WHITE BRICK MANUFACTURE

UTILIZING KLINE MOUNTAIN, NEW MEXICO CLAY

ISKENDER ISIK

Department of Geological Sciences

APPROVED:

Dr. Kenneth F. Clark, Chair

Dr. G. Randy Keller

Dr. Jerry M. Hoffer

Dr. David V. LeMone

Dr. John C. McClure

Dr. George S. Austin

Associate Vice President for Research
and Graduate Studies

WHITE BRICK MANUFACTURE
UTILIZING KLINE MOUNTAIN, NEW MEXICO CLAY

by

ISKENDER ISIK, B.Sc., M.Sc.

DISSERTATION

Presented to the Faculty of the Graduate School of

The University of Texas at El Paso

in Partial Fulfillment

of the Requirements

for the Degree of

DOCTOR OF PHILOSOPHY

Department of Geological Sciences

UNIVERSITY OF TEXAS AT EL PASO

December, 1993

This dissertation is dedicated to my father, Abdulkadir Isik, my mother, Gulnaz Isik, my wife, Zuhal Isik, my son, C. Eren Isik and my daughter, Merve B. Isik.

ACKNOWLEDGEMENTS

I would particularly like to thank my advisor, Dr. Kenneth F. Clark, for counseling me throughout my time at the University of Texas at El Paso (UTEP). I would like to thank Dr. George S. Austin, Senior Industrial Minerals Geologist of the New Mexico Bureau of Mines and Mineral Resources, Socorro, New Mexico, and Dr. George F. Cudahy, the President of the American Eagle Brick Company, for suggesting the dissertation study, and providing guidance and support during the course of my dissertation, together with my advisor. I am grateful to the other members of my committee, Dr. G. Randy Keller, Dr. Jerry M. Hoffer, Dr. David V. LeMone, and Dr. John C. McClure (Department of Metallurgy and Materials Engineering), for their contributions, reviews and suggestions toward the completion of this dissertation.

I am indebted to Timothy J. Maciejewski, a senior in geology, for accompanying and assisting me during the larger part of my field work; Mr. Alejandro C. Moreno, for providing laboratory equipment and chemicals to prepare and run analyses; Dr. Ibrahim Gundiler for allowing me to prepare my samples in the Metallurgical Laboratories of the New Mexico Bureau of Mines and Mineral Resources, Socorro, New Mexico; Dr. Murat Bengisu for furnishing the XRD equipment of the Department of Metallurgical Engineering at New Mexico Tech; and Mr. Christopher G. McKee for performing my chemical analysis by XRF in the laboratories of the New Mexico Bureau of Mines and Mineral Resources.

My appreciation is extended to Dr. Miguel Picornell-Darder, for allowing me to use the Soils Mechanic Laboratory in the Civil Engineering Department at UTEP; Mr. Ron J. Clark for performing my firing experiments in the kilns of the Art Studio of El Paso

Community College; Mr. Dennis J. Menual, scanning electron microscopy (SEM) technician, for providing valuable assistance in the SEM work at the Department of Metallurgy and Materials Engineering, UTEP; Ms. Judith Waggoner, realty specialist of the Bureau of Land Management, Las Cruces, New Mexico, for furnishing official information on mining claims in the study area; and Mr. Pat Roche, the owner of some of the claims and agent for the others, for allowing me to conduct my field work on his claims.

I would also like to express my sincere gratitude to the Chancellor and other Administrators of Anadolu University for their financial support during the course of my stay in the United States of America.

I am thankful to all those who made my and my family's stay in the United States of America a happy and good experience. The William N. McAnulty fund in Economic Geology at UTEP provided funds during the last few months of my stay, as did the American Eagle Brick Company.

A special thanks goes to my family, who provided the emotional support and encouragement so needed during the course of my study for an undertaking such as this. This work would probably never have been finished without their encouragement and sacrifice.

This dissertation was submitted to the committee on August 17, 1993.

ABSTRACT

The Kline Mountain kaolin deposit is situated on the northwestern flank of Kline Mountain in the complex Black Range uplift, Sierra County, New Mexico. It is located within the Gila National Forest. The deposit, discovered by Dr. F. L. Schneider in 1958, was used experimentally for its kaolin content in making ceramic tile. In 1962 and 1980, samples from the deposit were examined in some detail by the private sector to be utilized as paper coater. However, fine-grained silica (cristobalite and/or tridymite) within the kaolin has been reported as a major drawback for use in the paper industry. The whole deposit was reported to have 200 million tons reserve with 38 to 39 percent Al_2O_3 and a very high Standard Brightness of 94 percent. The production of kaolin has been by open pit mining methods. About 900 tons of kaolin were sold in 1969 for use as an oil absorbent by Union Oil Company. After screening crushed kaolin ore, it was shipped by trucks to Elephant Butte Lake for use in the Santa Barbara Channel Oil Spill.

The kaolinized tuff of the Kline Mountain area lies on the eastern margin of the Mogollon Plateau volcano-tectonic province, a major mid-Tertiary volcanic center. The later stage of the evolution of this center was related to the extensional environment of Basin and Range province and the Rio Grande rift. Local faults in the study area could have originated by the intrusion of Kline Mountain rhyolitic domes, which may be a set of ring fracture intrusions possibly related to the Gila Cliff Dwellings cauldron to the west. These faults have probably been reactivated by Basin and Range extension in the past 21 Ma. Faults in the study area display two dominant trends: northwest and northeast. The dominant structural style found in the study area is high-angle normal faulting. The stratigraphy in the

Kline Mountain clay deposit area consists of mid-Tertiary bimodal volcanic and volcanoclastic deposits that consist of basaltic andesite lavas, high-silica rhyolite lavas, and pyroclastic material.

The kaolin deposit occurs as a result of hydrothermal alteration within the advanced argillic zone of the tuff of Kline Mountain. The hydrothermal origin is indicated by clay minerals, silicification, volcanogenic materials and textures, structural and stratigraphic controls of the original volcanic sequence. The deposit is a result of kaolinization, alunitization and silicification that appears to have come from mid-Tertiary alteration and mineralization, both of which have affected the Kline Mountain rhyolite porphyry and the Taylor Creek rhyolite porphyry.

Relative to the Kline Mountain intrusive contact, the more distally located kaolinitic clay shows an inverse relationship between SiO_2 and Al_2O_3. In the proximal alunitic samples, SiO_2 has the lowest percentage, while Al_2O_3 and loss on ignition (LOI) are in the higher percentages, and K_2O is the highest. Thus, the ratio $Al_2O_3+K_2O+LOI:SiO_2$ is very low in the kaolinitic clays and is high in the alunite samples.

Based on the chemical analyses of surface localities and one drill core, the mineral compositions of each sample were calculated. The detected mineral percentages correspond to minerals present from XRD data. Minerals are calculated under four categories: kaolinite, alunite, silica (quartz, tridymite, opal, and cristobalite), and accessory minerals. Variations in the proportions of minerals was found with respect to depth of the drill core. Within the kaolinization zone, the kaolinite proportion is between 30.97 % and 58.20 % by weight. However, this percentage drops drastically to 5.27 %, and silica increases to 72.63 % in the

basal breccia zone, indicating the limit of economically viable kaolin deposits at 158 ft (48 m) depth. On the basis of calculated mineral composition and XRD data, there is an inverse relationship between kaolinite percentage and proximity to the intrusion. Conversely, there is a proportional relationship between alunite content and the proximity of the intrusion.

XRD data indicates that kaolinite is present in both whole-rock and clay-size fractions of each sample, while smectite was identified in two clay-size samples as the second clay mineral present due to the increasing amount of this clay mineral in this fraction. Elsewhere, alunite dominant samples in the both sizes show weak, small peaks of kaolinite reflection.

According to SEM photomicrographs of three outcrop samples studied, four kaolinite textures are recognizable as follows: columnar covered by very fine silica silcretes, well-crystallized, relatively poorly crystallized, and stacks. These SEM photomicrographs demonstrate the variability of kaolinite crystallinity, plus silica overgrowths (mostly silica lepispheres). The SEM images show that alunite crystals are hexagonal and pseudo-rhombohedral associated with bladed silica crystals, which are intergrown with lepispheres.

Particle-size analyses show that the shallowest drill core sample has the highest percentage of clay-size particles. With the exception of alunitic clay, there is a proportional relation between kaolinite content percentages and clay-size fraction percentages of kaolinitic surface samples. Larger clay-size fractions by weight in some samples indicate larger amounts of kaolinite. The alunitic clay sample demonstrates that the silt-sized fraction is the chief constituent.

There is a proportional linear relation between compressive strength and increasing firing temperature. Kaolin+#3 clay+nepheline syenite+white silica shows the highest compressive strength at the lowest firing temperature (3617 psi at 1900 °F) which is higher than the required compressive strength (2500 psi for Grade Severe Weathering, 2200 psi for Grade Moderate Weathering, and 1250 psi for Grade Negligible Weathering). In addition, #3 clay improves plasticity and green strength of brick made from Kline Mountain kaolin.

The fired brick specimens also demonstrated excellent white color properties. The bright whiteness of the fired specimen can give more market flexibility to the local brick company to produce various shades of white colored brick from this kaolin by adding from 15 to 50 % by weight of #3 and/or #1 clay from the Cerro de Cristo Rey deposit, in the El Paso area, with nepheline syenite to the kaolin so that a complete range of white-to-gray brick can be produced. This has the additional advantage of lowering the cost of producing white brick, because the #3 clay has negligible transportation cost to the firing plant.

Water absorption is the only physical property determined to be high for the specimens. However, all the brick specimens were prepared without using a vacuum which can reduce the porosity in a brick body and thus reduce water absorption. Water absorption is determined to be lowest in experimental mixtures that contain kaolin+#3 clay+nepheline syenite and white silica, which fire at lower temperatures than other mixtures. Thus, this mixture appears to be not only favorable for lowering the water absorption but also for providing highest compressive strength at low temperature. By using these clay mixtures followed by extrusion with vacuum, water absorption should be reduced in the fired brick to

the required limit and possibly lower than the required limit which is 20 percent for Grade SW, 25 percent for Grade MW, and no limit for Grade NW.

Consequently, these experiments have determined that the experimental brick specimens made with the Kline Mountain kaolin have the plasticity, green strength, workability and extrudability properties needed for utilization by the brick industry without any defects as a result of firing and chemical composition.

On the average, the available clay is calculated to be composed of kaolinite (40.67 %), alunite (16.37 %), silica (37.89 %) and accessories (1.16 %). The amount of clay available, for which there are chemical and mineralogical control, is probably 3,158,024 m tons. The Net Present Value (NPV) of brick made with Kline Mountain clay at American Eagle Brick Company for the next 30 years using the single factor Discounted Cash Flow method is $4,132,138. The NPV by the Hoskold method is $3,532,430. The discounted cash flow return on investment (DCFROI) is found to be approximately 48 %. On the basis of the NPV and DCFROI, exploiting the Kline Mountain clay and manufacturing white brick at the American Eagle Brick Company plant in El Paso is found to be economically viable under the projected conditions.

TABLE OF CONTENTS

LIST OF TABLES

LIST OF FIGURES

CHAPTER 1
INTRODUCTION

1.1. Location and Geographic Setting

The Kline Mountain kaolin deposit occurs within an advanced argillic alteration zone in volcanic and volcaniclastic rocks of mid-Tertiary age (Patterson and Holmes, 1965; Ericsen, 1970; Coney, 1976; Eggleston, 1987; Eggleston and Norman, 1983; and Harrison, 1986). The deposit lies within the Black Range, Sierra County, New Mexico. This range has the potential to host to a number of kaolin deposits as a consequence of the wide varieties of feldspathic volcanic and volcanoclastic rocks present as well as the appropriate hydrothermal alteration conditions that once existed. The source rock potential and hydrothermal alteration of the Kline Mountain tuffs therefore is significant in delineating areas likely to contain commercial reserves of kaolin. Clay minerals, such as kaolinite which is a common constituent of altered tuff, are also indicators of the hydrothermal alteration that can accompany feldspathic volcanic and volcaniclastic rocks.

The Kline Mountain kaolin deposit is situated on the northwestern flank of Kline Mountain in the Black Range, Sierra County, New Mexico (Figure 1). It is about 170 miles northwest of El Paso on New Mexico Highway 59 (NM 59). The elevation of the deposit is 7670 feet (2338 m) above sea level. There are no electric facilities. The kaolin deposit is located within the Gila National Forest (Figure 2). Nearby settlements are Winston and Chloride. The prevailing climate in the area is semiarid, and precipitation varies from about 8 in (20 cm)/yr to more than 20 in (50 cm)/yr. Rainfall occurs predominantly in July and August.

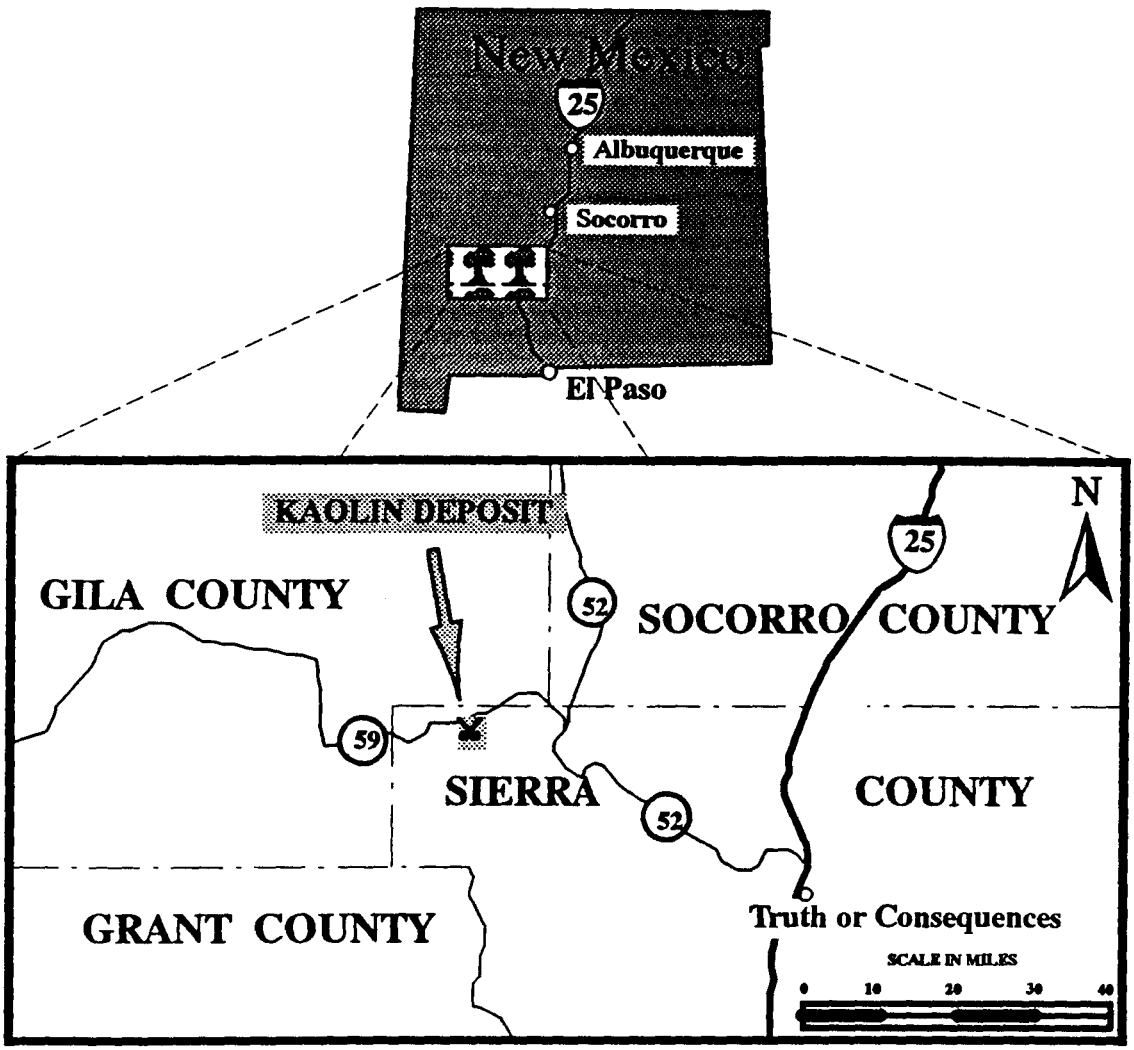

Figure 1: Location map of Kline Mountain kaolin deposit.

Figure 2: Panoramic view of Kline Mountain koalin mine at the sorted materials site. Mining activities have locally removed the pervasive forest at this elevation.

1.2. History of Mining and Exploration

The deposit, discovered by Dr. F. L. Schneider in 1958, was used experimentally for its kaolin content in making ceramic tile. Samples from the deposit were examined in some detail by DeViliers and Sallee in 1962 and by Chowdhury in 1980. Evaluation for use of the kaolin as paper coater were completed by the private sector. Fine-grained silica (cristobalite or tridymite ?) within the kaolin has been reported as a major drawback for use in the paper industry. The whole deposit is estimated to have 200 million tons reserve with (pers. comm., P. Roche, August 1991) 38 to 39 % Al_2O_3 and a very high Standard Brightness of 94 %. About 900 tons of kaolin were sold in 1969 to be used as oil absorbent by Union Oil. The production of kaolin has been by open pit mining methods (Figure 3). After screening crushed kaolin ore, it was shipped by trucks to Elephant Butte Lake for use in the Santa Barbara Channel Oil Spill (pers. comm., P. Roche, August 1991). American Eagle Brick Company (formerly known as El Paso Brick Company) has begun to explore the possibility of making white brick from Kline Mountain kaolin so as to increase the production and to meet El Paso's brick needs.

1.3. Purpose of Investigation

This dissertation primarily concerns the kaolin deposit and its application as raw white brick material. Thus, the objectives of this study were to: 1) identify clay minerals and other minerals within the deposit, 2) identify a genetic model, 3) investigate the kaolin properties to determine if the material would be more suitable for consideration as a

Figure 3: Panoramic view of Kline Mountain kaolin mine at the excavation site.

white brick material, and 4) evaluate the mine under todays economic conditions and determine whether it would be economically viable in terms of ore quality, reserves, mine life, investment, the net present value (NPV), and the discounted cash flow return on investment (DCFROI).

1.4. Methods of Investigation

Detailed geologic mapping of the study area was completed during the summer of 1992, as seen in Plates 1 and 2. Measurements, descriptions, and samplings of the drill core (Figures 16 through 20), whose exact locality is unknown, and throughout the advanced argillic alteration zone that contains the clay deposit, provided the primary data base for many aspects of this study.

X-ray diffraction (XRD), with both random and oriented mounts, and scanning electron microscopy (SEM) were used to identify clays and other alteration minerals within the deposit. The former analysis was done both at the Materials Department of New Mexico Tech and at the Department of Metallurgy of the University of Texas at El Paso (UTEP). The latter was done at the Department of Metallurgy of the University of Texas at El Paso.

Twenty four samples, seven of which were drill core chips, were selected for bulk major-element analysis (Tables 1 and 2). The analysis were done at the New Mexico Bureau of Mines and Mineral Resources by X-ray fluorescence methods under the supervision of Christopher G. McKee. On the basis of chemical analyses, semiquantitative mineral composition percentages were calculated, as explained in Appendix 1.

CHAPTER 2
GEOLOGY

The Kline Mountain kaolin deposit is located in part of the complex Black Range uplift which lies on the eastern margin of the Mogollon Plateau volcano–tectonic province (Figures 4 and 5). Locally, it occurs in a structurally simple block bounded on the west by the Glenwood graben and on the east by the Winston graben, both of which are related to the Basin and Range Province and Rio Grande rift. The Mogollon Plateau, mid–Tertiary volcanic field consisting of intermediate to felsic volcanic rocks and volcaniclastic sedimentary rocks, underwent minor subsidence from about 33 Ma to 21 Ma BP and has interacted with the extensional tectonism as an essentially coherent block. The Mogollon Plateau was depressed, covered with Gila group volcano–sedimentary rocks, later uplifted, as presently exposed (Eggleston and Norman, 1983). The distribution of the lava and the location of some of the calderas are shown in Figures 4 and 5.

2.1. Previous Studies

Many investigations have centered on the Black Range occurrences of tin, perlite, topaz, copper, lead, zinc, gold, and silver, but only a few studies have dealt with the clay deposits of the range. Patterson and Holmes (1965) stated that the highly crystalline kaolinite, which occurs in hydrothermally altered tuffs and other volcanic rocks, has been tested for use in making ceramic tile and as coating for paper products. Ericsen et al. (1970) reported that tests indicate the kaolin was an intermediate to heavy–duty refractory material. Coney (1976) defined the kaolin deposit as part of the heavy alteration and high silicification of the

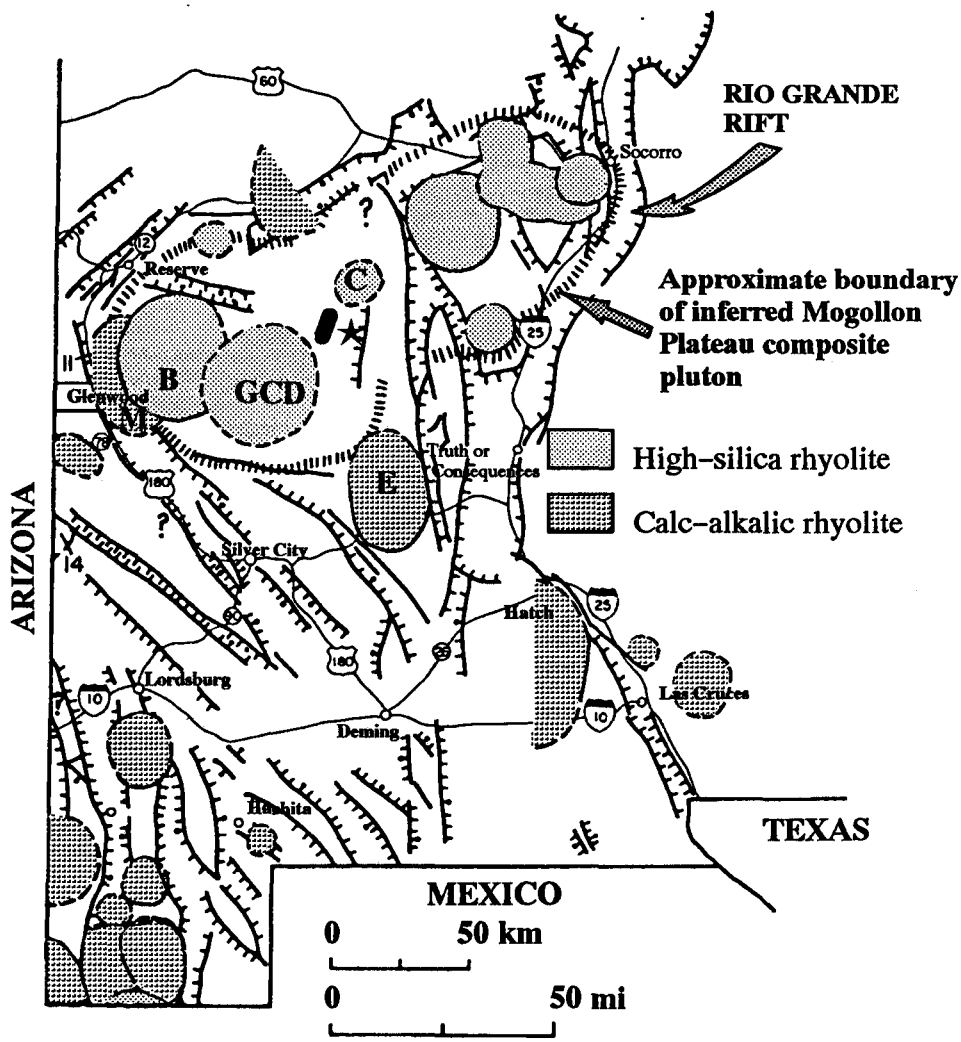

M: Mogollon Caldera
B: Bursum Caldera
GCD: Gila Cliff Dwellings Caldera
C: Corduray Canyon Caldera
E: Emory Caldera
: Taylor Creek Rhyolite
★ : **The Kline Mountain Kaolin Deposit**

Figure 4 : Tectonic map of southwestern New Mexico showing the relationship of the Kline Mountain kaolin deposit to the major Cenozoic faults and calderas in the region (modified from Elston, 1984).

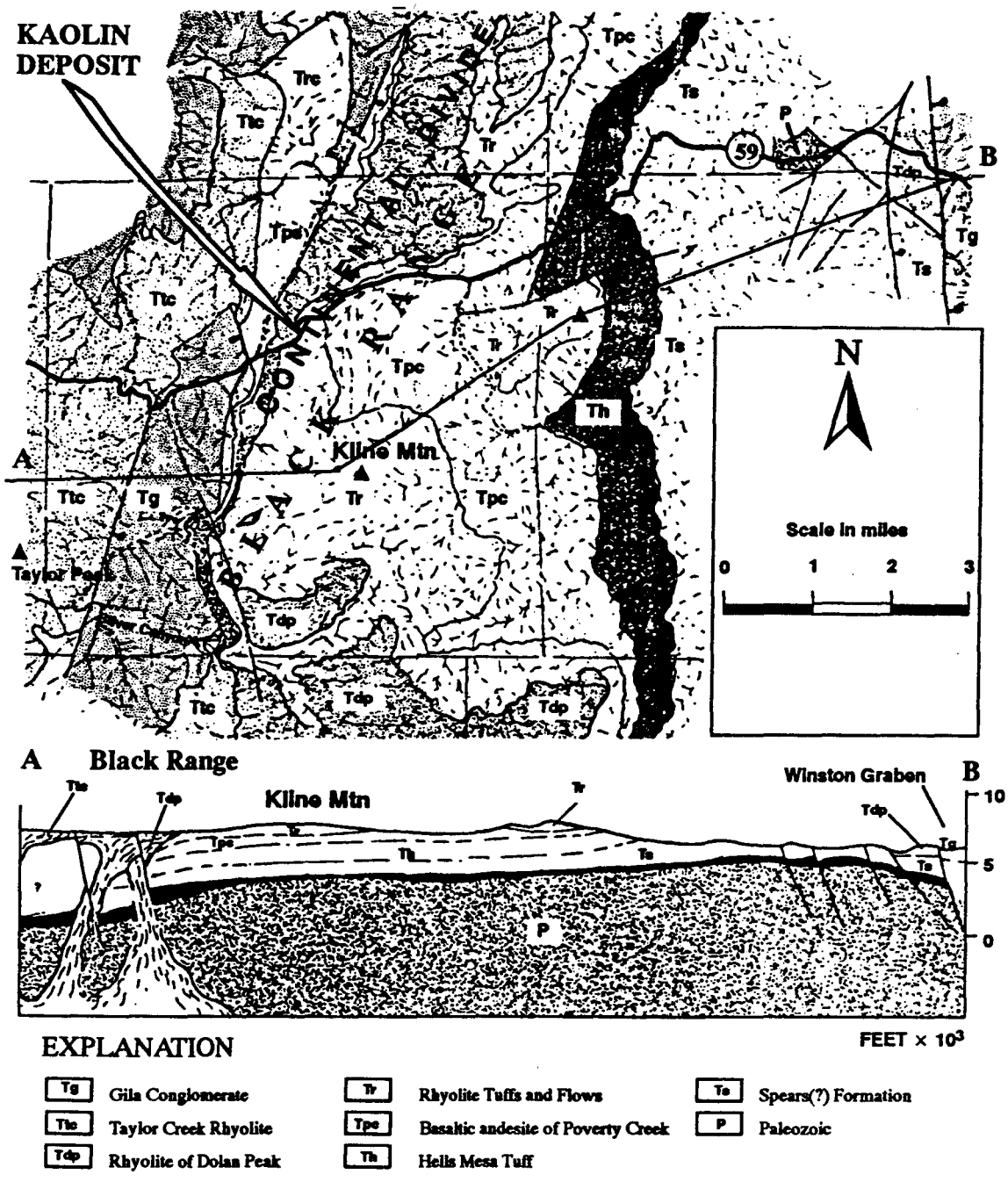

Figure 5: Geological map and cross section of the Black Range uplift showing the configuration of the Kline Mountain kaolin deposit (Coney, 1976).

basal and upper tuffs, mineralized by gasses and tin-bearing fluids associated with ascent of the younger tin-bearing Taylor Creek Rhyolite through the tuffs.

On a regional scale, Elston et al. (1976) postulated that the Mogollon-Datil volcanic field of southwestern New Mexico consisted of three overlapping volcanic rock suites, one of which is high-silica alkali rhyolite hosting the kaolin deposit. They stated that the high-silica alkali rhyolite is the volcanic equivalent of an underlying granitic pluton and was formed as a result of partial melting of upper mantle and/or lower crust. According to them, the alkali rhyolite suite consists of ash-flow tuff, ring fracture and moat deposits of large central volcanoes, and enormous masses of flow-banded rhyolite. Moreover, they stated that the high-alkali rhyolite suite is nearly confined to the Mogollon Plateau, unlike the other two volcanic suites.

Eggleston and Norman (1983) reported that the tuff of Kline Mountain is a sequence of interbedded ash-flow and air-fall tuffs and volcanosedimentary rocks that were altered by the Kline Mountain intrusion. They indicated an advanced argillic alteration zone near the contact with the intrusive and an argillic alteration zone further from the contact, where kaolin is deposited. On the basis of the close association of the altered mineral assemblages and their genetic relation to the northern end of the Kline Mountain rhyolite porphyry, Eggleston and Norman (1983) have reported normal zoning of alteration. According to the authors, zoning of the alteration around this part of the intrusion is not complex. On the basis of the close association of the altered mineral assemblages and their genetic relation to the northern end of the Kline Mountain rhyolite porphyry, they have reported normal progression of alter-

ation, intense near the intrusive and gradually decreasing away from the core toward north. Moreover, they stated a genetic relation between the tuff of Kline Mountain and the rhyolite of Dolan Peak (Figure 5), based on similar vitric clast content in the upper few meters of the tuff of Kline Mountain and overlying rhyolite of Dolan Peak, which is outside the map area. They defined two periods of alteration and mineralization in the Taylor Creek region (Figure 5), the older period of which is associated with the Taylor Creek Rhyolite and consists of argillic alteration and hematite–cassiterite veining, and the younger period is associated with the Kline Mountain Rhyolite porphyry and consists of argillic, advanced argillic, and quartz–sericite–pyrite alteration. They estimated the age of the alteration at post 23.5 Ma or much younger.

Elston (1984) concluded that hydrothermal activity in southwestern New Mexico is generally in the ring–fracture zone of the cauldrons (Figure 4) which may have been the ground preparation for later mineralization. He postulated that the ring–fracture volcanism in the region acted as a safety valve by carrying vapor pressured magma through fractures and diluting it by convecting meteoric water, resulting in alteration and mineralization during the hydrothermal activity stage. Harrison (1986) described the epithermal vein deposits in the Chloride district and concluded that alteration occurred in the district because of hydrothermal convective cells generated by intrusion of rhyolitic domes, which is believed to be in a ring fracture of a cauldron (Elston, 1984).

2.2. Geology of the Kline Mountain Kaolin Deposit Area

The geological maps of the Kline Mountain kaolin deposit area (Plate 1 and Plate 2) were completed by the author (after Eggleston, 1987) during the summer of 1992. Plate 1 covers an area of about 15.5 km^2 and the mapping scale is 1:10,000. Plate 2 shows detailed geological mapping of mine sites and covers an area (as shown in Plate 1) of about 0.41 km^2 at a map scale of 1:1,500. Location of the maps is shown in Figures 1, 4, and 5.

The basic tools used for these surveys were Brunton compass, pacing, hammer, rod, and tape measure. Pick and shovel were employed for some surface sample recoveries. Ground survey control points include a USGS bench mark, surveyed mine sites, surveyed cross cuts of the Continental Divide, NM 59, and topographic features.

These geological maps are outcrop maps in which geological contacts are controlled at three levels. However, intense forest and thick overburden were the two formidable barriers in tracing outcrops and contacts in the field. Advantages of an outcrop map is that the distribution of outcrops is controlled exactly, which is helpful for the interpretation of hydrothermal alteration, concealed contacts, faults, and folds, as well as geochemical, mineralogical, and geophysical data.

Along with the geological maps are two cross sections compiled from the surface geological map. Section ABC is in a northwest–southeast direction, it cuts through a northwest–striking fault as well as Kline Mountain Rhyolite porphyry, kaolinized tuff unit, silica cap, La Jencia tuff, and an alluvial deposit. Section DE is in a east–northeast and west–south-

west direction, and shows the kaolin mine sites. These cross sections demonstrate the gross relation of stratigraphy, structural features and the extension of the kaolin deposit.

2.3. Tertiary Stratigraphy

The stratigraphy in the Kline Mountain clay deposit area consists of mid-Tertiary (mostly Oligocene to Miocene) bimodal volcanic and volcanoclastic deposits that consist of basaltic andesite lavas, high-silica rhyolite lavas, and pyroclastic material. Eggleston's (1987) nomenclature was the basis for this study (Figure 6). The mid-Tertiary volcanic/volcaniclastic sequence is divided, in stratigraphically ascending order, into basaltic andesite of Poverty Creek (Tpc), tuff of Stiver Canyon (Tsc), tuff of Kline Mountain (Tkm), Silica Cap (S), La Jencia tuff (Tlj), unnamed pyroclastic deposits (Tt), tuff of Garcia Camp (Tgc), sandstone of Inman Ranch (Tir), and rhyolite porphyry of Kline Mountain (Tkmpr). Quaternary alluvium and colluvium overlie this mid-Tertiary section in the area. Detailed stratigraphic description below are based on field mapping and observations, Eggleston (1987), and of other investigators work.

2.3.1. Basaltic Andesite of Poverty Creek (Tpc)

This is the oldest stratigraphic unit that crops out in the kaolin deposit area. In the study area, this unit crops out extensively in the northeast part along the northern flank of Kline Mountain (Plate 1). Woodard (1982) reported that the thickness of this unit is between 60 and 240 m. The author stated a K-Ar date of 28.3 $\pm$ 0.6 Ma for the basaltic andesite of Poverty Creek. Eggleston (1987) reported mild propylitization in the top flows of the unit

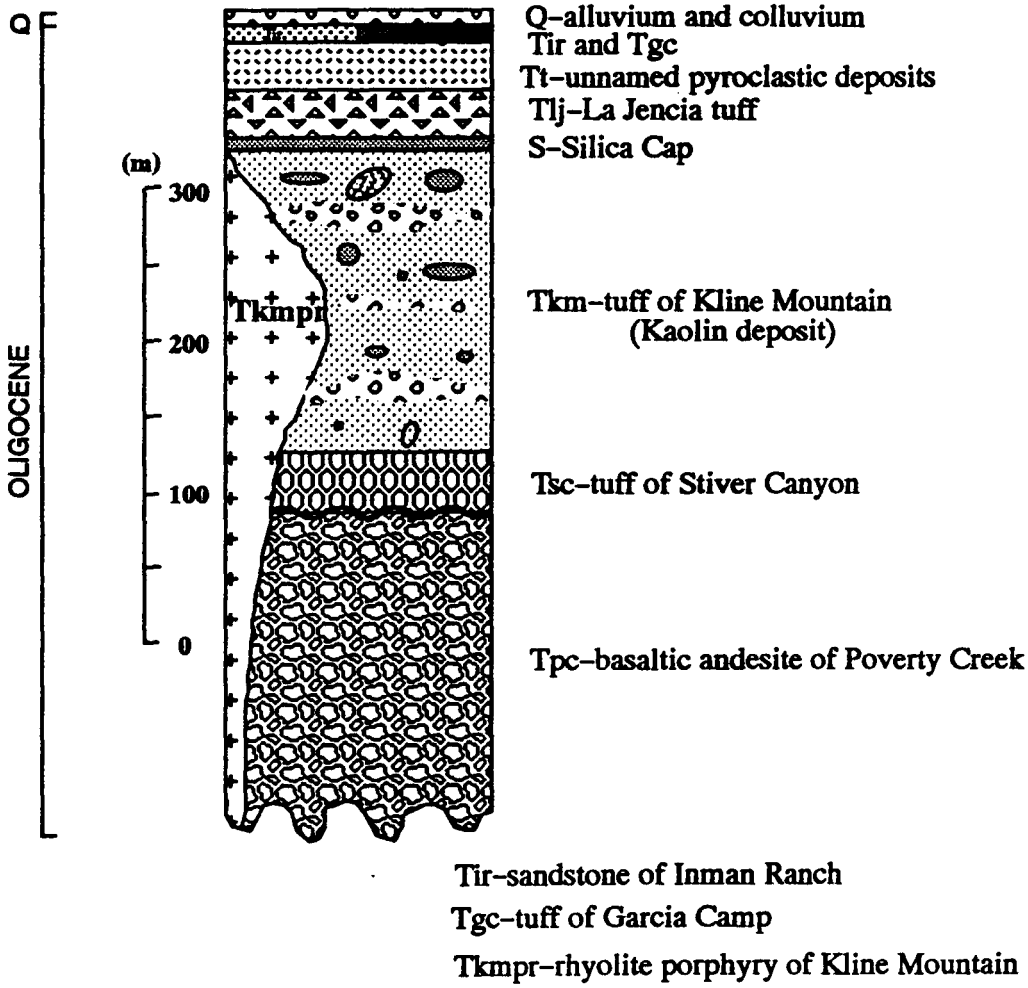

Figure 6: Stratigraphic Column of the Kline Mountain Kaolin Deposit (after Eggleston, 1987).

on the basis of thin section studies. Contrary to Woodard (1982), Eggleston (1987) reported a thickness of 40 to 200 m for the unit.

The basaltic andesite of Poverty Creek contains lava flows with minor intercalated volcaniclastic sedimentary rocks, which were probably locally derived (Figure 7). According to Eggleston (1987), the andesite has a fine-grained trachytic texture with sparse phenocrysts, consisting of clinopyroxene and plagioclase. Plagioclase microlites are reported to be the chief minerals of this rock (Woodard, 1982). Accessory minerals were reported to be iddingsite, bowlingite, and amphibole (Eggleston, 1987).

2.3.2. Tuff of Stiver Canyon (Tsc)

The tuff of Stiver Canyon is pink, orange, or white colored, poorly welded, pumiceous rhyolitic ash-flow tuff, containing phenocrysts. According to the Woodard (1982), this unit unconformably overlies the basaltic andesite of Poverty Creek and is a crystal-poor to moderately crystal-rich, high-silica rhyolite-ignimbrite named for exposures in Stiver Canyon, which is located on the west of Kline Mountain between Kline Mountain and Taylor Creek (Figure 5). Eggleston (1987) reported that this unit consists of phenocrysts of sanidine (2 %), quartz (1 %), and biotite (trace) in a vitroclastic groundmass on the north side of Kline Mountain where this unit is exposed in the study area (Plate 1). The tuff of Stiver Canyon is about 40 m thick in the area. Eggleston (1987) states that the source of the tuff is unknown.

Figure 7: Basaltic andesite of Poverty Creek showing alteration in the top flow and intercalated volcaniclastic sedimentary debris.

2.3.3. The Tuff of Kline Mountain (Tkm)

Tuff of Kline Mountain was named by Eggleston (1987) for the sequence of ash-flow tuffs that crop out on the northern flank of Kline Mountain in the study area (Plate 1). According to Eggleston (1987), the tuff is a high-silica rhyolitic ignimbrite which contains a sequence of nonwelded, thinly bedded, and moderately crystal-rich units. Eggleston (1987) reports numerous 1 to 3 m thick flow units that contain as much as 50 % pumice fragments. He recognized variable crystal content from flow to flow unit with an average of 12 %. The author reports, in decreasing order, sanidine and quartz as the phenocrysts, and plagioclase, biotite, zircon, and opaque minerals as the trace constituents. He believed that the tuff of Kline Mountain fills a shallow paleovalley with as much as 200 m of thickness and may have a genetic relation with the rhyolite of Dolan Peak, which overlies this unit outside the study area.

In the study area (Plate 1), much of the tuff of Kline Mountain has been converted to an assemblage of kaolinite-alunite-silica due to the intrusion of the Kline Mountain Rhyolite Porphyry (Figure 8). This is the unit of commercial interest that was intermittently mined for its kaolin content where NM 59 crosses the Continental Divide. This lithologic unit is the focus of this dissertation.

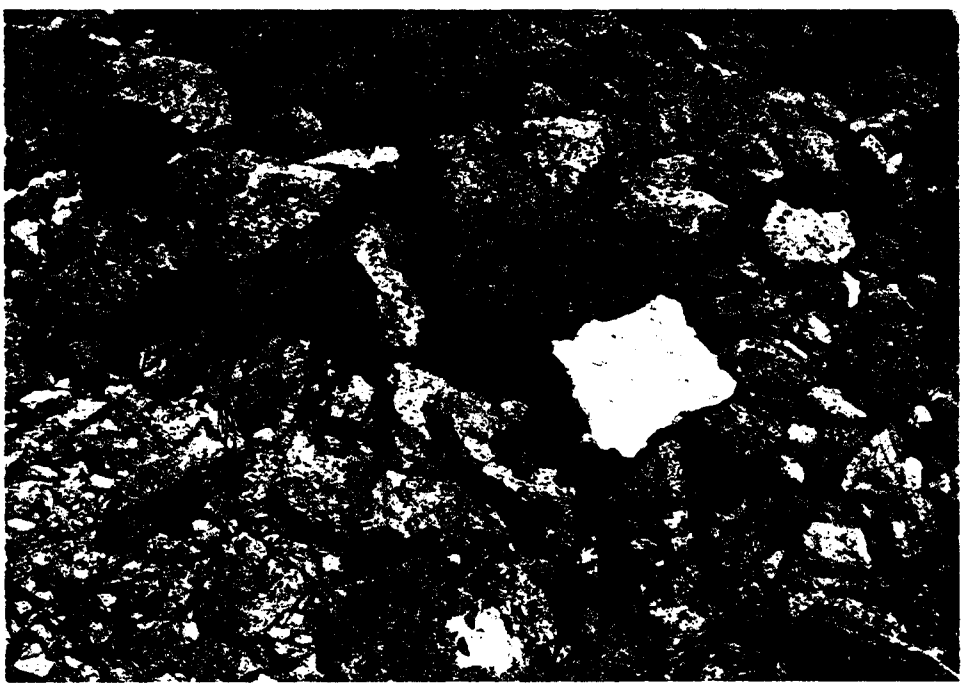

Figure 8: Typical exposures of the altered tuff of Kline Mountain in the clay pit showing kaolinization.

2.3.4. Silica Cap (S)

Silica caps were mapped as an individual stratigraphic unit in Plates 1 and 2. They cover a significantly large portion of the study area. Silica caps are well developed on the south of the Strip Mine (Figure 9). They appear to be replacement bodies of the tuff above the kaolin deposits. Subhedral to euhedral quartz crystals within the silica cap (chalcedony) are believed to be relict phenocrysts and lead to the interpretation of these units as chalcedonic replacements of lavas. The massive replacement type silica consists mostly of chalcedony with some opal CT (?) and minor kaolinite in some places. Figure 10 is an SEM image of a silica cap displaying quartz crystals and opal CT (?) within the fibrous cryptocrystalline texture. Its thickness is a maximum of about 3.5 m on the west of the Strip Mine, indicating the degree of silica supersaturation of the fluid.

Figure 9: Silica cap showing massive chalcedony body.

Silica caps display close association with faults in the area indicating that the faults were the conductive zones for silica bearing fluids, as evidenced by the altered and silicified fault zones in the area. In some places in the kaolin deposit, the silica caps display sinter type texture with alteration rims of chalcedony indicating ancient hot–spring related alteration as evidenced by hard, dense and spongy porous (in places) textures indicating various flow regimes of ancient hydrothermal fluids (Figure 11). Banded texture in places suggests paleo hot–spring fluid conduits where geothermal steam was prevalent. The alteration rims in the silica caps are common especially in places that they are associated with fracture zones. This silica sinter may have been formed by SiO_2 precipitating from cooling water supersaturated with dissolved SiO_2. The sinter appears to be amorphous and hydrous (?); however, fibrous cristobalite and hexagonal quartz images in Figure 10 display slow crystallization as postulated in Browne (1992) for silica sinter. Silica sinter in the area is generally white, but in some places, grey and brown.

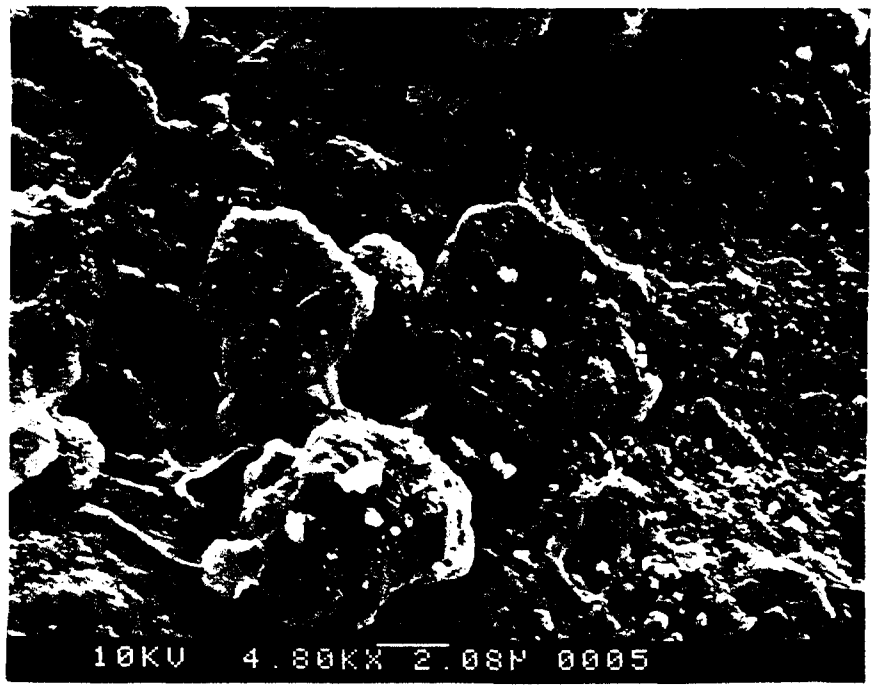

Figure 10: Scanning electron image of a silica cap, chalcedony. Note fibrous cryptocrystalline texture containing quartz and opal (?) (Scale bar=2.08 µm).

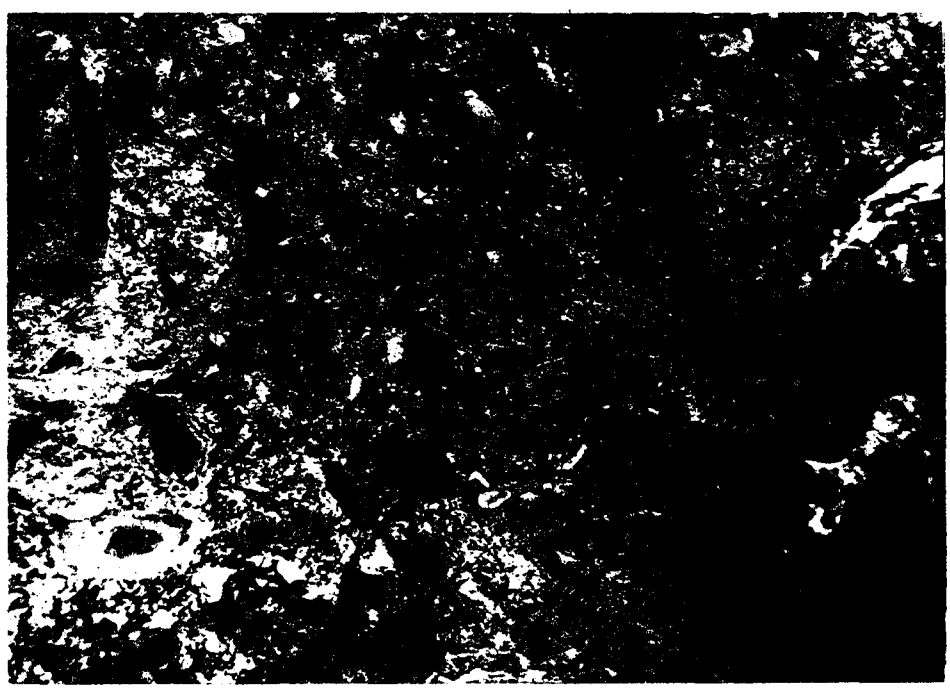

Figure 11: Siliceous sinter showing alteration rims of chalcedony in the kaolin mine indicating ancient hot-spring related alteration.

2.3.5. La Jencia Tuff (Tlj)

Within the study area, the La Jencia Tuff is exposed along the Continental Divide north of NM 59 and west of Kline Mountain (Plate 1). Eggleston (1987) defined this unit as a crystal poor, densely welded, foliated, and locally lineated rhyolitic ignimbrite. He reported a SiO_2 content of about 73 % and a mineral assemblage that contains 7 % sanidine and a traces of quartz, plagioclase, biotite, zircon, and pyroxene as phenocrysts in a vitroclastic groundmass. Eggleston (1987) reported a 28.76 $\pm$ 0.15 Ma age of the La Jencia tuff. He postulated its thickness to be between 20 and 30 m. The tuff is light to dark gray in color.

2.3.6. Unnamed Pyroclastic Deposit (Tt)

This unit is exposed on the northwest corner of the study area (Plate 1). Eggleston (1987) defined it as a multiple flow nonwelded crystal-poor, moderately pumice-rich ignimbrite, which consists of massive pyroclastic flow unit (10 m thick) overlain by numerous thin pyroclastic flow units. He reported about 5 % sanidine and a trace of plagioclase as phenocrysts. The pumice is dark gray to black in a tan to light gray groundmass. He postulated up to 30 m thickness for this unit.

In the study area, the top of the deposit consists of a coarse breccia believed by Eggleston (1987) to have been emplaced as a hot pyroclastic flow. The deposit consists of blocks of clasts in a matrix of vesiculated rhyolite lava. The blocks are generally 12 to 27 cm in diameter.

2.3.7. Tuff of Garcia Camp (Tgc)

Within the study area, this unit is exposed on the west flank of Kline Mountain (Plate 1). It is essentially a high-silica rhyolite ignimbrite with abundant pumice fragments. Eggleston (1987) reported about 10 % quartz, 6 % sanidine, 1 % biotite, and a traces of plagioclase, amphibole, zircon, and opaque minerals as phenocrysts in a vitroclastic groundmass. He stated that this unit is a cliff former as much as 20 m thick and developed a granophyric groundmass texture with overgrowths on quartz and sanidine phenocrysts caused by intense vapor-phase crystallization.

2.3.8. Sandstone of Inman Ranch (Tir)

In the study area, this unit is the least-well exposed rock. The unit is essentially tuffaceous siltstone, sandstone, and conglomerate. On the basis of high-angle crossbedding in well-sorted sandstones near the base of the unit, Eggleston (1987) suggested an aeolin deposition. He noted the dominating clasts of the pre-existing lithologies in the region and believes that these were the local sources for the sandstone of Inman Ranch. He described the unit as distinctive 1 to 2 m thick sandstone. According to the author, the unit contains, poorly welded ignimbrite exposed near the top of the unit. Eggleston (1987) reported an age of Upper Oligocene to Lower Miocene.

2.3.9. Kline Mountain Rhyolite Porphyry (Tkmpr)

The only intrusive exposed in the study area is the rhyolite porphyry of Kline Mountain, which caused gently doming of the overlying volcanic rocks. Eggleston (1987) recognized about 15 % phenocrysts consisting of quartz (5 %) and sanidine (10 %) in a

granophyric groundmass with biotite and possibly amphiboles as trace constituents that are rarely preserved. Near the margin of the intrusive, vertical flowbanding is common.

The entire intrusive is altered to some degree as evidenced by silicification and argillic alteration. The primary texture of the intrusive is affected and obscured by intense alteration. Thus, the contact of the rhyolite porphyry and surrounding rocks is only approximated on Plate 1. Eggleston (1987) noted a common quartz–pyrite stockwork of the intrusive, to the southeast of the study area. The alteration associated with this intrusive is described in a later section.

Eggleston (1987) reported a conventional K–Ar date of 28.4 $\pm$ 1.2 Ma age for the rhyolite porphyry of the Kline Mountain. The author suggests that the Kline Mountain intrusive is younger than the Taylor Creek Rhyolite, a ring fracture type volcanic unit associated with the Gila Cliff Dwellings Caldera (GCD) in the region (Figure 4).

2.3.10. Quaternary Deposits

In the study area, these Quaternary deposits consist of alluvium (Qal) in the larger active stream channels and colluvium (Qca) on gentle hillslopes and in small stream channels, which are drainage systems in the study area. The Piedmont slope deposit (Qpg) is exposed to the northwest of the study area and is poorly sorted. All of three deposits contain fine to coarse–size volcano–sedimentary materials.

2.4. Structures

The Kline Mountain kaolin deposit is located in the southeastern edge of the Mogollon Plateau volcano–tectonic province (Figures 4 and 5), which is related to the extensional environment of Basin and Range Province and the Rio Grande rift (Isik and Clark, 1992). Local faults in the study area could have originated by the intrusion of Kline Mountain rhyolitic domes, which may be part of a set of ring fracture intrusions related possibly to the Gila Cliff Dwellings Cauldron to the west (Figures 4 and 5). These faults have probably been reactivated by the Basin and Range extension in the past 21 Ma.

On the basis of geologic mapping and gravity studies, Coney (1976) reported that the Mogollon Plateau is bounded on the east by Winston graben and on the west by Glenwood graben. He also stated that the rims of the plateau are marked by the Black Range uplift (Figure 5) on the east and Mogollon uplift on the west, both of which are complex and contains economically viable mineral deposits. He determined the gravity highs over the uplifts and the gravity lows over the interior plateau were due to the presence of a pluton buried at shallow depth beneath the interior plateau.

A tectonic sketch map of the region surrounding the study area is shown in Figure 4. The study area lies on the west side of the Black Range (Figure 5), which is reported by Woodard (1982) and Coney (1976) as a west–dipping homocline bounded on the east by the range–margin–fault of the Winston graben that has dropped relative to the Black Range uplift. Faults in the study area display two dominant trends: northwest (Figure 12) and northeast (Plate 1). They are silicified and altered in zones, as at the Jeep Trial, displaying

wide silicified and altered zones (Plate 1 and Figure 13). At the Prospect locality close to the intrusive, the fault zone displays about 75 m wide hematite–cassiterite (?) mineralized zone (Figure 14). According to Coney (1976), the mineralizations in the altered tuff were occurred by gasses and tin-bearing fluids associated with ascent of the younger tin-bearing Taylor Creek rhyolite through the tuffs.

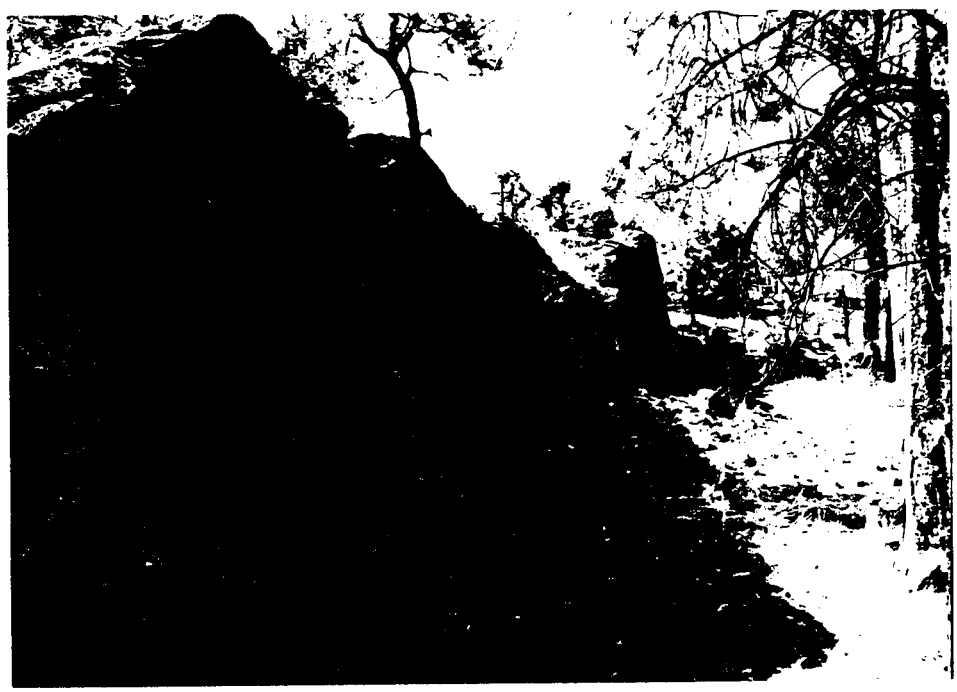

Figure 12: Normal fault displaying northwest trend.

The dominant structural style found in the study area is high-angle normal faulting. A fault shows evidence for strike-slip motion along a northwest trend is shown by slicenside striations (Figure 13), indicating reactivation of previous trends by a new stress regime, possibly due to the intrusion of the rhyolite porphyry of Kline Mountain. Also, Eggleston (1987) stated that the intrusion of the rhyolite porphyry of Kline Mountain possibly changed the strikes of faults in the study area from north-south to northeast.

Figure 13: Normal fault showing silicified zone at Jeep Trial.

Figure 14: Prospect location displaying hematite-cassiterite (?) mineralization fracture zone along with fault zone.

CHAPTER 3
HYDROTHERMAL ALTERATION

Due to the unstable, reactive nature of many volcanic minerals and glasses, post–depositional changes of volcanogenic deposits are typically rapid and pronounced. Alteration is the term commonly employed by geologists to describe these post–depositional changes in hydrothermal environments.

The factors that can affect the formation of hydrothermal minerals are classified by Browne (1992) as temperature, pressure, type of parent rock, reservoir permeability, fluid composition, and duration of activity. Browne (1992) postulated the types of hydrothermal alteration as direct deposition–from solution deposited along with passages such as joints, faults, vugs, pores, and fissures; replacement–permeability dependent interaction for some primary minerals, stable or metastable under the new conditions influenced by hydrothermal environment; and leaching–dissolving primary minerals without replacing the voids. They generally cause chemical changes as a function of mineralogy whose constituents are added and removed from a reservoir.

Volcanic units in the field have undergone hydrothermal alteration. Alteration is most intense near the intrusive contact of the Kline Mountain rhyolite porphyry and gradually fades out distally. The altered zone has an elliptical shape that trends roughly northwest. The Kline Mountain rhyolite intrusion is also affected. Four distinct alteration assemblages are recognized in the study area (Plate 3). These assemblages are: (1) weak propylitic alteration, (2) argillic alteration, (3) advance argillic alteration, and (4) silicification. Alteration

of the volcanic units occurs primarily as replacement, that is, a new mineral assemblage takes place of the primary minerals. The distribution of these alteration assemblages in the area is discussed in detail below.

3.1. Weak Propylitic Alteration

This alteration assemblages is the dominant alteration type in the top of the basaltic andesite of Poverty Creek (Figure 7). Eggleston (1987) reported epidote, calcite, and possibly chlorite indicating a propylitic assemblage along fracture surfaces in the basaltic andesite of Poverty Creek. He did not find pervasive propylitic alteration in the region and remarked on the rapid decreasing degree of the alteration immediately northwest of the area.

3.2. Argillic Alteration

This alteration assemblage overlaps the advanced argillic assemblage in the study area. According to the Eggleston (1987), the argillic assemblage begins about 2 km northeast of where NM 59, crosses the Continental Divide and increases in intensity southward. He stated that argillic alteration is characterized by a kaolinite–chalcedony assemblage that has replaced alkali–feldspars in high–silica rhyolite ignimbrites such as the tuff of Kline Mountain. The author reported that potassic feldspar and sodic plagioclase feldspar is altered to clay minerals, ferromagnesian minerals are altered to various opaque oxides, manganese oxides coat fractures, and hematite is disseminated throughout the tuff near the northern extremity of the argillic alteration. He noted that with increasing intensity of alteration, the groundmass was converted to clay minerals and alkali–feldspars also were locally converted

to clay minerals. He postulated that the end stage of argillic alteration is marked by conversion of the groundmass of the tuffs to clay minerals, conversion of all alkali–feldspars to clay minerals, and deposition of veinlets of chalcedonic quartz in the tuff host rock. According to him, the transition from argillic to advanced argillic alteration occurs an a zone about 1 km wide and is characterized by the first occurrence of alunite.

3.3. Advanced Argillic Alteration

This alteration zone contains commercial kaolin deposits which have been explored intermittently. Advance argillic alteration, characterized by kaolinite–alunite–silica (chalcedony, tridymite, and quartz) mineral assemblage, is widespread in the study area (Figure 2 and Plate 3). This pervasive alteration in the area developed in situ and is related to hydrothermal regimes developed concurrent with or subsequent to the intrusion of the rhyolite porphyry of Kline Mountain, which has also undergone the same alteration to some degree.

Kaolinite and alunite are the most diagnostic indicators of advance argillic alteration, both of which are the characteristic minerals in the advanced argillic alteration assemblage. On the basis of calculated mineral composition (Table 3), kaolinite is the dominant clay mineral in the northern part of this alteration zone where the abandoned mines are, while alunite is the dominant mineral to the south near the contact of the intrusive. The alunite dominant mineral assemblage around the intrusive contains hematite–cassiterite (?) mineralization (Figures 14 and 15).

On the basis of representative drill core fragments (R5–I through VII) furnished by G. S. Austin, New Mexico Bureau of Mines and Mineral Resources, the depth of kaoliniza-

tion zone is 48 m. Figures 16 through 20 depict the character of this drill core with respect to kaolinization depth and physically different levels. According to the map by Mr. P. Roche, the owner of part of the claims and agent for the others, the location of this drill core is estimated to be between the two mines in the study area, as seen in Figure 21. The description of drill core logs shown in Figure 21 have been reported to be lost. Between 0 and 48 m the tuff is completely altered to kaolinite–alunite–silica mineral assemblage with a characteristic white color and softness. However, drill core fragments display a relatively fresh breccia type texture below 48 m, indicating the end of the commercially viable kaolin deposit at this location. This observation is supported by XRD graph (Figure 26 through 32), chemical analyses (Table 1), and calculated mineral compositions (Table 3) of the drill core samples.

Figure 15: Hematite–cassiterite(?) mineralization within the alunitization dominant advanced argillic alteration close to (approximately 0.9 km or 0.56 miles) the Kline Mountain intrusive.

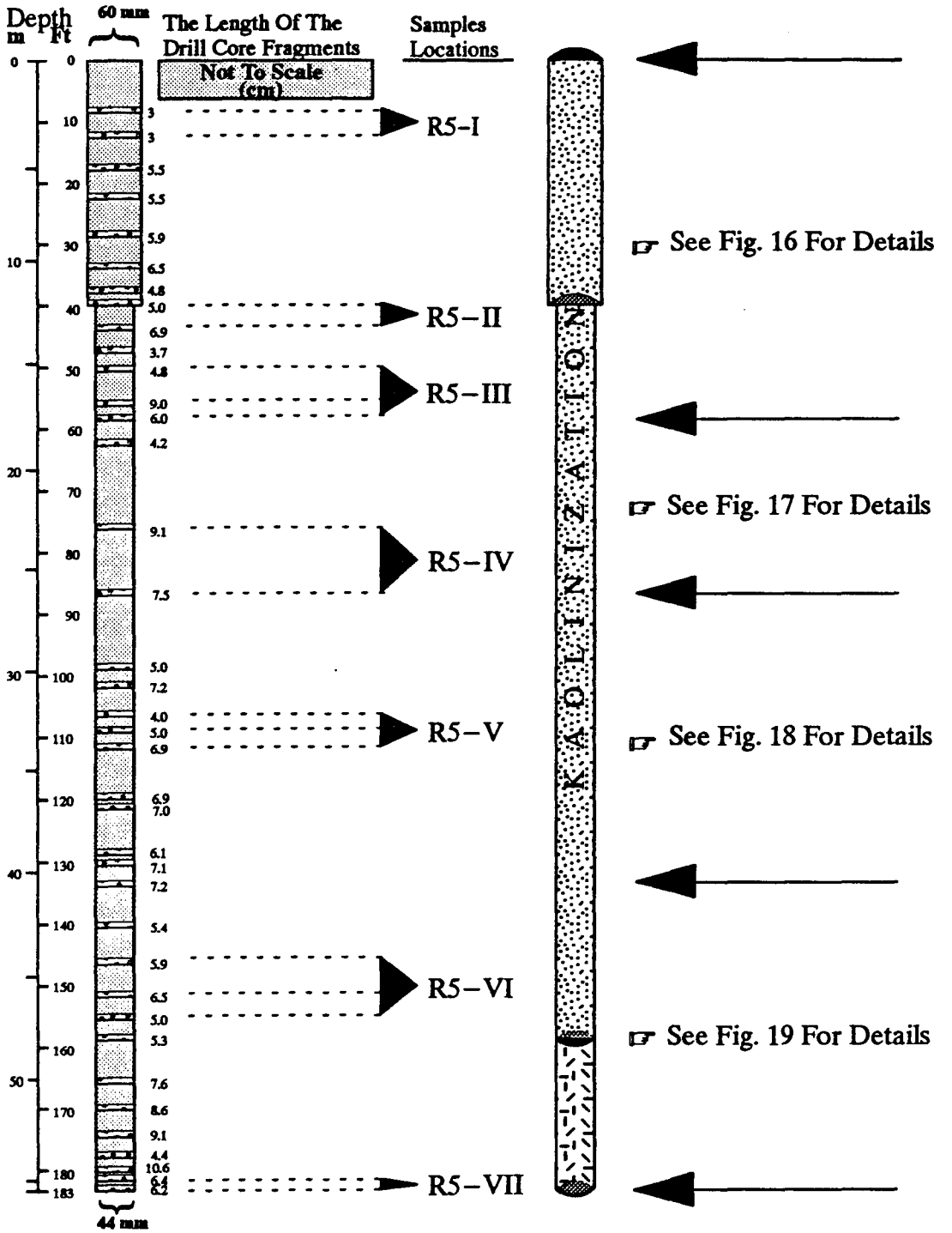

Figure 16: Schematic drill core showing depth, core fragments, samples locations, kaolinization depth, at different levels.

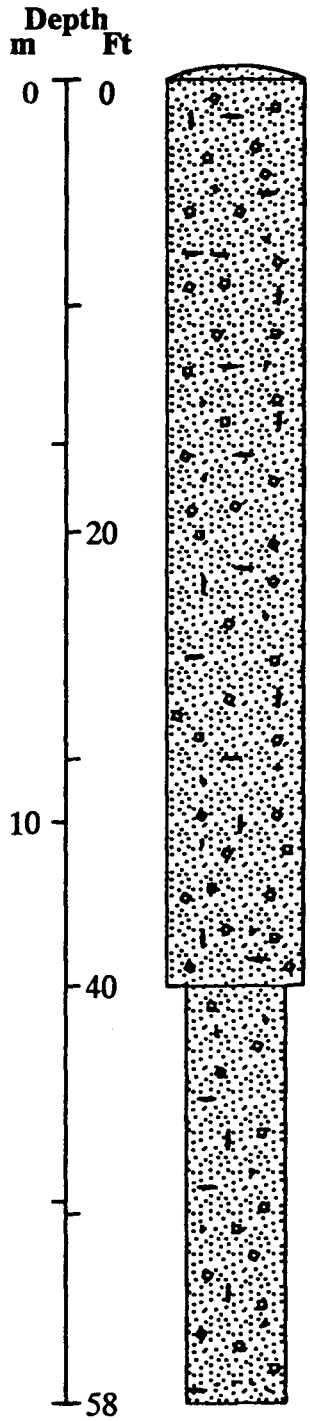

Description

The vertical lengths of the drill core fragments in this interval are between 3.5 and 10.6 cm. On the basis of these core fragments, this part of the tuff is completely altered; kaolinite being the most common mineral. The fragments of the core are as soft as chalk and are white with light yellowish stains. The hardness of the drill core fragments increases relatively with depth. However, all the core samples can be scratched easily with a fingernail. Kaolinite and disseminated quartz are the only two minerals that can be identified easily by the unaided eye. The quartz crystals range in size from 1.5 mm and smaller.

Figure 17: Schematic drill core and its description showing the physical properties of the interval surface to 58 ft (17.7 m) depth.

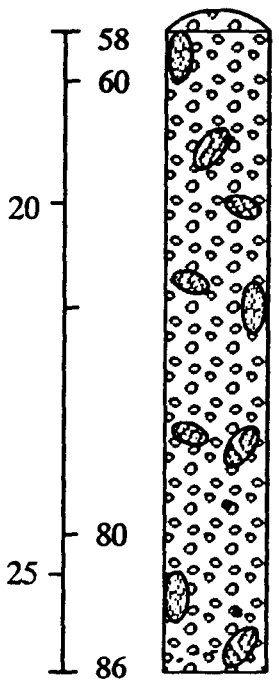

Description

Color of the core fragments is whitish pink with pumice imbedded in the matrix. All the core fragments are highly altered and in some places the volcanic fragments have been leached out, as evidenced by the voids (1.7 cm and smaller) in the core samples. The core fragments are soft and can be scratched with a fingernail. Pumice fragments, kaolinite, and disseminated quartz are the only minerals that can be seen by the unaided eye.

Figure 18: Schematic drill core and its description showing the physical properties of the interval from 58 ft (17.7 m) to 86 ft (26.2 m) depth.

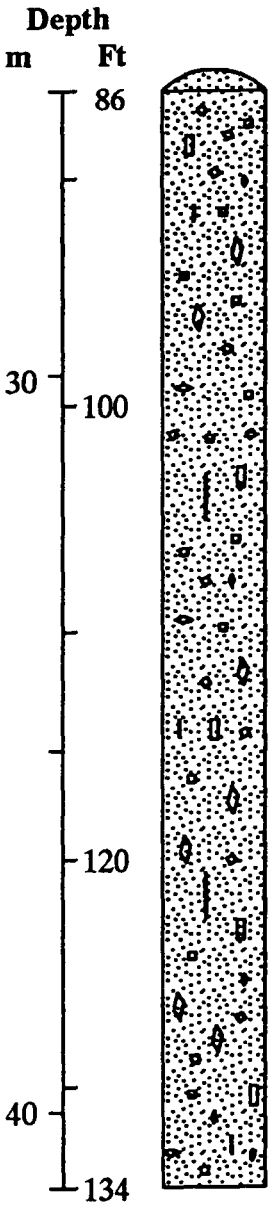

Description

This part of the drill core fragments displays about the same physical properties as the interval of 0–58 ft. However, relatively course grains of quartz are the only physical difference. These grains are mostly smaller than 1 mm in size but some of them are between 2 and 4 mm in size. In some places, pinkish color seems to be the physical appearance of alunite content. Toward the bottom of these core fragments, there are very fine disseminated brown volcanic fragments (in the size of 1 mm to 10 mm) within the matrix, which could be hematite. The core fragments can be scratched with a fingernail.

Figure 19: Schematic drill core and its description showing the physical properties of the interval from 86 ft (26.2 m) to 134 ft (40.8 m) depth.

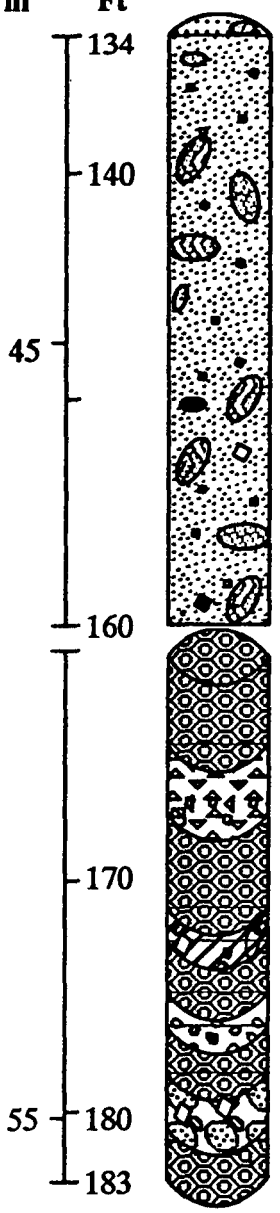

Description

This is the deepest interval of the kaolinization. Thus, the fragments are completely altered to kaolinite with the exception of some brownish pumiceous fragments, which carry possible hematitic stains. Kaolinite, quartz crystals, and pumice fragments (between 5 mm and 12 mm in size) can be identified with the unaided eye. The core fragments are relatively hard and can scarcely be scratched with a fingernail.

This interval of the drill core fragments has breccia type texture which carries reddish silicified fragments that are relatively least altered. However, the matrix contains kaolinite in some places. At the bottom of this interval, three core fragments are relatively fresh from their alteration points of view, as evidenced by a hexagonal quartz crystal which is located in next to the other silica carrying alteration rim. Most silica fragments (quartz ?) are opaque, but some look transparent. The size of the fragments ranges from 2 mm to 41 mm.

Figure 20: Schematic drill cores and their descriptions showing the physical properties of the interval from 134 ft (40.8 m) to 183 ft (55.8 m) depth.

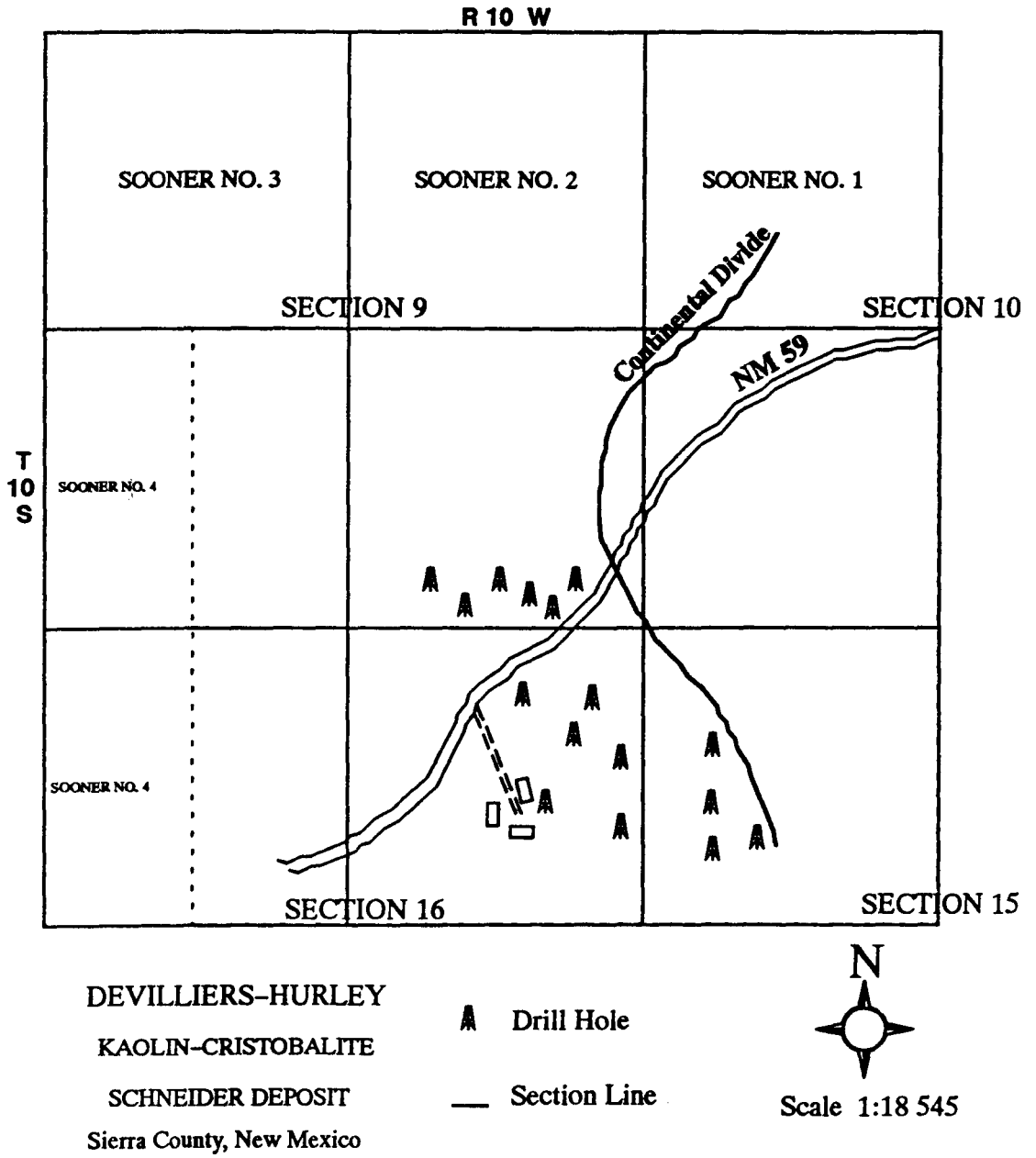

Figure 21: Claim map showing drill core locations. Depicted from the map furnished by Mr. P. Roche. Further detail of this area can be found in Appendix 3.

In this part of the alteration, the rhyolitic tuff of Kline Mountain has suffered complete alteration of the original minerals and textures. Eggleston (1987) believed that this may be related to as yet unrecognized faults. The shallow intrusive could be another explanation to the high intensity of the hydrothermal alteration (Plate 3). The resulting alteration mineral assemblages may best be described, from north to south, as a kaolinization zone with alunite to alunitization zone with kaolinite. Near NM 59, no pure kaolinite is observed, as postulated by Eggleston (1987).

In the advanced argillic alteration assemblage adjacent to the Kline Mountain intrusive, alunite inevitably contaminates the kaolin deposit, as shown by XRD graphs (Figures 48 and 49) and calculated mineral compositions (Table 3). Based on the calculated average mineral composition within the 48 m kaolinization zone of the drill core (Figure 16 and Table 27), kaolinite and alunite proportions increase with depth; on the other hand, the silica proportion decreases with depth, indicating possible proximity and/or shallow depth of the Kline Mountain Rhyolite Porphyry that may have caused these changes.

3.4. Silicification

Silicification is considerable in the study area, and is primarily restricted to three localities within the tuff of Kline Mountain and Kline Mountain Rhyolite Porphyry. They are (Plates 1, 2 and 3): (1) silicified tuffs at the top of the Kline Mountain tuff, (2) chalcedonic quartz within the kaolin deposit, and (3) widespread silicification at the top of the rhyolite porphyry of Kline Mountain. In the study area, silicification mainly occurs as fine-grained replacement of groundmass and matrix (Figures 10 and 11), as evidenced by relict quartz

phenocrysts within the silicification zones. The hydrothermal alteration may have occurred while the intrusive was cooling, possibly due to fumarolic processes. Condensation of fumarole gasses may provide both acids to attack the rhyolite and produce clay minerals as well as silica for replacement of the volcanic lavas and tuffs. The most silicified rocks in the area are white to light gray.

As stated above, the silica proportion decreases with depth at least in the one core studied indicating possible proximity to the rhyolite porphyry of Kline Mountain. However, silica may have been also supplied by the kaolinization of feldspars as shown on the following equation:

$$2KAlSi_3O_8 + 2H^+ + H_2O \Rightarrow 2K^+ + Al_2Si_2O_5(OH)_4 + 4SiO_2$$

(Orthoclase or sanidine) (Kaolinite) (Silica)

This kaolinization remnant silica are believed to have accompanied silicification either in the silica cap (Figure 10) or as chalcedonic relicts within the kaolin deposit (Figure 11) or both.

The hydrothermal activity was responsible for the silicification as well as kaolinization in the study area. It lasted intermittently for a long period of time, probably millions of years. Thus, it appears that silicification in the study area was formed as a result of precipitation from cooling waters supersaturated with dissolved SiO_2, as evidenced by colloform and botryoidal habits of chalcedonic silica in the SEM images (Figure 10 and 79), and also as a result of a strong acidic environment that altered volcanic units (pumice and rhyolite) to kaolinite and alunite by liberating SiO_2, as seen in the above equation.

Some of the silicified unit (sinters) readily break down into fragments when the deposits become desiccated due to shifting hydrothermal activity and exposure to weathering. Depending on the weathering environment, the fragments may remain in place, or more commonly may be transported locally by wind or water, and occasionally become cemented by later hot-spring activity. A great amount of chalcedonic nodules and fragments are distributed to the north of the Strip Mine location (Figure 11) and are believed to be eroded silica fragments possibly from the top of the silica cap. As seen in Figure 11, these chalcedonic nodules and fragments developed a spongy porous texture indicating a possible ancient hot-spring vent, which implies paleo-hot spring fluid conduits.

Post depositional weathering may have affected the hydrothermal minerals in the deposit to some extent. However, the wide extent of the silica cap on the top of the deposit may have protected the deposit against the effects of post depositional weathering, since it is highly resistant to both chemical and physical erosion, as postulated by Browne (1992).

CHAPTER 4
CLAY MINERALS

Clays have been very important materials to the development of mankind since the beginning of recorded history. From the beginning, clays were used as raw materials for making pottery and construction material. Also, research into clays is finding new applications in developing industries. Today, the uses of clay are expanding. New applications are being used for clay in the storage of hazardous waste and aerospace industry. Even after thousands of years of technological advancement, mankind still relies upon clays.

Because aspects of clay mineralogy studies show differences with respect to disciplines, the definition of clay is somewhat a discipline dependent issue. Thus, clay still does not have a general definition. In geology, clay can be extremely fine (<2 μm) particle-size material or it can refer to one or more of the clay minerals. A civil engineer would interpret a clay as a material that has plasticity, while a materials engineer would define a clay as a material that hardens upon firing. One commonly referred to definition of clay is: "In general the term clay implies a natural, earthy, fine-grained material which develops plasticity when mixed with a limited amount of water" (Grim, 1968).

Clay minerals are the most abundant minerals at the surface of the earth. They usually do not occur as monomineralic deposits, but there are usually several kinds in any sample. When formed in place they represent a response to the geochemical and physical conditions under which they formed or altered. Clay minerals generally form within the five types of geological environment: weathering, sedimentation, burial, diagenetic, and hydrothermal

alteration (Velde, 1985). Of these, hydrothermal alteration is the most complicated and variable of the environments, often accompanied in nature by other mineral deposition.

The properties of clay minerals are directly or indirectly related to their unique mineralogical, chemical, and physical characteristics such as cation exchange capacity, interaction with water, interaction with organic compounds, plasticity, thixotropy (the tendency of a slip to gel on standing and become fluid when agitated), consolidation, emulsion, etc. (Moore and Reynolds, 1989). It is these properties that make them versatile materials for industry. Many of the properties of clays are dependent on the nature and amounts of various minerals in them, so that their identification and determination are of very great importance (Grimshaw, 1971).

Practical applications and understanding of clay minerals are vital in agriculture, engineering, and industry. In agriculture, the soil productivity is often a function of the kind and amount of clay minerals present, namely, cation exchange capacity which influences the nutrients exchanged or extracted from clay minerals. However, in engineering the study of the properties present in clay minerals is very important because without this information engineers can not predict how the material will perform. Roads, foundations, tunnels, and other structures have been built in many large cities which are built on expandable clay minerals. Presumably, information on clay mineralogy for engineers is vital to the reliability of construction projects. According to researchers, a growing engineering, industry, and societal concern is the isolation of radioactive wastes; commercial, medical, industrial, academic, and military procedures increasingly generate nuclear critical waste. Clay minerals are

highly significant in critical radioactive waste disposal for isolating and retaining because of their desirable high sorptivity, long-term structural stability, and very low permeability.

Clay and clay minerals are most widely used by industry in several ways, as principal raw material in ceramics and cement, as clarifiers in alcoholic beverages and cooking oil production, and as fillers in paper, pharmaceuticals, rubber, plastic, etc.

Clay minerals are classified fundamentally on the basis of the type of layer (1:1 and 2:1), layer charge, the cation content of octahedral sheet (dioctahedral or trioctahedral), and the type of interlayer material (Eslinger and Pevear, 1988). Most clay minerals are mica-like phyllosilicates, and have a crystal structure made up of sheeted tetrahedral and octahedral layers (Figures 22 and 23) which contain strong covalent bonds between ions within each sheet, and among sheets but weak bonding between adjacent two or three sheet layers. This crystal structure is a very stable one and accounts for the high relative abundance of clays and clay minerals. The weak bonding between layers permit good cleavage in clay minerals, and also allows clay minerals to adsorb metallic cations and organic substances on their surfaces.

As seen in Figure 22 and 23, the tetrahedral sheet consists of corner-linked tetrahedra with the dominant cation Si^{4+}, less commonly Al^{3+}, and rarely Fe^{3+}. The octahedral sheet is composed of edge-linked octahedra, each of which consists of oxygen and hydroxide ions around Al^{3+}, Mg^{2+}, Fe^{2+}, and Fe^{3+} cations. When aluminum cations are in the centers of the octahedra, only two-thirds of the octahedral centers are filled (dioctahedral or gibbsite-like, cation-to-anion ratio in the sheet is 1:3). When magnesium cations are in the centers, all the octahedra centers are filled (trioctahedral or brucite-like, the cation-to-anion ratio is 1:2).

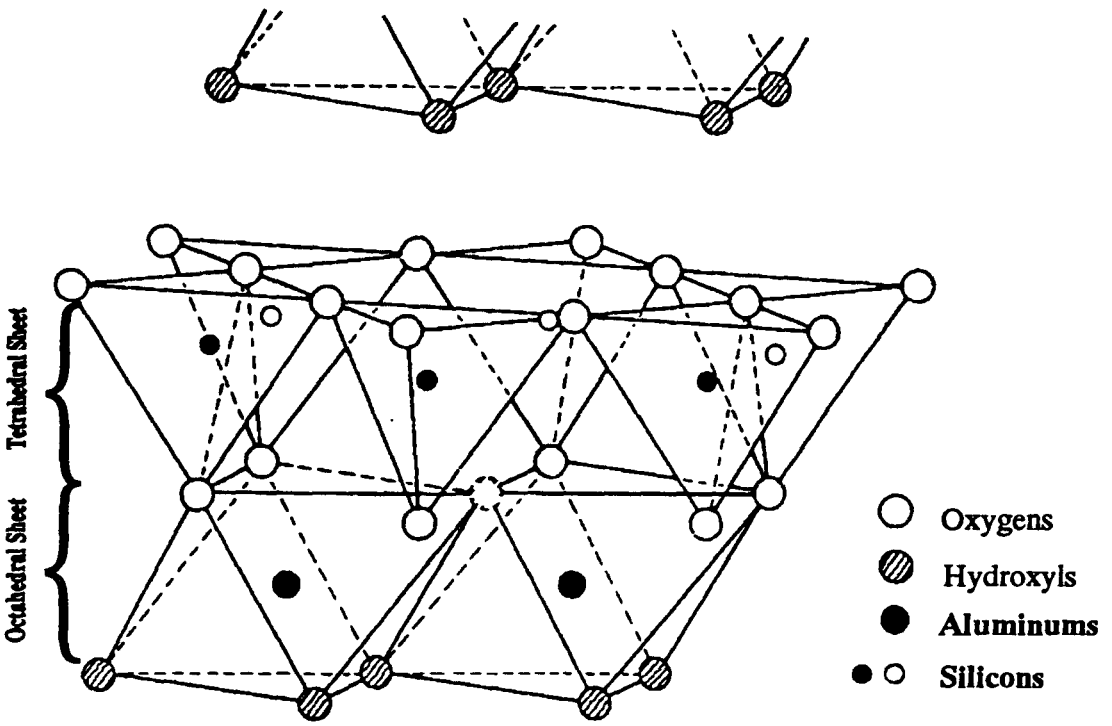

Figure 22: Diagrammatic sketch of kaolinite structure as an example of 1:1 layer type (Grim, 1968).

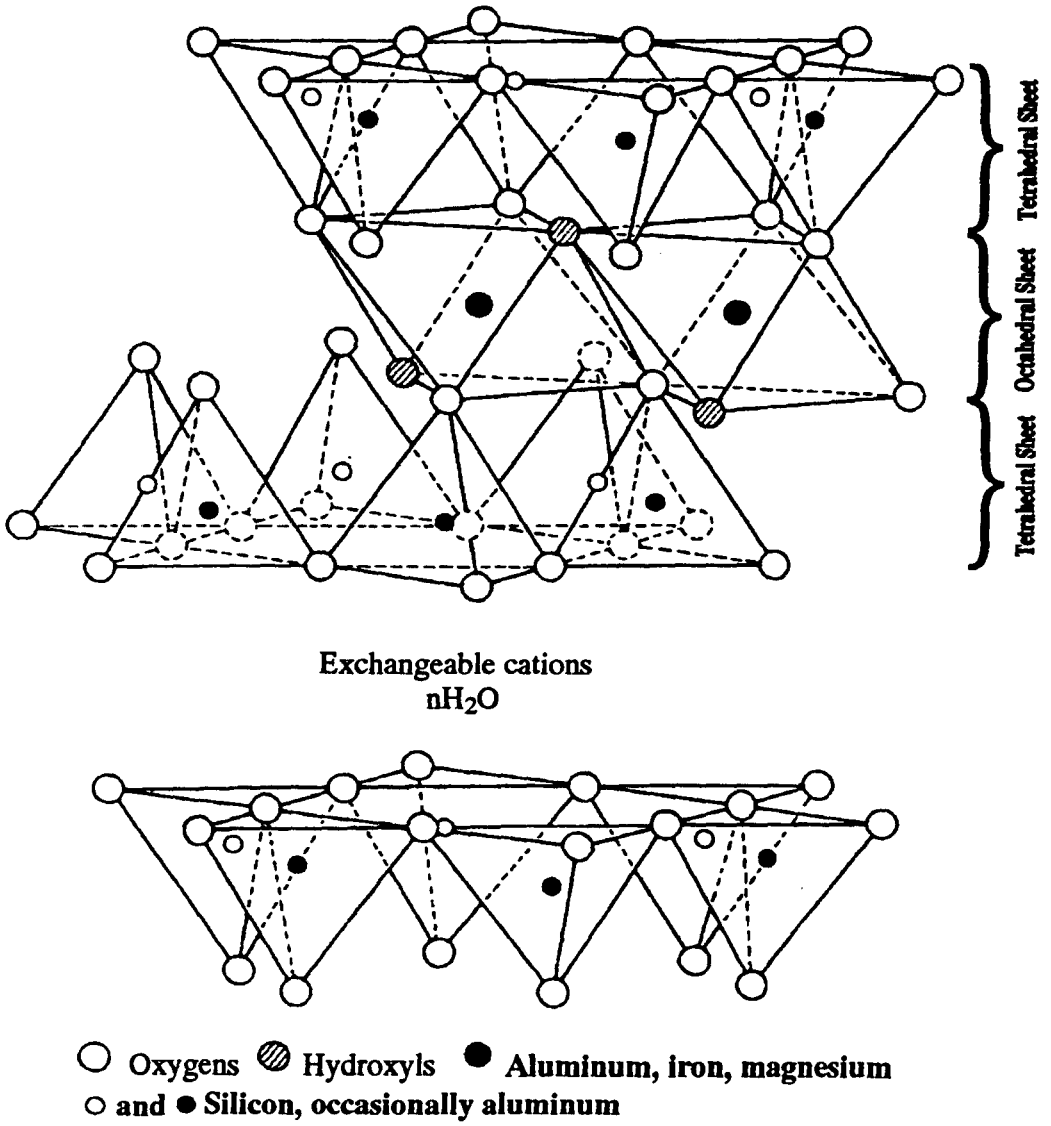

Figure 23: Diagrammatic sketch of montmorillonite structure as an example of 2:1 layer type (Grim, 1968).

Tetrahedral coordination can accommodate only the smaller cations whereas octahedral coordination accommodates the larger cations (Moore and Reynolds, 1989).

The simplest phyllosilicate clay mineral structure combines a single aluminum octahedral sheet and a single silica tetrahedral sheet to form a 1:1 layer (Figure 22). Another major layer type consists of two tetrahedral and one octahedral sheets which together form the 2:1 layer (Figure 23). The three layer can be either dioctahedral or trioctahedral.

Individual 1:1 or 2:1 layers (neglecting broken bonds on the edges) can be either neutral or bear a negative charge, balanced by the cations between the layers in the interlayer space. The layer charge is controlled by the substitution of cations in both sheets (Moore and Reynolds, 1989).

4.1. Kaolinite Group Minerals

Deposits of kaolin–containing clay are formed by geological processes that ranges widely in variety and complexity. Kaolinite, the chief constituent of kaolin, is always a secondary mineral formed by weathering or hydrothermal alteration of aluminum silicates, particularly feldspar. The mineralogical and chemical composition of the kaolin depends on the nature of the parent rock and the type and degree of alteration.

The mineral of this group consists 1:1 layer type lattice consisting of a tetrahedra layer linked to an octahedral layer (Figure 22). There is no ionic substitution in the kaolins and the unit does not expand with varying water content. The general formula for this group is $Al_2Si_2O_5(OH)_4$. The kaolinite group of minerals are kaolinite, dickite, nacrite, 7 A°–halloysite, and 10 A°–halloysite that has a layer of water about 2.9 A° thick between the 7 A°–lay-

ers, giving a 10 A°-spacing. The water can easily be driven off at 60 C° (Moore and Reynolds, 1989).

Kaolin is an important industrial raw material in world trade averaging $ 1.9 billion market value in 1987 (Roy Woodal, 1991, written communication). Historically, kaolin was first used in ceramics and this is perhaps still the best known application, although the total tonnage sold for this use is small compared with that marketed for paper, paint, and rubber manufacturing. Ballclays, fireclays, flintclays, and underclays, that are kaolinitic sedimentary clays with special characteristics, are the commercial clay names used primarily in ceramic and refractory industries (Moore and Reynolds, 1989). The largest user of kaolin by far with special specifications is the paper industry where it is utilized as a filler in the paper sheet and as a coating on the surface. Other important clay groups are illite, smectite, mixed layer, chlorite, vermiculate, and sepiolite-polygorskite.

4.2. Silica

Silica (SiO_2), tridymite, and cristobalite, are the primary non-phyllosilicate fine grain (clay size) minerals in hydrothermal clay deposits. Hydrothermal kaolin deposits are almost invariably accompanied by one or more of the silica minerals as formed by silica sinter and/or silica residue which commonly contains quartz, cristobalite, and tridymite.

Other constituents associated with kaolinite in the deposit are alunite and accessory minerals. Hematite and cassiterite (?) occur dominantly within the alunitic zone of the alteration, close to the Kline Mountain intrusion.

4.3. Alunite

Alunite is represented by the formula $KAl_3(OH)_6(SO_4)_2$. It is a secondary mineral formed under high Eh, low pH (<3) conditions (Long et al., 1992). It is often associated with acid-mine drainage, weathering of sulfide ore deposits, hydrothermal alteration, oxidation of pyrite, or weathering in acidic soils. Alunite forms during both hypogene and supergene processes (in the zone of acid-sulfate hydrothermal alteration). In low-temperature environments the formation of alunite has also been related to microbial oxidation of iron and sulfur (Long et al., 1992). These investigators postulated that the principal mechanism for the formation of alunite is thought to be by dissolution/re-precipitation reactions involving pyrite and aluminosilicates. In some cases, alunite precipitates after local migration (on the order of 1 m) of the constituents (i.e. K, Al, Fe, SO_4). According to the authors, long distance migration of the constituents prior to their precipitation as alunite has not been previously documented.

Alunite is frequently found in kaolin deposits together with kaolinite, silica silcretes and other minerals. This kaolinite-alunite close association was thought by King (1953) on the basis of chemical, petrographic, and X-ray data to indicate that kaolinite is an intermediate stage in derivation of alunite from feldspars. On the other hand, Meyer and Reis (1983) postulated alunite precipitation within silcrete as an impermeability and acid environment related formation.

CHAPTER 5
MINERALOGICAL ANALYSIS

A precondition for the success of any research connected with clay minerals is the correct identification of the clay mineral(s) present in the sample studied. Among the many instrumental methods X-ray diffraction (XRD), scanning electron microscopy (SEM), transmission electron microscopy (TEM), infrared spectroscopy, chemical methods, and differential thermal analysis (DTA) are used primarily for identifying and analyzing clay minerals. Of these, the X-ray diffraction method is principal identification method that has been used in making the greatest strides toward an understanding of the crystallographic mineralogy of clay minerals. Thus, it is of paramount importance for studying kaolin by XRD to identify and interpret its crystal structure (Keller, 1978).

The purpose of this mineralogy study is to examine the occurrence and distribution of kaolinite, together with other alteration mineral assemblages in the deposit, and to analyze the composition of the kaolin deposit. The result of this study will also assist in the calculated semiquantitative mineral composition and material application for making white brick. Altogether, they will be used to constrain the alteration mineral paragenesis as well as the geochemical conditions of mineralization.

5.1. Sampling Procedure

This study has utilized drill core fragments as shown in Figure 16, which were provided by G. S. Austin. Surface sampling was conducted during the time of the geological field mapping in the summer of 1992. Three sampling techniques were employed: (1) sur-

face samples (about 1 kg each) were collected at intervals along an approximately north to south direction to observe mineralogical composition changes with respect to the intrusive body, (2) detail surface sampling in and around the two abandoned open pit sites close to NM 59 (Plate 2), and (3) about 200 kg representative samples from each abandoned open pit (SM 200–from the open pit and CS 200–from the prospect on the Continental Divide). These samples were secured to run experimental analyses in addition to XRD, SEM, particle size, and bulk chemical analyses. Plates 1 and 2 show the sample locations utilized in this study, with the exception of the exact drill core location which is estimated to be between the two pits in the study area as shown in Figure 21.

5.2. Methods of Investigation

Whole–rock major element chemical analyses of the samples were done by X–ray fluorescence method (XRF) at New Mexico Bureau of Mines and Mineral Resources under the supervision of Christopher G. McKee. The semiquantitative mineral compositions were calculated on the basis of the chemical analyses, as explained in Appendix 1.

A total of seven drill core samples and eighteen surface samples were examined by XRD analysis for bulk and clay–size mineral identification, random and oriented mounted, at the Department of Metallurgy of New Mexico Tech and the Department of Metallurgy at UTEP. Powdered whole–rock samples (–100 mesh in size) were scanned from 5° to 65° 2θ, using Cu K_α radiation and a Norelco diffractometer with scanning speed of 2° 2θ/min. Oriented, <2 μm–size fractions of these samples were sedimented on glass slides as outlined in Appendix 2. Half of the samples were then examined using a Norelco diffractometer at New

Mexico Tech with Cu K_α radiation at 40 kV and 40 mA. The other half of the samples were examined using a Scintag Inc., USA–XDS 200 XRD unit at the Department of Metallurgy at UTEP with Cu K_α radiation at 40 kV and 25 mA. They were scanned from 5° to 35° 2θ, using a vertical goniometer, and graphite crystal monochromator.

Several techniques can be used to prepare specimens for SEM viewing. In this study, the sample preparation procedure was to break off with a small hammer, a fragment of the specimen so as to expose a clean, natural, freshly fractured surface. It is simply the same process as is used to break the rock from the outcrop. After fracturing and blowing away any dust, the surface was coated with a very thin conducting layer of gold to carry away excess charge from the electron beam. By this procedure, the natural break is preserved without introduction of an artifact by grinding, polishing, chemical etching or other processing.

Texture of a rock or mineral is one property commonly used to identify the material and/or to estimate its quality for industrial utilization. To observe the texture of clays requires high magnification, commonly 1,000X to 10,000X (even though higher or lower magnifications also may be used). Thus, SEM magnification was employed for the visual observation of clay texture of different samples as well as single crystals or particles. The qualitative energy–dispersive X–ray analysis (EDS) of the SEM was used to identify some crystal and particles by their atomic and weight percent ratios and was completed by a dual stage scanning electron microscope, ISI–DS130, at the Department of Metallurgy at UTEP under the supervision of Dennis Joseph Manuel, SEM technician.

5.3. Results

5.3.1. Chemical Analysis

Tables 1 and 2 show the bulk chemical major element analyses of the drill core and outcrop samples, respectively. Minor to major chemical differences and conceivably mineralogical differences are seen in the samples from the tuff of Kline Mountain, depending on the locality from which the sample was collected with respect to the rhyolitic intrusion as well as depth in the drill core samples. In the kaolinitic clay, SiO_2 shows an inverse relationship with Al_2O_3 in both Tables. In the alunitic samples (Tkm 18 and 20), SiO_2 has the lowest percentage, while Al_2O_3 and loss on ignition (LOI) are in the highest percentages. In these samples K_2O is the highest. Alunite content can be easily seen by high K_2O, LOI and low SiO_2 percentages. Also, the ratio K_2O+LOI:SiO_2 is very low in the kaolin clays (i.e. R5–II and Tkm 8) and is high in the alunite samples (Tkm 18 and 20).

Based on the chemical analyses, the mineral compositions of each sample were calculated (Table 3) as explained in Appendix 1. The detected mineral percentages are coincident with XRD data. Minerals are calculated under four categories: kaolinite, alunite, silica, and accessory minerals. Silica should be taken account of as quartz, tridymite, opal, and cristobalite. The amount of each mineral is reported as a weight percentage.

As seen in Table 3 and Figure 24, variations in the proportions of minerals was found with respect to depth of the drill core. Within the kaolinization zone, the kaolinite proportion is between 30.97 % and 58.20 %. However, this percentage drops drastically down to 5.27 %, with an 72.63 % of silica in the breccia zone (Sample R5–VII), indicating the limit of

economically viable kaolin deposits at 158 ft (48 m) depth. The kaolinization zone of the drill core samples and two representative 200 kg pit samples (SM 200 and CS 200) have about the same mineral distribution in surface samples (Table 4 and 5), suggesting that the drill core location is between these two pits as previously stated.

Table 1: Chemical analysis of the drill core samples of the tuff of Kline Mountain[1] (see Figure 21 for estimated location).

	R5–I	R5–II	R5–III	R5–IV	R5–V	R5–VI	R5–VII
SiO_2	68.51	65.43	47.65	69.29	47.32	54.73	74.69
Al_2O_3	17.90	24.66	25.72	17.26	25.08	24.22	8.29
Fe_2O_3	0.02	0.00	0.00	0.04	0.30	0.23	1.44
MnO	0.04	0.03	0.03	0.03	0.03	0.04	0.04
MgO	0.20	0.13	0.04	0.09	0.44	0.28	0.00
CaO	0.11	0.15	0.08	0.18	0.11	0.12	0.02
Na_2O	0.00	0.00	0.00	0.00	0.00	0.00	0.00
K_2O	1.69	0.35	3.61	1.25	3.69	2.54	1.91
TiO_2	0.15	0.10	0.21	0.22	0.17	0.14	0.29
P_2O_5	0.11	0.16	0.10	0.09	0.10	0.09	0.08
%–LOI	12.52	11.22	22.20	12.22	21.52	17.87	12.71
TOTAL	101.25	102.23	99.64	100.67	98.76	100.26	99.47

[1] The chemical analyses in Table 1 and 2 were performed by XRF method at New Mexico Bureau of Mines and Mineral Resources, Socorro, New Mexico, on March 11, 1993, (File: SYO:LAB93B.MJD and Generator Settings: 35 kV and 75 mA).

Table 2: Chemical analysis of the outcrop samples of the tuff of Kline Mountain (see Plate 1 and 2 for locations).

	SM200	CS200	Tkm1	Tkm2	Tkm3	2Tkm2	2Tkm4	2Tkm5	3Tkm1	3Tkm3	3Tkm5	Tkm8
SiO_2	69.38	62.55	93.92	68.68	41.26	69.99	67.53	56.04	42.67	73.18	80.99	72.17
Al_2O_3	15.13	17.91	0.57	19.93	22.65	14.29	17.82	21.77	18.42	16.22	11.70	17.92
Fe_2O_3	0.04	0.17	0.03	0.02	0.00	0.33	1.23	0.04	0.10	0.04	1.11	0.63
MnO	0.04	0.04	0.05	0.04	0.04	0.04	0.06	0.04	0.03	0.05	0.05	0.05
MgO	0.19	0.07	0.03	1.19	0.02	0.00	0.07	0.00	0.00	0.50	0.10	0.03
CaO	0.09	0.11	0.10	0.20	0.03	0.11	0.11	0.09	0.06	0.09	0.08	0.12
Na_2O	0.00	0.08	0.00	0.00	0.00	0.00	0.00	0.00	0.00	0.00	0.00	0.00
K_2O	1.43	1.50	0.11	0.76	6.03	2.22	0.32	2.98	5.23	0.11	0.11	0.09
TiO_2	0.14	0.18	0.32	0.14	0.07	0.22	0.37	0.22	0.16	0.21	0.19	0.24
P_2O_5	0.08	0.11	0.08	0.16	0.09	0.07	0.09	0.10	0.08	0.07	0.05	0.07
%–LOI	12.54	15.75	4.87	11.37	27.83	15.32	11.86	18.77	27.16	10.43	7.45	8.63
TOTAL	99.06	98.47	100.08	102.49	98.02	102.59	99.46	100.05	93.91	100.90	101.83	99.95

Table 2: (continued)

	S7	S7.5	S8	Tkm 18	Tkm 20
SiO_2	77.03	69.00	61.74	15.72	32.54
Al_2O_3	11.73	9.70	13.09	29.27	24.83
Fe_2O_3	0.00	0.00	0.05	0.82	0.09
MnO	0.04	0.04	0.04	0.02	0.03
MgO	0.14	0.02	0.22	0.11	0.02
CaO	0.11	0.08	0.04	0.04	0.02
Na_2O	0.00	0.00	0.37	0.09	0.00
K_2O	1.26	3.08	3.85	7.73	6.97
TiO_2	0.12	0.36	0.11	1.24	0.21
P_2O_5	0.06	0.06	0.06	0.17	0.11
%–LOI	11.76	15.77	19.07	36.77	28.79
TOTAL	102.25	98.11	98.64	91.98	93.61

Table 3: Calculated mineral composition of the samples (see Appendix 1 for calculation method).

SAMPLE	KAOLINITE (%)	ALUNITE (%)	SILICA[1] (%)	ACCESSORIES (%)	TOTAL (%)
R5–I	30.97	14.70	53.25	0.62	99.54
R5–II	58.20	3.01	36.94	0.56	98.71
R5–III	35.46	31.94	31.33	0.46	99.16
R5–IV	33.14	10.94	53.41	0.65	98.14
R5–V	33.47	32.91	32.34	1.16	99.88
R5–VI	40.23	22.31	35.88	0.90	99.32
R5–VII	5.27	16.91	72.63	1.88	96.69
SM 200	26.73	12.72	57.60	0.59	97.64
CS 200	33.47	13.41	47.95	0.77	95.6
Tkm 1	0.53	0.97	93.60	0.61	95.71
Tkm 2	43.09	6.53	46.97	1.71	98.30
Tkm 3	7.79	54.19	38.47	0.26	100.71
2Tkm 2	17.43	19.06	57.71	0.75	94.95
2Tkm 4	42.67	2.83	48.05	1.94	95.49
2Tkm 5	30.51	26.24	41.82	0.49	99.06
3Tkm 1	3.72	49.06	43.71	0.46	96.95
3Tkm 3	39.76	0.96	54.03	0.95	95.70
3Tkm 5	28.16	0.95	66.43	1.55	97.09
Tkm 8	44.62	0.79	51.45	1.14	98.00
S7	18.88	10.86	66.55	0.46	96.75
S7.5	0.00	27.65	70.33	0.57	98.55
S8	1.44	34.38	61.92	0.90	98.64
Tkm 18	11.31	74.03	11.83	2.71	99.88
Tkm 20	5.78	65.59	32.07	0.51	103.95

[1] Quartz, tridymite, cristobalite, and opal.

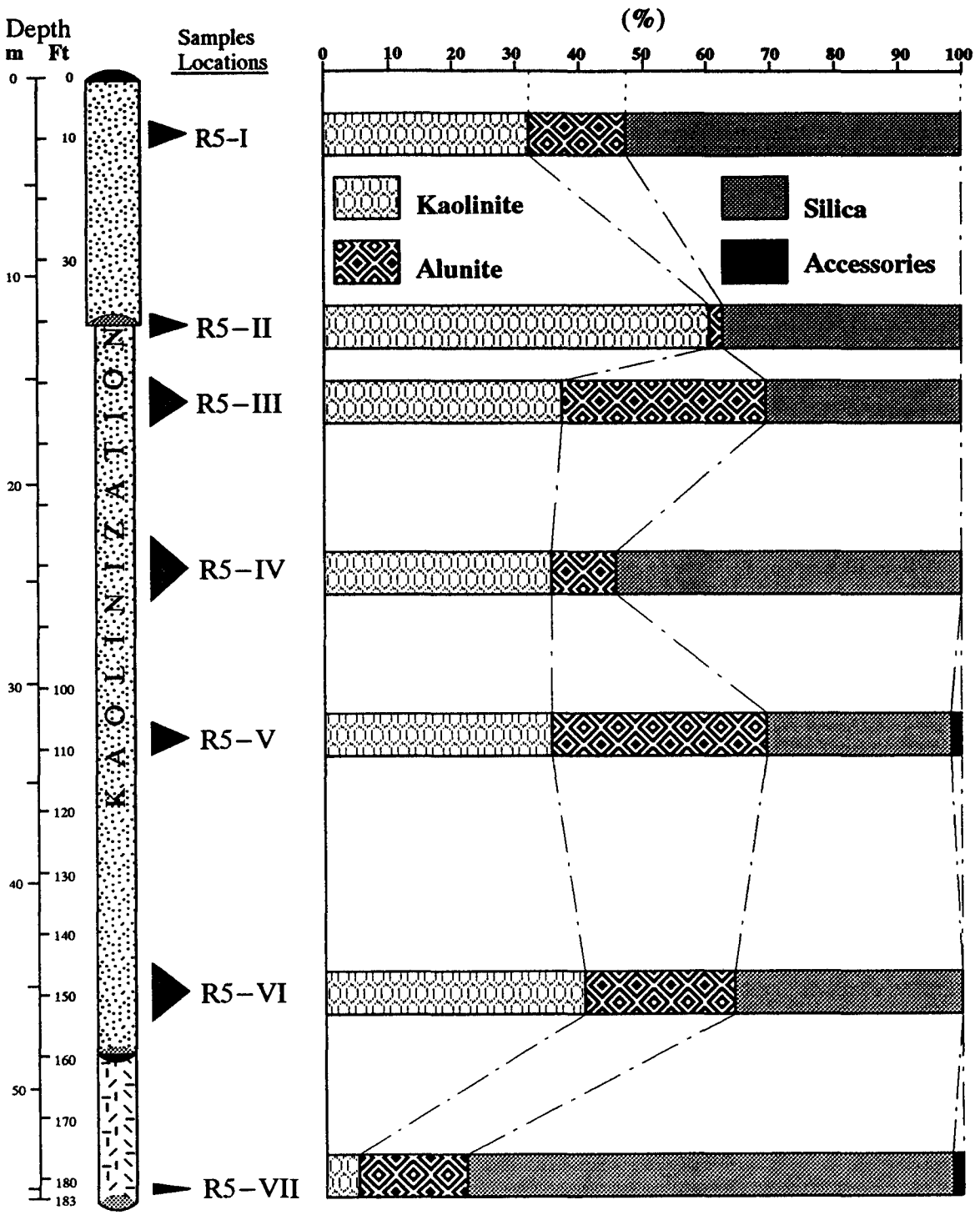

Figure 24: Kaolinization zone and mineral distribution in drill core R5.

Semiquantitative calculated mineral composition of outcrop samples from chemical analysis (Table 3) shows an inverse relationship between kaolinite percentage and proximity to the intrusion, as seen in Figure 25. Conversely, it displays a proportional relationship between alunite content (%) and the proximity of the intrusion. As previously stated, this evidence also suggests that around the intrusion the advanced argillic alteration zone contains dominantly alunite, while in the pits, which are further away from the intrusive contact, but still within the advanced argillic alteration zone, kaolinite predominates.

5.3.2. X-Ray Diffractogram Analysis

On the basis of individual minerals identical d-spacing (A°) and their corresponding relative peak intensity, clay mineral groups are identified from X-ray diffractogram patterns according to the criteria of Brindley and Brown (1980). Figures 26 through 49 show the whole-rock mineralogy of the Kline Mountain, first seven of which belong to drill core samples. The whole-rock minerals, both drill core and surface, are listed in Table 4. As seen in Table 4, most of the tuff is composed of kaolinite, alunite, tridymite, quartz, cristobalite, and accessory minerals. The clay-size minerals (<2μm) of the tuff of Kline Mountain are listed in Table 5, in order of decreasing abundance. Figures 50 through 71 display the mineralogy of the clay-size particles X-ray diffractograms. Kaolinite is present in both size fractions of each sample, as indicated by the reflections from 7.15 A° and 3.57 A°, the identical d-spacings. However, alunite dominant samples (Tkm 18 and Tkm 20) in both sizes show weak, small peaks of kaolinite reflection that would indicate very minor kaolinite content. Cristobalite is detected only in the bulk sample of Tkm 1 as a major constituent. Tridymite is

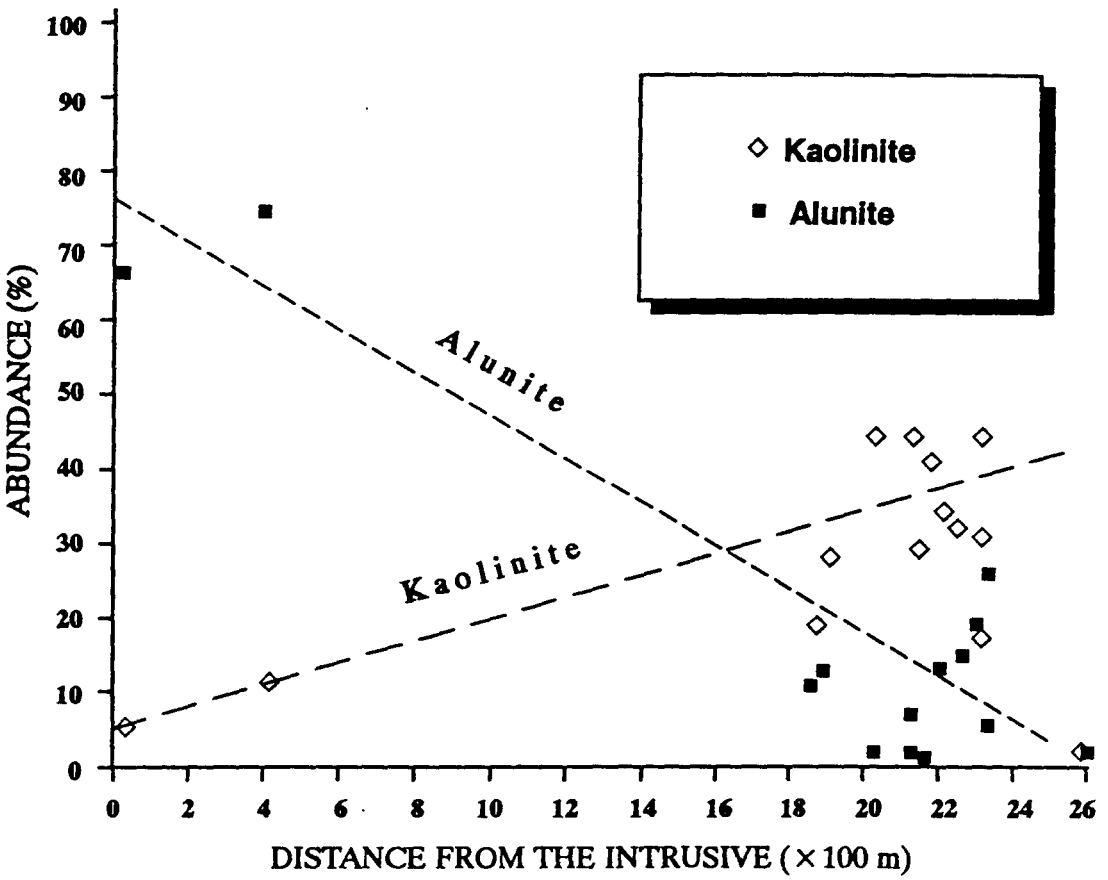

Figure 25: Graph showing kaolinite and alunite abundance in surface samples relative to the distance from the Kline Mountain intrusion.

present in each sample at different intensities except for alunitic tuff, Tkm 20.

Kaolinite is the most common clay mineral detected in <2μm samples. However, smectite was identified in two samples as the second clay mineral present due to the increasing amount of this clay mineral in clay-size fractions. The presence of smectite in the two clay-size oriented fractions is based on the appearance of a high background level in the 7.40° 2Θ, which was only observed on the R5-III (drill core) and SM 200 (outcrop sample) XRD patterns. It was not detected in any other samples. No change in ordering of XRD patterns of the glycolated and heated samples were observed in the preliminary study of deposit, indicating no significant amount of expandable clay minerals (Isik, 1990). The kaolinite is well-crystallized as evidenced by the sharp 001 and 002 reflections (Figures 51 and 58).

XRD data indicates that the mineralogy of the clay-size fractions is different from that of the drill core. The mineralogical difference among the different size fractions within given samples show that quartz is concentrated in the coarse fractions (>2 μm) as seen in Tables 4 and 5. In the < 2 μm fraction, kaolinite predominates with ten exceptions and quartz is absent with five exceptions (Table 5). In the drill core samples, kaolinite is the chief mineral followed by alunite and tridymite. However, alunite is the chief mineral followed by kaolinite in the drill core sample of R5-VII, which is the deepest core sample obtained.

In the SEM studies of these samples, no halloysite image is detected, as inferred in the preliminary study on the basis of an X-ray diffractogram.

Table 4: Kline Mountain mineralogy showing distribution of the minerals in the samples detected by X-ray diffraction (m: minor constituent).

Sample	Kaolinite	Alunite	Tridymite	Quartz	Cristobalite
R5-I	X	X	X	X	
R5-II	X	m	X	X	
R5-III	X	X	X	X	
R5-IV	X	X	X	X	
R5-V	X	X	X	X	
R5-VI	X	X	X	X	
R5-VII	m	X	X	X	
SM 200	X	X	X	m	
CS 200	X	X	X	m	
Tkm 1			X		X
Tkm 2	X	m	X		
Tkm 3	m	X	X	m	
2Tkm 2	X	X	X	X	
2Tkm 4	X	m	X	X	
2Tkm 5	X	X	X	X	
3Tkm 1	m	X	X		
3Tkm 3	X		X	X	
3Tkm 5	X		X	X	
Tkm 8	X		X	X	
S7	X	X	X	m	
S7.5		X	X	X	
S8	m	X	X	m	
Tkm 18	m	X	X		
Tkm 20	m	X		X	

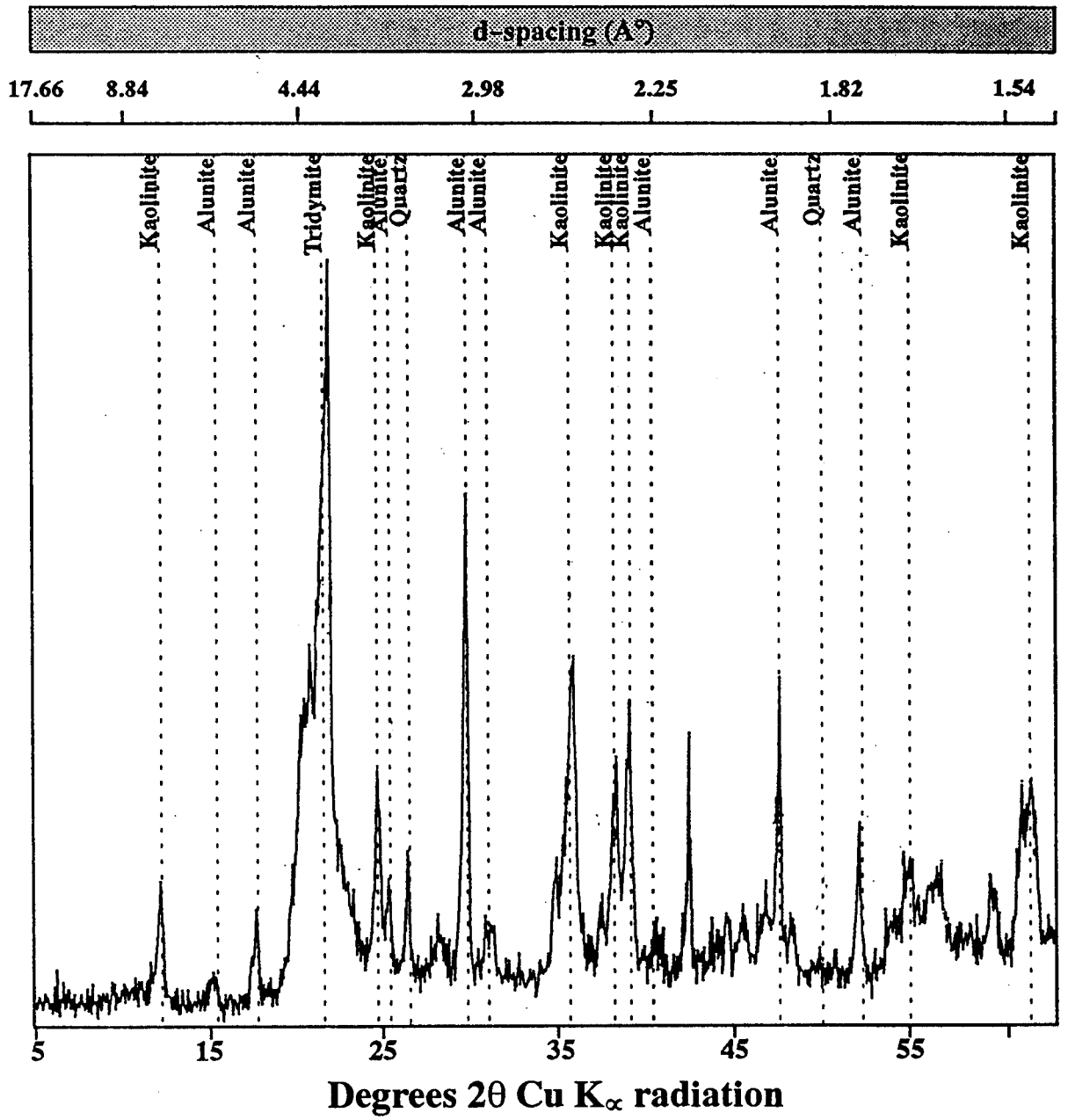

Figure 26: X-ray diffractogram of unoriented >2μm fraction showing the minerals in sample R5-I of the Kline Mountain kaolin deposit.

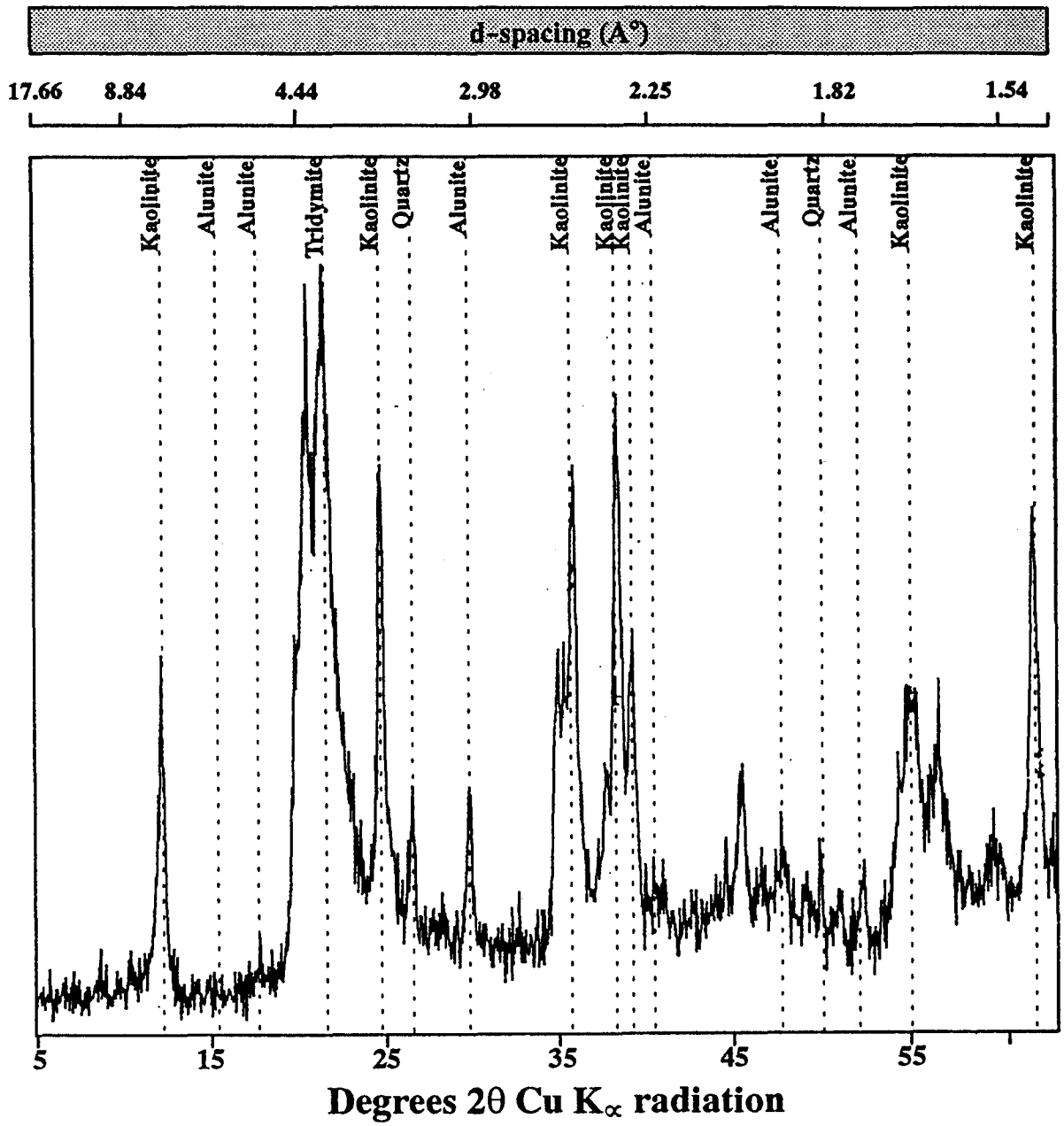

Figure 27: X-ray diffractogram of unoriented >2μm fraction showing the minerals in sample R5-II of the Kline Mountain kaolin deposit.

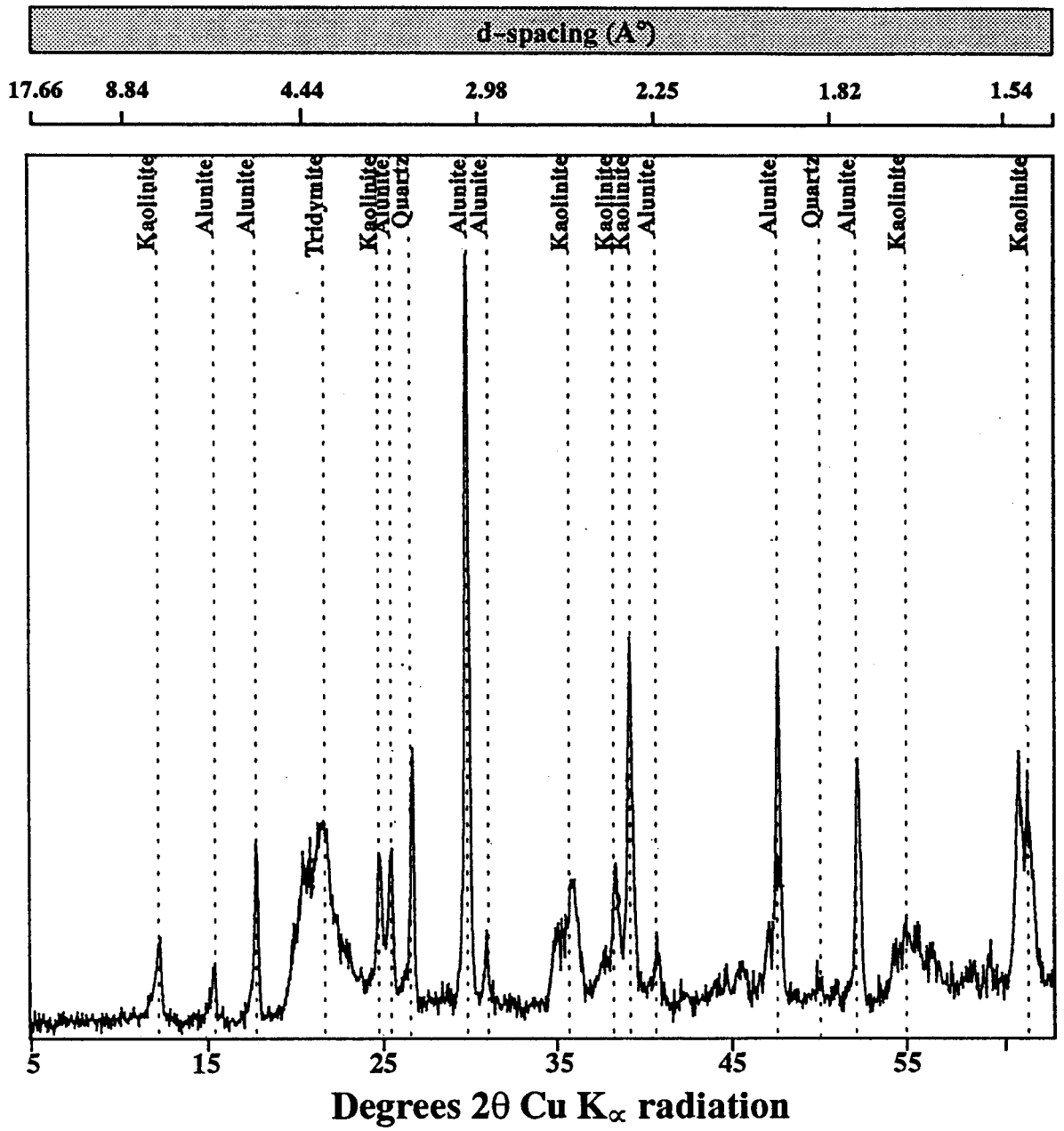

Figure 28: X-ray diffractogram of unoriented >2μm fraction showing the minerals in sample R5-III of the Kline Mountain kaolin deposit.

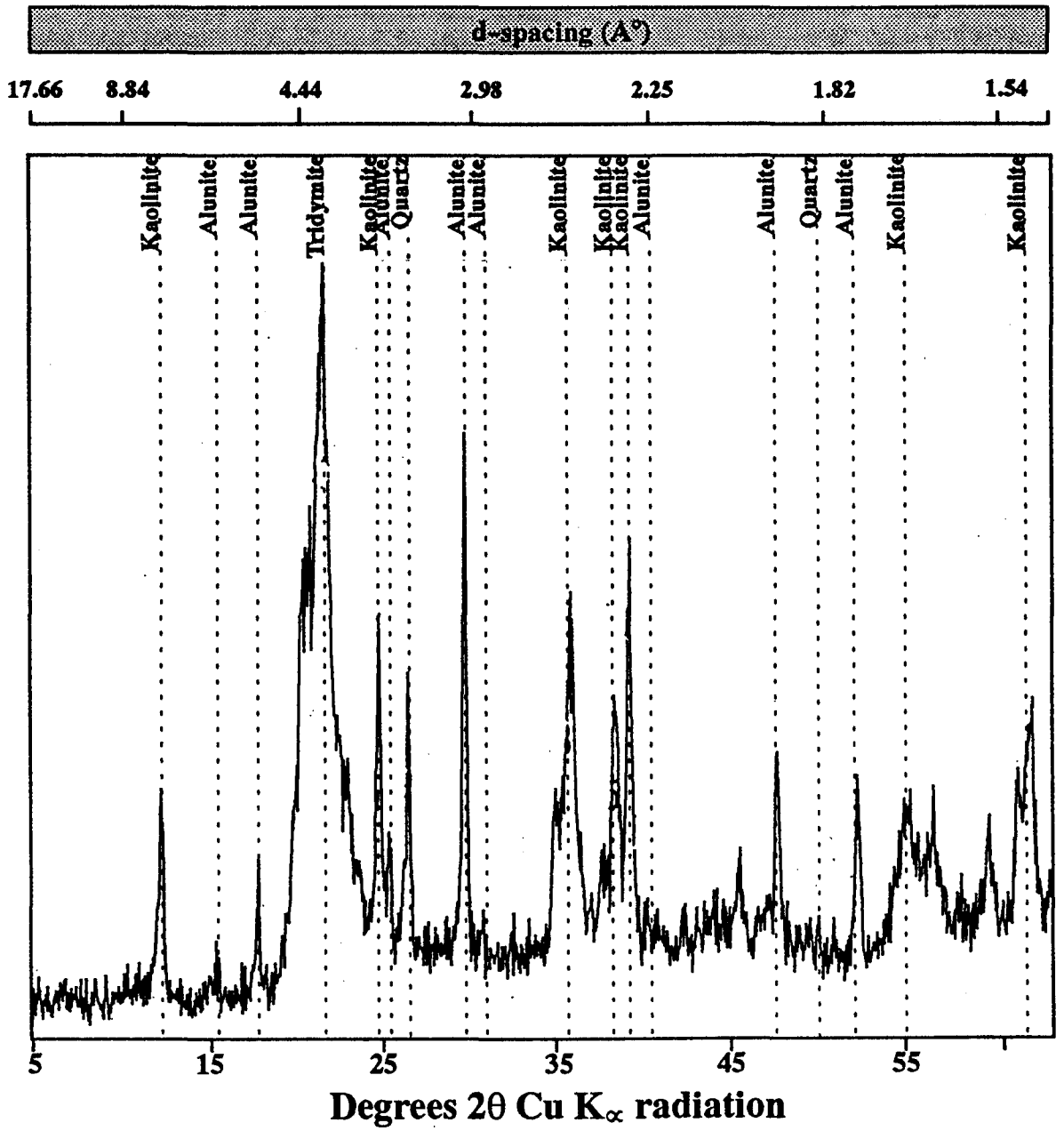

Figure 29: X-ray diffractogram of unoriented >2μm fraction showing the minerals in sample R5-IV of the Kline Mountain kaolin deposit.

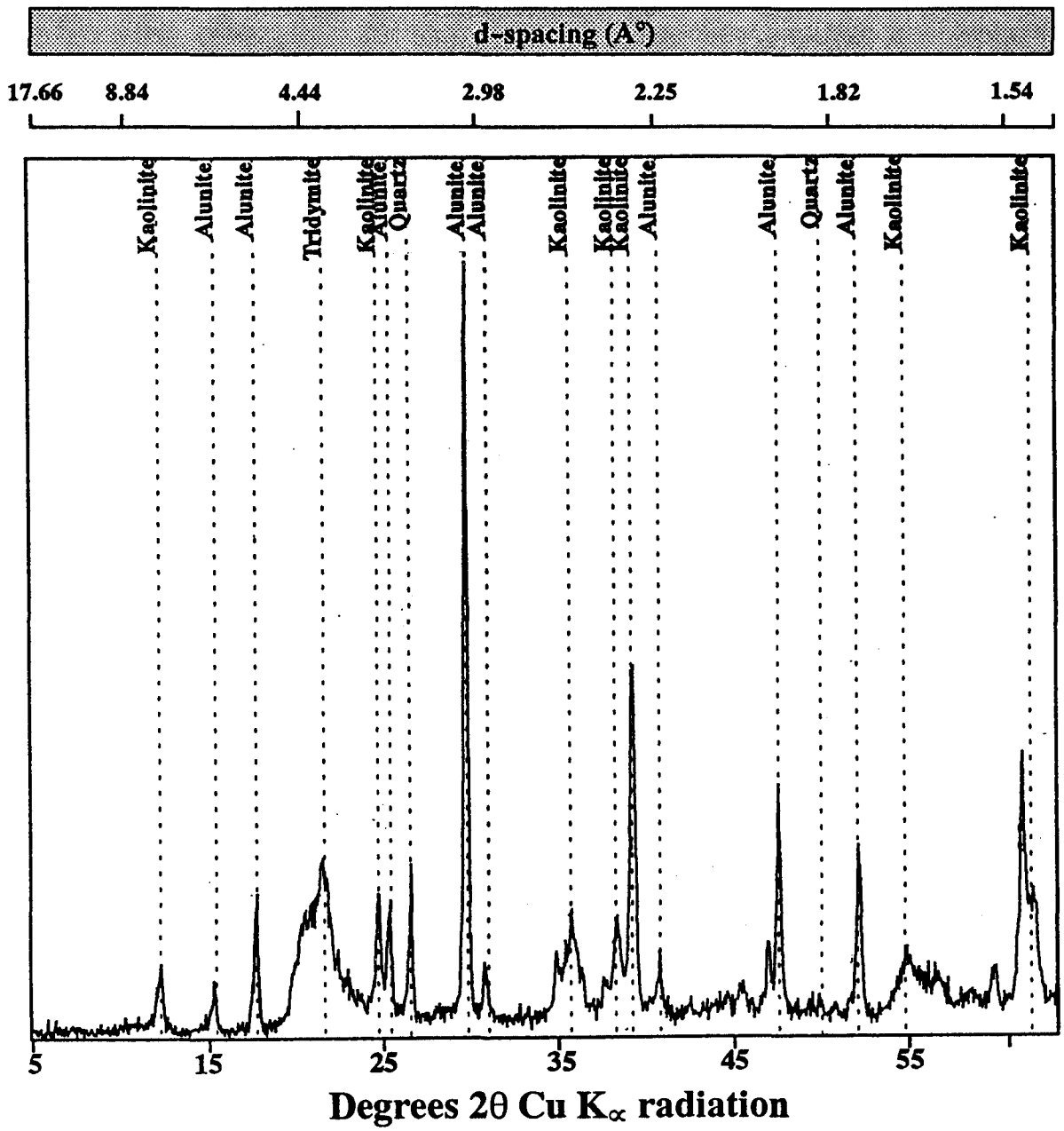

Figure 30: X-ray diffractogram of unoriented >2μm fraction showing the minerals in sample R5-V of the Kline Mountain kaolin deposit.

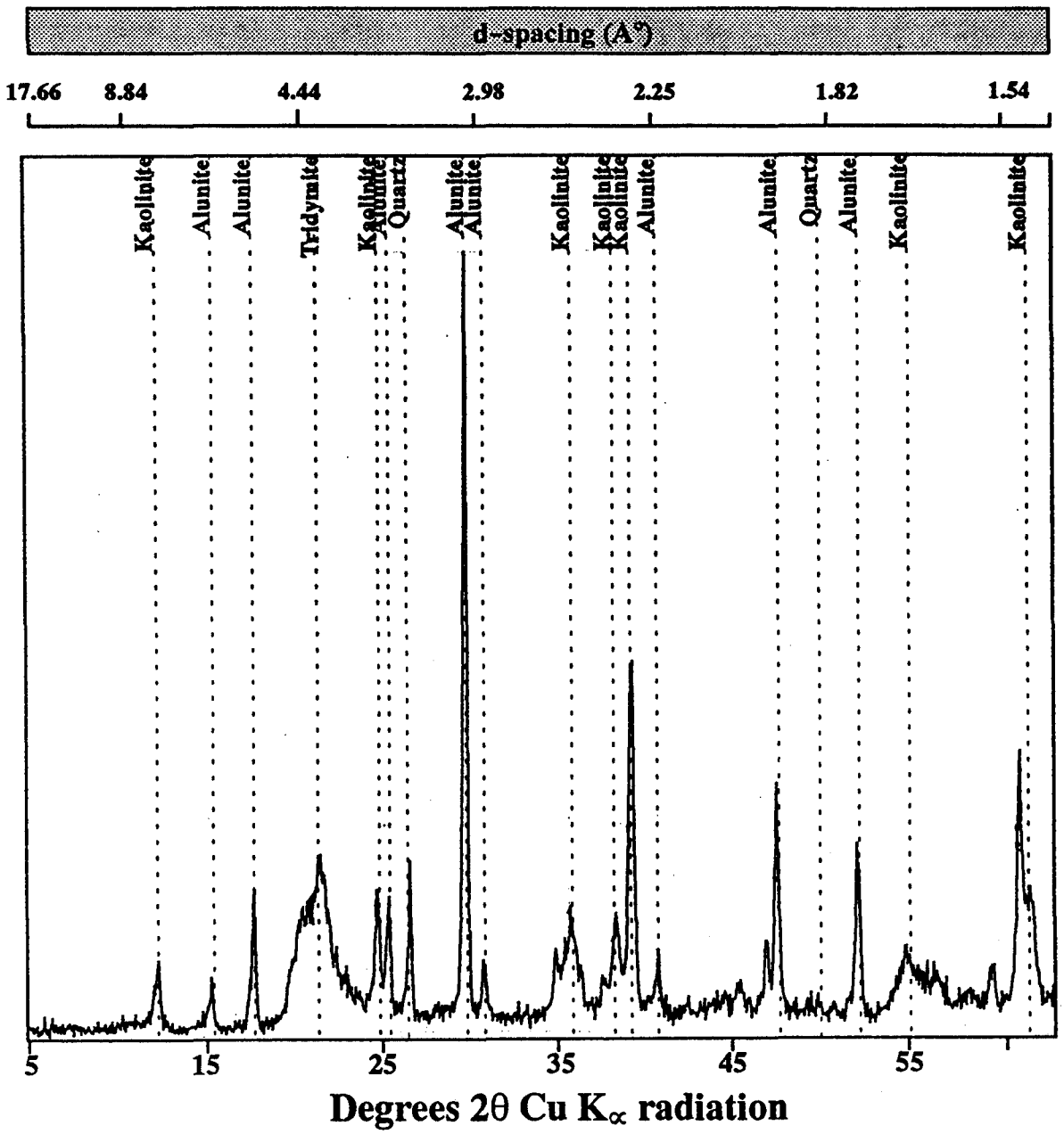

Figure 31: X-ray diffractogram of unoriented >2μm fraction showing the minerals in sample R5-VI of the Kline Mountain kaolin deposit.

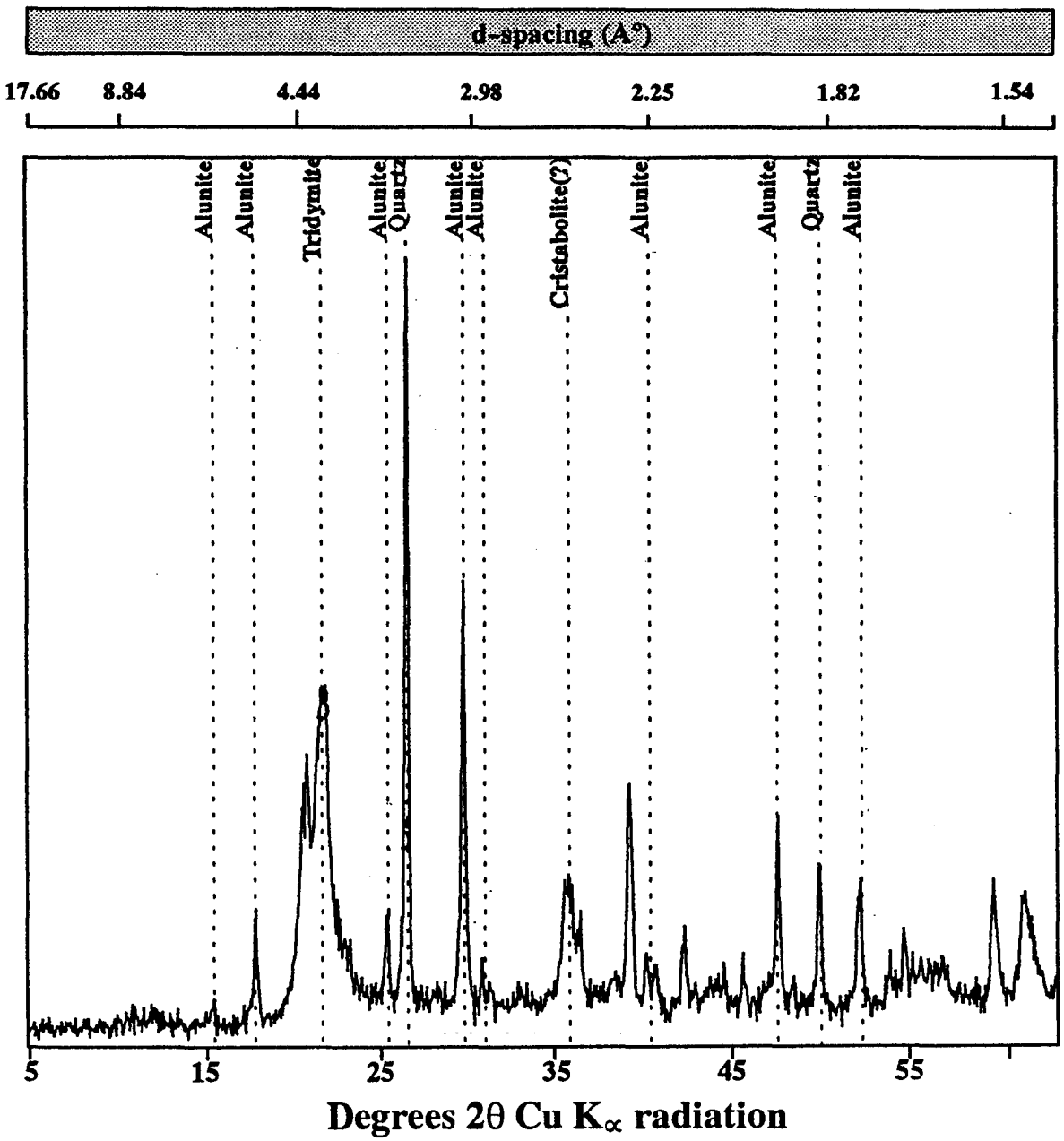

Figure 32: X-ray diffractogram of unoriented >2μm fraction showing the minerals in sample R5-VII of the Kline Mountain kaolin deposit.

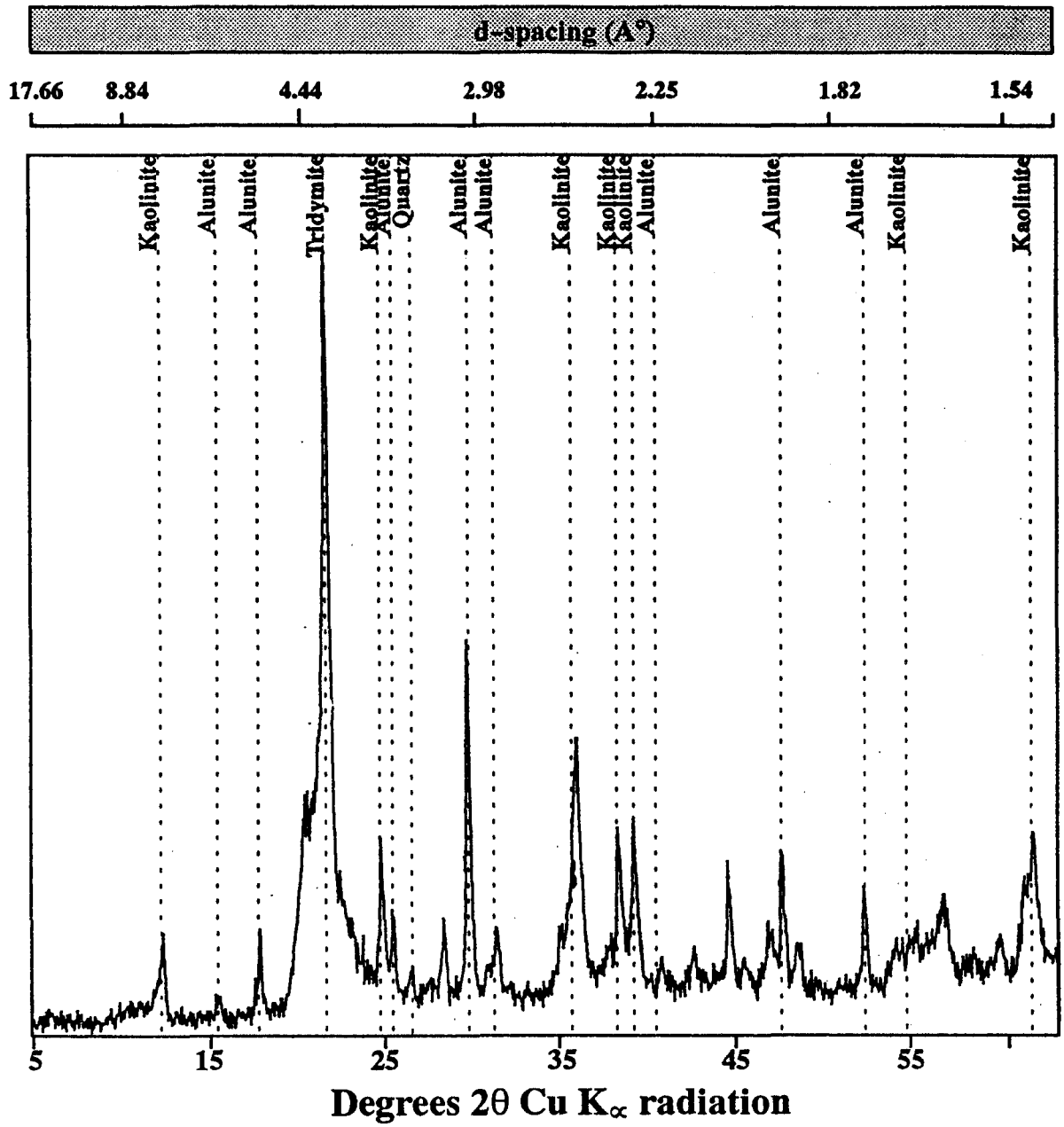

Figure 33: X-ray diffractogram of unoriented >2μm fraction showing the minerals in sample SM 200 of the Kline Mountain kaolin deposit.

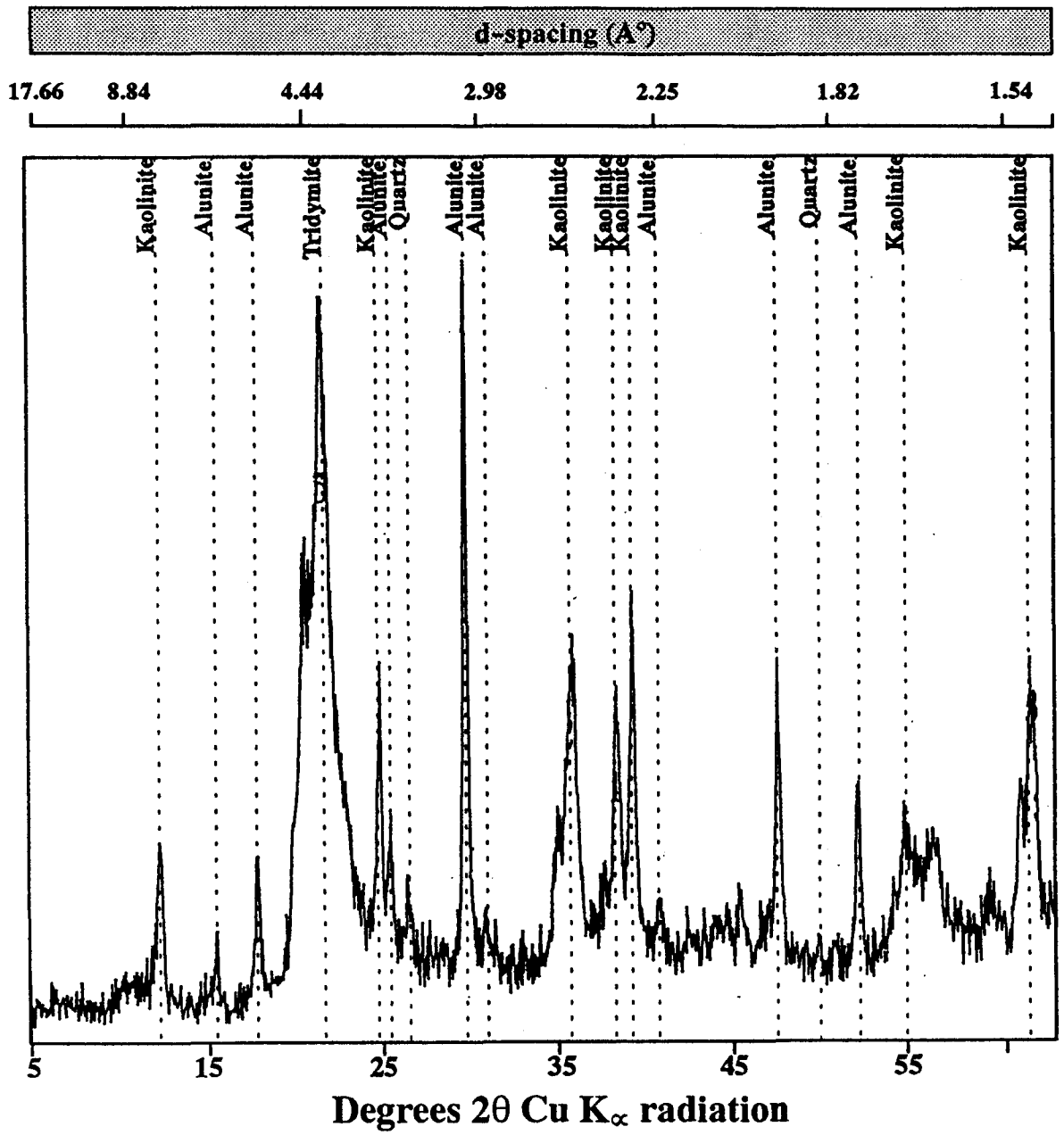

Figure 34: X-ray diffractogram of unoriented >2μm fraction showing the minerals in sample CS 200 of the Kline Mountain kaolin deposit.

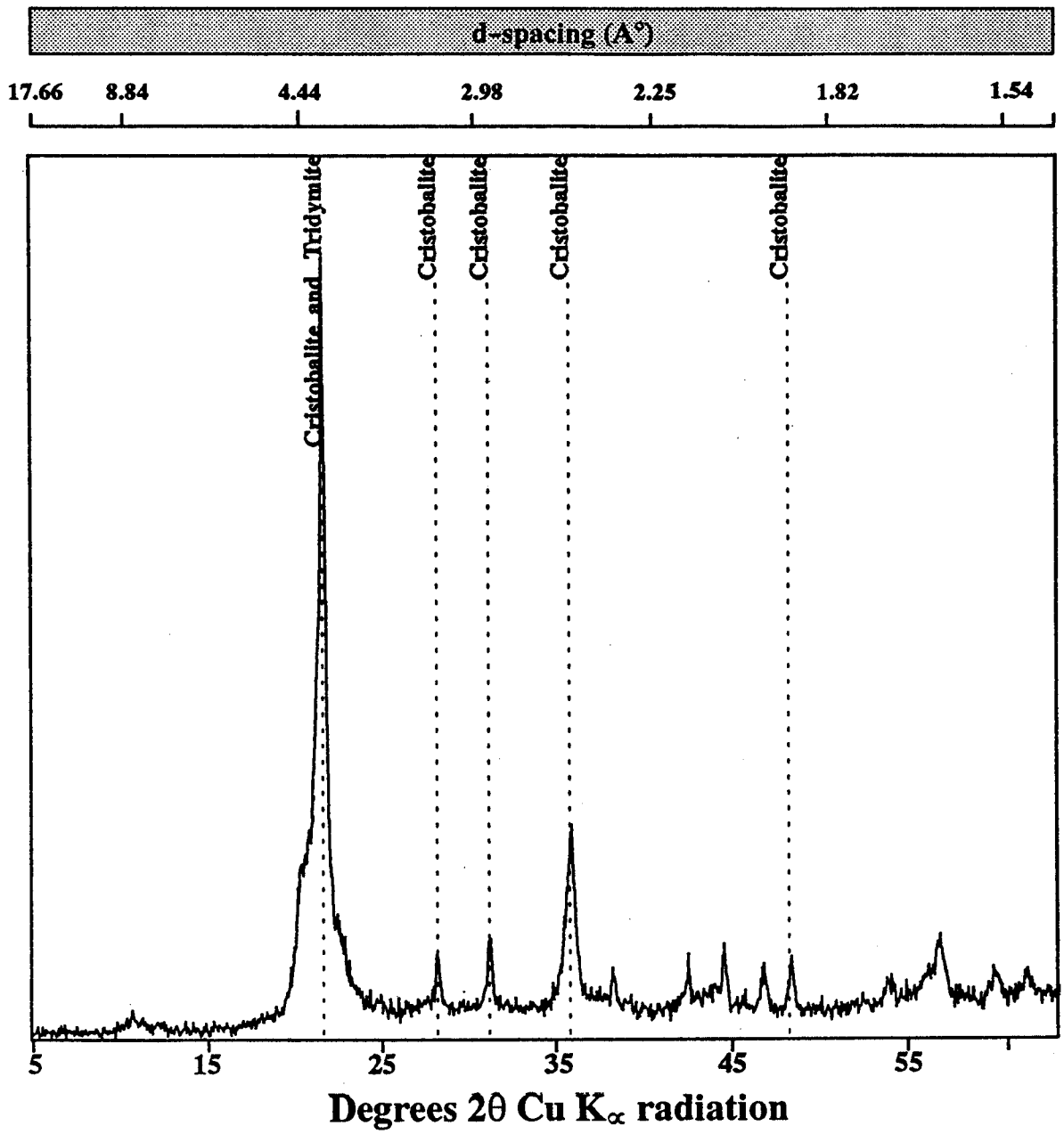

Figure 35: X-ray diffractogram of unoriented >2μm fraction showing the minerals in sample Tkm 1 of the Kline Mountain kaolin deposit.

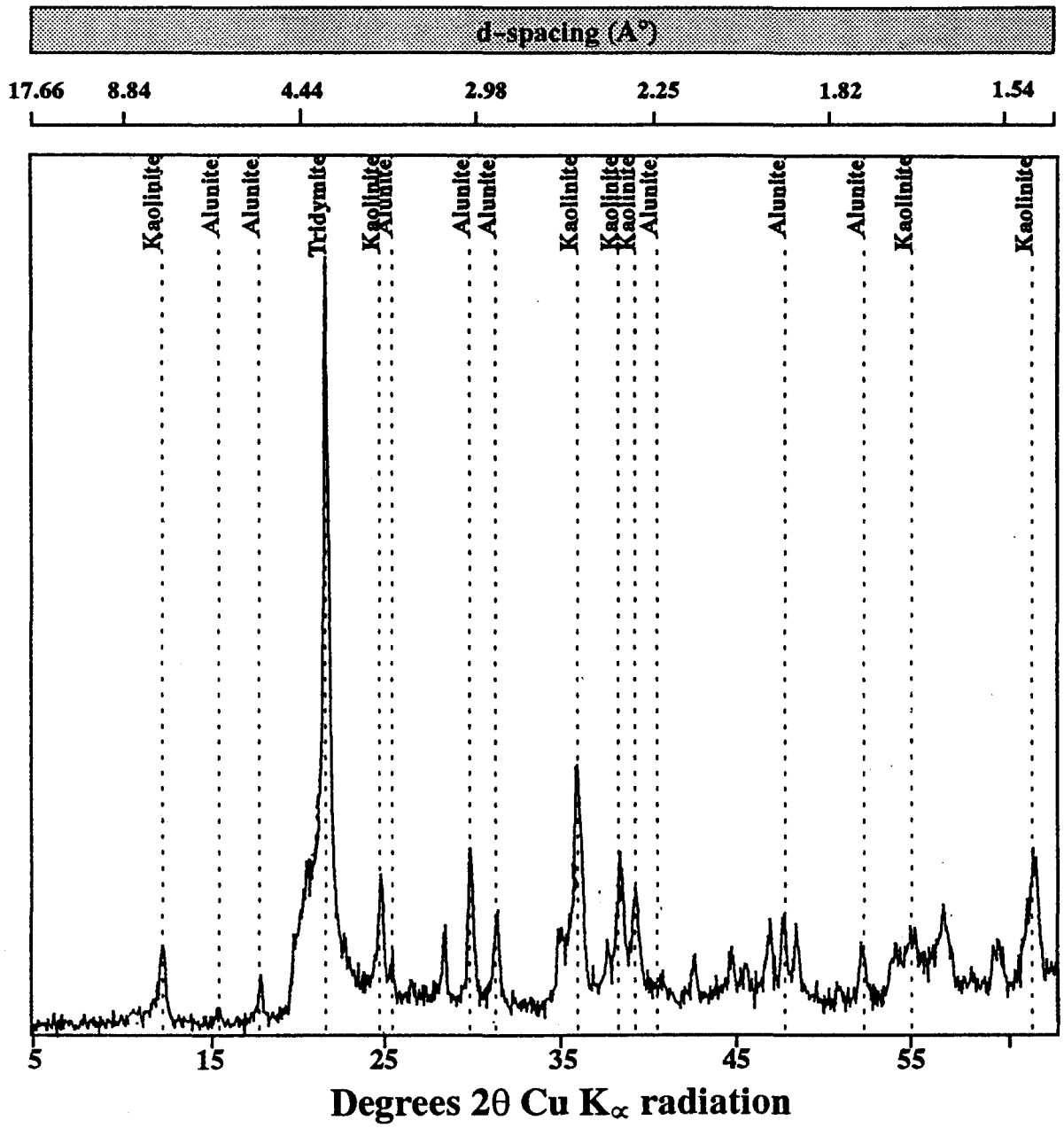

Figure 36: X-ray diffractogram of unoriented >2μm fraction showing the minerals in sample Tkm 2 of the Kline Mountain kaolin deposit.

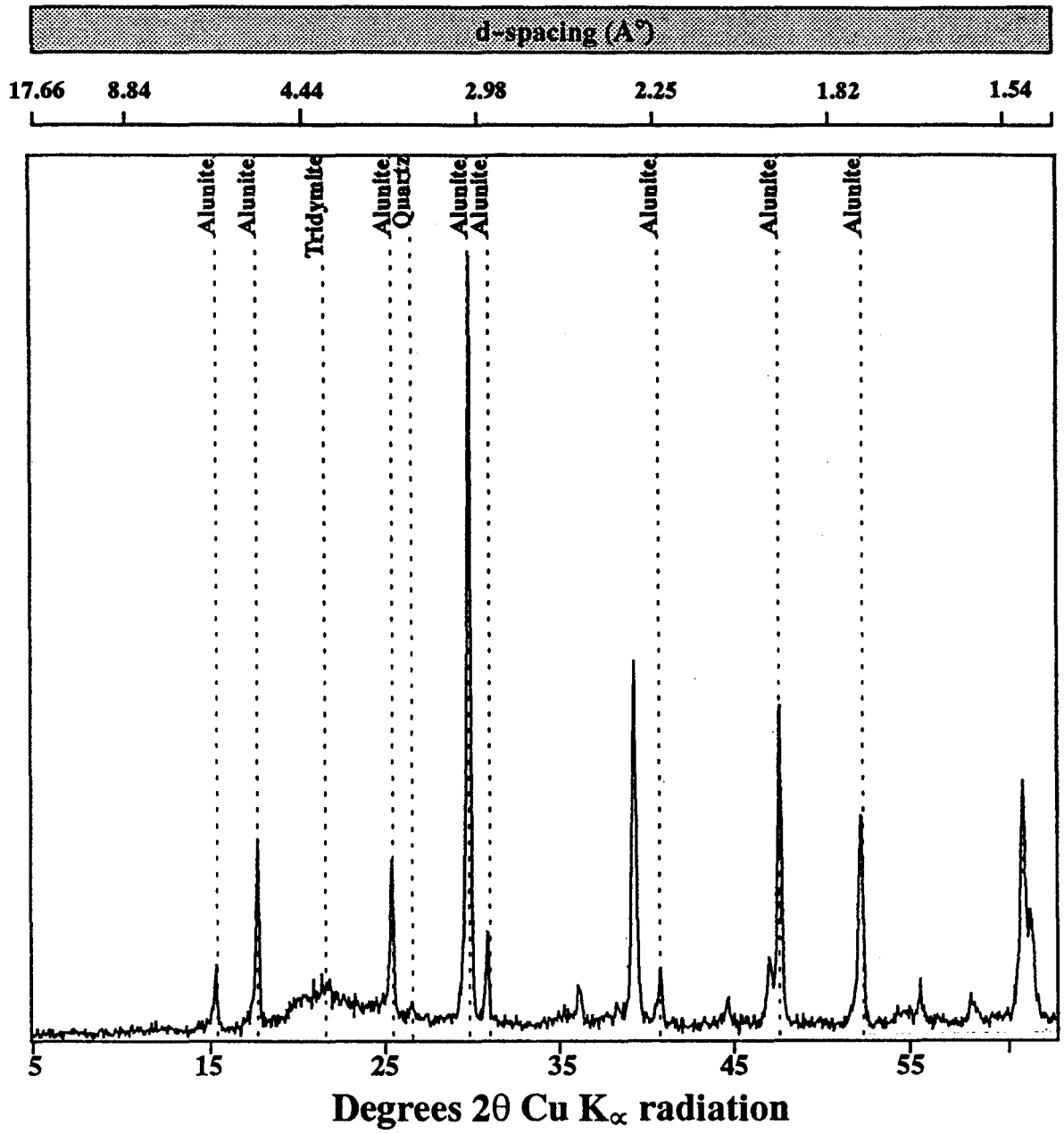

Figure 37: X-ray diffractogram of unoriented >2μm fraction showing the minerals in sample Tkm 3 of the Kline Mountain kaolin deposit.

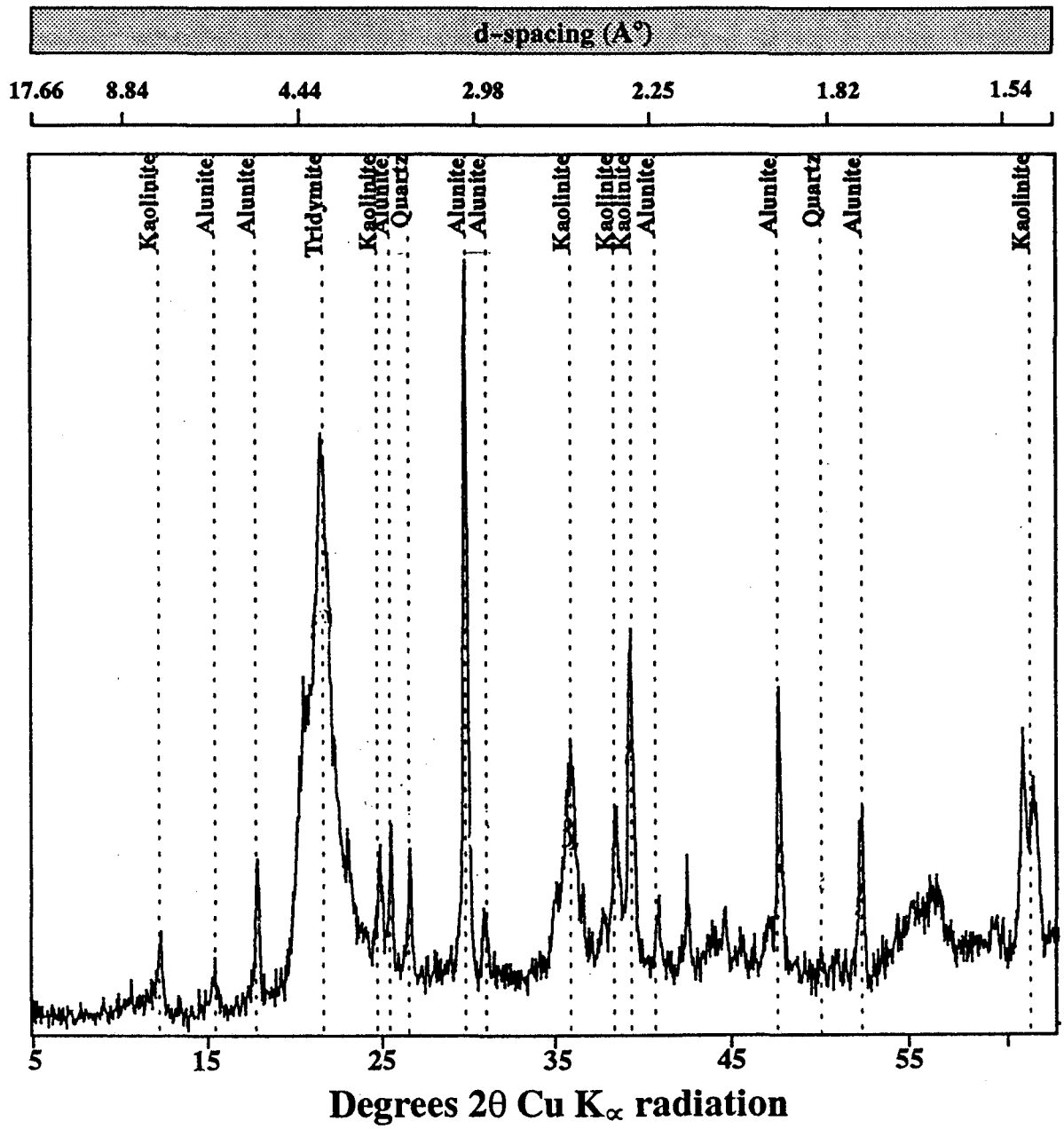

Figure 38: X-ray diffractogram of unoriented >2μm fraction showing the minerals in sample 2Tkm 2 of the Kline Mountain kaolin deposit.

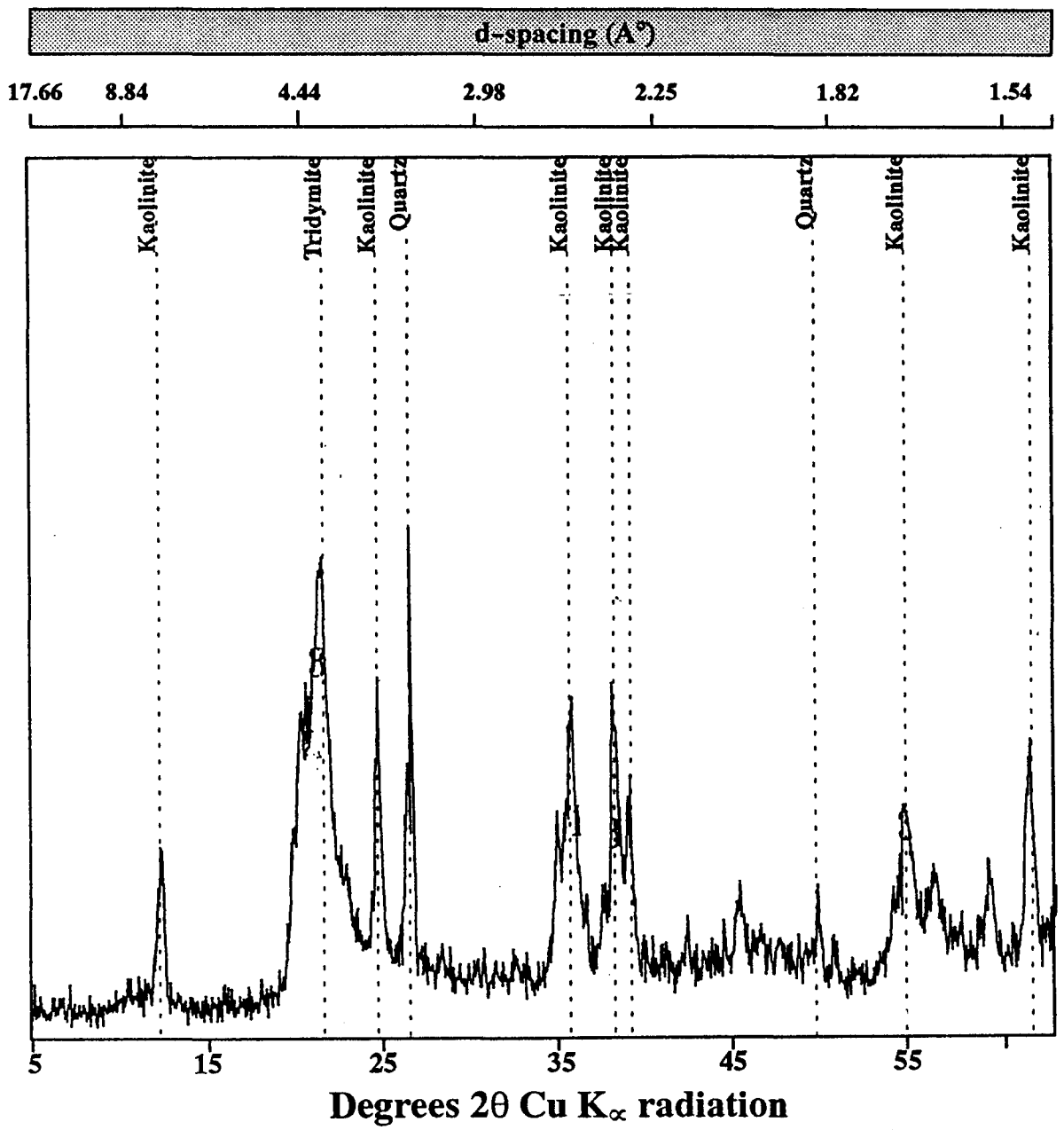

Figure 39: X-ray diffractogram of unoriented >2μm fraction showing the minerals in sample 2Tkm 4 of the Kline Mountain kaolin deposit.

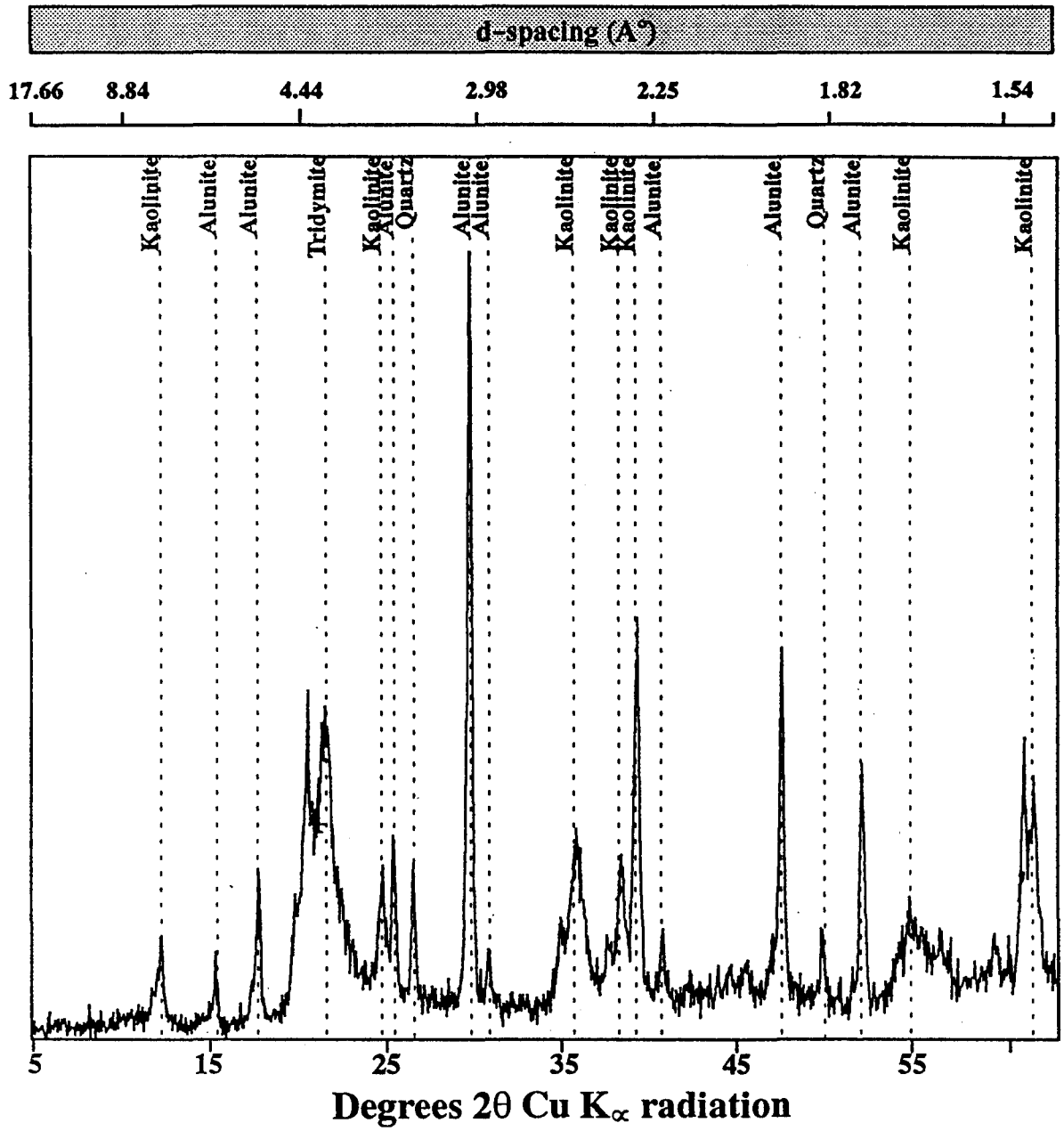

Figure 40: X-ray diffractogram of unoriented >2μm fraction showing the minerals in sample 2Tkm 5 of the Kline Mountain kaolin deposit.

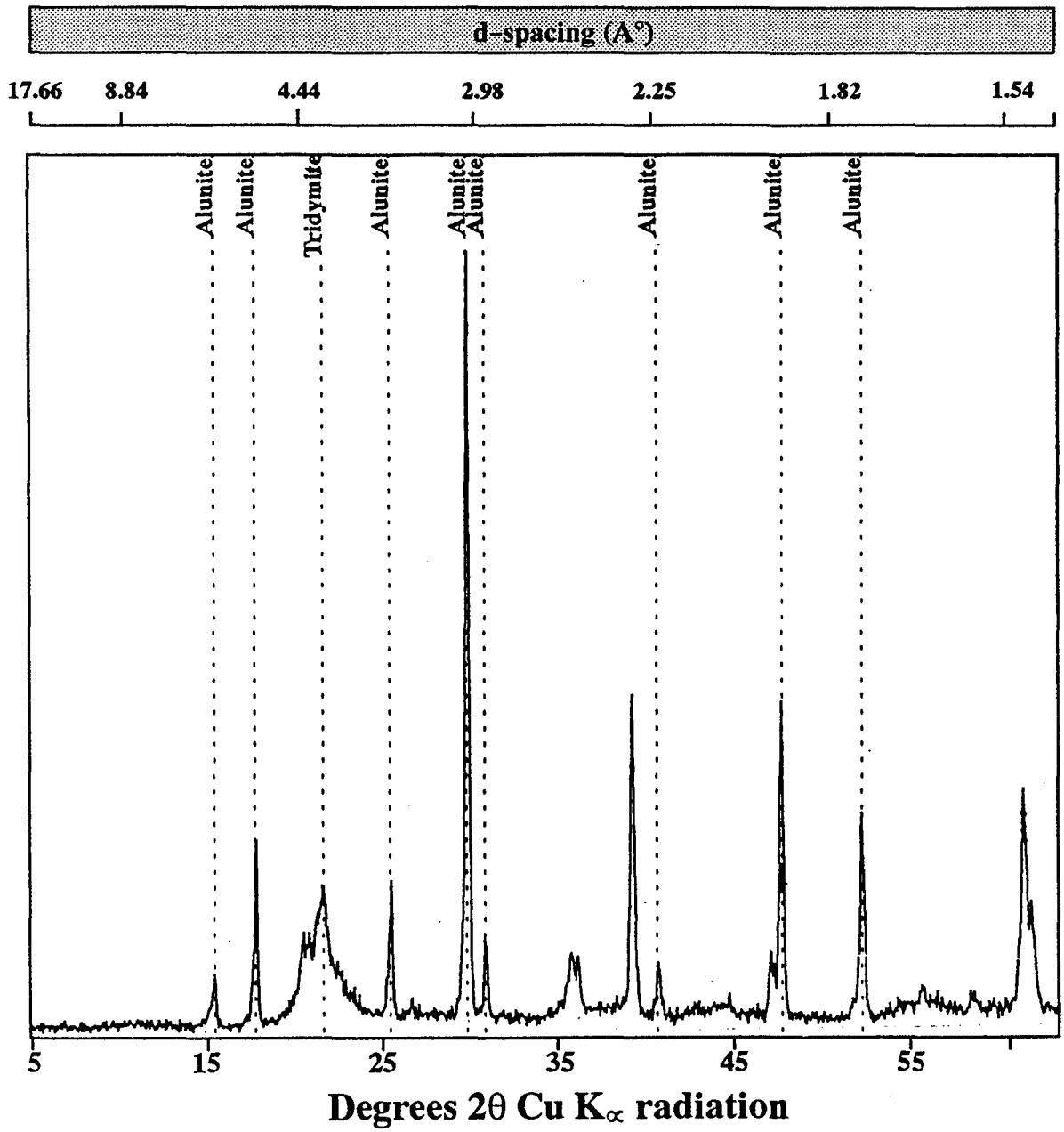

Figure 41: X-ray diffractogram of unoriented >2μm fraction showing the minerals in sample 3Tkm 1 of the Kline Mountain kaolin deposit.

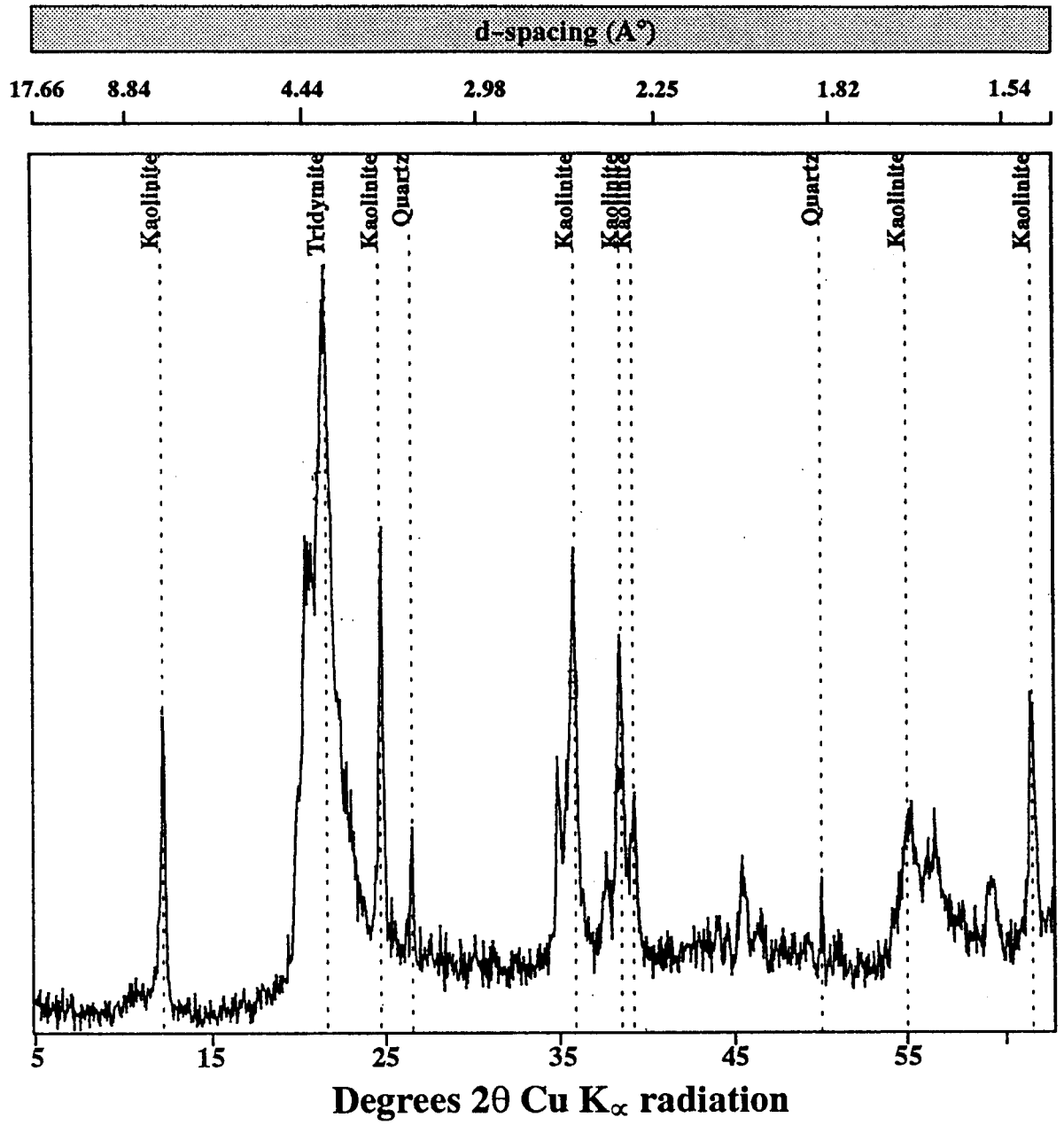

Figure 42: X-ray diffractogram of unoriented >2μm fraction showing the minerals in sample 3Tkm 3 of the Kline Mountain kaolin deposit.

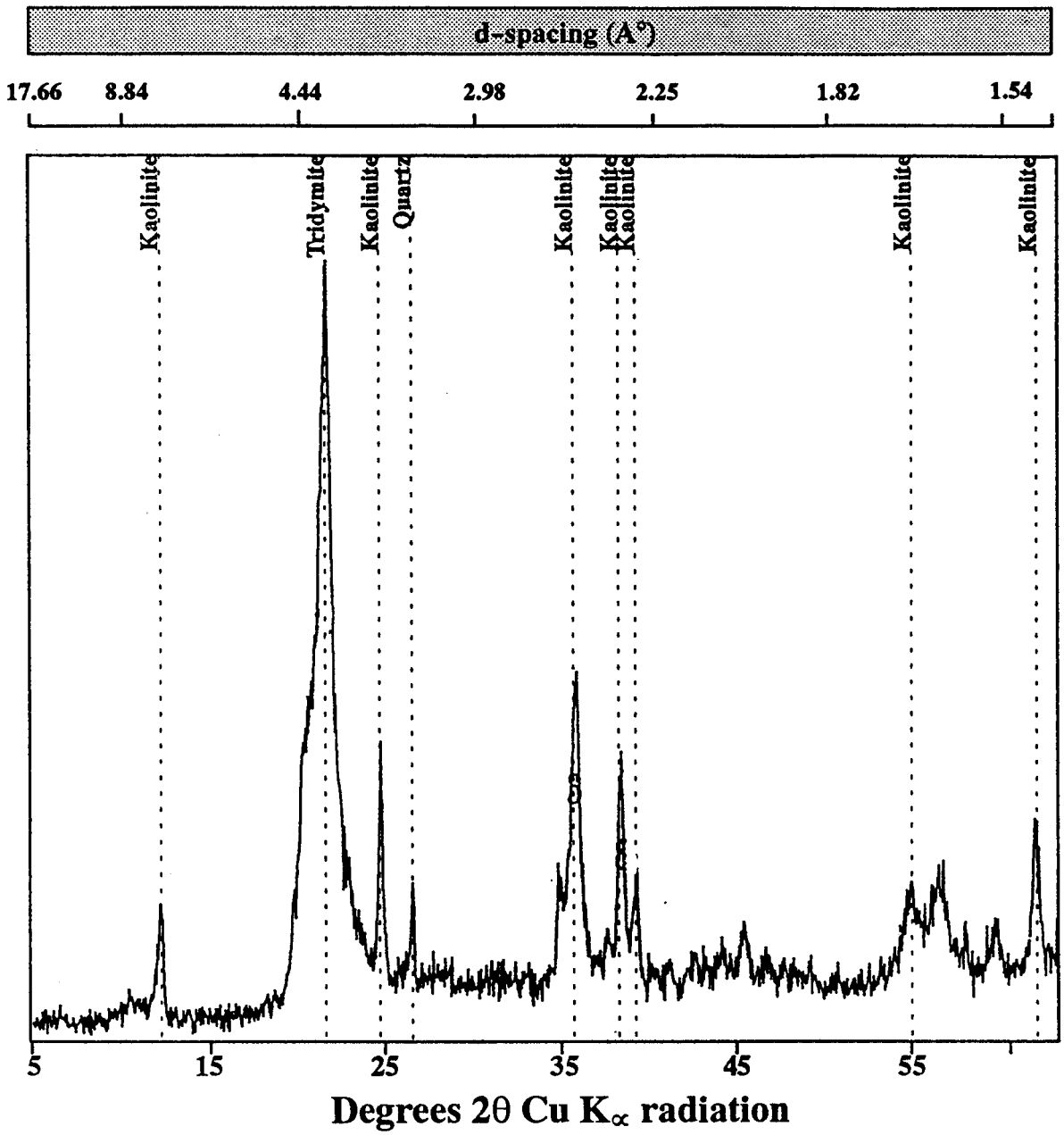

Figure 43: X-ray diffractogram of unoriented >2μm fraction showing the minerals in sample 3Tkm 5 of the Kline Mountain kaolin deposit.

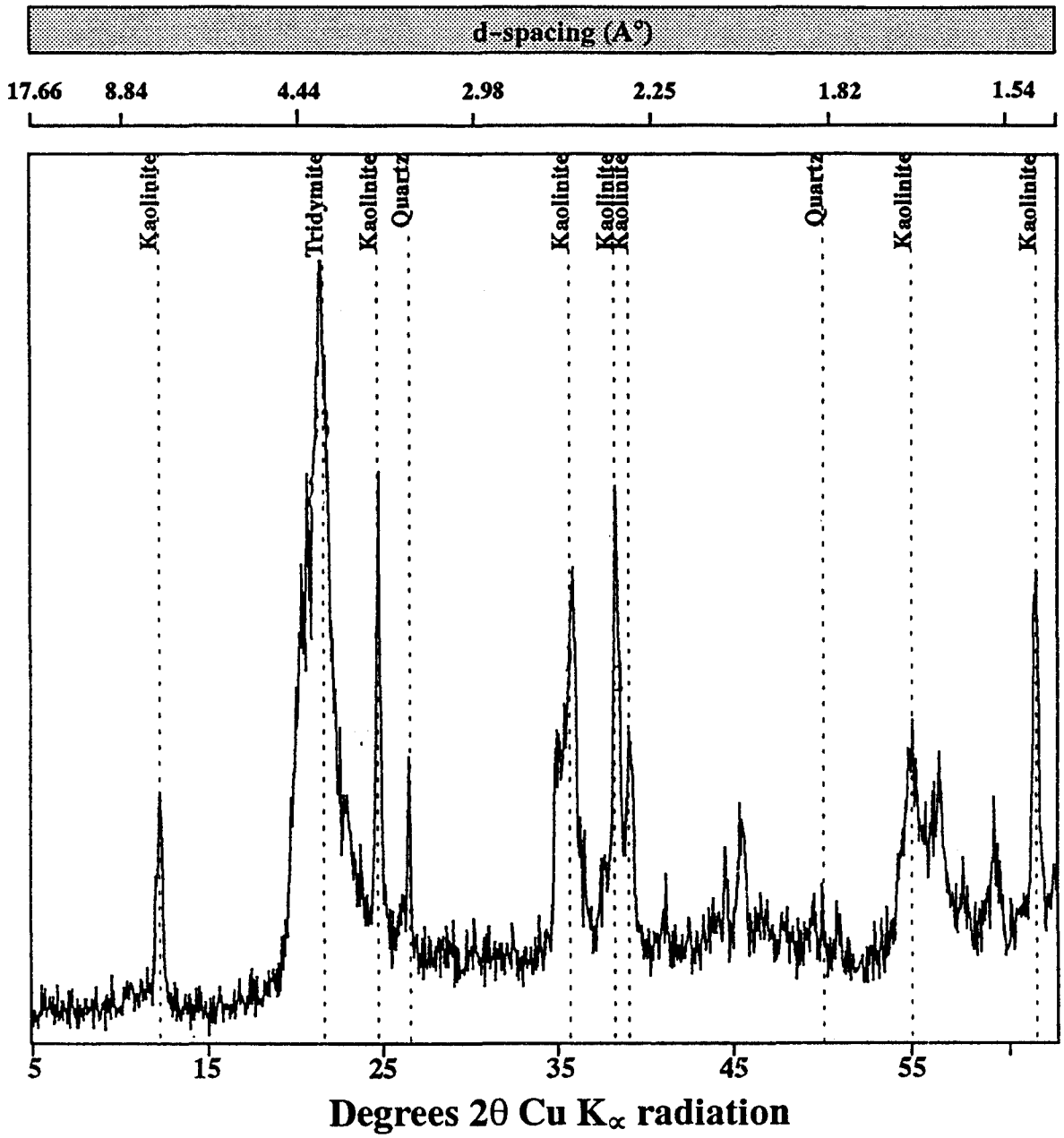

Figure 44: X-ray diffractogram of unoriented >2μm fraction showing the minerals in sample Tkm 8 of the Kline Mountain kaolin deposit.

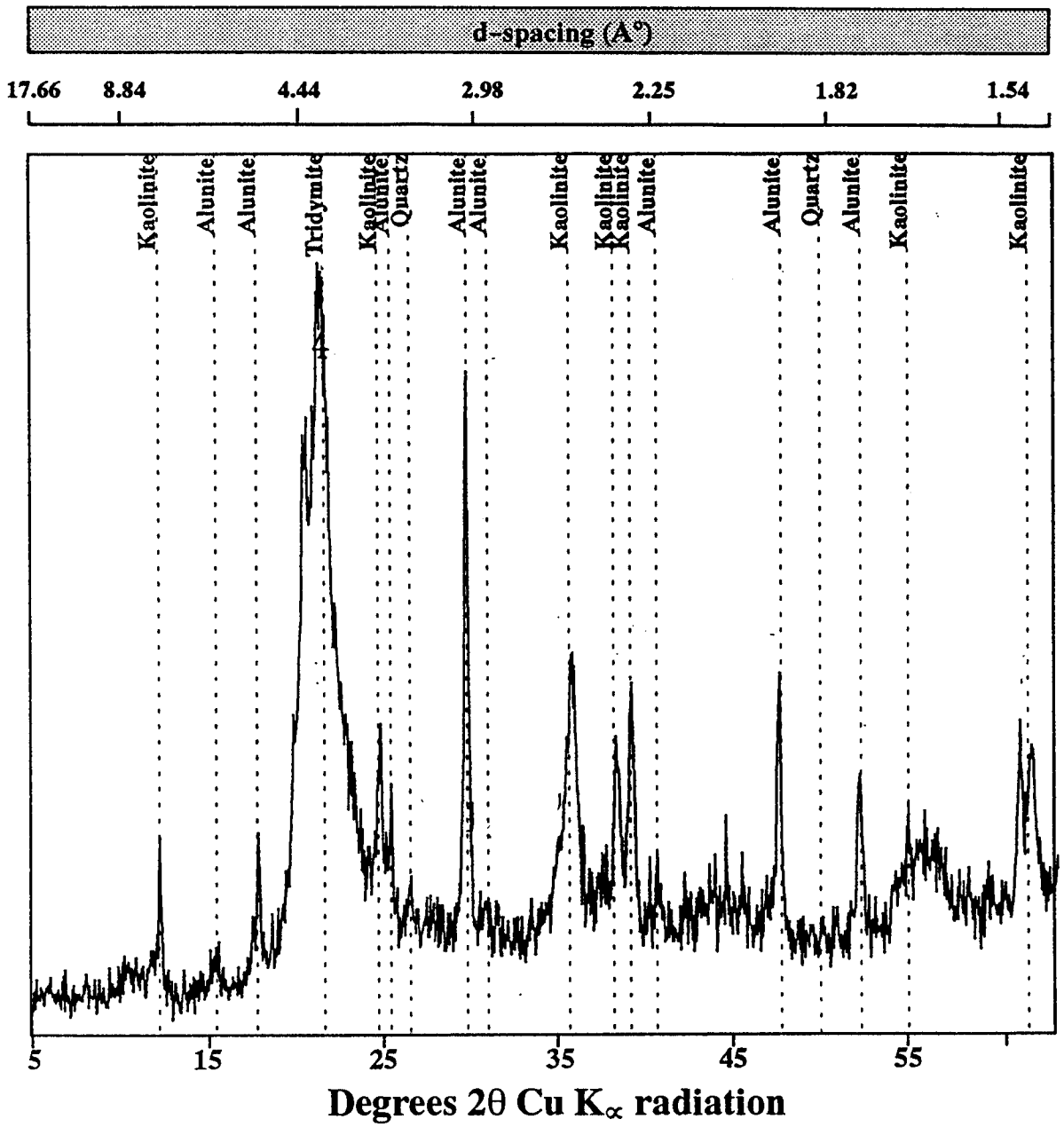

Figure 45: X-ray diffractogram of unoriented >2μm fraction showing the minerals in sample S7 of the Kline Mountain kaolin deposit.

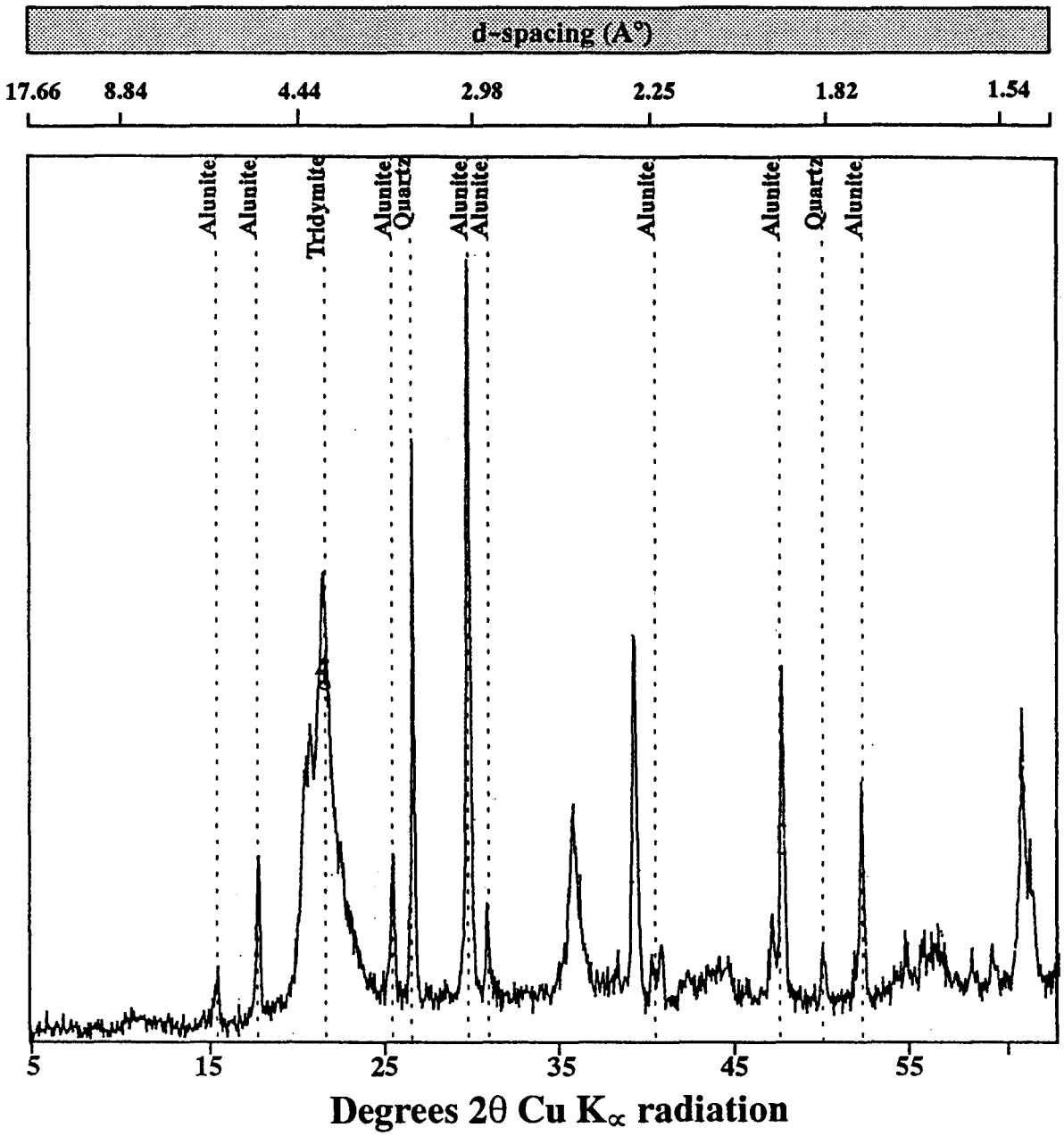

Figure 46: X-ray diffractogram of unoriented >2μm fraction showing the minerals in sample S7.5 of the Kline Mountain kaolin deposit.

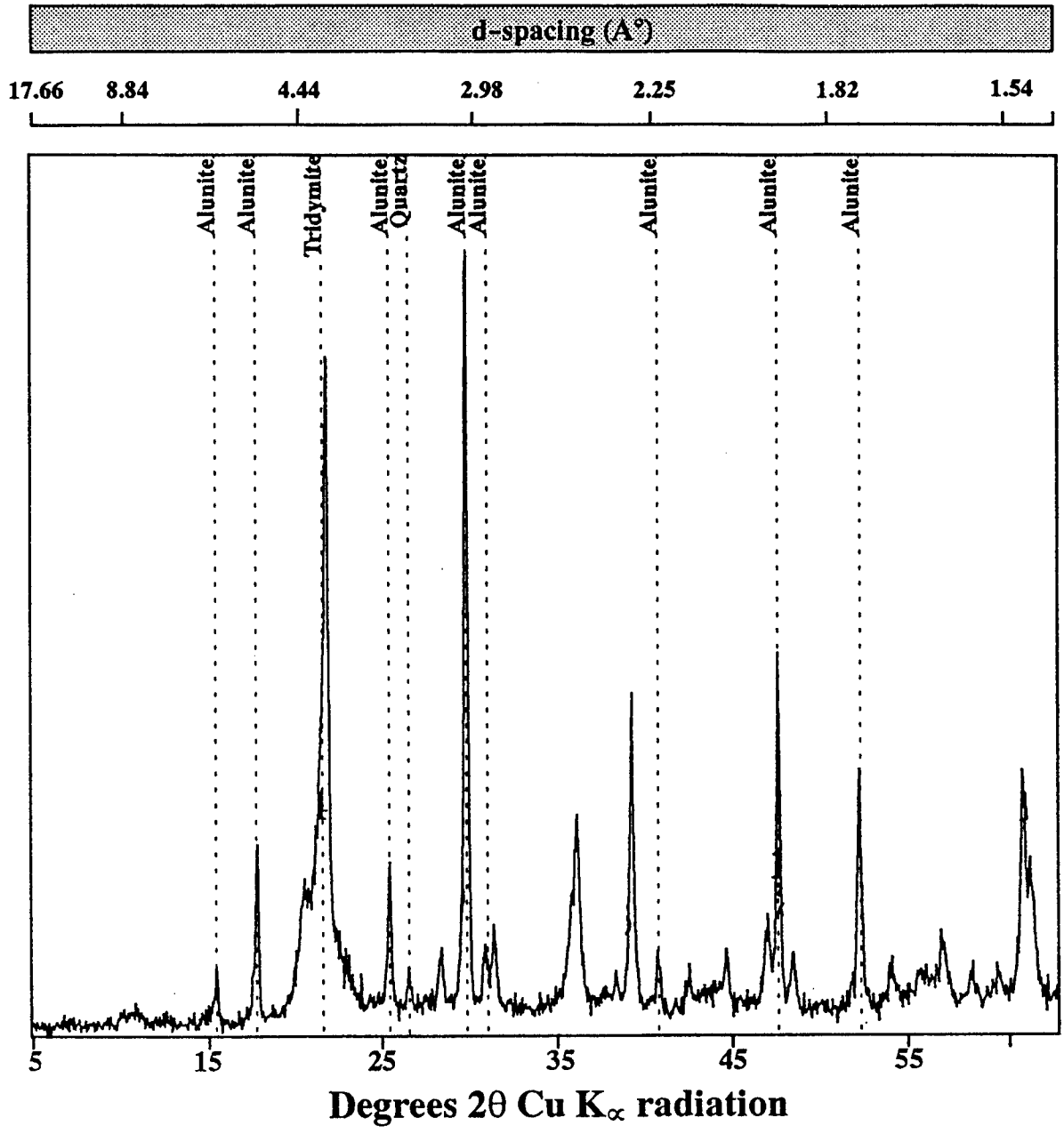

Figure 47: X-ray diffractogram of unoriented >2μm fraction showing the minerals in sample S8 of the Kline Mountain kaolin deposit.

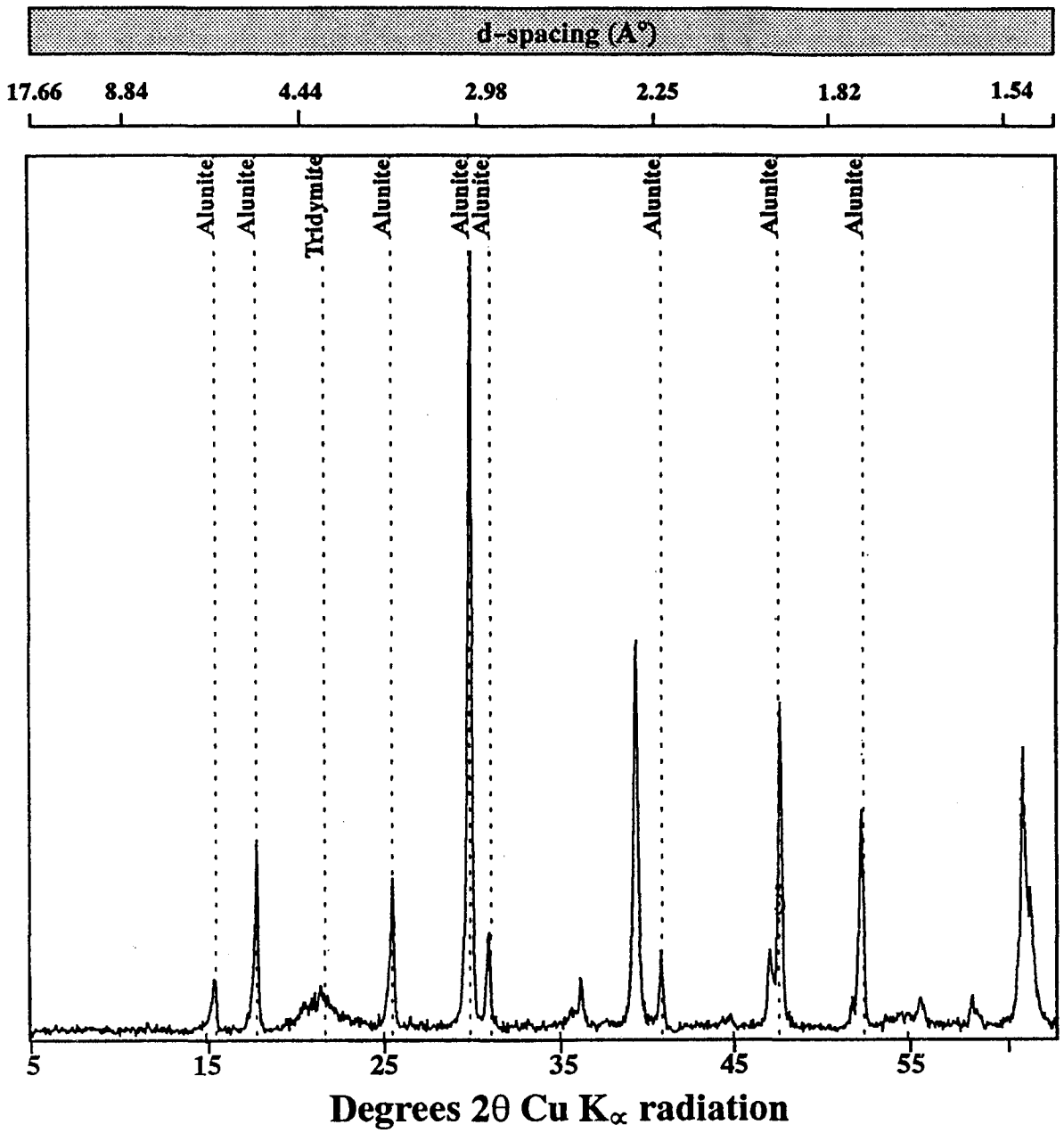

Figure 48: X-ray diffractogram of unoriented >2μm fraction showing the minerals in sample Tkm 18 of the Kline Mountain kaolin deposit.

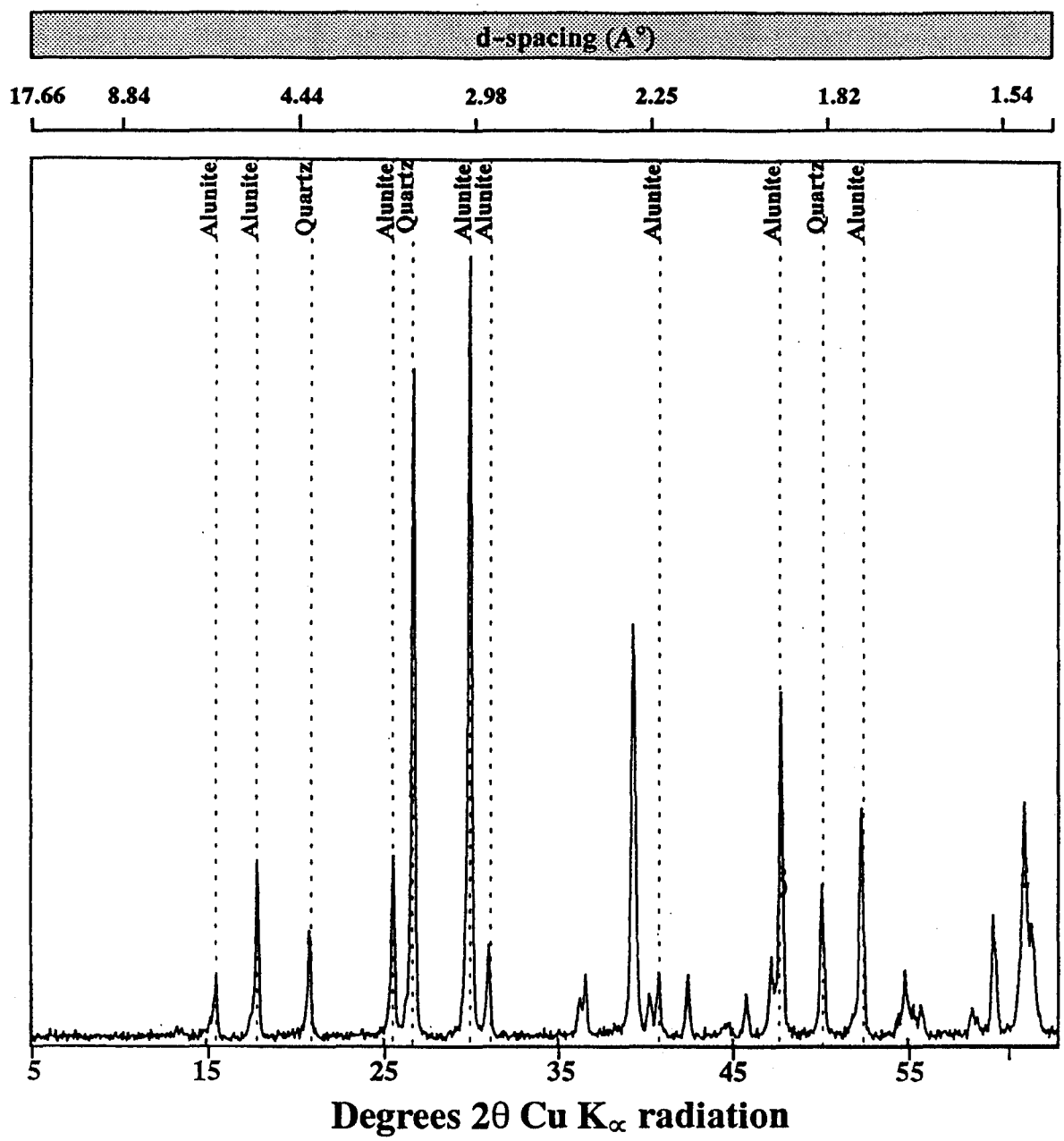

Figure 49: X-ray diffractogram of unoriented >2μm fraction showing the minerals in sample Tkm 20 of the Kline Mountain kaolin deposit.

Table 5: Clay-size fraction (<2 μm) mineralogy showing the distribution of the clay-size minerals in the samples of Kline Mountain tuff detected by X-ray diffractogram analysis (the order of numbers shows the decreasing order of abundance).

Sample	Kaolinite	Alunite	Tridymite	Quartz	Smectite
R5-I	1	3	2	4	
R5-II	1	2	3		
R5-III	1	2	4		3
R5-IV	1	3	2	4	
R5-V	1	2	3		
R5-VI	1	2	3		
R5-VII	2	1	3	4	
SM 200	1	2	4		3
CS 200	1	2	3		
Tkm 1	3		2		
Tkm 2	1	2	3		
Tkm 3	2	1			
2Tkm 2	3	1	2		
2Tkm 4	1		2	3	
2Tkm 5	2	1	3	4	
3Tkm 1	3	1	2		
3Tkm 5	1		2		
Tkm 8	1		2		
S7	4	2	1	3	
S8	2	1	3	4	
Tkm 18	?	1	2		
Tkm 20	?	1		2	

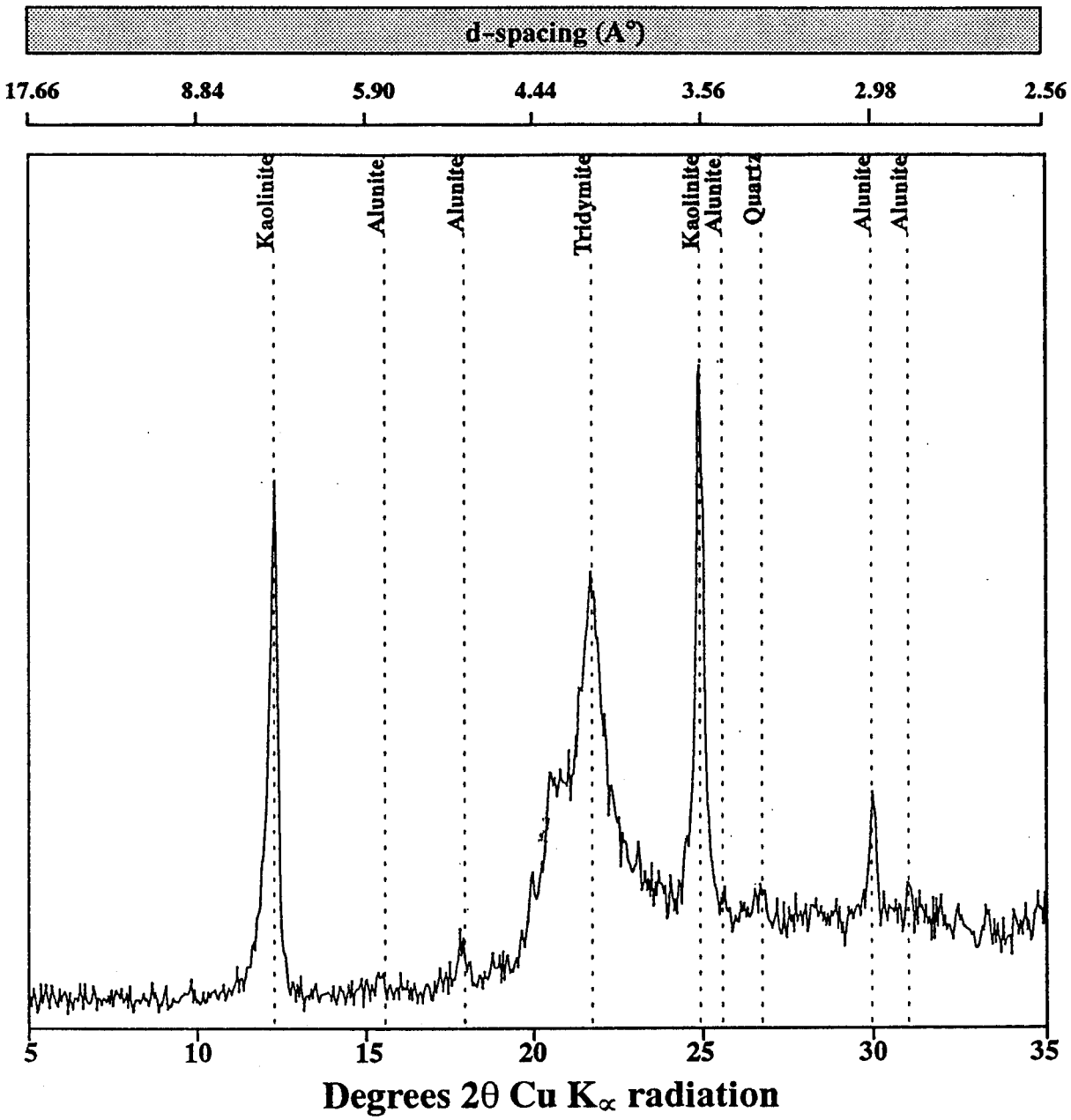

Figure 50: X-ray diffractogram of oriented <2μm fraction showing the minerals in sample R5-I of the Kline Mountain kaolin deposit.

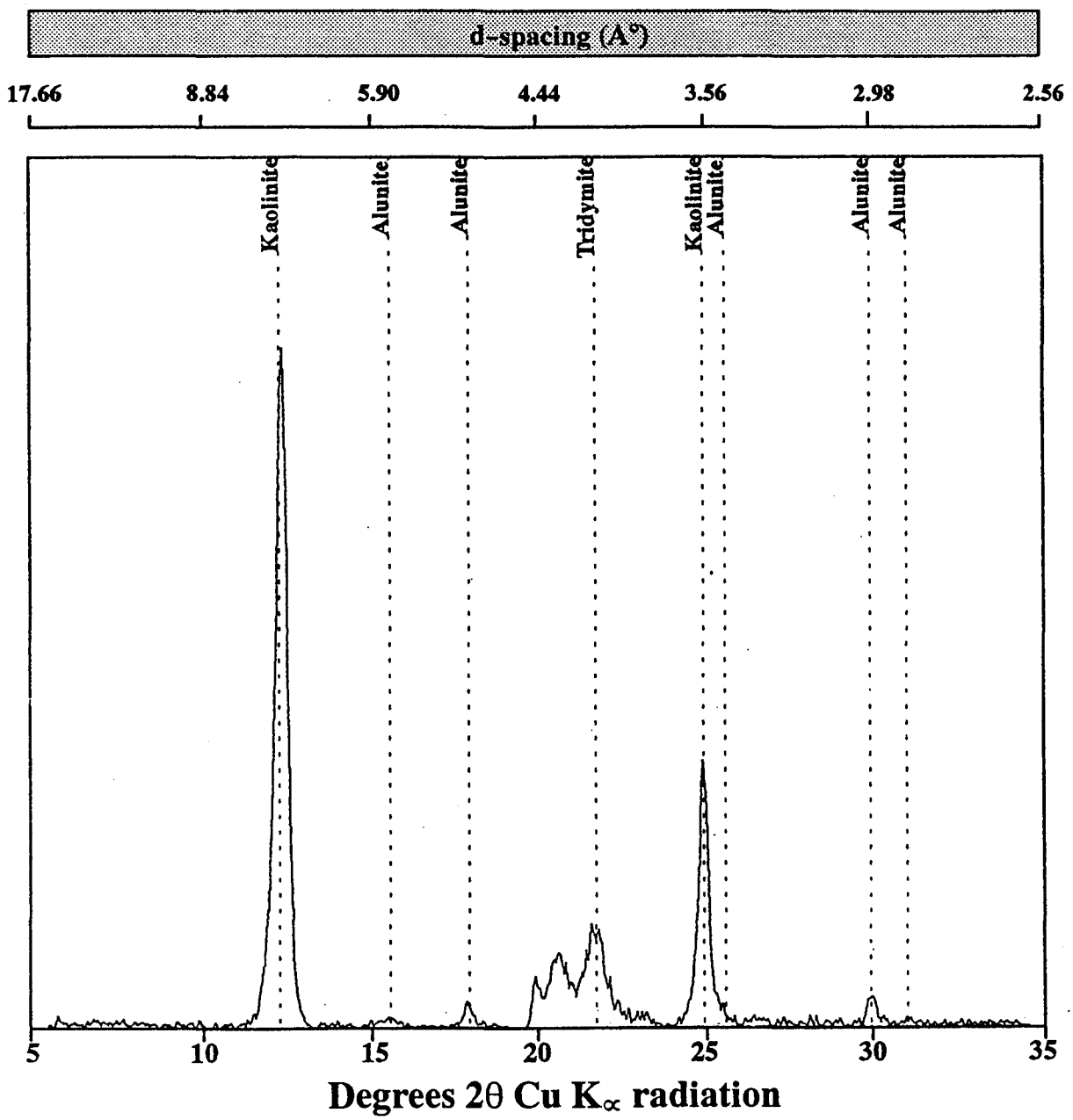

Figure 51: X-ray diffractogram of oriented <2μm fraction showing the minerals in sample R5-II of the Kline Mountain kaolin deposit.

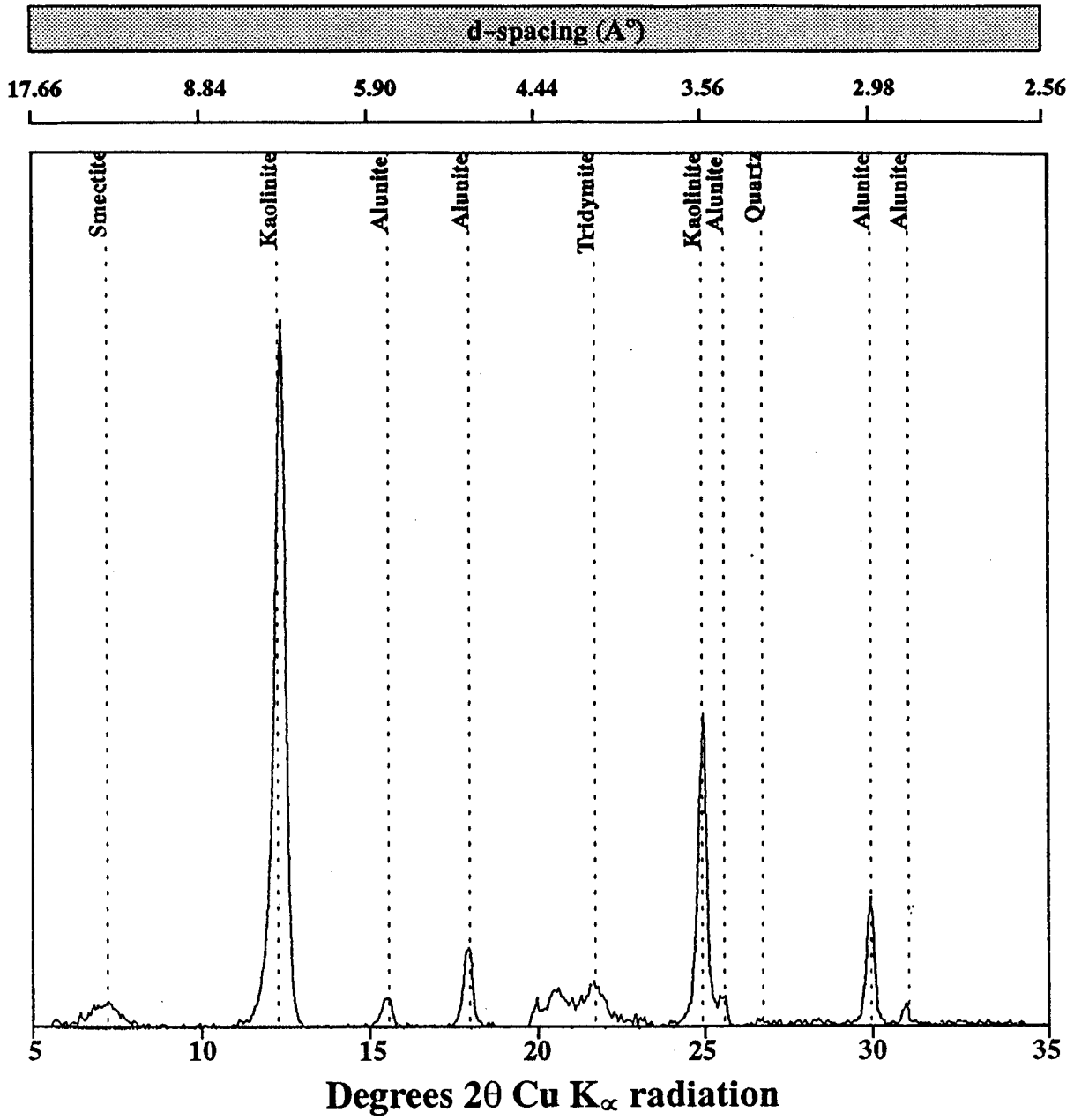

Figure 52: X-ray diffractogram of oriented <2μm fraction showing the minerals in sample R5-III of the Kline Mountain kaolin deposit.

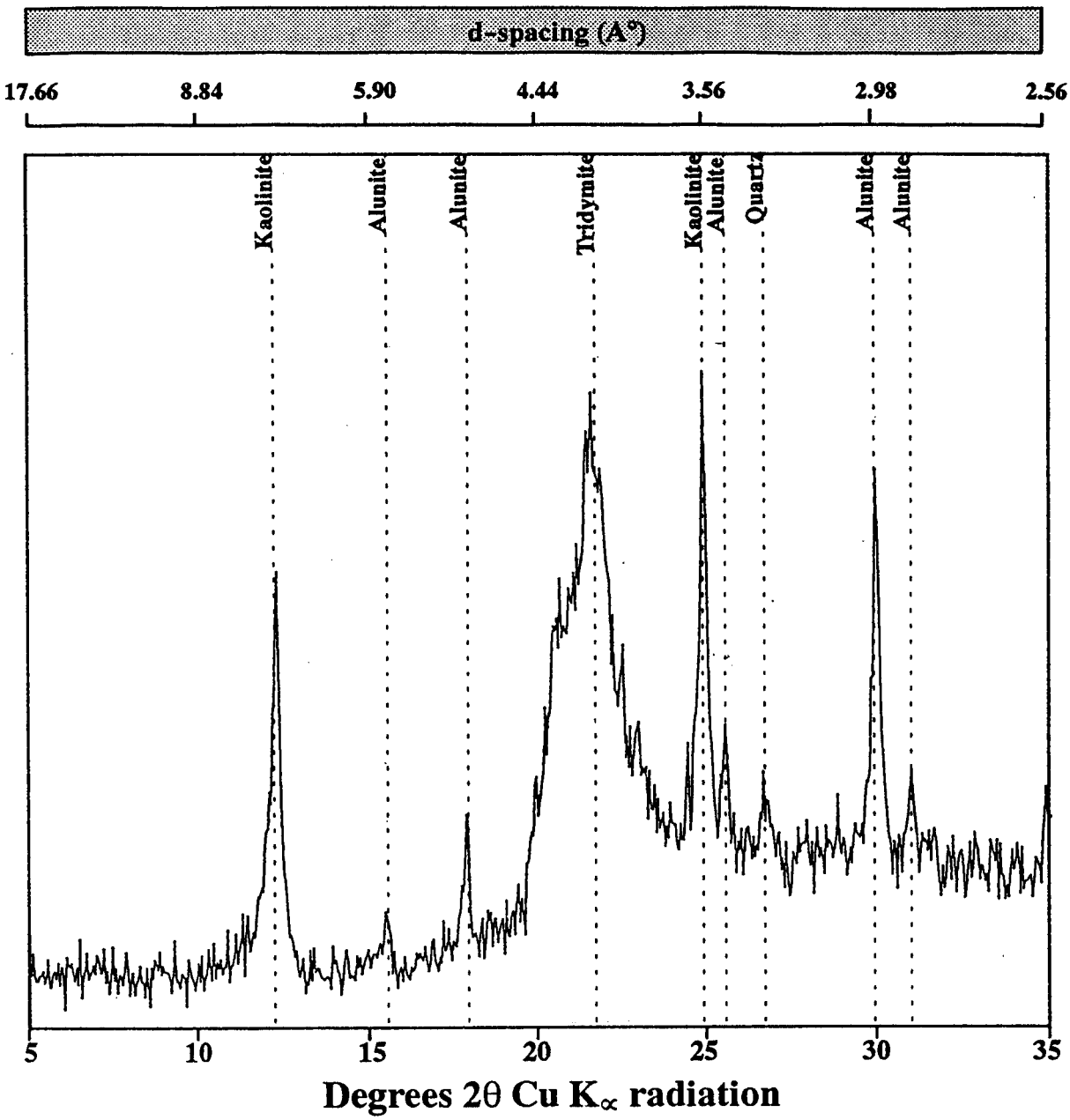

Figure 53: X-ray diffractogram of oriented <2μm fraction showing the minerals in sample R5-IV of the Kline Mountain kaolin deposit.

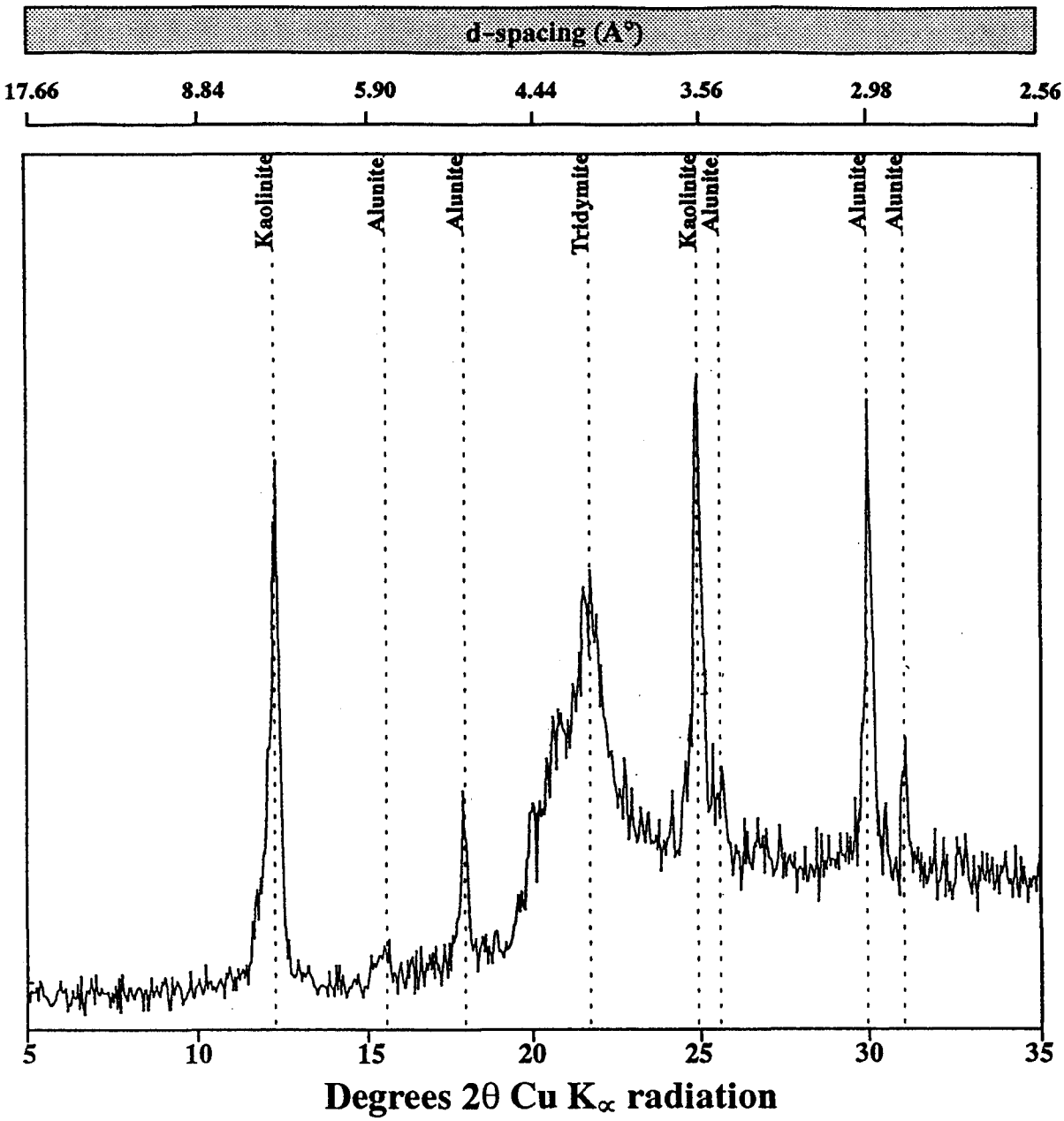

Figure 54: X-ray diffractogram of oriented <2μm fraction showing the minerals in sample R5-V of the Kline Mountain kaolin deposit.

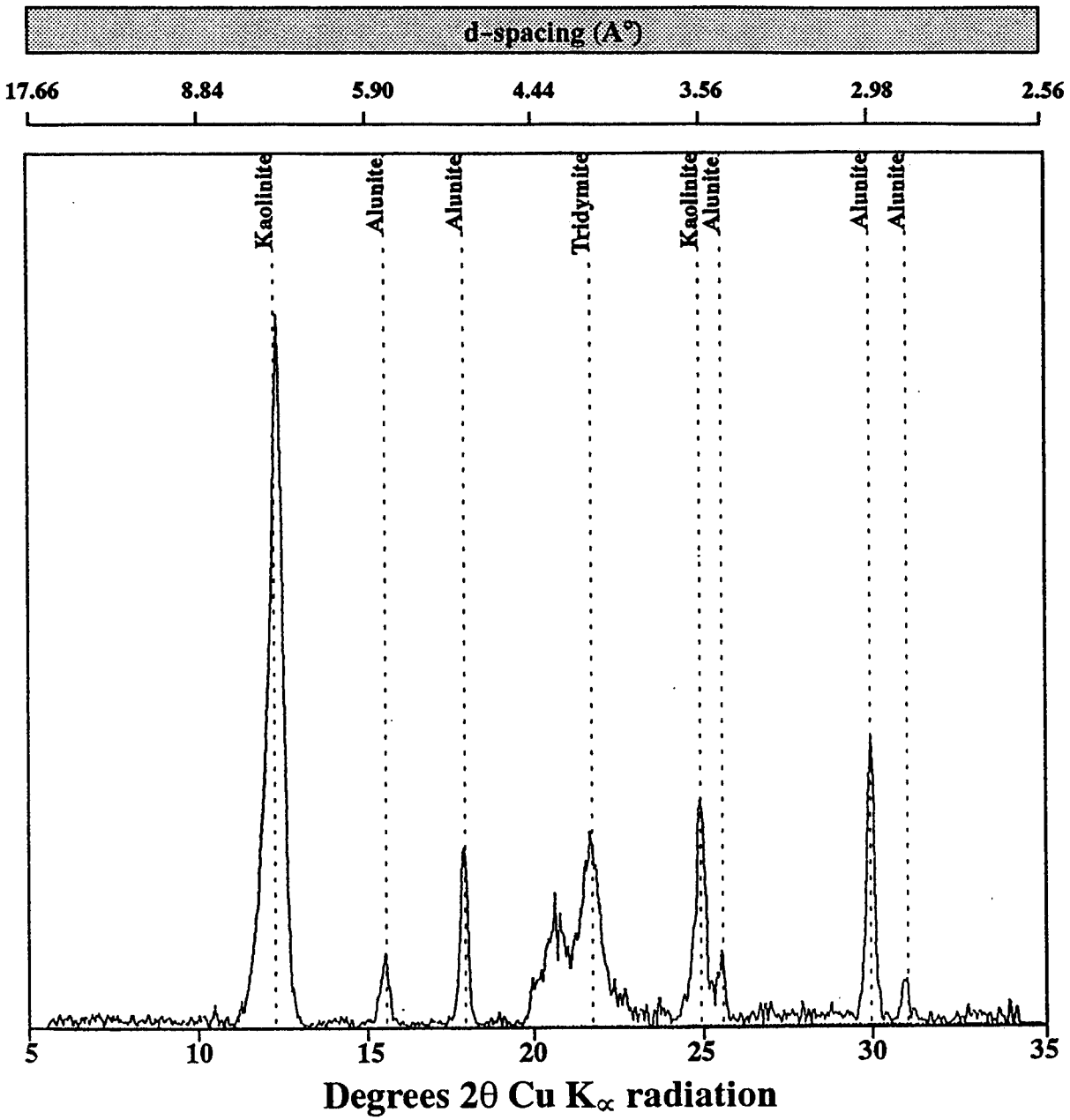

Figure 55: X-ray diffractogram of oriented <2μm fraction showing the minerals in sample R5-VI of the Kline Mountain kaolin deposit.

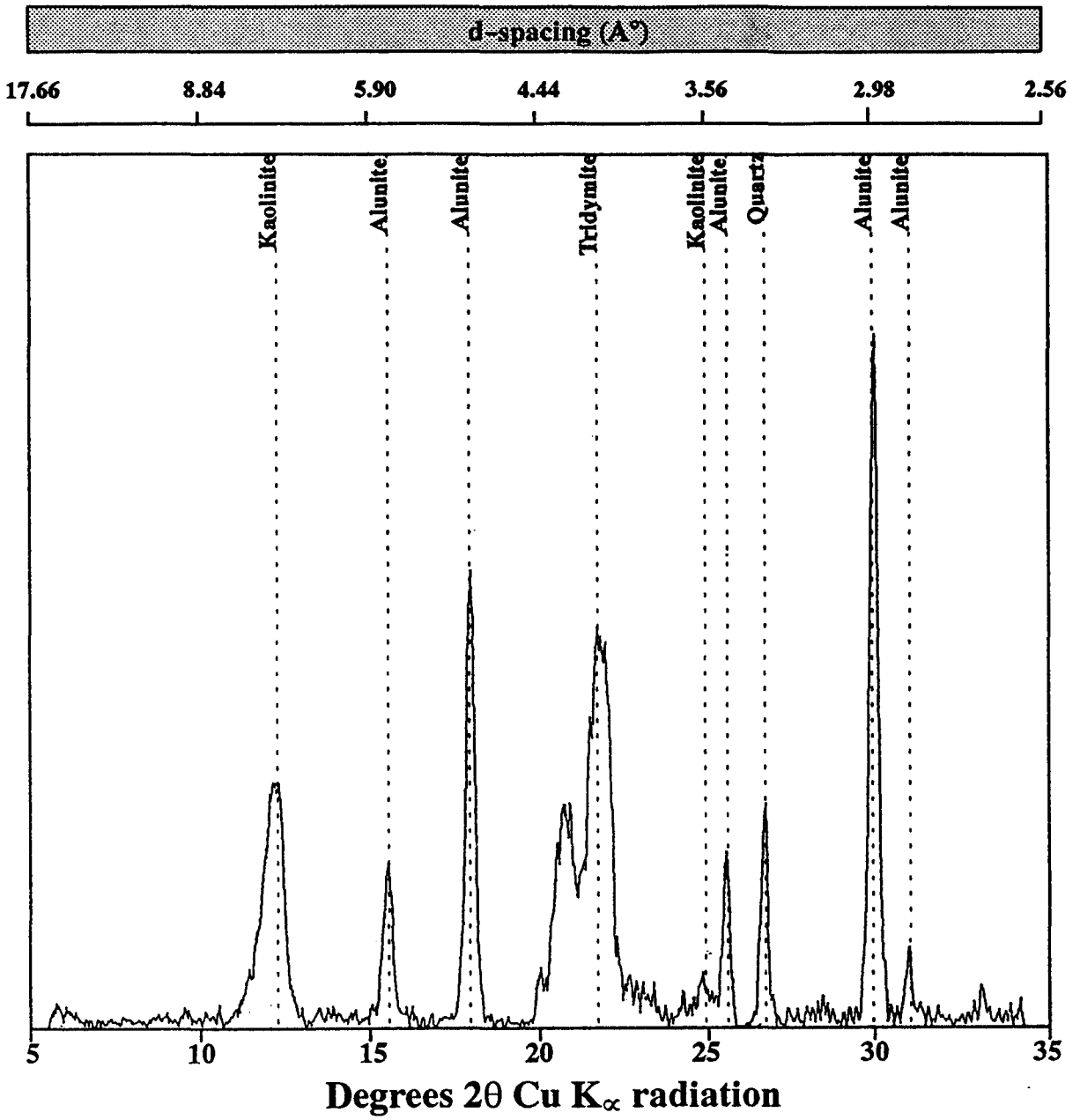

Figure 56: X-ray diffractogram of oriented <2μm fraction showing the minerals in sample R5-VII of the Kline Mountain kaolin deposit.

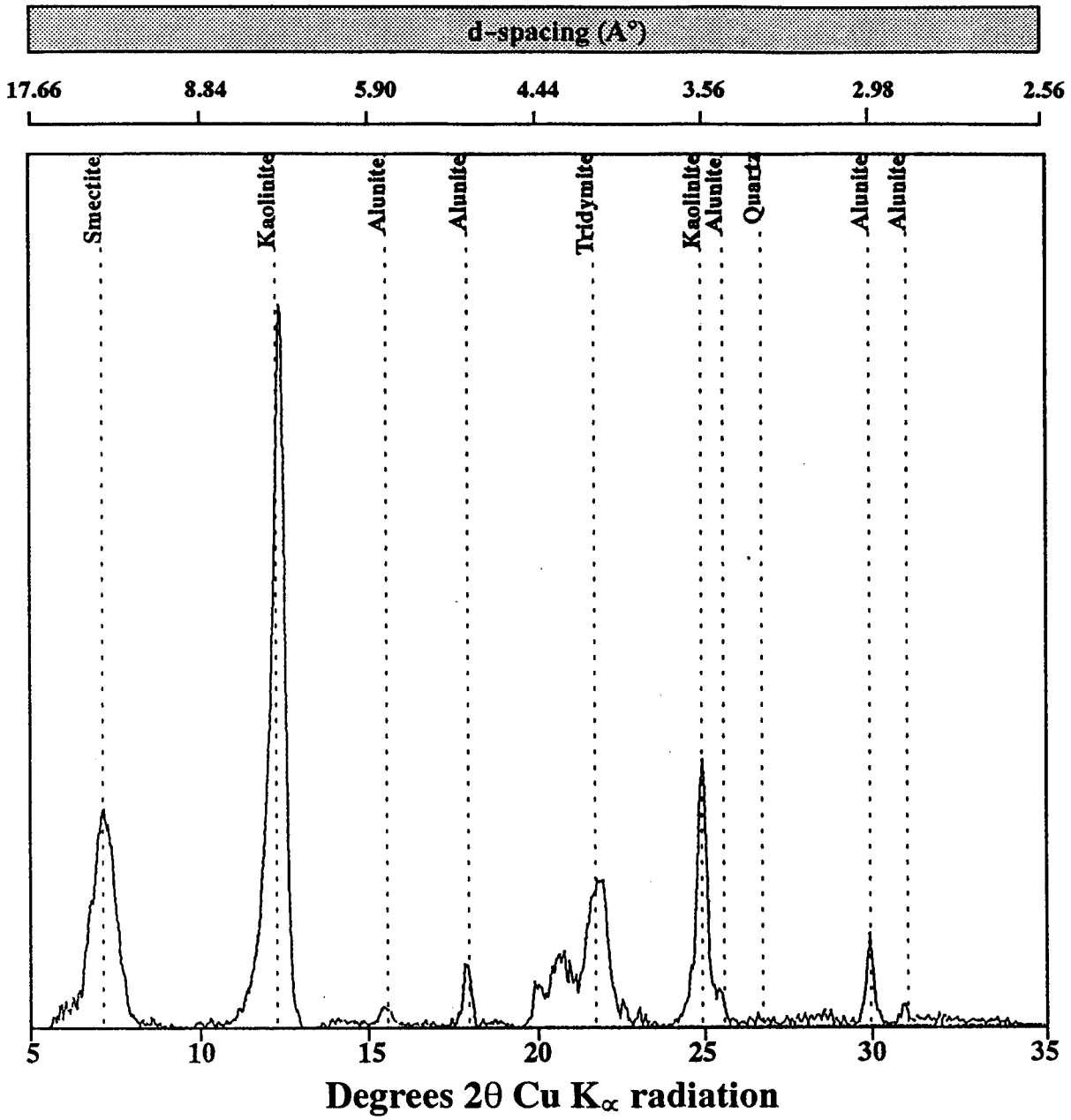

Figure 57: X-ray diffractogram of oriented <2μm fraction showing the minerals in sample SM 200 of the Kline Mountain kaolin deposit.

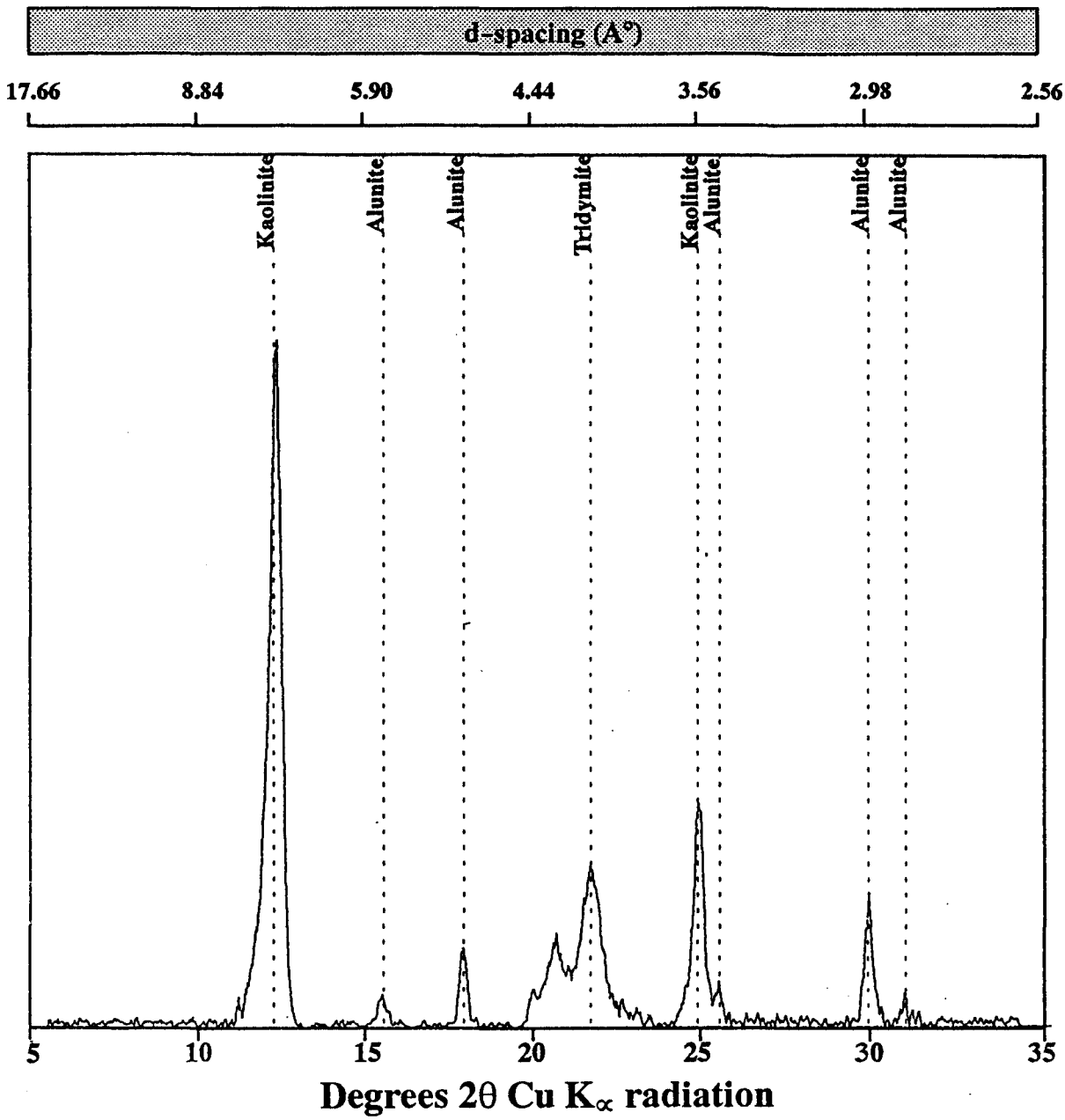

Figure 58: X-ray diffractogram of oriented <2μm fraction showing the minerals in sample CS 200 of the Kline Mountain kaolin deposit.

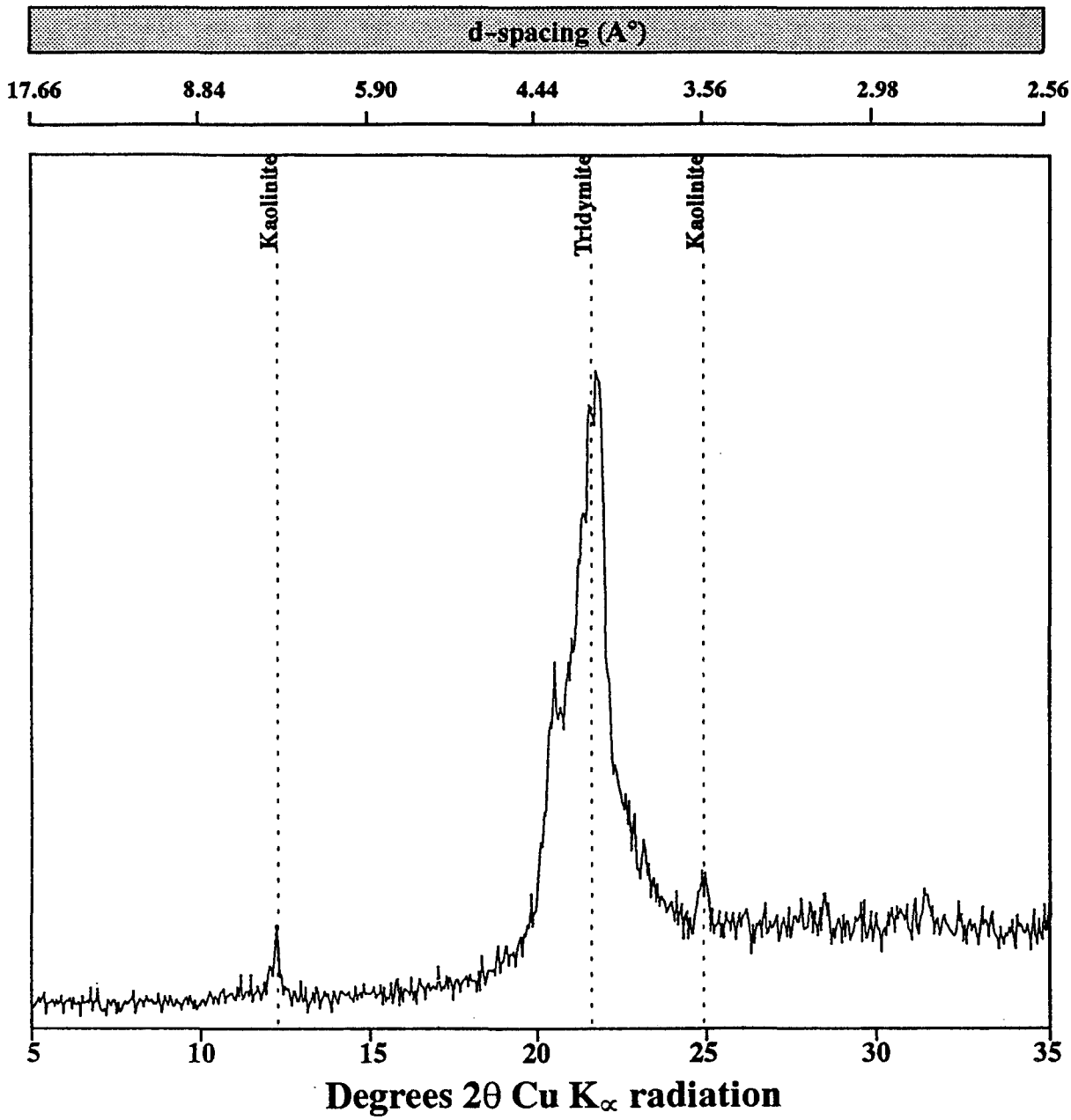

Figure 59: X-ray diffractogram of oriented <2μm fraction showing the minerals in sample Tkm 1 of the Kline Mountain kaolin deposit.

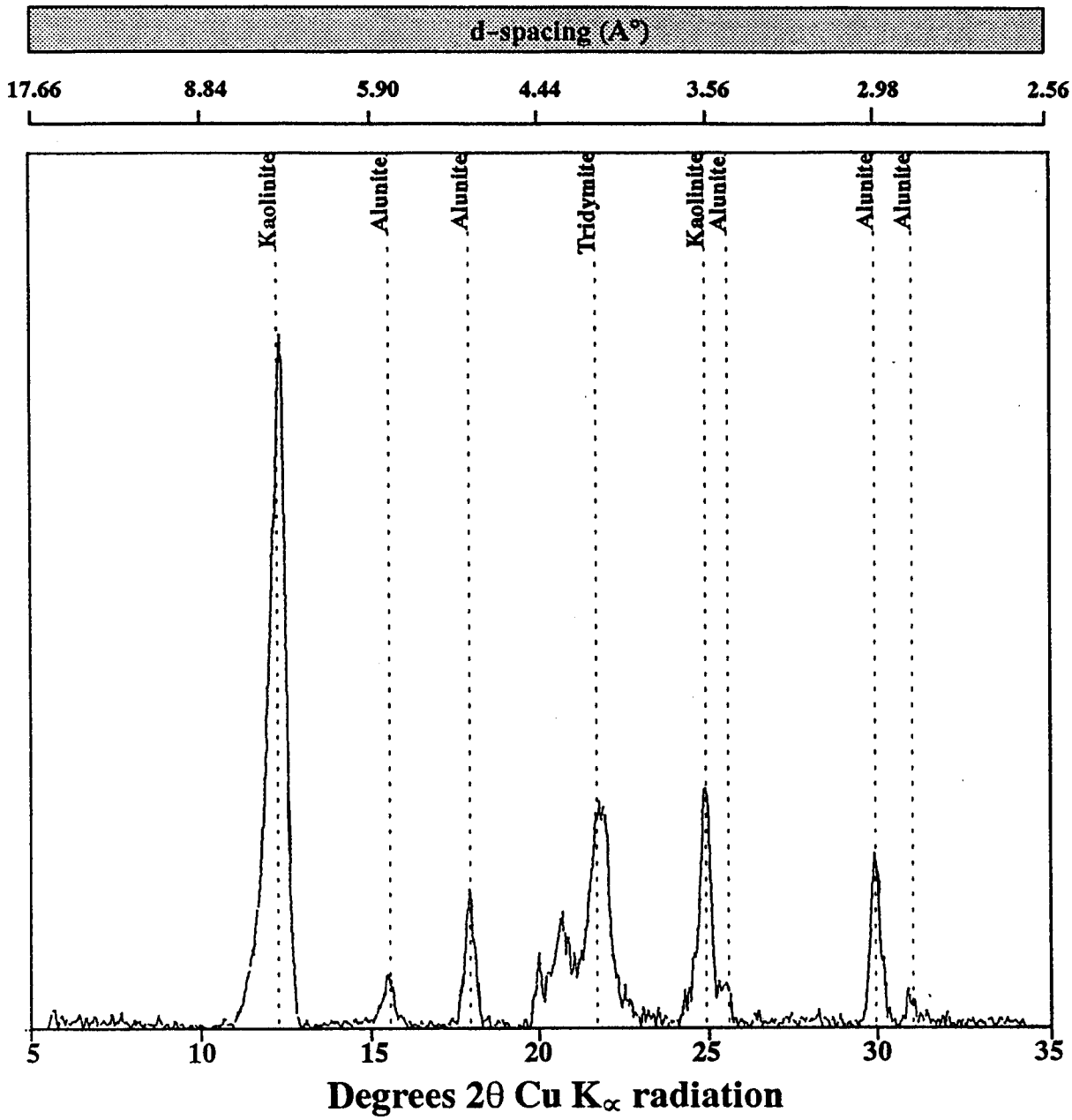

Figure 60: X-ray diffractogram of oriented <2μm fraction showing the minerals in sample Tkm 2 of the Kline Mountain kaolin deposit.

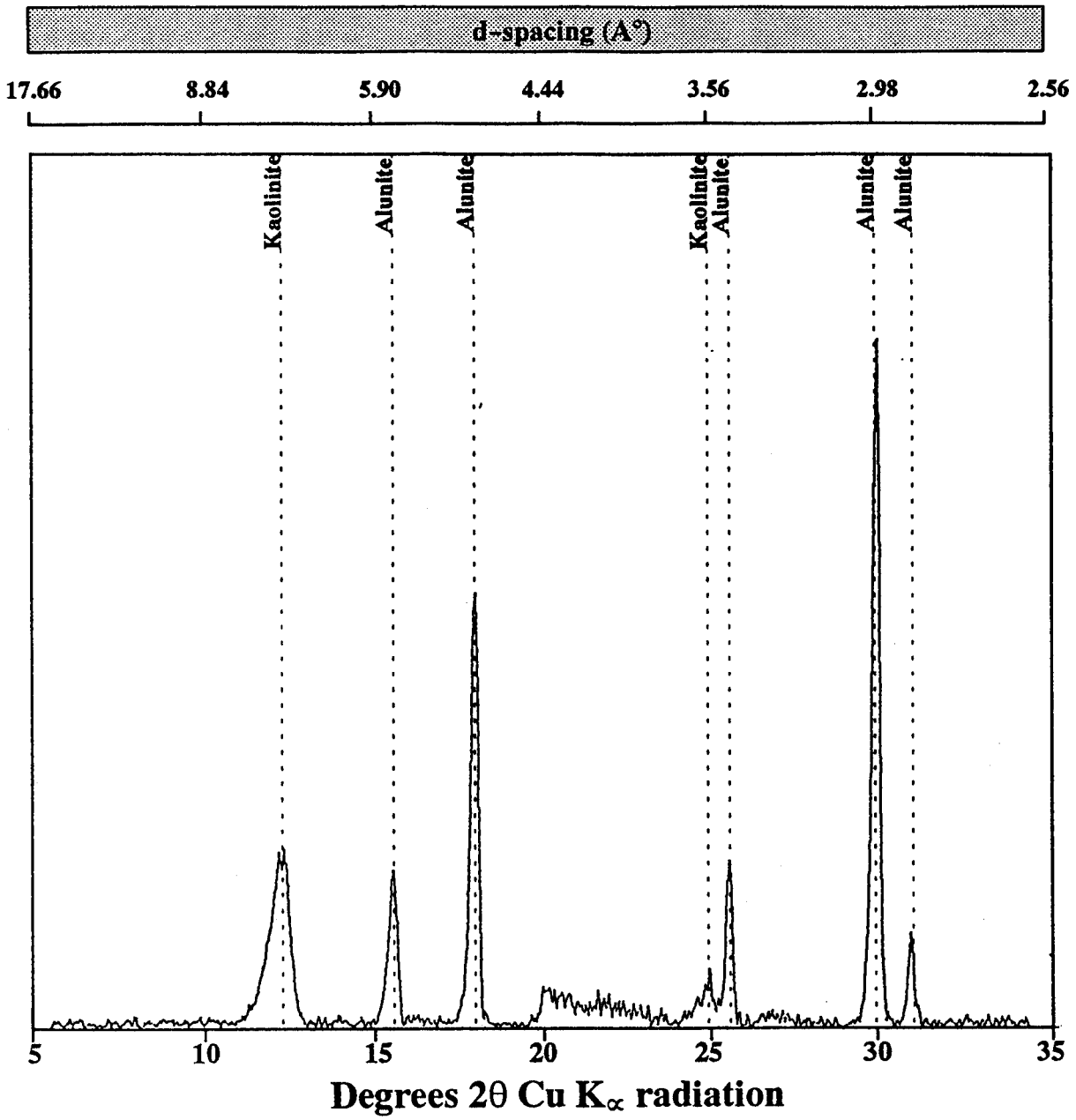

Figure 61: X-ray diffractogram of oriented <2μm fraction showing the minerals in sample Tkm 3 of the Kline Mountain kaolin deposit.

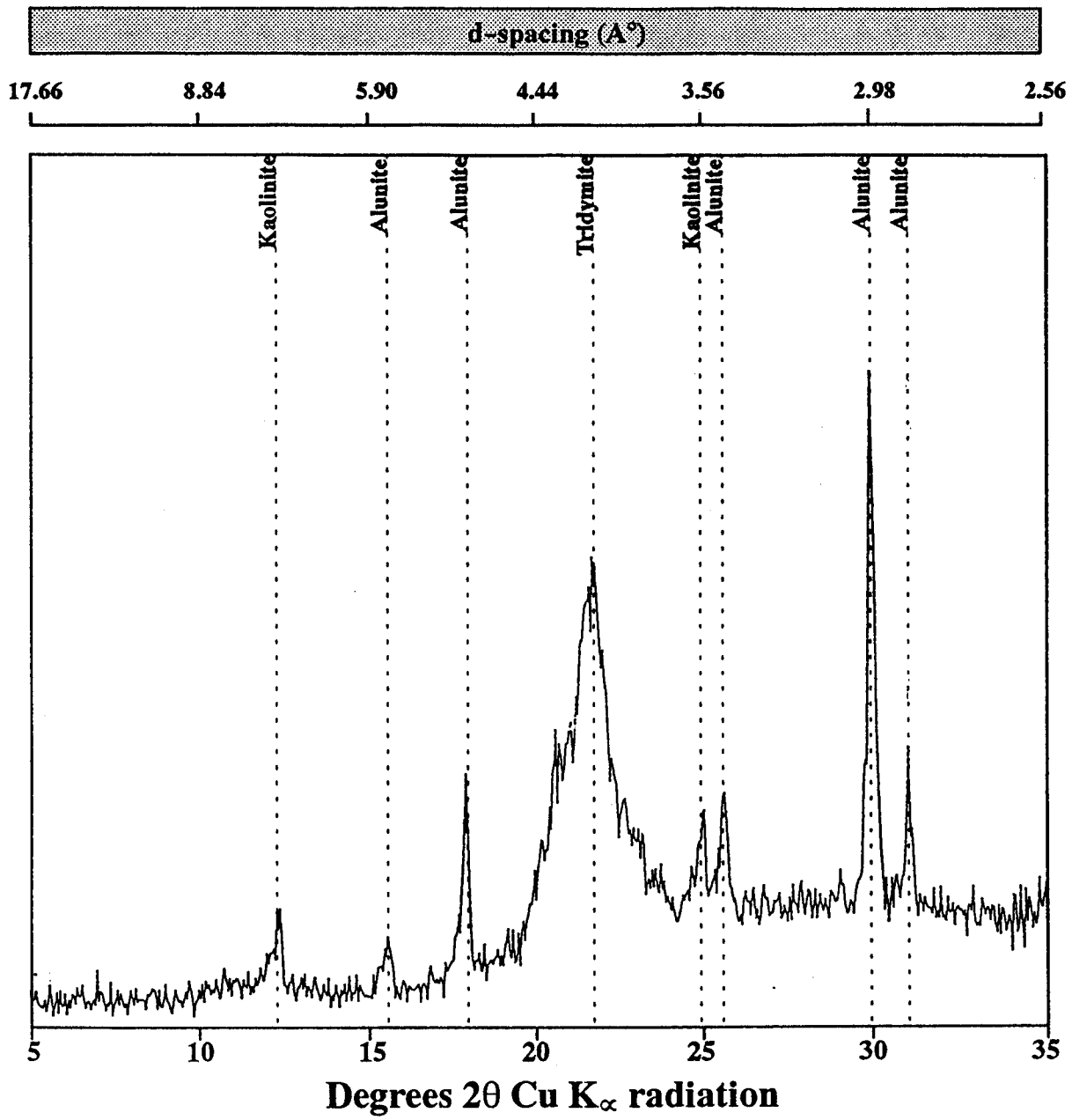

Figure 62: X-ray diffractogram of oriented <2μm fraction showing the minerals in sample 2Tkm 2 of the Kline Mountain kaolin deposit.

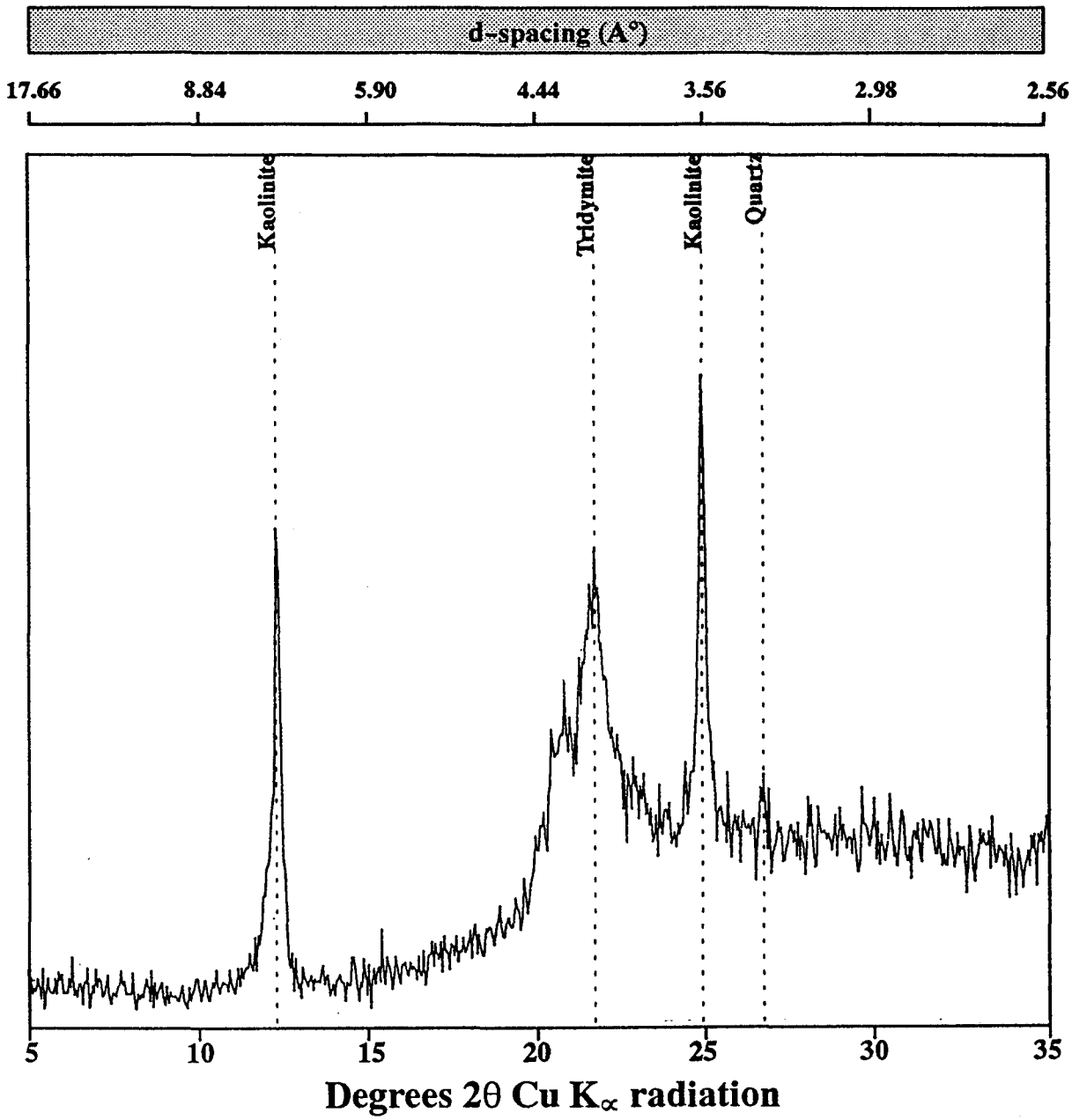

Figure 63: X-ray diffractogram of oriented <2μm fraction showing the minerals in sample 2Tkm 4 of the Kline Mountain kaolin deposit.

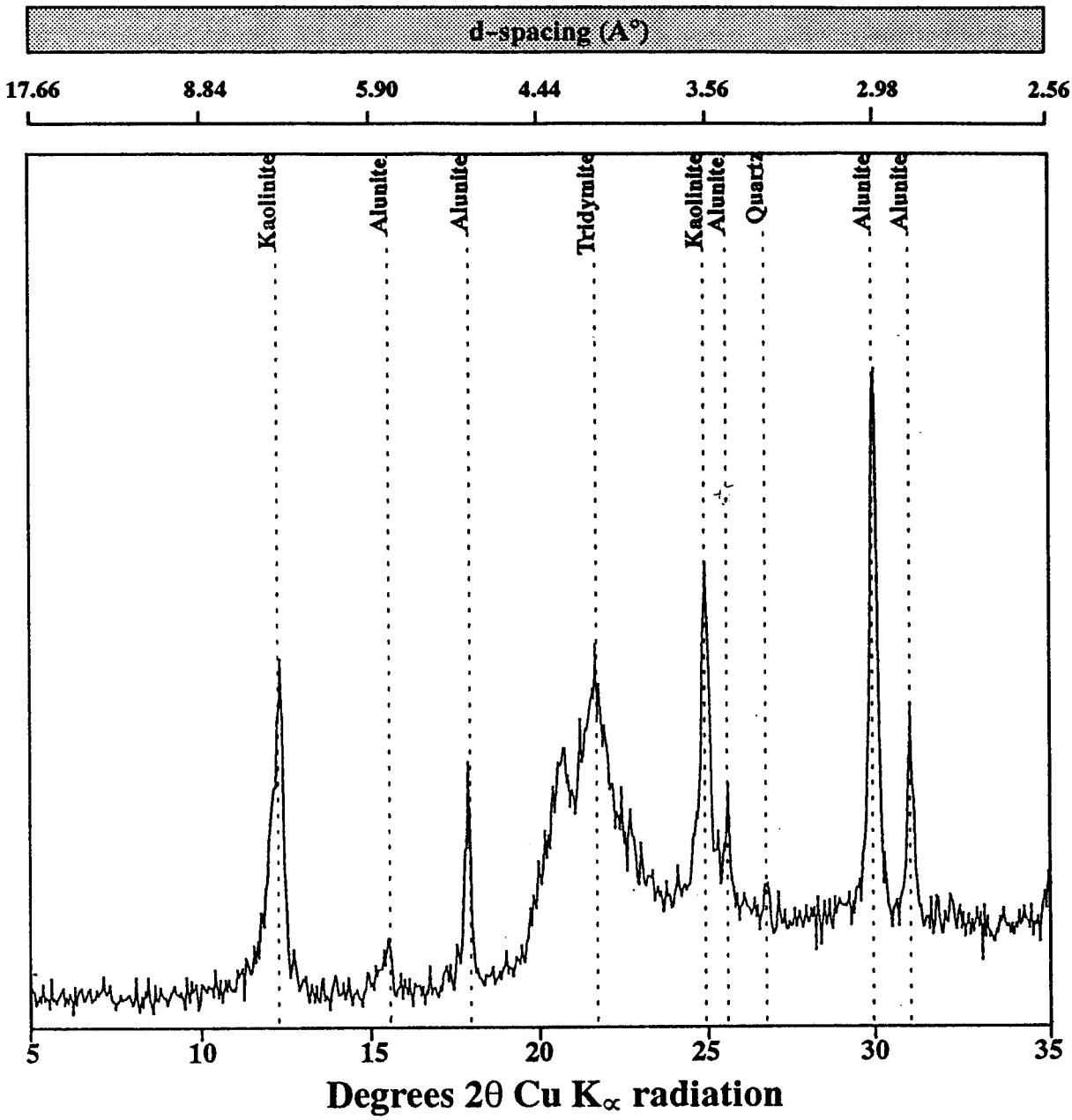

Figure 64: X-ray diffractogram of oriented <2μm fraction showing the minerals in sample 2Tkm 5 of the Kline Mountain kaolin deposit.

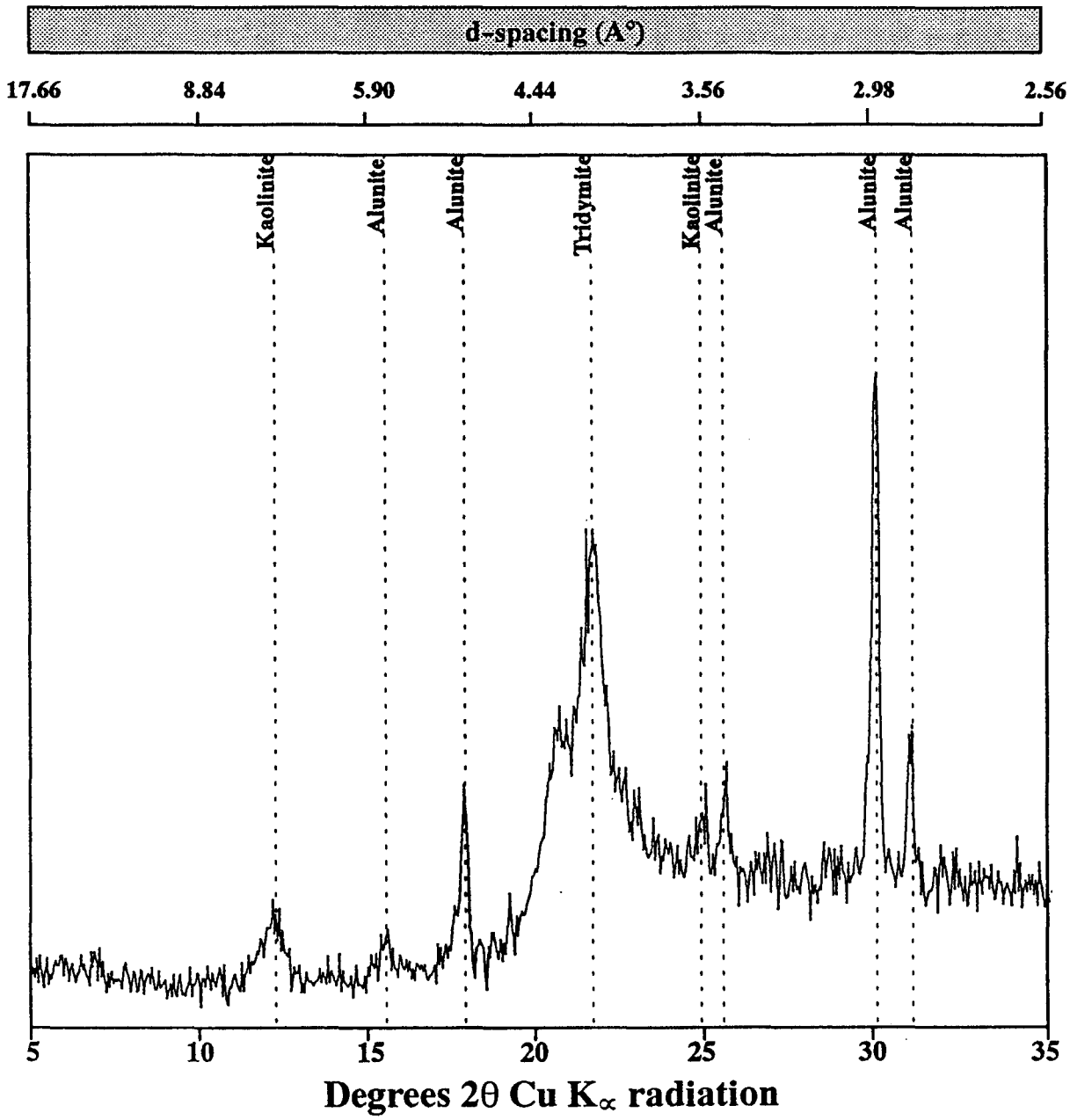

Figure 65: X-ray diffractogram of oriented <2μm fraction showing the minerals in sample 3Tkm 1 of the Kline Mountain kaolin deposit.

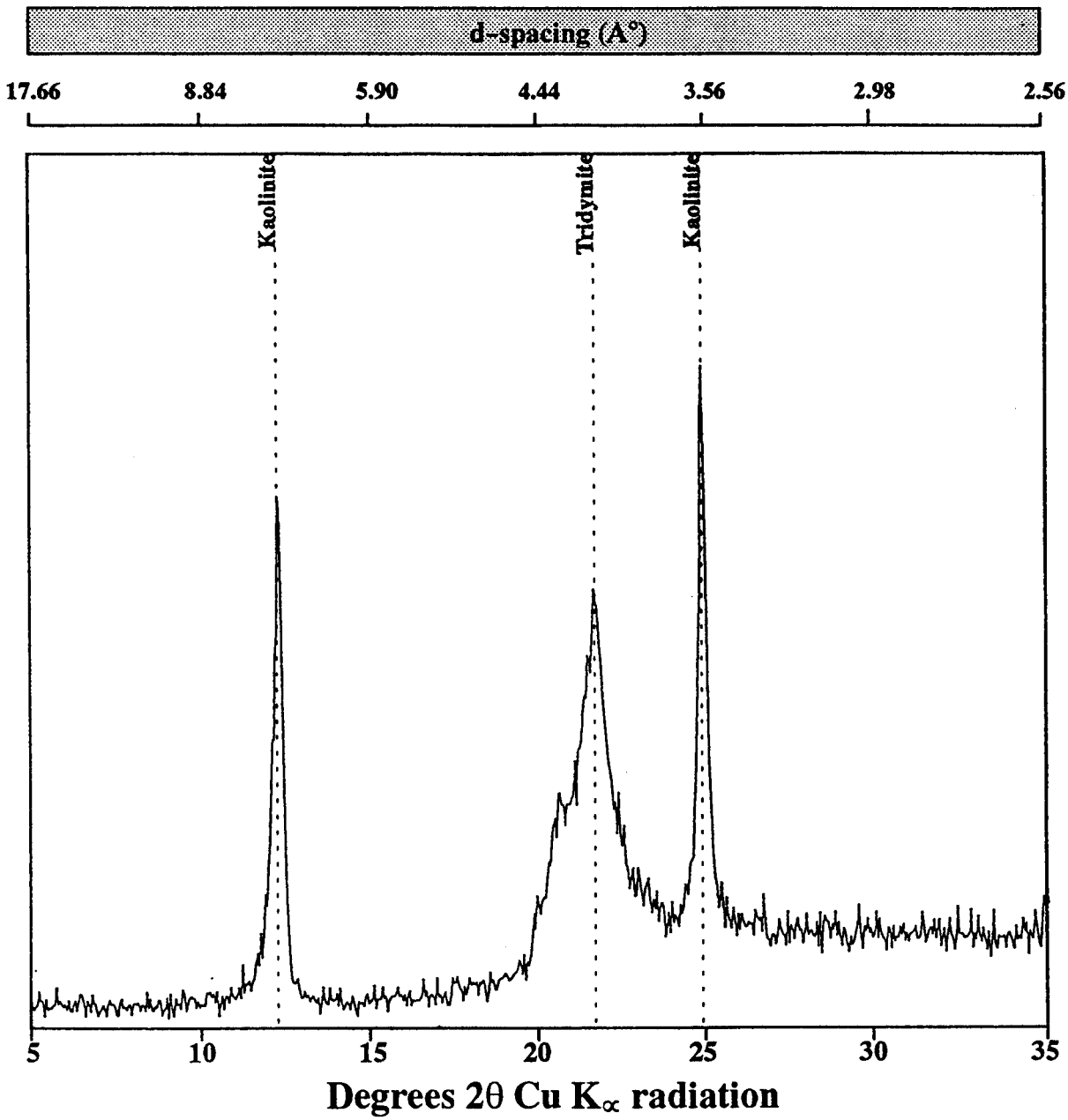

Figure 66: X-ray diffractogram of oriented <2μm fraction showing the minerals in sample 3Tkm 5 of the Kline Mountain kaolin deposit.

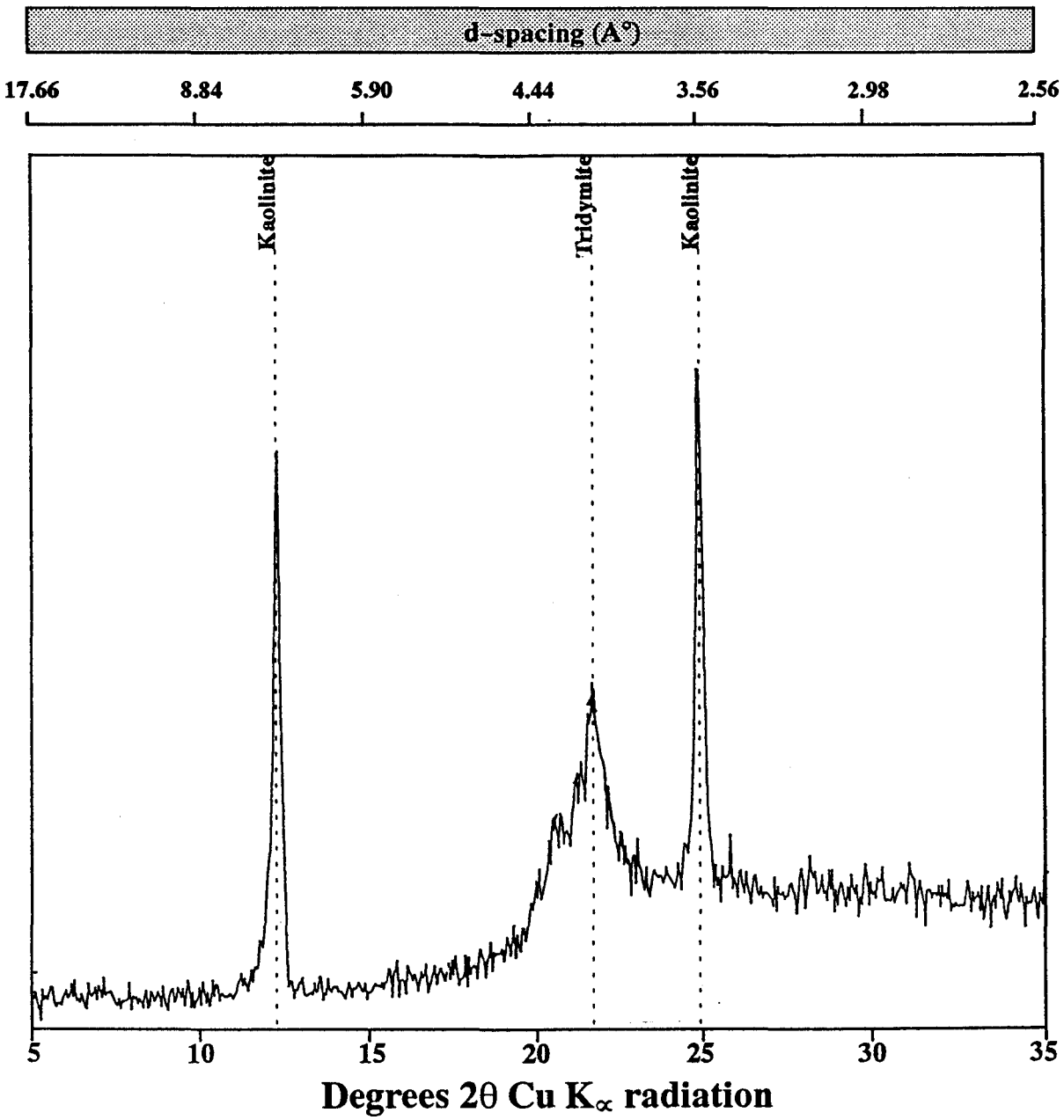

Figure 67: X-ray diffractogram of oriented <2μm fraction showing the minerals in sample Tkm 8 of the Kline Mountain kaolin deposit.

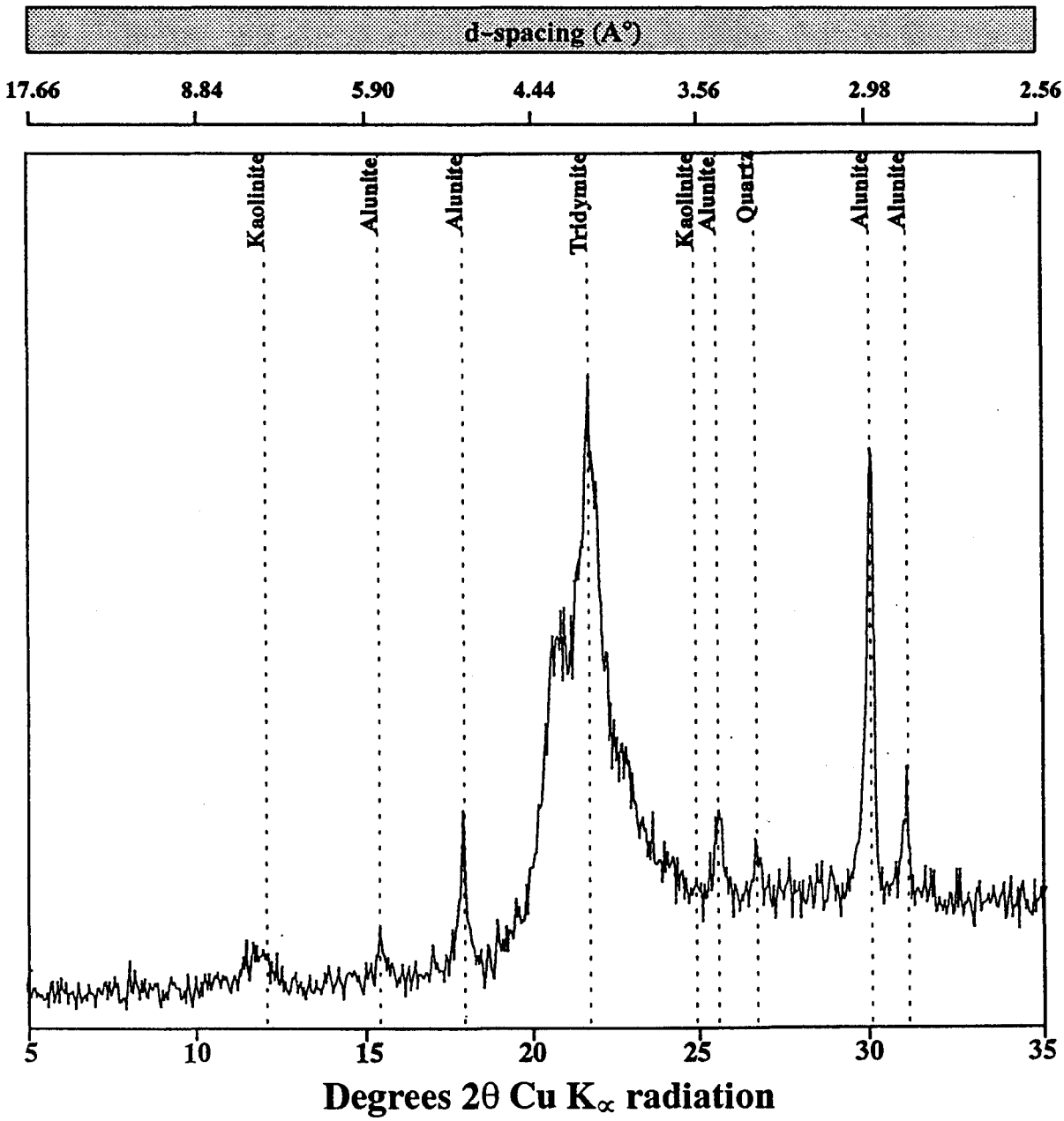

Figure 68: X-ray diffractogram of oriented <2μm fraction showing the minerals in sample S7 of the Kline Mountain kaolin deposit.

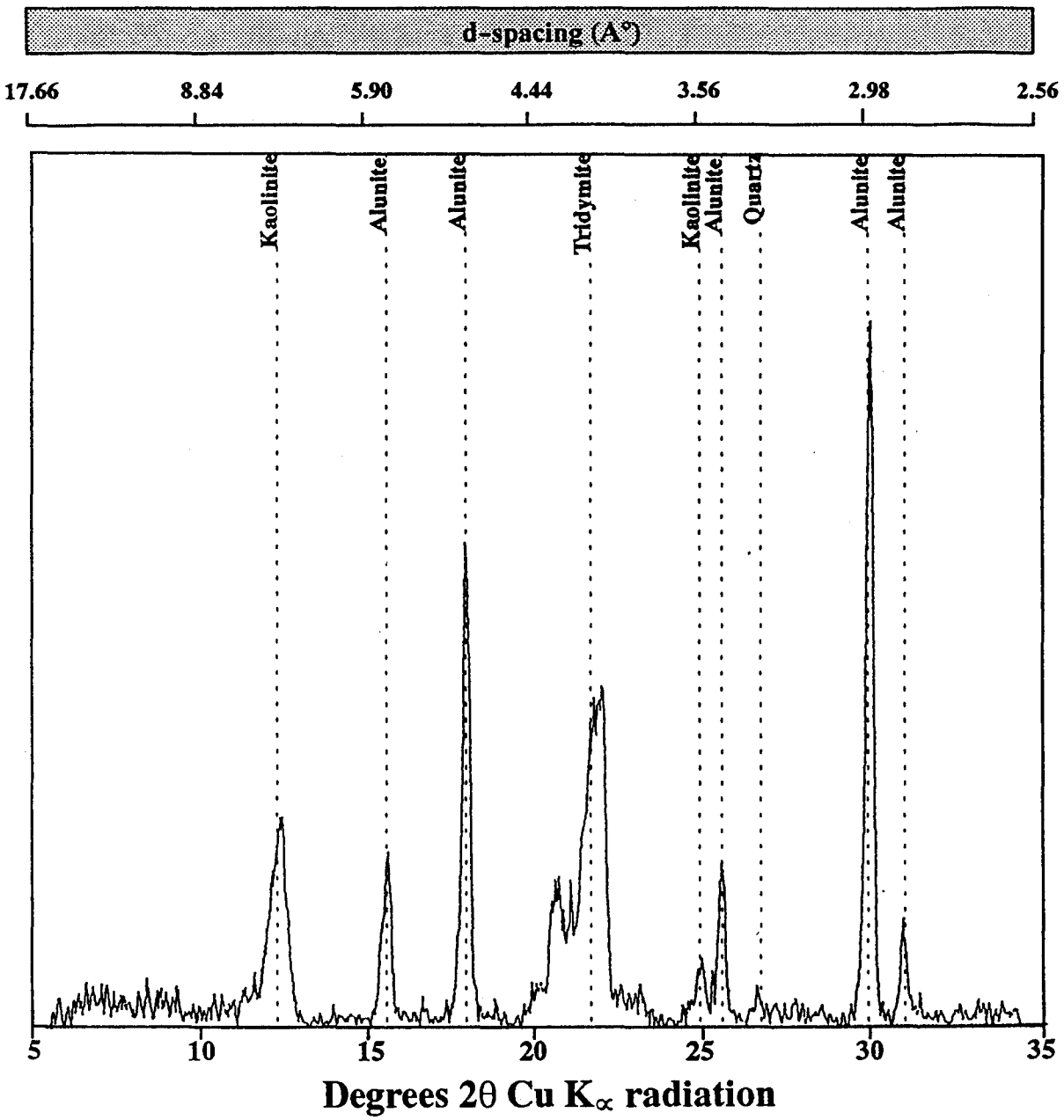

Figure 69: X-ray diffractogram of oriented <2μm fraction showing the minerals in sample S8 of the Kline Mountain kaolin deposit.

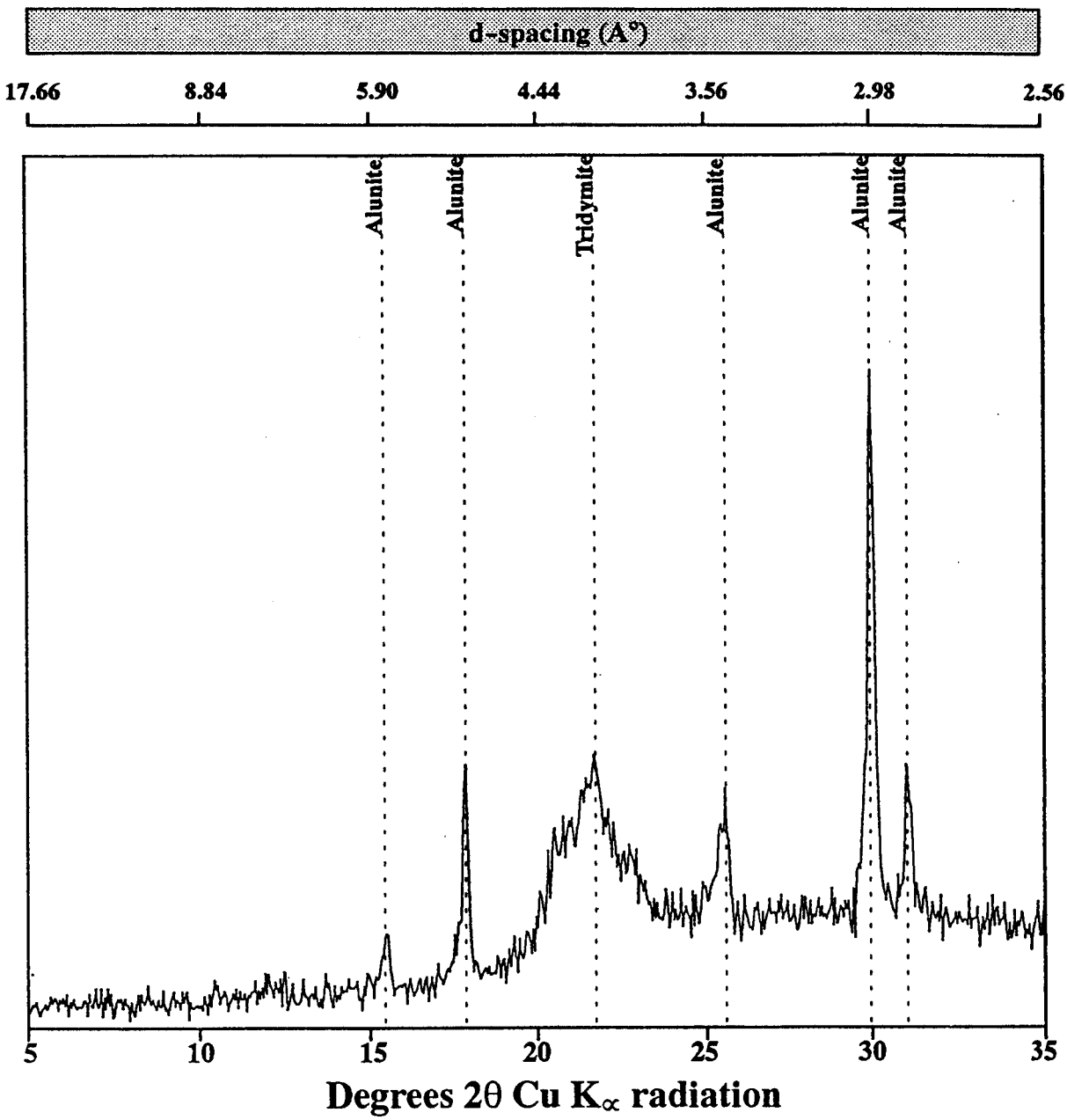

Figure 70: X-ray diffractogram of oriented <2μm fraction showing the minerals in sample Tkm 18 of the Kline Mountain kaolin deposit.

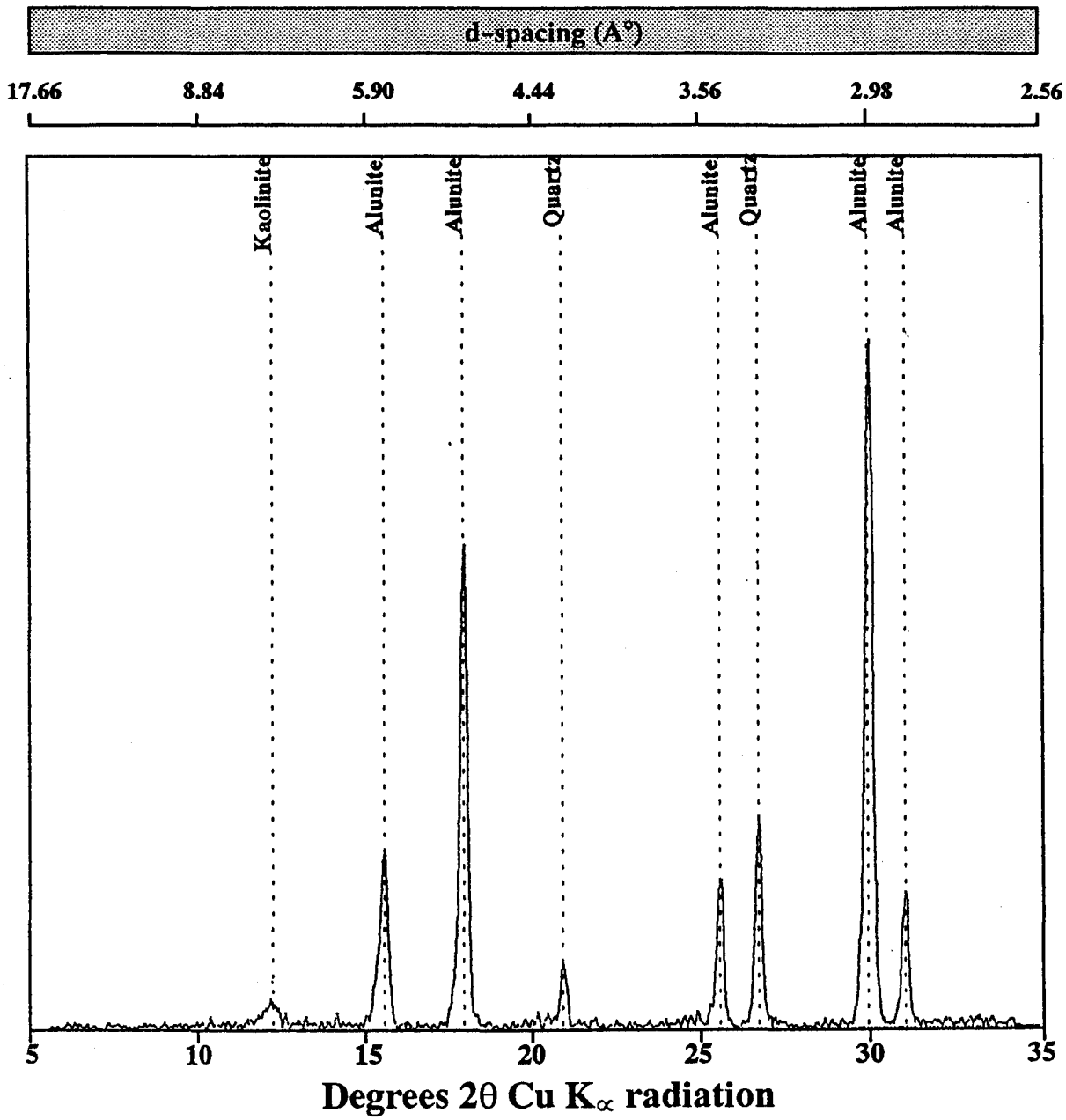

Figure 71: X-ray diffractogram of oriented <2μm fraction showing the minerals in sample Tkm 20 of the Kline Mountain kaolin deposit.

5.3.3. Scanning Electron Microscope (SEM) Photomicrography

SEM photomicrographs of three outcrop samples show different varieties of kaolinite textures: columnar covered by very fine silica silcretes, and well–crystallized, relatively poorly crystallized, and stacks. Kaolinite images in the sample of CS 200 contain kaolinite crystals covered by the clay–size silcretes (Figure 72) as indicated by qualitative EDS analysis in Table 6. The clay fraction is a mixture of kaolinite, alunite, and tridymite on the basis of X–ray diffractogram data in Figure 58. In the scanning electron micrograph of the clay (Figure 72), plates of kaolinite show columnar morphology. The kaolinitic clay of sample 3Tkm 5 contains pseudohexagonal plates of well–developed kaolinite crystals in the SEM photomicrograph associated with possible silica lepispheres (Figure 73). The photomicrograph in Figure 73 displays the typical texture of kaolinite at the indicated scale bar, which is 1.87 μm in length. A portion of it is magnified to about 60 % more in Figure 74 showing the loosely packed kaolinite flakes. Similarly, the SEM photomicrograph of sample 2Tkm 5 demonstrates more or less the same textures as 3Tkm 5, with the exception of its relatively poor crystallinity in some kaolinite flakes and stacks of kaolinite (Figure 75). A portion of Figure 75 is enlarged to about 40 % more in Figure 76, showing the pseudohexagonal packed kaolinite flakes associated with poorly crystalline kaolinite flakes and possibly some lepispheres. These SEM photomicrographs of the kaolinitic clay samples demonstrate the variability of kaolinite crystallinity, plus silica overgrowths. Another kaolinitic clay sample of 2Tkm 5 displays relatively poor crystallinity in some kaolinite particles (Figure 77), as evidenced by qualitative EDS analysis in Figure 78 and Table 7. These flakes of kaolinite are small to moderate in size.

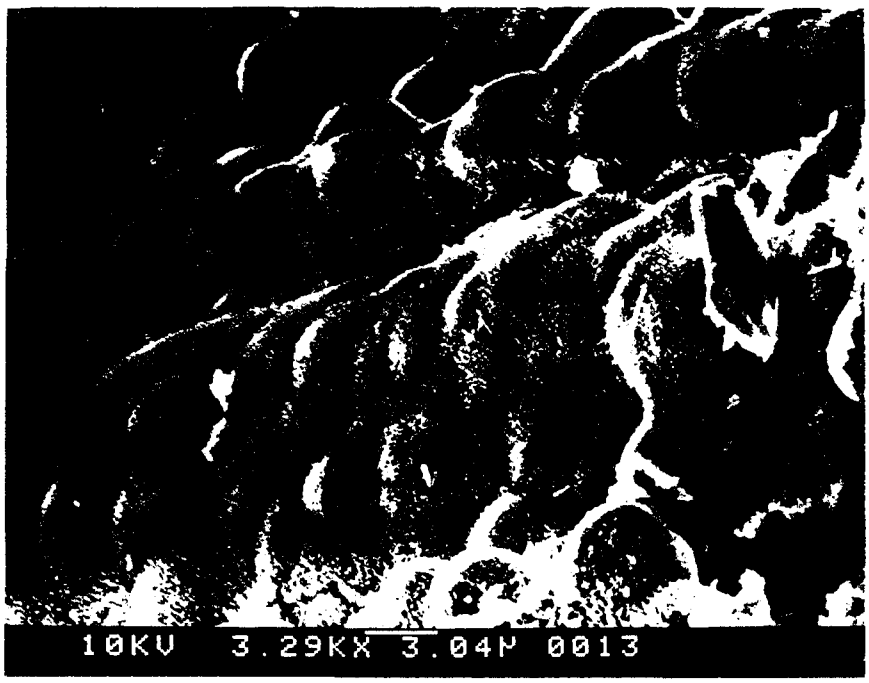

Figure 72: Scanning electron micrograph of the highly silicified clay particles within sample CS 200 demonstrating columnar kaolinite flakes covered by silcretes. See Table 6 below for the weight and atomic percentages of the elements in the image (Scale bar=3.04 μm).

Table 6: The weight and atomic percentages of the elements by energy dispersive X-ray spectra of highly silicified clay particles shown in Figure 72 indicating kaolinite.

ELEMENT	RELATIVE K	WT %	ATOMIC %
Al	0.1252	12.42	12.88
Si	0.7644	87.02	86.68
S	0.0016	0.28	0.24
K	0.0023	0.29	0.20
Total		100.00	100.00

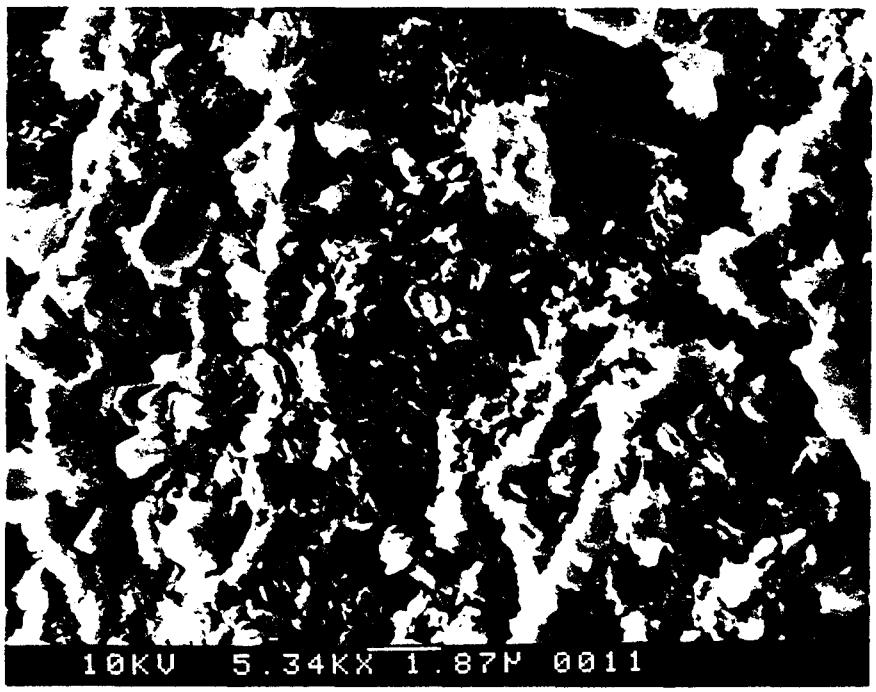

Figure 73: Scanning electron micrograph of well–crystallized kaolinites within the sample 3Tkm 5 displaying high clay crystallinity and silica lepispheres (Scale bar=1.87 μm).

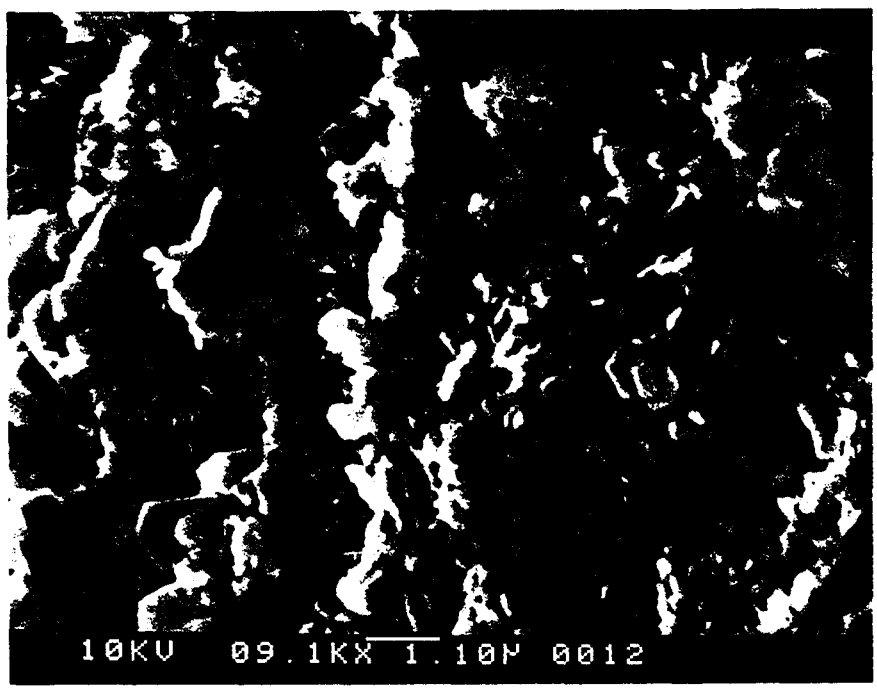

Figure 74: Enlargement of sample in Figure 73 (Scale bar=1.10 μm).

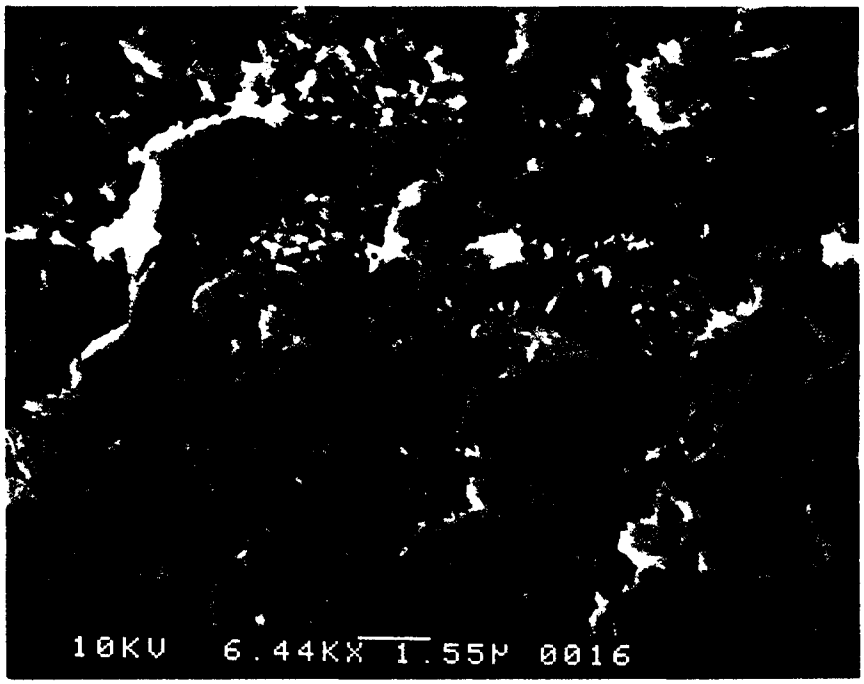

Figure 75: Scanning electron micrograph of kaolinite flakes within the sample 2Tkm 5 showing stacks of well-developed kaolinites (Scale bar=1.55 µm).

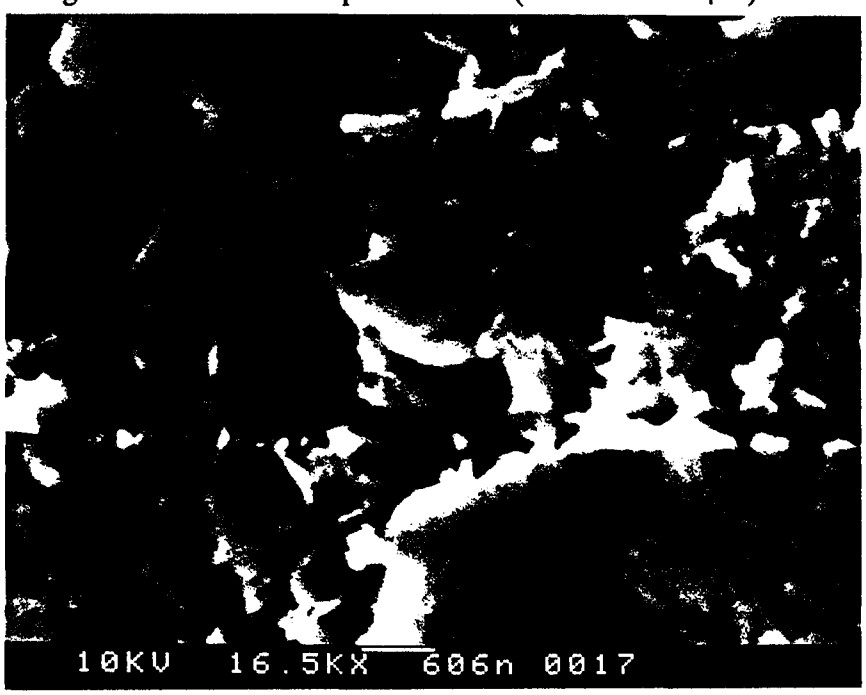

Figure 76: Enlargement of sample in Figure 75 (Scale bar=0.606 µm).

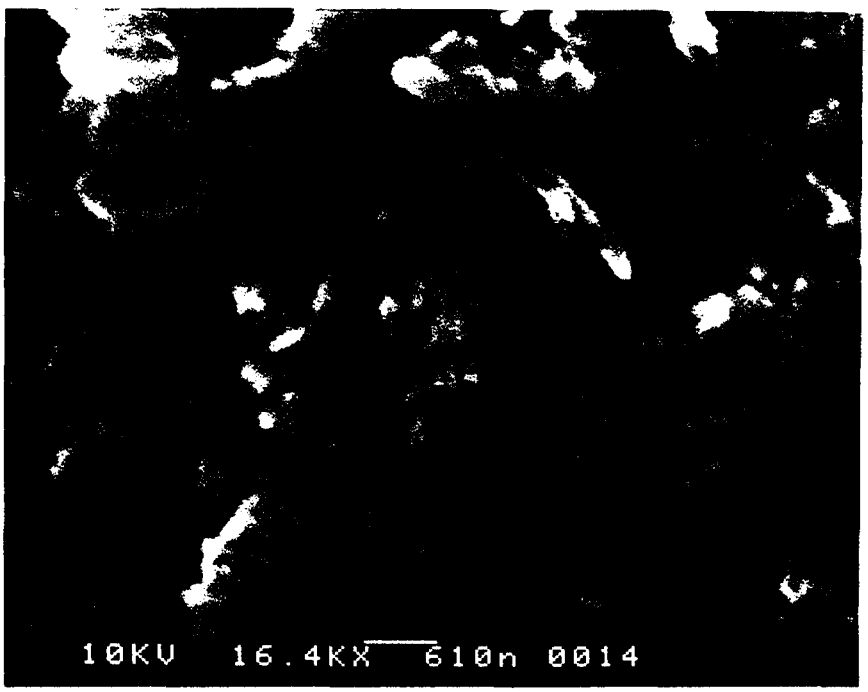

Figure 77: Scanning electron micrograph of kaolinites within the sample 2Tkm5 demonstrating the clay crystallinity. See Figure 78 and Table 7 for energy dispersive X-ray spectra of the indicated kaolinite flake in center (Scale bar=0.610 μm).

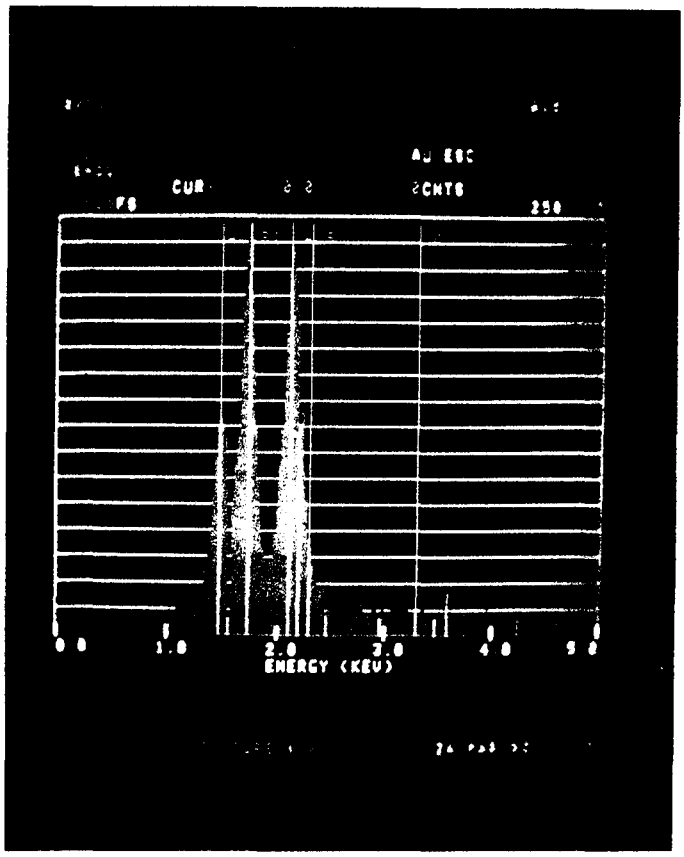

Figure 78: Energy dispersive X-ray spectra of the clay particles shown in Figure 77. Note the Si/Al ratio. The Au is due to the process of coating which gives also a false S content. See Table 7 for the weight and atomic percentages of the elements.

Table 7: The weight and atomic percentage of the elements by energy dispersive X-ray spectra of clay particles shown in Figure 77 and 78 indicating kaolinite.

ELEMENT	RELATIVE K	WT %	ATOMIC %
Al	0.2452	25.21	26.51
Si	0.4477	58.46	59.05
S	0.1058	16.31	14.43
K	0.0001	0.01	0.01
Total		100.00	100.00

As previously stated, the fine-size silica content was reported as a major drawback for this kaolin deposit to be utilized in the paper industry. Even though all the SEM micrographs demonstrate evidence for fine-size silica content (lepispheres), SEM photomicrograph of sample SM 200 in Figure 79 displays strikingly these fine-size silica textures with high porosity associated with alunite flakes. Energy-dispersive spectroscopy indicates aggregates of bladed crystals composed of individual lepispheres consisting dominantly of silica minerals (tridymite and/or cristobalite), which is believed to be formed as a result of precipitation related with groundwater. These minerals are presumed to be tridymite and/or cristobalite, based on X-ray characterization, and X-ray fluorescence data conducted during a preliminary study (Isik, 1990), and comparison with scanning-electron micrographs of Meyer and Reis (1985), Welton (1984), and Scholle (1979).

Figures 80 through 82 show SEM images of alunite which demonstrate identical crystal forms and flakes within the typical texture. The EDS analysis of the flake in Figure 80 and the crystals in Figure 81 and 82 are composed of Al, K, and S (Table 8, 9 and 10). This indicates that the flake and the crystals are alunite and are consistent with the observation of the close association of alunite and silica (tridymite and/or cristobalite) from the XRD results (Table 4 and Figures 33, 41 and 48). The SEM images show that alunite crystals are hexagonal and pseudo-rhombohedral associated with bladed silica crystals, which are intergrown to form lepispheres. In Figure 81 and 82, SEM alunite crystal photomicrographs demonstrate well-developed and tightly packed textures.

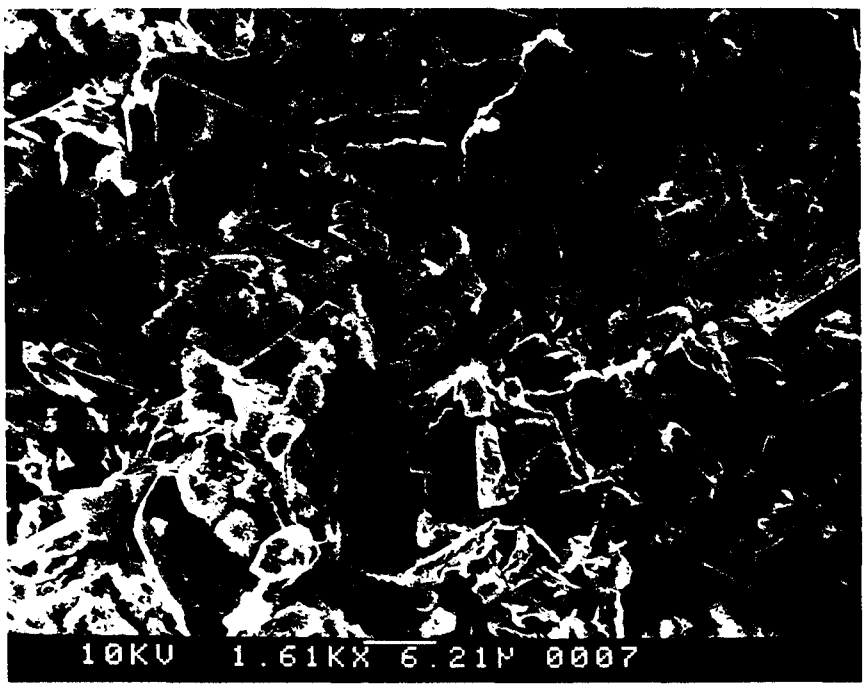

Figure 79: Alunite crystals and silica lepispheres within the sample SM 200, as seen by scanning electron microscopy. Note the fine grain sizes of the silica lepispheres. Large angular flakes are examples of alunite (Scale bar=6.21 μm).

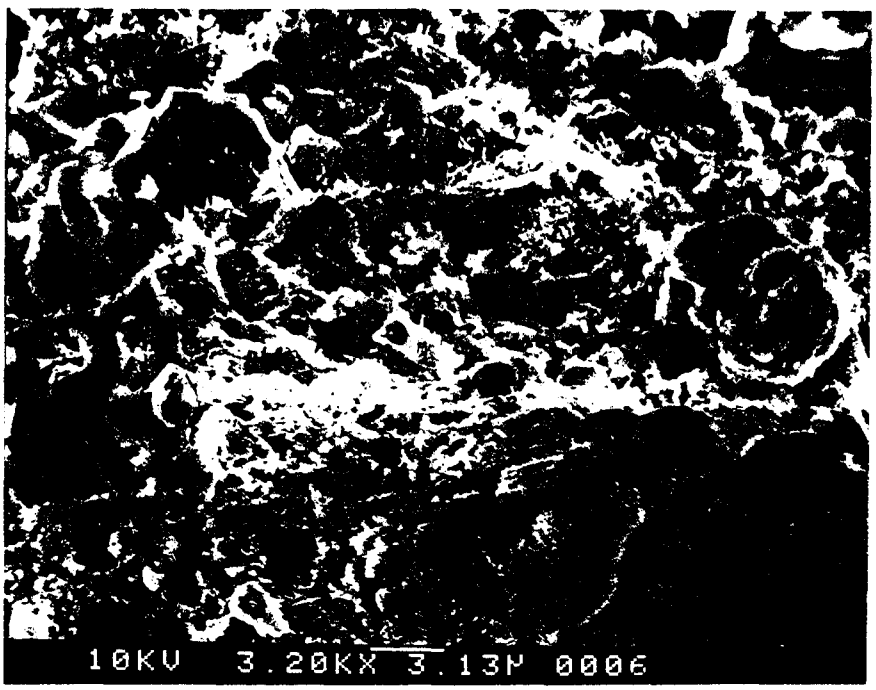

Figure 80: Alunite crystal (hexagonal) and silica lepispheres within the sample SM 200, as seen by scanning electron microscopy. See Table 8 below for the weight and atomic percentages of the elements in the marked alunite flake (Scale bar=3.13 μm).

Table 8: The weight and atomic percentages of the elements by energy dispersive X-ray spectra of alunite flake shown in Figure 80.

ELEMENT	RELATIVE K	WT %	ATOMIC %
Al	0.3586	38.87	42.82
Si	0.0900	13.54	14.32
S	0.3123	40.09	37.16
K	0.0597	7.50	5.70
Total		100.00	100.00

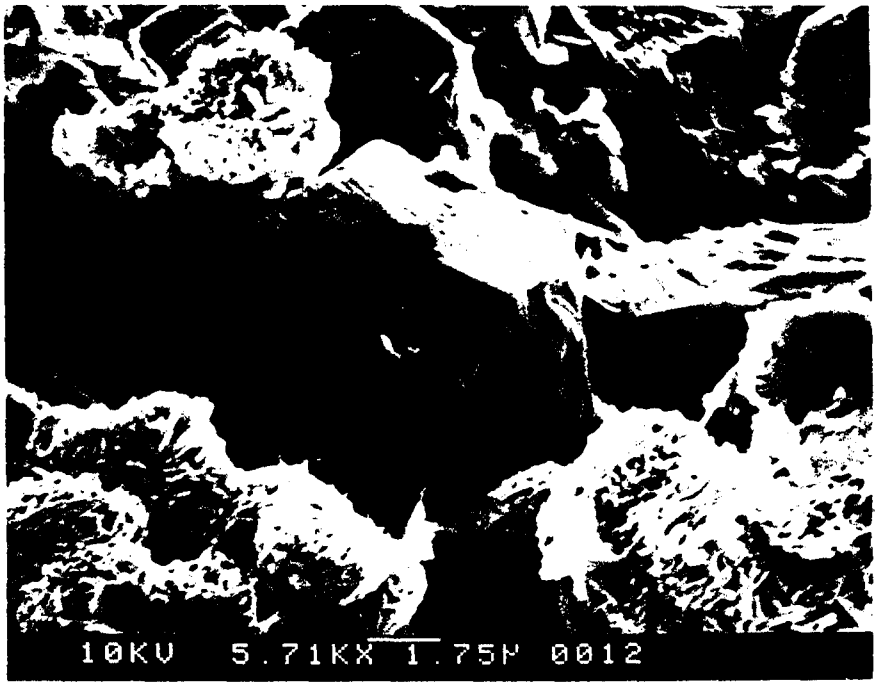

Figure 81: Well-developed alunite crystal within the sample 3Tkm 1 with characteristic hexagonal face (Scale bar=1.75 μm).

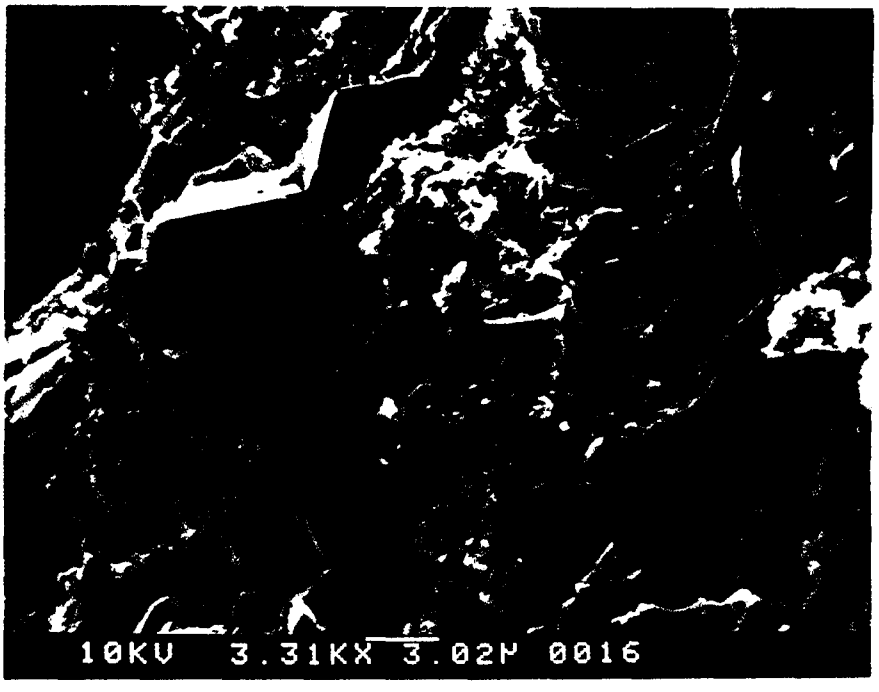

Figure 82: Scanning electron micrograph of alunite crystals within the sample Tkm 18 demonstrating characteristic hexagonal and rhombohedral faces. See Table 9 and 10 for the weight and atomic percentages of the contained elements for the alunite crystals (Scale bar=3.02 μm).

Table 9: The weight and atomic percentages of the elements by energy dispersive X-ray spectra of large hexagonal alunite crystals shown in the upper left part of Figure 82.

ELEMENT	RELATIVE K	WT %	ATOMIC %
Al	0.2090	22.11	23.90
Si	0.3866	49.41	51.30
S	0.1496	21.75	19.78
K	0.0537	6.73	5.02
Total		100.00	100.00

Table 10: The weight and atomic percentages of the elements by energy dispersive X-ray spectra of rhombohedral alunite crystals shown in Figure 82. The end of these crystals appear as laths in the lower central part of the SEM image.

ELEMENT	RELATIVE K	WT %	ATOMIC %
Al	0.4083	44.75	49.70
Si	0.0378	6.01	6.41
S	0.2900	36.57	34.18
K	0.1027	12.67	9.71
Total		100.00	100.00

CHAPTER 6
PHYSICAL AND STRUCTURAL PROPERTIES OF KLINE MOUNTAIN KAOLIN

In making brick, physical properties of clay play a more important role than its chemical properties. In addition to a sufficient reserve of clay deposit to be considered as a structural clay for the brick industry, the physical properties are principally: particle size, plasticity (to be molded easily into brick shape), green strength (to retain that shape in both wet and dry states), and firing temperature (to form hard brick without excessive deformation at temperature of 1745 °F–2015 °F by sufficient vitrification). In fired brick, they are: compressive strength, firing color, and water absorption.

According to DeVilliers (1962 a,b,c), a sample of a refined clay was found to have a very high Standard Brightness of 93.9%, an abrasion loss of only 11 mg. wire*, low moisture content, and very easily dispersed by 1 mili- equivalent of sodium hydroxide per 100 grams of the clay to bring the pH to 7.0 or above. He concluded that this clay has good possibilities in the coating field. In his further study, he reported that the coating had high values for smoothness, gloss, and glare. However, the brightness value and bonding strength of the refined clay were the characteristics considered to be most attractive.

*: "The Valley abrasion tester has been designed to simulate the wear which occurs in the paper machine wires, and has been widely used in evaluating the relative abrasiveness of different pigments. The device consists of a perforated composition block (Micarta) which rests on a weighed piece of 70 by 48–mesh bronze screen. A slurry containing 100 grams of the test pigment in 3200 ml. of water is continuously circulated through the perforated block as it moves back and forth across the screen 6000 times in 70 minutes. At the end of the run the wire is reweighed and the weight of the wire abraded away is determined by difference. Abrasion values below 20 mg. are considered to be acceptable for either filler–or–coating–grade pigments. Values from 20 to 60 mg. are borderline cases and values above 60 mg. are not considered commercially acceptable" (Sallee, 1962).

In contrast, Sallee (1962) stated that the clay sample was difficult to disperse due to the preparation, which had been flocculated with acid and not adequately washed. Thus, he added that the true characteristic of the particle size was uncertain. However, he concluded that the mineral was good quality kaolinite with a standard brightness of 87.7%, an abrasion loss of only 12 mg. wire, and low grit content.

6.1. Particle Size

The purpose of particle size measurements is to determine the percentages of clay-sized particles, silt-sized particles, and sand-sized particles in the raw, unfired samples. The particle size distribution is a most important factor with both filling and coating materials. The brick industry uses a large amount of relatively coarse material. The use of fine, coarse, and well-distributed particles have advantages and disadvantages in regard to producing a more vitreous and homogenous ceramic body. Tichane (1990) reported that particle size manipulation is one of the important factors which enables evaluation and improvement of strength of ceramic body without any defect such as high shrinkage, distortion, and low plasticity. Also, Grimshaw (1971) reported the finess of particle size as a main factor influencing the dry strength of a clay body.

The clay particles are very small (<2 μm) and occur mostly in form of plates and rods, and rarely spherical which make determination of clay particle size a complex problem with respect to Stoke's Law. Grimshaw (1971, pp. 373-374) reported several other difficulties in clay particle size analysis, which essentially lies in the existence of extremely fine portions (< 0.5 μm) and also in breaking down the harder types of clays to their real particle size etc.

Consequently, it should always be remembered that the methods of clay particle size measurements are not fully satisfactory nor desirable procedures at least from the academic stand point (Klinefelter and Hamlin, 1957) because of the physical properties of clays as well as their behavior when treated with water and chemicals.

Grimshaw (1971) has classified the particle size measurements using three methods: geometric symmetry, hydrodynamic symmetry, and surface area measurement, each of which has its limits in terms of a certain range of size suitability and interpretation. Electron microscopy and electrically induced birefringence are also recommended methods by Dixon and Weed (1989) for clay particle size measurement.

6.1.1. Samples

In order to represent the Kline Mountain clay deposit size distribution vertically and horizontally, five surface and three core samples are analyzed. Four of the surface samples (SM 200, CS 200, Tkm 2, and 3Tkm 3) are kaolinitic clay taken from two open pits and their vicinity, while the other (Tkm 18) was secured from alunitic clay close to the intrusion. The drill core samples (R5–I, R5–IV, and R5–VI) belong to the kaolinization zone of the tuff of Kline Mountain (see Figure 16, for the depth of the drill core samples).

6.1.2. Methods of Investigation

Even though numerous procedures exist, the method used by the New Mexico Bureau of Mines and Mineral Resources was employed for determining the percentages of clay–size, silt–size, and sand–size particles (Brickell, 1989). This analysis incorporates

sieve analysis for the sand-and-larger-(sand+) and silt-size particles and the pipette method for the clay-size fraction. Sieve analysis is one of the quickest and simplest, most widely used method of particle size analysis. In the pipette method of particle size analysis, the concentration changes that occur within a settling suspension are followed by drawing off definite volumes by means of a pipette.

For this analysis, the equipment used are: a 1000 ml beaker, two 80 ml beakers, a number 230 sieve, a large pan, a glass pipette, an oven, a desiccator, and a balance. The procedure of particle size measurement is explained in Appendix 2.

6.1.3. Results

The grain size distribution is listed in Table 11 as a percent of sand-size and greater (>63 μm), silt-size (63-2 μm), and clay-size (<2 μm). For most of the samples, the majority of the material is clay-sized, followed by sand^{+}-sized, then silt-sized particles. Material compositions, based on grain-size, are plotted on a sand-silt-clay ternary diagram in Figure 83 for visual demonstration and relation of the particle size distribution among the samples.

Particle-size analyses show that R5-I (drill core), which includes silica (tridymite, quartz, and cristobalite), kaolinite, and alunite, has the highest percentage of clay-size particles. With the exception of alunitic clay (Tkm 18), there is a proportional relation between kaolinitic content percentages (Table 3) and clay-size fraction percentages of kaolinitic surface samples (Table 11 and Figure 83). Higher clay-size fractions in some samples indicate larger amounts of kaolinite (Table 3). The two open pit samples, SM 200 and CS 200, show more sand-size fraction than the other samples. For the samples of the drill core, the majority

of the material is clay-sized, followed by silt-sized, then sand$^+$-sized particles. On the other hand, two kaolinitic surface samples (Tkm 2 and 3Tkm 3) carry clay-sized particles as a principal dominant fraction. The alunitic clay sample Tkm 18 demonstrates that the silt-sized fraction as the chief constituent. The open pit mine sample SM 200 contains the least percentage of the clay-sized fraction, while the shallowest drill core sample R5-I contains the least percentage of sand+ sized fraction.

Table 11: Grain-size distribution of Kline Mountain clay.

SAMPLE	SAND+ >63 μ (%)	SILT 63−2 μ (%)	CLAY <2 μ (%)
R5−I	1	37	62
R5−IV	17	38	45
R5−VI	11	44	45
SM 200	46	26	28
CS 200	45	22	33
Tkm 2	16	30	54
3Tkm 3	33	27	40
Tkm 18	18	49	33

R5 is number of core

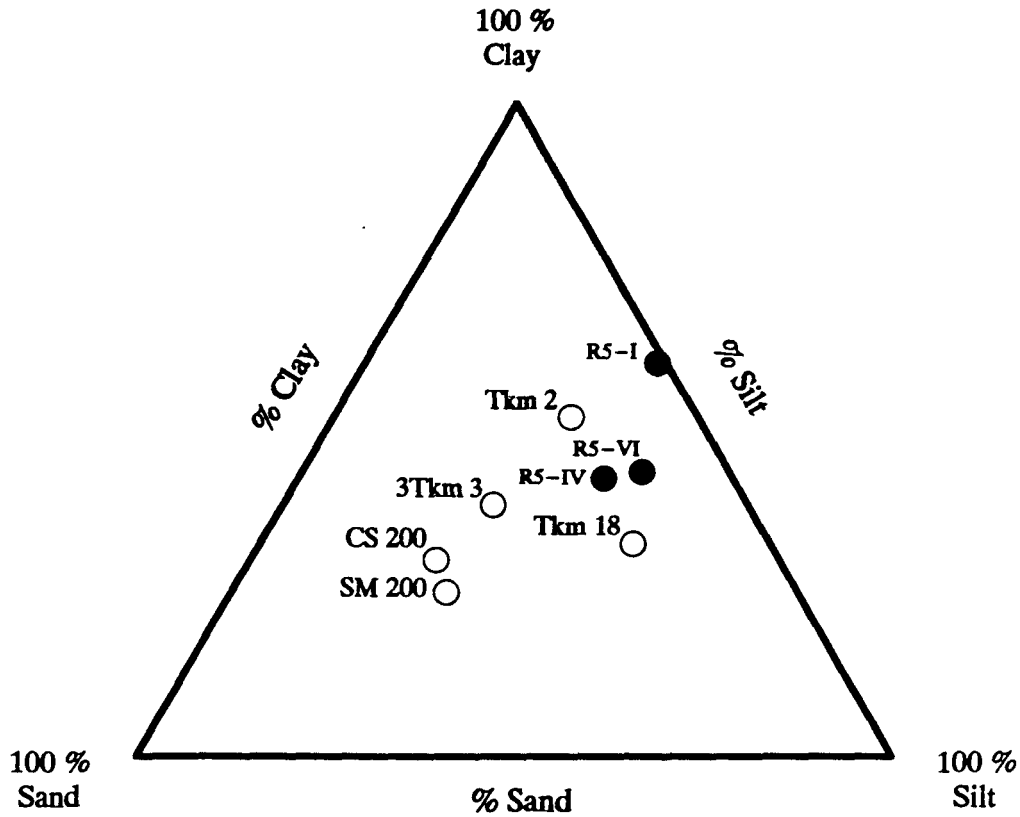

Figure 83: Ternary diagram showing sand-silt-clay size distribution of the samples. The filled circles (●) designate drill core samples, while the others (○) designate surface samples.

6.2. Clay Firing Experiments

A ceramic body is an aggregate of crystals and glass and can be considered a grouping of loose crystals cemented together by a glassy matrix, which can be obtained by firing. Thus, the firing process is one of the most important parts of making any kind of a ceramic body. After methodical firing, one can draw many important conclusions about the ceramic body, such as vitrification temperature, firing color, fusion temperature, and compressive strength. Various firing temperatures conducted on the same clay can produce different ceramic properties until a fusion forms which destroys the usefulness of the ceramic article. It is very important for a ceramic body to be fired at a specific temperature so that a desirable ceramic product can be obtained without any defects such as fusion deformation, undesirable color or weak compressive strength.

The purpose of these experiments is to determine: (1) firing color, (2) compressive strength, and (3) water absorption of experimental ceramic brick with or without fluxing agents. In addition to the above stated objectives, workability, green strength, and molding properties of the mixes are also observed as other important required properties for making brick and will be discussed later.

A good drying cycle to remove free water from the molded ceramic body is the first important step in a firing process. The drying process begins when the green–ware, for example brick, is exposed to the atmosphere. Most of the molding process in ceramics, including brick, is performed with bodies containing up to 30 % or more of water to facilitate extruding and binding properties. Prior to firing, all of the hygroscopic water must be re-

moved, as the firing in the kilns takes place so fast that the hygroscopic water contained in the green-ware would evaporate too quickly, and develop vapor pressures which would disintegrate the body or would otherwise cause damages due to the water expanding explosively.

Flux is a substance that is added to a clay body to enable it to fuse more readily and for strength. In ceramics, including the brick industry, fluxes are incorporated into the clay bodies in order to lower the temperature at which fusion begins during firing. This liquid, when cooled, forms a glass which binds the grains of the body together. By means of fluxes, a strong ceramic body can be produced at lower temperature and at a lower cost.

Vitrification varies and depends primarily on the nature and amount of fluxes present in a ceramic body. The most effective fluxes are materials rich in alkali oxides–Na_2O, K_2O or Li_2O. Calcium and magnesium oxides also act as fluxes. Cost and availability are the main factors that influence the choice of fluxing materials; hence, naturally occurring minerals that contain the above oxides are preferred to pure chemicals.

6.2.1. Samples

For this study, 200 kg of sample CS 200 was recovered from the abandoned pit to be utilized. The calculated mineral content of this sample is kaolinite (33.47 %), alunite (13.41 %), silica (47.95 %), and accessory minerals (0.77 %). Table 11 displays the grain-size distribution of the sample.

Fluxing agents used in this study were nepheline syenite, calcined talc, salt (NaCl), $CaCl_2$, hydrated lime ($Ca(OH)_2$), and #3 clay (Anapra Shale) of the American Eagle Brick Company. With the exception of calcined talc, all of them were provided by Dr. George F.

Cudahy, the President of the American Eagle Brick Company. Ntsimanyana (1990a) reported that the nepheline syenite, $(Na, K)_2O.Al_2O_3.2SiO_2$, was provided by Allied Marketing Services of Austin, Texas, to American Eagle Brick Company (then El Paso Brick Company) for experimentation as a brick and tile mix component. He also stated that the Granite Mountain Quarries at Sweet Home, Arkansas, was the producer of the nepheline–syenite. Table 12 displays the chemical and mineralogical analysis of the nepheline syenite.

The calcined talc was obtained during the field trip in the Industrial Rocks and Minerals course (Geol. Sci. 3515) on November 22, 1992. Kyle and Clark (1990) reported that this ceramic–grade talc contains disseminated quartz and dolomite between 5 and 30 % by volume as accessory minerals.

The kaolin sample, CS 200, has been crushed by hammer and crusher followed by grinding in the Metallurgy Laboratory of the New Mexico Bureau of Mines and Mineral Resources. Then, 95 % of this ground sample has been sieved to -100 mesh (-150 μm) by repeated grinding of the +100 mesh particles after each sieving.

Nepheline syenite, calcined talc and #3 clay were crushed, ground and sieved to -35 mesh in the American Eagle Brick Plant prior to mixing as a fluxing agent. Factory produced salt (NaCl), $CaCl_2$, and hydrated lime was provided by the American Eagle Brick Company.

Table 12: Chemical and mineralogical analysis of the nepheline syenite used in the mixtures of firing experiments (Ntsimanyana, 1990a).

Chemical Analysis in Weight Percent (wt %)	
SiO_2	60.30
TiO_2	1.10
Al_2O_3	19.93
Fe_2O_3	4.67
MgO	1.19
CaO	1.27
Na_2O	6.25
K_2O	5.30
L.O.I.	0.11
Mineralogical Analysis in Approximate Modal Amounts (%)	
Alkali Feldspars	60
Nepheline	10
Hornblende	10
Diopside	5
Titanite	-
Apatite	15
Magnetite	combined
Biotite	total

6.2.2. Methods of Investigation

For the firing experiment, four different sets of samples were prepared. The first set was prepared without any additive fluxing agent, while the others were prepared with a certain amount of fluxing agents. Also, the laboratory extruder of American Eagle Brick Company was employed for the second set of the samples.

For the first set of experiments, 30 g. of ground kaolin were mixed with 14.5 g. water to make it plastic. Then, these "muddy" kaolin materials were molded by hand into four patties (1 through 4). These patties were left at room temperature for 12 hours. Afterwards, the patties were placed in an oven to be dried at 50 °C for about 6 hours. In order to determine if there was a vitrification without adding any flux to the clay, the patties were fired at different temperature by using the Standard Large Orton Pyrometric Equivalents (PCE) to observe the temperature (Figure 84). The PCE is a standard determination universally used to evaluate the refractoriness of both clays and refractory bodies. For the first two of these specimens (1 and 2), firing was conducted in the electric kiln (Figure 85), while the firing of the last two (3 and 4) was done in the gas kiln (Figure 86). Firing tests were performed as a fast-firing. Four firing temperatures, 1120 °C (2048 °F) for sample 1, 1162 °C (2124 °F) for sample 2, 1222 °C (2232 °F) for sample 3, and 1305 °C (2381 °F) for sample 4, were used for the first set of experiments. Large Standard Orton PCE Cones (04–02–6–10) was employed to control the temperatures, which correspond to those reported above. The numerical part of the PCE cones indicate certain fusion temperature for specified cones.

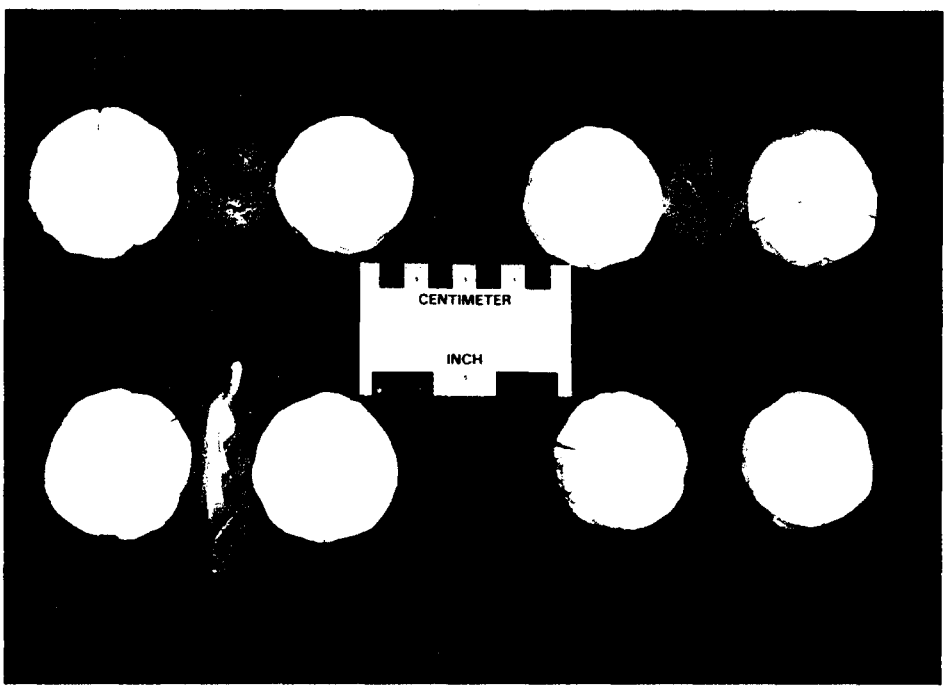

Figure 84: Fired brick specimens of the Kline Mountain kaolin showing the white fired specimen at different temperatures. The two in the left corner at the top are fired at 1120 °C (2048 °F); the two in the right corner at the top are fired at 1162 °C (2124 °F); the two in the left corner at bottom are fired at 1222 °C (2232 °F); and the two in the right corner at the bottom are fired at 1305 °C (2381 °F).

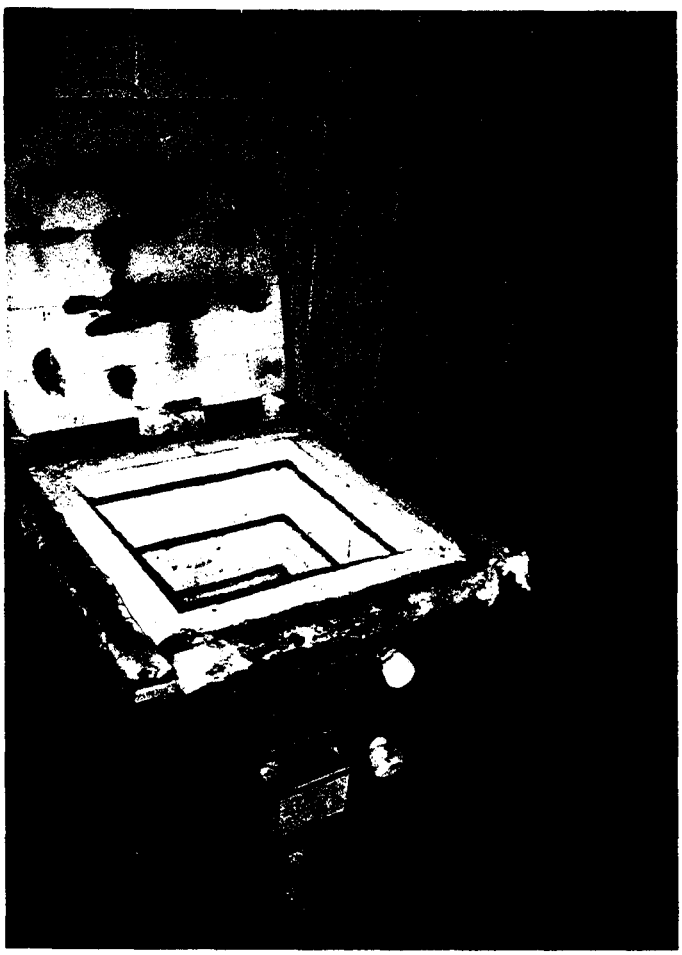

Figure 85: Electric kiln of El Paso Community College Art Studio used in the low temperature firing of the experimental brick.

Figure 86: Gas-fired kiln of El Paso Community College Art Studio used in the high temperature firing of the experimental brick.

In the second set of experiments, a 4.364 kg kaolin sample of CS 200 (91 %) was mixed with equal amounts of 218 g. (4.5 %) of nepheline syenite and white silica, respectively. The experimental mixtures were moistened with water for a workable plasticity to be extruded. In the following step, the laboratory extruder of the American Eagle Brick Company (Figure 87) was employed to make the brick. The mix was extruded with a very poor (almost no) vacuum because the vacuum system was inoperative. Then, the bricks were left under room conditions for 2 days (Figure 88). On the following day, they were placed in an oven at 65 °C for 2 hours, at 85 °C for 2 hours and at 105 °C for 2 hours. Next, they were fired at the Community College Art Studio's kiln (Figure 89) by employing large Orton Standard cones to monitor the temperatures. The second firing tests were conducted with the same method as the first firing test. Three firing temperatures, 1121 °C (2050 °F), 1190 °C (2175 °F), and 1288 °C (2350 °F), were employed for the nepheline syenite and white silica fluxing.

For the third set of experiments, eight specimens were prepared by using talc, NaCl, $CaCl_2$, Hydrated lime–$Ca(OH)_2$, and #3 clay (Anapra Formation) of the American Eagle Brick Company. Table 13 lists the amount of kaolin, fluxing agent and water utilized to make these specimens. The firing temperatures conducted for each specimen are also indicated. Samples numbered 01 through 04 were prepared by adding the indicated amount of talc to reported amounts of kaolin. Then, these patties were molded after plasticity was obtained by the reported amount of water, as shown in Table 13. For sample 05, 25 g of salt (NaCl) was mixed into 75 g of water. Then, it was stirred, and 20 g of this solution, which contained 5 g NaCl, was added to the clay. By adding given amounts of water for plasticity, it was molded by hand.

Figure 87: Laboratory extruder of American Eagle Brick Company used in the second set of experimental brick specimens.

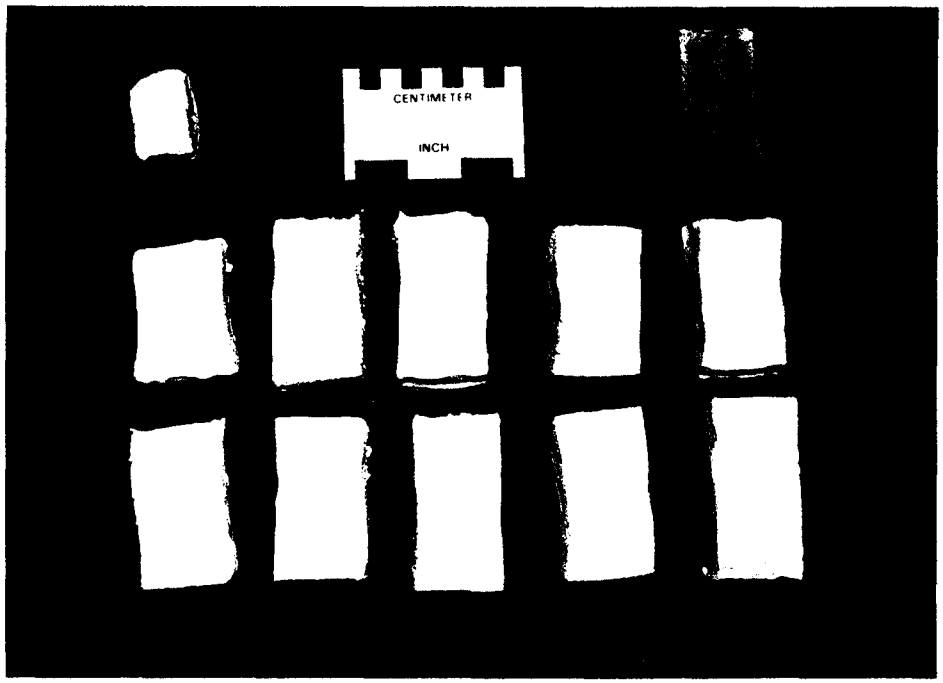

Figure 88: Unfired dried specimens of the extruded brick specimen showing green-ware brick body. The gray specimen at the right corner contains the #3 clay.

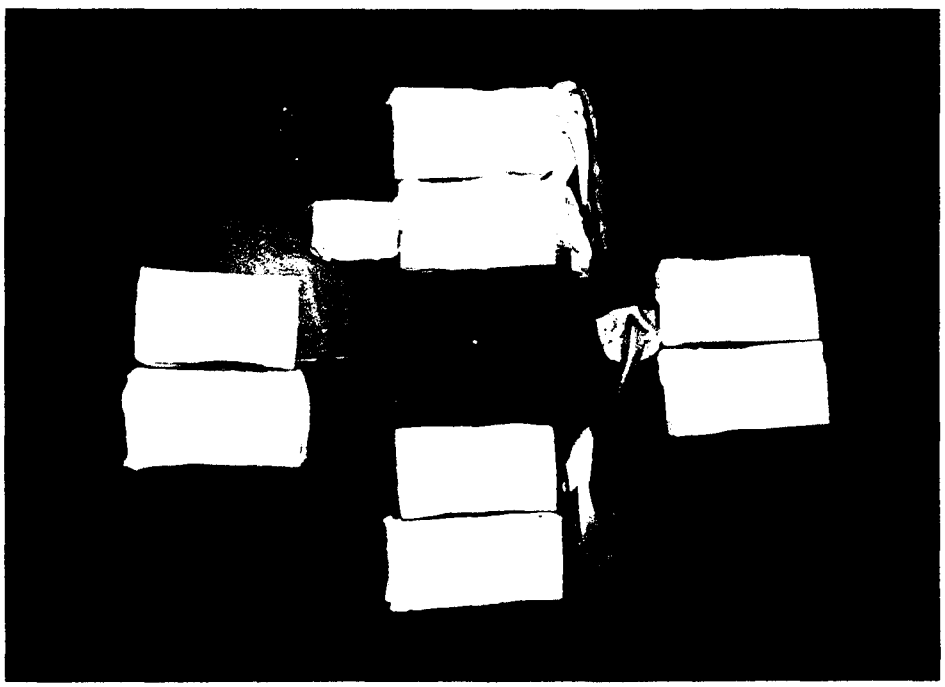

Figure 89: Fired brick specimens of the Kline Mountain kaolin with the fluxing agents of nepheline syenite and white silica showing the white fired specimen. The red fired specimen is the #3 clay fired specimen.

Table 13: The preparation list of the third firing experimental brick showing the amount of material and temperature utilized for these experiments.

SPECIMEN #	KAOLIN WEIGHT g	FLUXING AGENT NAME	FLUXING AGENT WEIGHT g	PLASTICITY WATER cc	FIRING TEMPERATURE °F
01	95	Talc	5	49	2095
02	95	Talc	5	48	2232
03	90	Talc	10	47	2095
04	90	Talc	10	47	2232
05	95	Salt (NaCl)	5	30	2095
06	95	$CaCl_2$	5	28	2095
07	90	Hydrated Lime	10	55	2232
08	92	Hydrated Lime+$CaCl_2$	5+3	38	2095

For sample 06, the same procedure was followed as in sample 05 but $CaCl_2$ was used instead of NaCl. For sample 07, dry hydrated lime was added to clay. Then, plasticity was obtained by adding the amount of water shown in Table 13. For sample 08, in addition to the indicated amount of hydrated lime, 12 g of $CaCl_2$ mixture from the solution of sample 06 was added to the clay. Then, varying degrees of plasticity were obtained by the amount of water shown in Table 13 (Figure 90). In the following step, samples were placed in an oven at 60 °C for 2 hours, at 75 °C for 2 hours and at 105 °C for 1 hour, and so dried. Then, they were fired at the temperatures shown in Table 13 by employing the PCE cones (Figure 91).

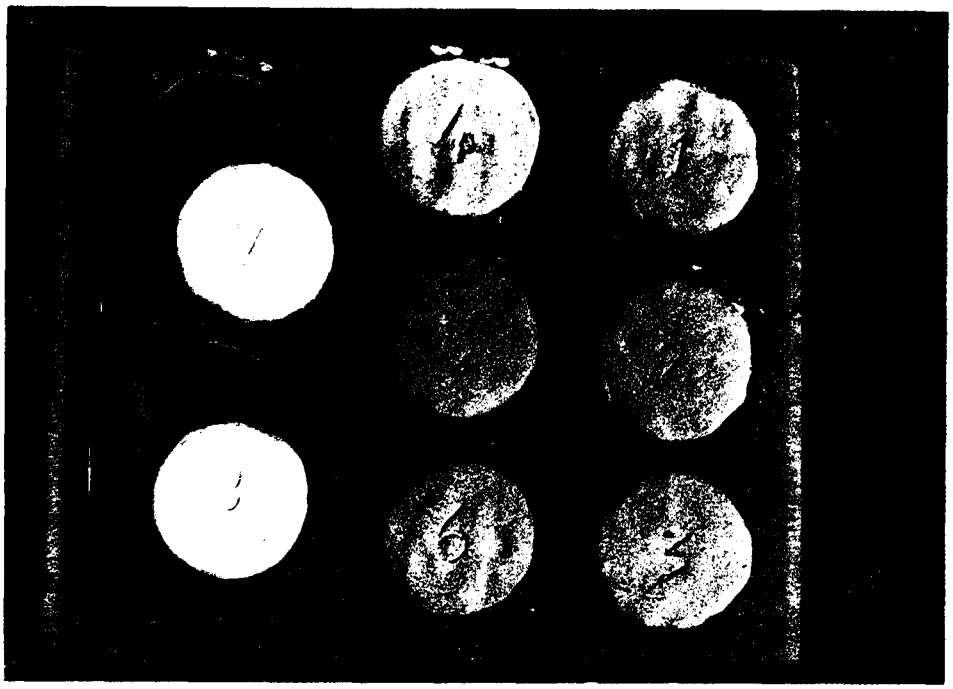

Figure 90: Unfired dried specimens of the experimental brick specimen of Kline Mountain kaolin with different fluxing agents showing green ware body.

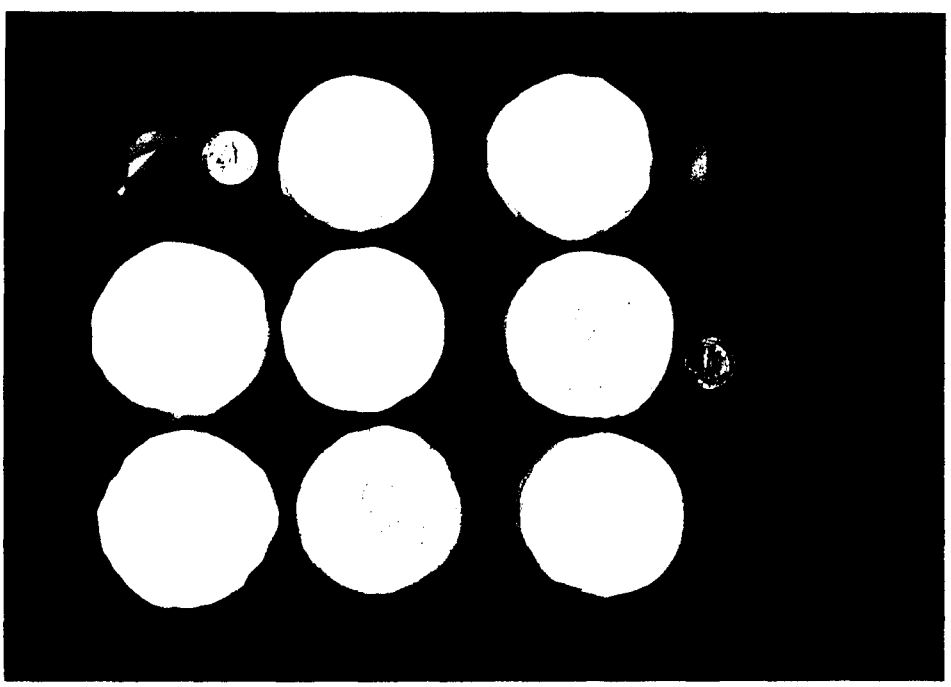

Figure 91: Fired brick specimens of the Kline Mountain kaolin with different fluxing agents showing the white fired brick specimen.

For the fourth set of experiments, eight specimens were prepared by using the #3 clay of the American Eagle Brick Company (Ntsimanyana, 1990 a) and the nepheline syenite. Table 14 lists the amount of kaolin, fluxing agent, and water utilized to make these specimens. The firing temperatures conducted for each specimen are also reported. Sample numbers 010, 030 and 070 were prepared by adding the indicated amount of #3 clay with the corresponding amount of Kline Mountain kaolin. Sample numbers 040, 050 and 080 were prepared by adding the indicated amounts of #3 clay and nepheline syenite with the reported amount of kaolin. Then, these specimens were molded after a plasticity was obtained by adding a given amount of water, which was 47 cc for the kaolin + #3 clay mixture and 45 cc for the kaolin + #3 clay + nepheline syenite mixture. The specimens were left under room conditions for 24 hours. Afterwards, the specimens were placed in an oven at 60 °C for 2 hours, at 75 °C for 2 hours and at 105 °C for 1 hour, to be dried. Then, the specimens were fired at the temperatures shown in Table 14 by employing the PCE cones (Figure 92).

Table 14: The preparation list of the fourth firing experimental brick showing the amount of material and temperature utilized for these experiments.

SPECIMEN #	KAOLIN WEIGHT g.	FLUXING AGENT NAME	FLUXING AGENT WEIGHT g.	PLASTICITY WATER cc.	FIRING TEMPERATURE °F
010	90	#3 clay	10	47	1900
030	90	#3 clay	10	47	2048
040	85	#3clay+neph. syenite	10+5	45	2048
050	85	#3clay+neph. syenite	10+5	45	2150
070	90	#3 clay	10	47	2150
080	85	#3clay+neph. syenite	10+5	45	1900

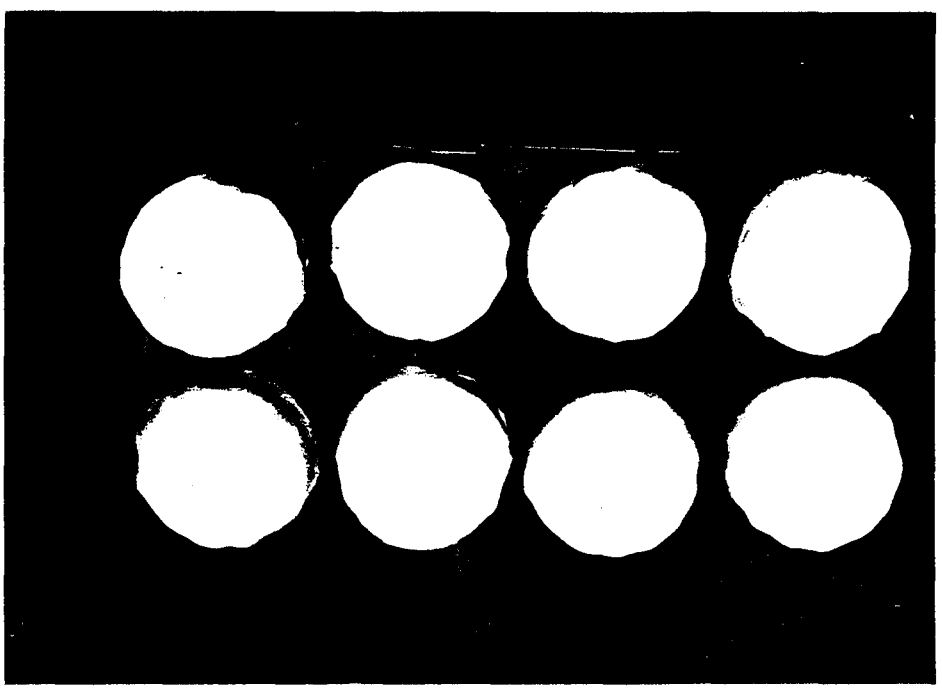

Figure 92: Fired brick specimens of the Kline Mountain kaolin with #3 clay, and #3 clay with nepheline syenite as fluxing agents showing the white fired brick specimens.

Firing was started at 75 °F, increasing it by 300 °F per hour until the plateau firing temperature was reached. As stated earlier, Standard Large Orton cones were employed to monitor the temperature within their corresponding temperature range. A pyrometer was also employed for the rate of firing as another monitoring device for the temperature. Each firing experiment spanned about 8 to 10 hours. Firing at the plateau temperature was always maintained for 20 minutes or more. All the firing experiments were performed in the Art Studio's kilns of El Paso Community College.

6.3. Water Absorption

The absorption tests were conducted for 24–hours, as outlined by the ASTM Standard Specifications for Brick and Applicable Testing Methods for Units and Masonry Assemblages. The fired samples were weighed prior to being submerged in distilled water for 24 hours. At the end of twenty four hours of water saturation, the samples were taken out of the water, dried with a moist cloth, and reweighed within a time limit of 5 minutes after being taken out of water. The absorption of each specimen was calculated as follows:

$$\text{Absorption} = 100 \times (W_s - W_f)/W_f$$

Where: Wf=fired dry weight of the sample and

Ws=water saturated weight of the sample.

Absorption tests were performed for four sets of the fired samples before the compressive strength test. However, for the third set, absorption tests were performed on the fragments of the samples that had been subjected to compressive strength tests first.

6.4. Compressive Strength Test

The compressive strength of a brick, as a masonry unit, is one of its most important physical properties. A brick has to meet at least the minimum standard requirement performed by a Standard Compressive Strength Test. The specifications, in pounds per square inch (psi) for the gross area, range from 1500 psi for the NW (Negligible Weathering) Grade to 2500 psi for MW (Moderate Weathering) Grade and 3000 psi for the SW (Severe Weathering) Grade (Figure 95). In general, brick strength is found to vary from 1,000 to over 20,000 psi (Klinefelter and Hamlin, 1957).

After the firing, the experimental brick specimens were smoothed before force application. This flattened surface area was calculated in square inches. The compressive strength tests were performed in accordance with ASTM C–67, Standard Test Method of Sampling and Testing Brick and Structural Clay Tile, by Danny R. Anderson Consultants, Inc., Geotechnical and Environmental Engineers, El Paso, Texas and Sunbelt Laboratories, El Paso, Texas, for the American Eagle Brick Company. For each specimen, the compressive strength was determined by dividing load in pounds, applied to the flattened surface vertically, into gross area in square inches.

6.5. Results

In order for wet brick to be handled or transported prior to drying and firing, the wet brick (green-ware) has to have sufficient green strength so that the molded shape will not be deformed when stacked on firing cars. Thus, the green strength is an important property of the clay body. Table 15 displays the compressive strength of the molded specimens. According to Dr. G. F. Cudahy, these green strengths indicate adequate strengths for brick making.

Table 15: Compressive strength showing green strength of the unfired experimental brick specimens as a function of the degree of drying.

SAMPLE #	DRYING TEMP. (°F)	GROSS AREA (Sq. In.)	LOAD (Lbs)	COMPRESSIVE STRENGTH (Psi)
1	212	0.3124	100	320
2	212	0.3406	150	440
20	77	1.5429	350	227
21	212	2.4147	750	311
The compressive strength test was performed in accordance with ASTM C-67, Standard Test of Sampling and Testing Brick and Structural Clay Tile, by Sunbelt Laboratories, El Paso, Texas, for American Eagle Brick Company, on June 8, 1993.				

As seen in Figure 89, the clay was extruded in the experimental extruder of the American Eagle Brick Company, indicating the required degree of material plasticity for making brick. The plasticity water for the kaolin is listed in Table 13 for the third set of the experimental brick. For the other experimental brick, the plasticity water was determined to be

between 45 and 47 percent by weight. This should be much lower when the clay is extruded in a full scale extruder with a vacuum in excess of 24 inches of Hg (Dr. G. F. Cudahy).

In the firing results of all experimental brick specimens with or without a fluxing agent, the desirable white color in the fired brick was achieved as seen in Figures 84, 89, and 91. From the color point of view, the Kline Mountain experimental brick specimen demonstrated a whiter color to meet the market need in comparison with Chihuahua white brick, which at one time was sold in the El Paso area. Moreover, the white color can be darkened by adding various amounts of the local brick company's #3 and/or #1 clay with nepheline syenite to supply various shades of white–to–cream brick, according to market demand. This can also bring additional advantages to the brick company in competing with its competitor(s) in the market by lowering the production cost of making white brick as well as supplying better quality white brick in terms of compressive strength and water absorption.

6.5.1. Water Absorption

The absorption tests were performed for 24 hours for the five experimental brick sets (Tables 16 through 20). The water absorption percentage was calculated by using the formula as stated in the methods of investigation (6.3).

For the experimental brick specimens, two weights were used for water absorption; dry fired weight (Wf) and absorbed brick weights (Ws) after 24 hours. Each water absorption was reported separately in the related water absorption table.

Other purposes of the firing experiments were to check the water absorption and compressive strength with or without a fluxing agent. For the first set of experimental brick,

kaolin was used without any fluxing additives. The four different temperatures were used for this experiment are reported in Table 16. The water absorption was calculated between 40.50 % at 2048 °F and 27.45 % at 2381 °F resulting in the highest percentage of water absorption among the experimental samples with respect to temperature. This is a linear inverse relationship between water absorption and firing temperature for all specimens as seen in Figure 93.

Table 16: Water absorption for the experimental brick of Kline Mountain kaolin (100 %). Absorption tests were performed at room temperature, approximately 25 °C.

SAMPLE #	FIRING TEMP. (°F)	FIRED WEIGHT (Wf) gr.	WATER SATUR. 24 Hrs (Ws) gr.	% ABSORPTION
1●	2048	10.00	14.05	40.50
2●	2124	7.20	10.09	40.14
3●	2232	11.30	15.45	36.73
4●	2381	11.13	14.18	27.40
The constituent of the specimens is the kaolin (100 %). The specimens were molded by hand, since the mechanical extruder was not functioning.				

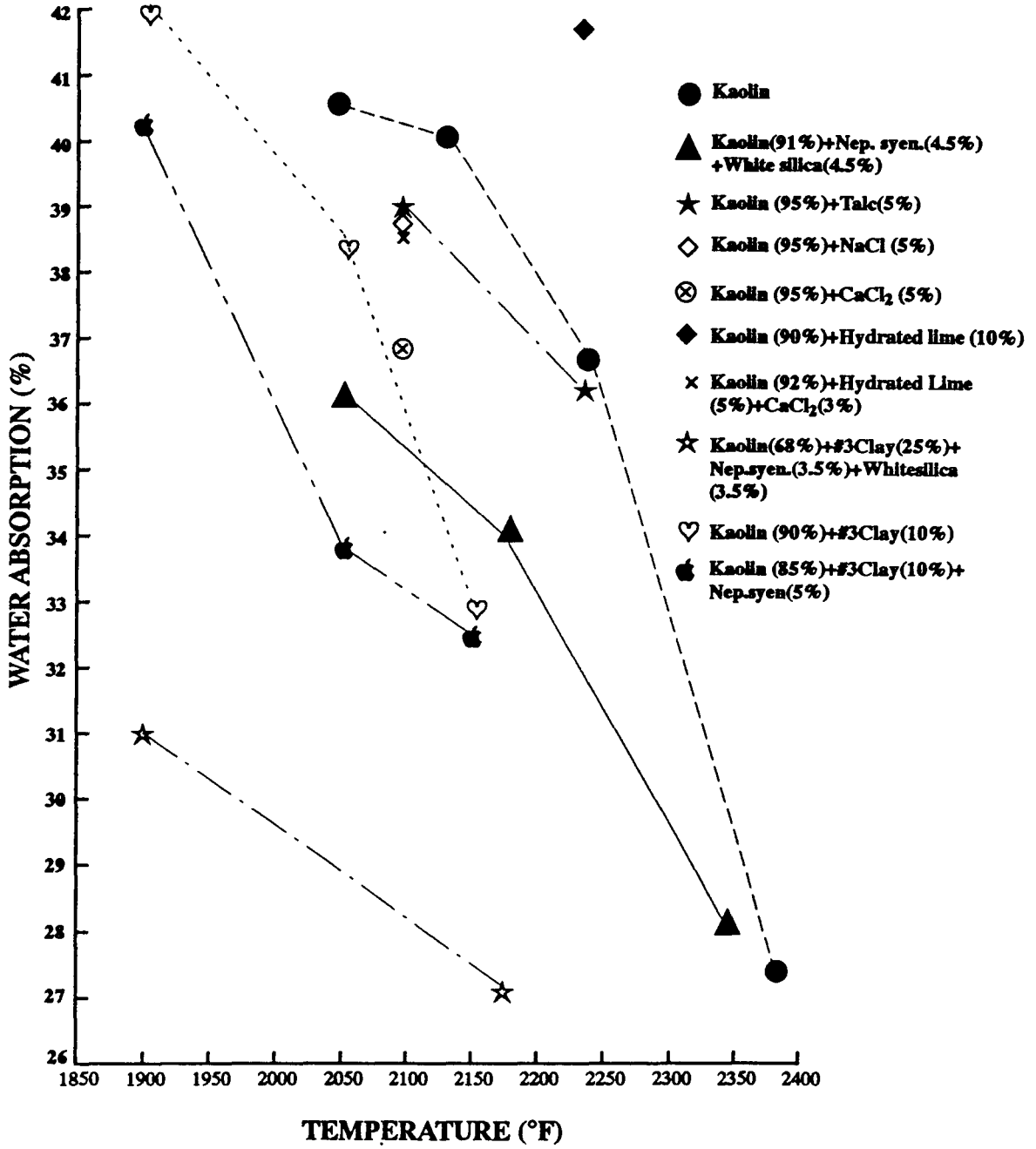

Figure 93: Graph showing the water absorption rates versus temperature. Note inverse linear relationship between water absorption rates and firing temperatures.

The brick specimens used in these absorption tests are the same ones used in the compressive strength tests (Table 21 through 24). With the nepheline syenite and white silica mixes, three different temperatures were employed for firing experiments as reported in Table 17. The water absorptions were determined as 36.15, 34.19 and 28.24 %, indicating a relatively lower water absorption than the first set of samples as seen in Figure 93. As observed in the first set, there is also an inverse relationship between firing temperatures and water absorption in this set. The specimens in this set were extruded without vacuum.

Table 17: Water absorption (wt %) for experimental brick set two. Absorption tests were performed at room temperature, approximately 25 °C.

SAMPLE #	FIRING TEMP. (°F)	FIRED WEIGHT (Wf) gr.	WATER SATUR. 24 Hrs (Ws) gr.	% ABSORPTION
20▲	2050	81.05	110.35	36.15
21▲	2175	79.70	106.95	34.19
23▲	2350	86.75	111.25	28.24
The constituents of the specimens are kaolin (91 %), nepheline syenite (4.5 %), and white silica (4.5 %). The specimens were extruded with no vacuum.				

In the third set, talc, NaCl, $CaCl_2$, and hydrated lime were utilized as a fluxing agent for the experimental brick made with the clay. Talc has been used in the first four specimens in amounts of 5 and 10 g, fired at 2095 °F and 2232 °F respectively. The highest water absorption percentage in this set was determined in sample 07 containing 90 % kaolin and 10 % hydrated lime, fired at 2232 °F followed by sample 01 containing 95 % kaolin and 5 % talc,

fired at 2095 °F, as seen in Table 18. No other specimens in this group, except for the talc specimens, show a correlation between water absorption and temperature. However, the talc graph in Figure 93 indicates an inverse linear relationship between water absorption and temperature.

Table 18: Water absorption (wt %) for experimental brick in third set. Absorption tests were performed at room temperature, approximately 25 °C.

SAMPLE #	FIRING TEMP. (°F)	FIRED WEIGHT (Wf) gr	WATER SATUR. 24 Hrs (Ws) gr	% ABSORPTION
01★	2095	5.45	7.57	38.90
02★	2232	9.60	13.08	36.25
03♣	2095	7.55	10.18	34.83
04♣	2232	16.10	21.95	36.34
05◇	2095	10.40	14.45	38.94
06⊗	2095	6.30	8.63	36.98
07◆	2232	3.75	5.32	41.87
08×	2095	9.70	13.46	38.76

Table 13 shows the mineral constituents of the specimens. The specimens were molded by hand. The tests were performed on the specimens that had been subjected to compressive strength tests first.

For the fourth set, kaolin was mixed with #3 clay (25 %), and nepheline syenite (3.5 %) and white silica (3.5 %) as fluxing agents (Table 19). Two temperatures were utilized for these experiments: 1900 °F and 2175 °F. As seen in Figure 93, a relatively lower water absorption was achieved at lower temperatures, which is the desirable goal in making brick.

The water absorptions were calculated between 33.72 and 27.16 %. These specimens were molded by the extruder with no vacuum.

Table 19: Water absorption (wt %) for experimental brick in the fourth set. Absorption tests were performed at room temperature, approximately 25 °C.

SAMPLE #	CONSTITUENT	FIRING TEMP. (°F)	FIRED WEIGHT (Wf) gr.	WATER SATUR. 24 Hrs (Ws) gr.	% ABSORP.
M1☆	Kaolin #3 clay Neph. syenite White silica	1900	60.55	79.50	31.30
M2☆	Kaolin #3 clay Neph. syenite White silica	1900	26.10	34.90	33.72
M3☆	Kaolin #3 clay Neph. syenite White silica	2175	27.80	35.35	27.16
The specimens were extruded without vacuum.					

For the last set, kaolin was mixed with #3 clay (10 %), and separately with #3 clay (10 %) and nepheline syenite (5 %) as fluxing agents (Table 20). Three temperatures were utilized for these experiments: 1900 °F, 2048 °F and 2150 °F. The water absorption percentages in kaolin and #3 clay mixture were determined as 42.06, 38.40 and 32.87 %, while the water percentages in kaolin, #3 clay and nepheline syenite mixture were determined as 40.38, 33.79 and 32.48 %. As seen in Figure 93, kaolin (85 %), #3 clay (10 %) and nepheline syenite

(5 %) mixture provided lower water absorption rates than that of kaolin (90 %) and #3 clay (10 %), indicating a high fluxing function property of nepheline syenite which provided a more glassy matrix to lower the porosity in the fired brick product at lower temperatures. Concordantly with the other experimental sets, there is an inverse relationship between firing temperatures and water absorption in this set as shown by Figure 93.

Table 20: Water absorption (wt %) for experimental brick set five. Absorption tests were performed at room temperature, approximately 25 °C.

SAMPLE #	FIRING TEMP. (°F)	FIRED WEIGHT (Wf) gr	WATER SATUR. 24 Hrs (Ws) gr	% ABSORP.
010♡	1900	13.10	18.61	42.06
030♡	2048	12.50	17.30	38.40
040	2048	10.95	14.65	33.79
050	2150	11.70	15.50	32.48
070♡	2150	10.80	14.35	32.87
080	1900	10.40	14.60	40.38
Table 14 shows the constituents of the specimens. The specimens were molded by hand.				

From the average absorption point of view (Tables 16 through 19) for each experimental brick specimen, the following conclusions can be drawn as shown by Figure 93:

1) The fluxing agents influence the water absorption rates of experimental brick positively, with the exception of hydrated lime.

2) Temperature appears to play a greater role in lowering the water absorption.

3) In increasing order, talc, nepheline syenite+white silica and #3 clay+nepheline syenite+white silica decreases the water absorption in the lower temperatures.

4) The kaolin (100 %) displays the highest percentages of water absorption after hydrated lime additive in the clay body.

5) There is an inverse linear relationship between water absorption and temperature.

6) Kaolin+#3 clay+nepheline syenite+white silica mixture shows a minimum amount of water absorption at lower temperatures.

6.5.2. Compressive Strength

Tables 21 through 24 list the compressive strength results of the four sets of experimental brick with or without a fluxing agent. In the first set of experimental brick containing 100 % kaolin without any additive (Table 21), the compressive strength was determined as 2206 psi after being fired at 2048 °F, 2840 psi at 2124 °F, 4541 psi at 2232 °F and 6296 psi at 2381 °F, indicating increasing compressive strength with respect to increasing firing temperature as seen in Figure 94.

In the second set of experimental brick (Table 22), the compressive strengths were determined as 2947 psi at 2050 °F, 3823 psi at 2175 °F, and 6958 psi at 2350 °F, indicating increasing compressive strength compared to the first set because of the nepheline syenite and probably white silica (Figure 94). This increase was determined as 741 psi at 2050 °F for the first two sets. The 6958 psi was the second highest compressive strength that was determined for these experiments as seen in Figure 94.

For the third set (Table 23), specimen 05, containing 5 % NaCl (by weight) as a flux, had the highest compressive strength, 5288 psi at 2095 °F, whereas specimen 01, containing 5 % talc as a flux, had the lowest compressive strength, 1665 psi at 2095 °F. Moreover, speci-

men 07, containing hydrated lime as a flux, had the second lowest compressive strength, 1890 psi at 2232 °F, in spite of high temperature firing. A flux of 5 and 10 % talc in the experimental brick body provided a positive proportional relationship between compressive strength and temperature as shown in Figure 94. $CaCl_2$, 3787 psi at 2095 °F, and $CaCl_2$+hydrated lime, 3623 psi at 2095 °F, as fluxing agents were also produced.

Table 21: Compressive strength of the first set for the fired kaolin without any additive as flux showing increasing compressive strength together with increasing temperature.

SAMPLE #	FIRING TEMP. (°F)	GROSS AREA (Sq. In.)	LOAD (Lbs)	COMPRESSIVE STRENGTH (Psi)
1●	2048	0.3627	800	2206
2●	2124	0.5105	1450	2840
3●	2232	0.5506	2500	4541
4●	2381	0.3812	2400	6296

The compressive strength test was performed in accordance with ASTM C-67, Standard Test of Sampling and Testing Brick and Structural Clay Tile, by Sunbelt Laboratories, El Paso, Texas, for American Eagle Brick Company on June 8, 1993. The major constituent of the specimens is the kaolin (100 %).

Table 22: Compressive strength of the second set for the fired kaolin with nepheline syenite and white silica as flux showing increasing compressive strength together with increasing temperature.

SAMPLE #	FIRING TEMP. (°F)	GROSS AREA (Sq. In.)	LOAD (Lbs)	COMPRESSIVE STRENGTH (Psi)
20▲	2050	4.31	12700	2947
21▲	2175	3.95	15100	3823
23▲	2350	3.78	26300	6958

The compressive strength test was performed in accordance with ASTM C–67, Standard Test of Sampling and Testing Brick and Structural Clay Tile, by Tannoy R. Anderson Consultants, Inc. Geotechnical and Environmental Engineers, 4601 Ripley, El Paso, Texas 79922, @ (915) 584–1317, for American Eagle Brick Company, on May 17, 1993, (Lab No. 65012 and File No. 93105).

Table 23: Compressive strength of the third set for the fired kaolin with talc, salt, $CaCl_2$, and hydrated lime as flux.

SAMPLE #	FIRING TEMP. (°F)	GROSS AREA (Sq. In.)	LOAD (Lbs)	COMPRESSIVE STRENGTH (Psi)
01★	2095	3.0625	5100	1665
02★	2232	2.4375	11100	4554
03✣	2095	3.0625	7500	2449
04✣	2232	3.1719	12200	3846
05◇	2095	2.7422	14500	5288
06⊗	2095	2.6406	10000	3787
07◆	2232	2.5391	4800	1890
08×	2095	2.5391	9200	3623

The compressive strength test was performed in accordance with ASTM C–67, Standard Test of Sampling and Testing Brick and Structural Clay Tile, by Danny R. Anderson Consultants, Inc. Geotechnical and Environmental Engineers, 4601 Ripley, El Paso, Texas 79922, @ (915) 584–1317, for American Eagle Brick Company on June 4, 1993, (Lab No. 65266 and File No. 93105). See Table 13 for the mineral constituents.

For the fourth set (Table 24), the compressive strengths of experimental brick specimens containing the kaolin, #3 clay, nepheline syenite, and white silica, were determined as 2734 psi and 3617 at 1900 °F, which is a desirable compressive strength at low temperatures (Figure 94). These specimens were extruded by the experimental extruder with no vacuum.

Table 24: Compressive strength of the fourth set firing kaolin with #3 clay, nepheline syenite, and white silica as flux.

SAMPLE #	FIRING TEMP. (°F)	GROSS AREA (Sq. In.)	LOAD (Lbs.)	COMPRESSIVE STRENGTH (Psi)
M1☆	1900	1.7554	6350	3617
M2☆	1900	1.5182	4150	2734
M3☆	2175	0.6375	6100	9569
Ch1 (Chihuahua white)■	?	3.9818	4000	1005
The compressive strength test was performed in accordance with ASTM C-67, Standard Test of Sampling and Testing Brick and Structural Clay Tile, by Sunbelt Laboratories, El Paso, Texas, for American Eagle Brick Company, on June 8, 1993.				

For the last set (Table 25), the strengths were determined as 1272 psi at 1900 °F, 2394 psi at 2048 °F and 3166 psi at 2150 °F for the first group containing kaolin (90 %) and #3 clay (10 %). For kaolin (85 %), #3 clay (10 %) and nepheline syenite (5 %) mixture, the compressive strengths were determined as 1908 psi at 1900 °F, 2101 psi at 2048 °F and 3272 psi at 2150 °F, indicating relatively higher compressive strength at lower temperatures with the addition of nepheline syenite as a fluxing agent (Figure 94).

Table 25: Compressive strength of the fifth set firing kaolin with #3 clay, and with #3 clay and nepheline syenite.

SAMPLE #	FIRING TEMP. (°F)	GROSS AREA (Sq. In.)	LOAD (Lbs.)	COMPRES-SIVE STRENGTH (Psi)
010♡	1900	2.0042	2550	1272
030♡	2048	2.2553	5400	2394
040	2048	1.9995	4200	2101
050	2150	2.1855	7150	3272
070♡	2150	2.0848	6600	3166
080	1900	2.2010	4200	1908

To make a comparison between the Chihuahua white brick and the Kline Mountain kaolin brick, a compressive strength test was conducted on the Chihuahua white brick. It was determined to be 1005 psi, which is weak under the required standards for all weathering grades, Negligible Weathering, Moderate Weathering, and Severe Weathering (Figure 95). This white brick was reported to have been fired in excess of 2000 °F (pers. comm., Dr. G. F. Cudahy, June, 1993), but this information has not been confirmed. Thus, the reported firing temperature should be taken into account with precaution until it is verified.

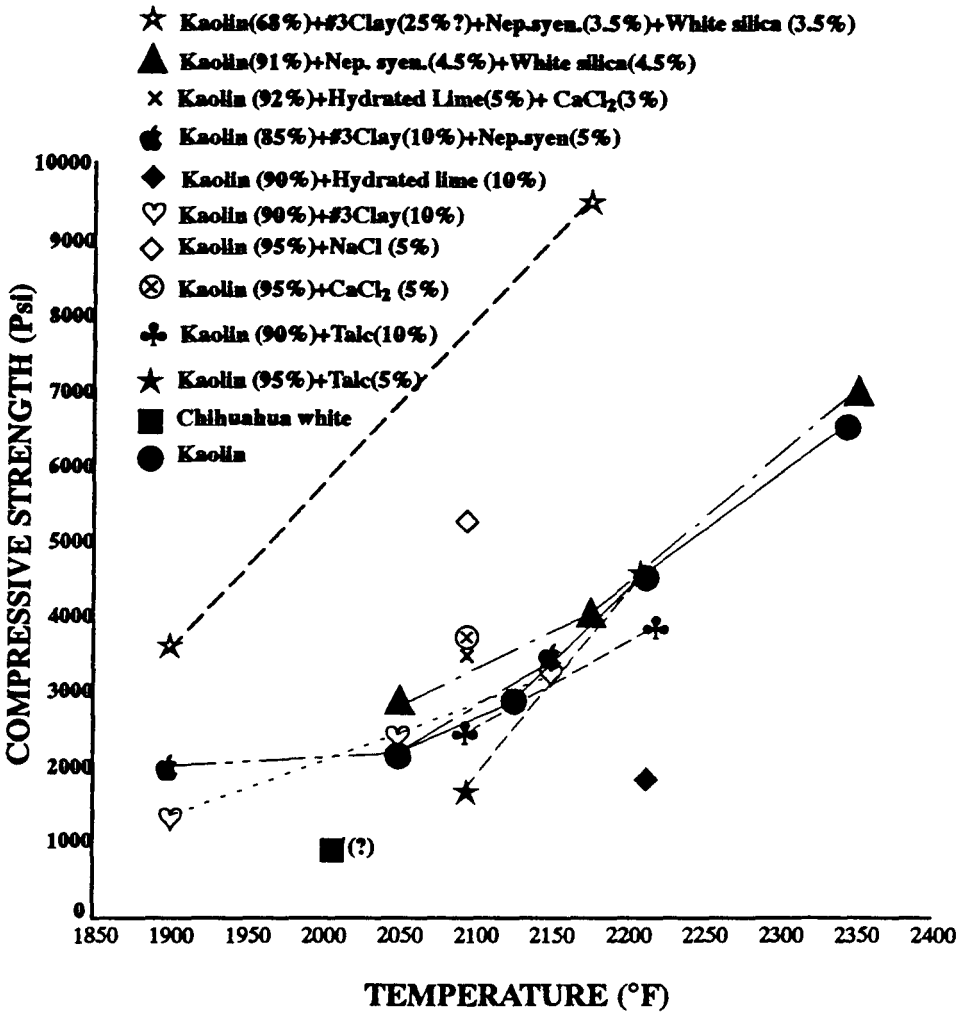

Figure 94: Graph showing the compressive strength versus the firing temperature. Note the proportional linear relationship between these two parameters, depending on the presence or absence of various fluxes.

6.6. Discussion of the Clay-Firing Experiments

About half of American Eagle's brick is sold in the El Paso area. The other half is sold to locations as far east as Dallas, Texas and as far north and west as northern New Mexico, Arizona, Nevada and California. The company also sells a relatively small amount of brick to Mexico (pers. comm., Dr. G. F. Cudahy, June 12, 1992). As seen in Figure 95, the company's market is primarily located in the Moderate Weather (MW) and Negligible Weather (NW) regions.

The main goals of these experiments were to check compressive strength, firing color, and water absorption of the experimental brick made from the Kline Mountain kaolin with or without a fluxing agent. Figure 94 demonstrates the compressive strengths of the experimental brick specimens with respect to temperature. As shown in the figure, there is a proportional linear relation between compressive strength and temperature. Kaolin+#3 clay+nepheline syenite+white silica shows the highest compressive strength at lower temperature (2734 and 3617 psi at 1900 °F) which is higher than the required compressive strength (2500 psi for Grade SW, 2200 psi for grade MW, and 1250 psi for Grade NW). As seen in Figure 94, kaolin+#3 clay and/or #1 clay with nepheline syenite plus white silica should be the best prescription for compressive strength at low temperature. Thus, this mixture appears to be not only favorable for lowering the water absorption but also for providing highest compressive strength at low temperature, both of which are desirable physical properties in making brick. In addition, #3 clay improves plasticity and green strength of brick made from Kline Mountain kaolin.

The fired brick specimens also demonstrated excellent white color properties. The bright whiteness of the fired specimen can give more market flexibility to the local brick company to produce various shades of white colored brick from this kaolin by adding from 15 to 50 % of #3 and/or #1 clay with nepheline syenite to the kaolin so that a complete range of white to gray colored brick can be produced. This has the additional advantage of lowering the cost of producing of white brick, because the #3 clay has negligible transportation cost to the firing plant.

The water absorption is the only physical property determined high for the specimens. However, all the brick specimens were prepared without using a vacuum which can reduce the porosity in a brick body and thus reduce water absorption. As seen in Figure 93, water absorption is determined in the lowest percentages at lower temperatures in the specimens containing kaolin+#3 clay+nepheline syenite and white silica, indicating #3 clay and nepheline syenite function as a fluxing agent and reduce water absorption, possibly filling in the pores in the specimen by providing a more glassy material at the lower temperature. Thus, using #3 clay and/or #1 clay in various percentages from 15 to 50 percent with nepheline syenite and by extruding and vacuuming the brick gives not only color manipulation but also reduces the water absorption. By using these clay mixtures followed by extrusion with vacuum, water absorption should be reduced in the fired brick to the required limit and possibly lower than the required limit which is 20 percent for Grade SW, 25 percent for Grade MW, and no limit for Grade NW.

The secondary goals of these experiments were to qualitatively evaluate the plasticity, green strength, workability, and extrudability of the experimental brick made with the Kline Mountain kaolin with or without fluxing agent. The experiments have determined that the experimental brick specimens made with the Kline Mountain kaolin have the plasticity, green strength, workability and extrudability properties needed for utilization by the brick industry without any defects as a result of firing and chemical composition. The specimens were extruded by a laboratory extruder and molded by hand without any defect, indicating appreciable plasticity, workability, and extrudability properties. Moreover, no defects during processing were observed in the molded and extruded wet clay body (green–ware) attesting to the clay's adequate green strength.

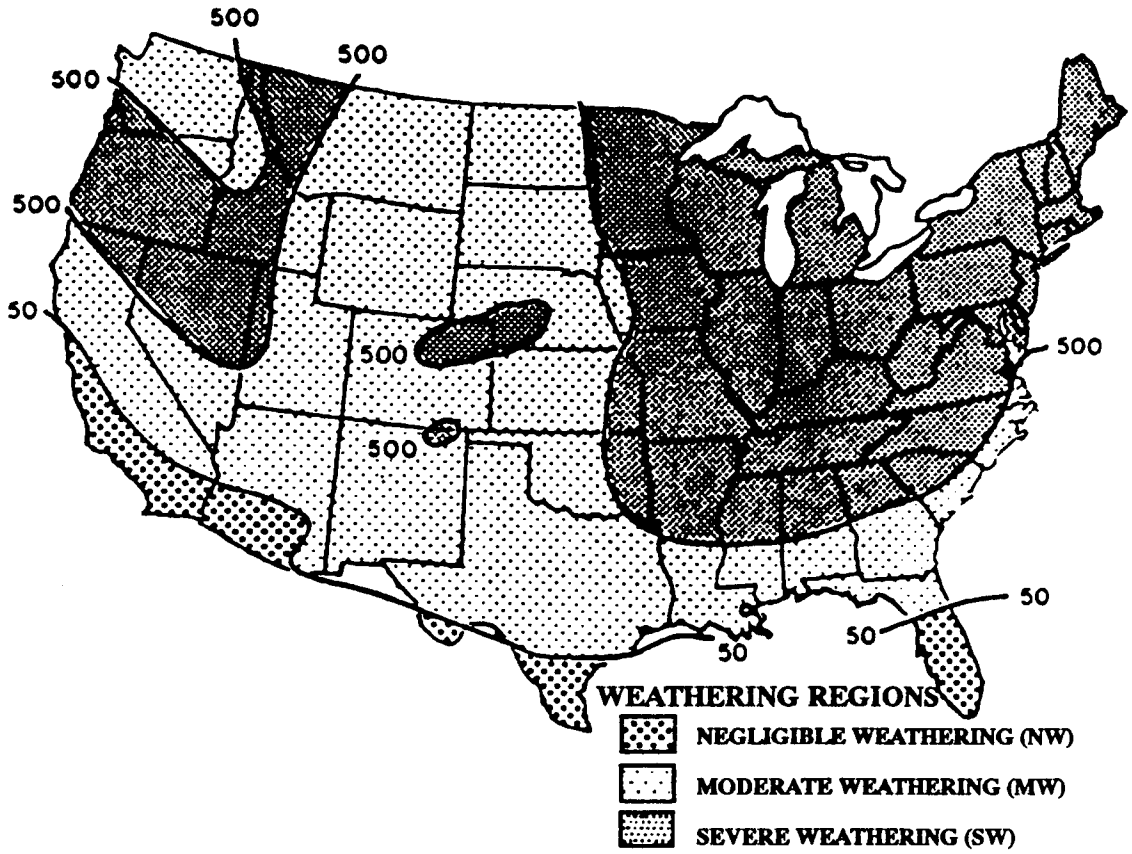

Figure 95: Weathering indexes in the United States (ASTM Standard Specifications for brick and applicable Standard Testing Methods for units and masonry assemblages, 1975).

CHAPTER 7

PROCESSING AND ECONOMIC EVALUATION

7.1. American Eagle Brick Company

The American Eagle Brick Company is situated on the eastern flank of Cerro de Cristo Rey, Doña Ana County, New Mexico (Figure 96). It is located about two miles west of the UTEP campus. The plant is found on the west side of the Rio Grande (Figure 97). Brick has been manufactured at this same location from 1897 until 1990 by El Paso Brick Company, and since 1990 as the American Eagle Brick Company.

In making brick, the company has been exploiting the Mesilla Valley shale and the Anapra shale/sandstone formations of Cretaceous age on the flank of the andesitic laccolith of Cerro de Cristo Rey. The formations have suffered very little low grade contact metamorphism by the Cerro de Cristo Rey intrusion and uplift. Ntsimanyana (1990 a and b), Lovejoy (1976), and Barnes et al. (1991) can be referred to for detailed information on the geology of the Cerro de Cristo Rey and also for the brick production process of American Eagle Brick Company.

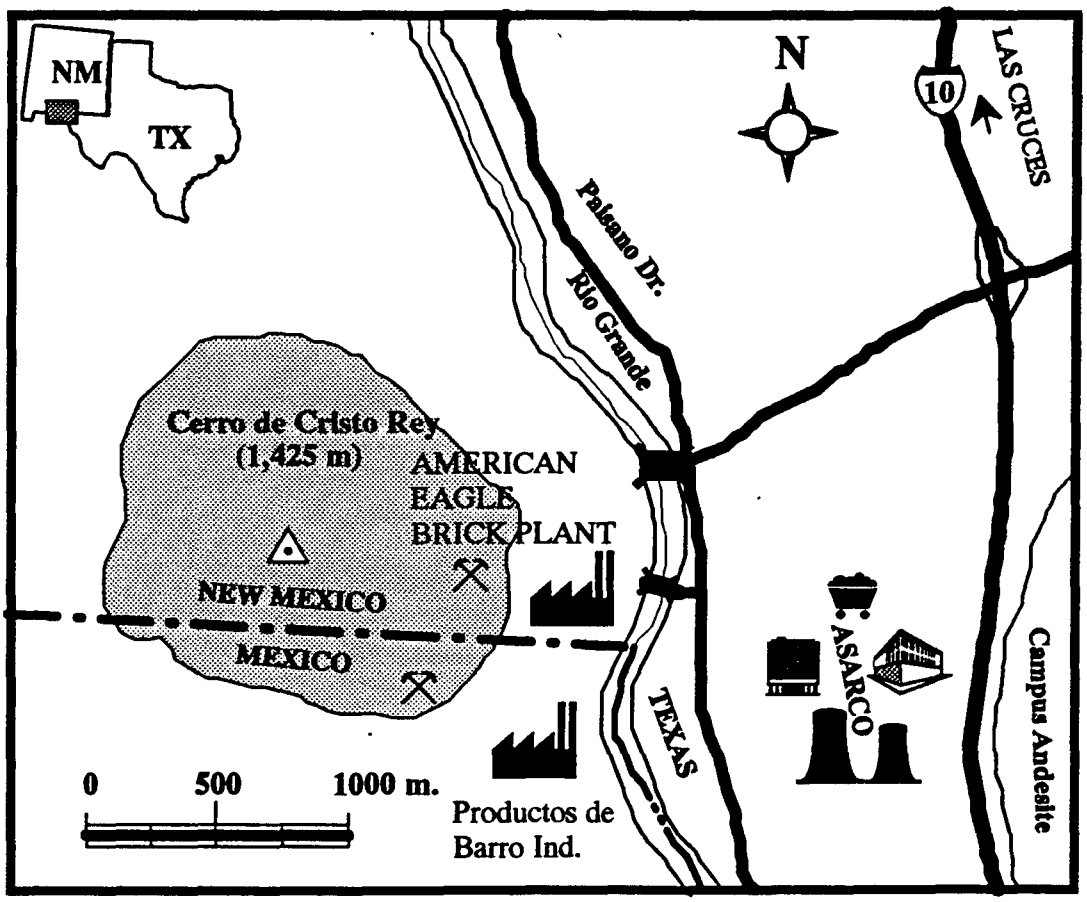

Figure 96: Location map of the American Eagle Brick Company.

Figure 97: The view of the Rio Grande showing the location of the American Eagle Brick Company. Cerro de Cristo Rey is in the background view to southwest. Immediately adjacent the river in the far distance is the Mexican brick company in the Ciudad Juarez, Productos de Barro Industrializados, S.A.

7.1.1. Processing and Production

Brick production of the Company is conducted by seven major processes from mining to final products, fired brick ,as shown by Figure 98. Mining has been performed by open pit methods producing about 3000 m tons per month. Stockpiling prepares the raw material by eliminating the cobbles and boulders easily during sieving as well as keeping the operation going under adverse weather conditions. After the shale and/or clay is milled to about 2 mm grain size, it is stored in silos. The clay, water and additive A (sulfo lignate, to stabilize soluble salts in the clay during drying) are combined in a pug mill, then the excess air is removed in a vacuum chamber.

In the next step, the plastic paste is continuously extruded in an extruder. For the brick to be extruded, the clay or shale must have a fair degree of plasticity. The shape of the brick can be determined by the optional dies. Then, the brick cutter cuts up to 18 bricks from the extruded brick shape column per cutter cycle. Approximately 65,000 bricks are loaded on to the kiln cars per 8 hour day.

The green brick enters the 13 car long dryer and the temperature is raised gradually from 80 °F to 270 °F. From the dryer, they enter the 13 car long gas fired kiln, and the temperature is raised gradually to about 1975 °F. The duration of time in the kiln is 1.5 days. At the exit end of the kiln, the brick is cooled where a portion of the hot air is circulated to the dryer and the rest is carried to the burning section and is subsequently exhausted along with the gases of combustion to the atmosphere near the entrance end of the kiln.

Some coloring agents such as manganese oxide and iron oxide are used to produce various color of brick. The compressive strength of the brick ranges from 10,000 to 15,000 psi (pounds per square inch).

The production is reported as 1.25 million bricks per month, as shown below. The company is currently employing over 40 people. In brick production, natural gas is used for heat energy and electricity is used for motivation energy.

Brick Production*
1,250,000 brick.month^{-1} x 12 months.year^{-1} = 15,000,000 brick.year^{-1} 15,000,000 brick.year^{-1} / 250 days.year^{-1} = 60,000 brick.day^{-1} (10 % production loss) 90 % (yield) x 60,000 brick.day^{-1} = 54,000 brick.day^{-1}
* Dr. G. F. Cudahy, the President of the American Eagle Brick Company (pers. comm., June,1993).

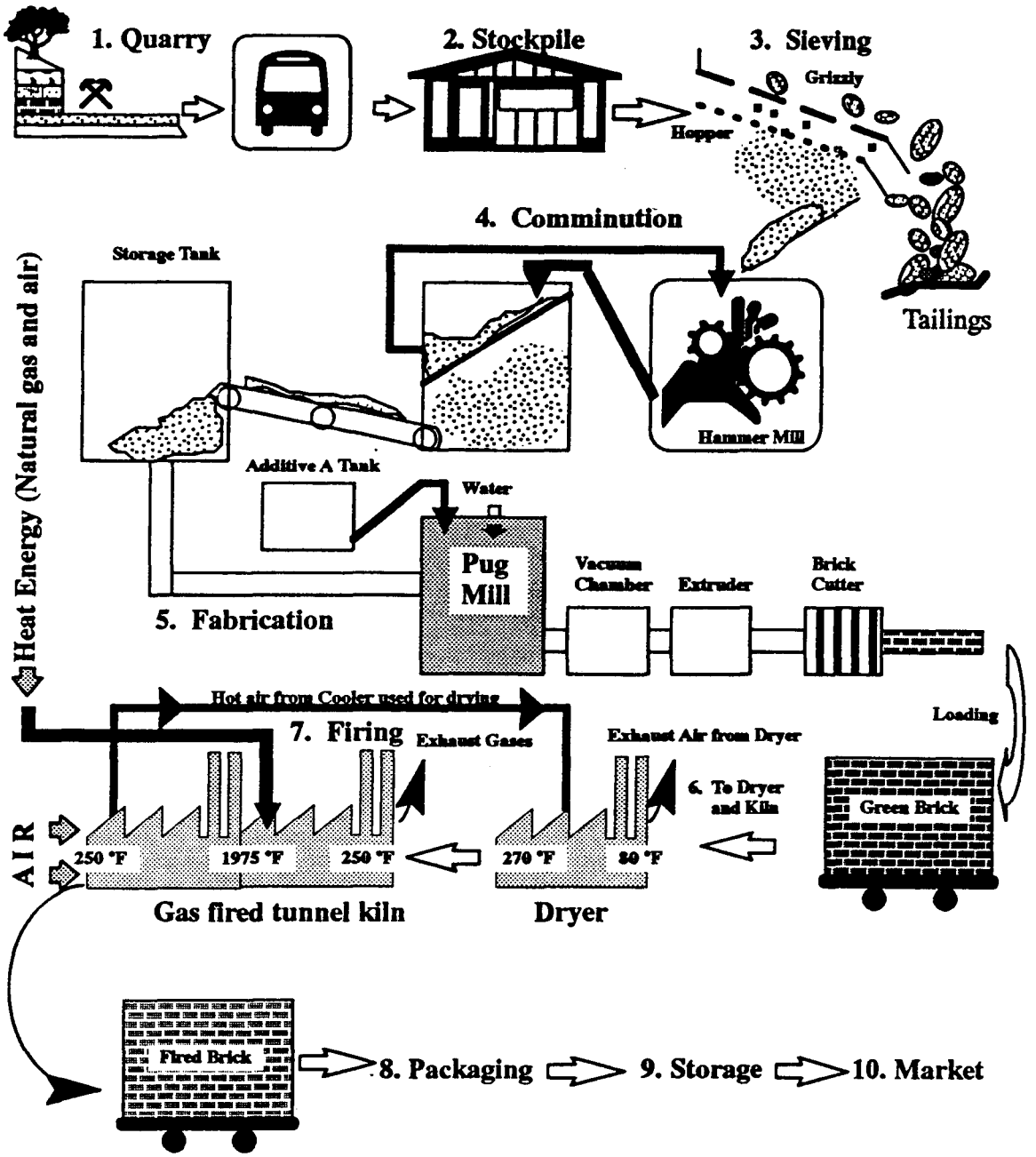

Figure 98: Steps in the manufacture of brick at American Eagle Brick Company (modified from Ntsimanyana, 1990 a).

Brick production and shipments in the U.S.A. are shown in Table 26.

Table 26: March summary of brick production and shipments in the USA (BIA* News, June 1993)[1]. See Figure 99 for BIA Region.

BIA Region	MARCH 1993 Production (1,000 brick)	MARCH 1993 Shipments (1,000 brick)	MARCH 1993 Value of Shipments ($1,000)	1993 YEAR TO DATE Production (1,000 brick)	1993 YEAR TO DATE Shipments (1,000 brick)	1993 YEAR TO DATE Value of Shipments ($1,000)
Total U.S.	535,793	462,491	64,086	1,371,575	1,199,999	159,943
1,2,3	28,484	17,381	3,505	60,794	47,073	9,196
4	30,798	24,832	4,555	81,429	59,232	10,974
5	15,089	12,053	1,743	43,259	30,753	4,403
6	10,758	8,202	1,361	33,973	24,402	4,145
7A	25,984	20,946	3,017	71,557	63,568	8,970
7B	77,972	69,384	11,392	190,514	180,953	25,512
7C	52,395	44,792	5,726	113,754	105,153	13,176
8,9	153,273	131,245	14,967	412,613	365,180	41,548
10	22,273	22,504	2,838	55,918	56,474	7,017
11,11A, 18	110,120	101,853	12,600	287,829	245,254	30.160
12	2,812	2,522	539	14,100	15,180	2,999
13—17	5,835	6,777	1,843	5,853	6,777	1,843

* BIA–Brick Industry Association

[1] Issued May 13, 1993

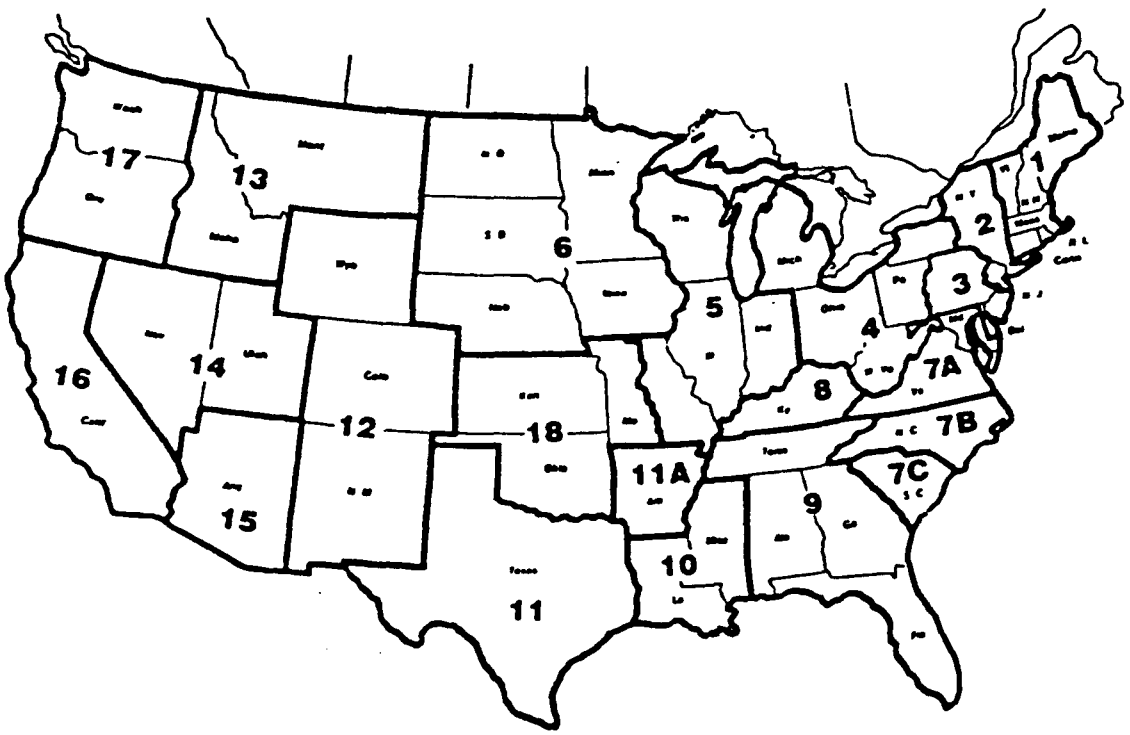

Figure 99: Brick Institute of America Regional Associations (Christine A. Subasic, written communication, June 1993)

7.2. Economic Analysis

The degree of success of any new project will ultimately depend on the underlying economic strength of the project as well as how successfully the parties involved can coordinate their interests. In the case of the kaolin deposit which had been used only sparingly by industry, the most striking attractions are its convenient location (crossed by NM Highway 59), large reserves, high brightness, cheap extraction methods, and readiness to be sold. Furthermore, there are no claim and flood water problems.

When a kaolin has been found to be of a certain industrial type and grade, the question immediately arises as to its possible market potential. The kaolin may be sold to some clay producer or directly to a firm using the clay in his product. The owner of the deposit may mine and ship the kaolin; or the buyer may do the mining and shipping and consequently pay a specified royalty per ton. That is, economic factors affecting kaolin deposits vary in importance with type, quality, and intended end use.

Brick, especially the common varieties, are made from a wide range of clays and shales. Occasionally, two or three more clays are blended, but the ideal is to use one clay or shale, if possible. The building–brick industry is the most localized of all ceramic industries. Thus, the cost of transportation will probably be an important factor in the future for the Kline Mountain kaolin deposit to be competitive.

The purpose of this analysis is to evaluate the mine in accordance with white brick production under today's economic conditions and to determine whether or not it would be economically viable in terms of projected conditions.

7.2.1. Clay Reserves

For a clay deposit to be utilized in the brick industry, a sufficient reserve is one of the principal requirements. Thus, the reserve calculation has been done as the first part of economic analysis.

7.2.1.1. Tonnage–Grade Calculation

The volume and tonnage of "probable ore" was calculated by triangular blocks as outlined by Patterson (1959). Plate 4 shows these blocks at a scale of 1:1500.

First, the average mineral compositions of the drill core samples in the kaolinization zone were determined as shown by Table 27. Then, the differences in mineral compositions

Table 27: Average mineral compositions of the drill core samples.

AVERAGE MINERAL COMPOSITIONS OF DRILL CORE SAMPLES (AMCDC) (R5-I THROUGH R5-VI)				
Kaolinite	**Alunite**	**Silica**	**Accessories**	**Total**
38.58	19.30	40.52	0.72	99.12

of the drill core samples between R5–I and the averages were calculated to determine the variability of the mineral contents in the deposit as shown in Table 28. The kaolinization zone depth, 48 m, in the drill core (Figure 16) was taken as the average depth for the triangular blocks (Table 29).

Table 28: Differences in mineral compositions between the averages in Table 27 and the surface samples (R5-I).

DIFFERENCES IN MINERAL COMPOSITION BETWEEN R5-I AND AMCDC (AMCDC)-(R5-I)			
Kaolinite	**Alunite**	**Silica**	**Accessories**
+7.61	+4.60	-12.73	+0.10

Table 29: Averages mineral percentages of the triangles.

1st TRIANGLE									
SAMPLE	DEPTH (h)	KAOLINITE (%)	KAOLINITE h*(%)	ALUNITE (%)	ALUNITE h*(%)	SILICA (%)	SILICA h*(%)	ACCESSORIES (%)	ACCESSORIES h*(%)
SM 200	48 m	34.34	1648.32	17.32	831.36	44.87	2153.76	0.69	33.12
3Tkm 3	48 m	47.37	2273.76	5.56	266.88	41.30	1982.40	1.05	50.40
2Tkm 4	48 m	50.28	2413.44	7.43	356.64	35.32	1695.36	2.04	97.92
Total	144 m		6335.52		1454.88		5831.52		181.44
AMC		44.00		10.10		40.50		1.26	

Average depth (AD): 48 m (from Figure 16)
Average mineral composition (AMC): 6335.52/144=44.00 % kaolinite

2nd TRIANGLE									
SAMPLE	DEPTH (h)	KAOLINITE (%)	KAOLINITE h*(%)	ALUNITE (%)	ALUNITE h*(%)	SILICA (%)	SILICA h*(%)	ACCESSORIES (%)	ACCESSORIES h*(%)
SM 200	48 m	34.34	1648.32	17.32	831.36	44.87	2153.76	0.69	33.12
3Tkm 1	48 m	11.33	543.84	53.66	2575.68	30.98	1487.04	0.56	26.88
2Tkm 4	48 m	50.28	2413.44	7.43	356.64	35.32	1695.36	2.04	97.92
Total	144 m		4605.60		3763.68		5336.16		157.92
AMC		31.98		26.14		37.06		1.10	

3rd TRIANGLE									
SAMPLE	DEPTH (h)	KAOLINITE (%)	KAOLINITE h*(%)	ALUNITE (%)	ALUNITE h*(%)	SILICA (%)	SILICA h*(%)	ACCESSORIES (%)	ACCESSORIES h*(%)
3Tkm 5	48 m	35.77	1716.96	5.55	266.40	53.70	2577.60	1.65	79.20
3Tkm 1	48 m	11.33	543.84	53.66	2575.68	30.98	1487.04	0.56	26.88
2Tkm 4	48 m	50.28	2413.44	7.43	356.64	35.32	1695.36	2.04	97.92
Total	144 m		4674.24		3198.72		5760.00		204.00
AMC		32.46		22.21		40.00		1.42	

4th TRIANGLE									
SAMPLE	DEPTH (h)	KAOLINITE (%)	KAOLINITE h*(%)	ALUNITE (%)	ALUNITE h*(%)	SILICA (%)	SILICA h*(%)	ACCESSORIES (%)	ACCESSORIES h*(%)
3Tkm 5	48 m	35.77	1716.96	5.55	266.40	53.70	2577.60	1.65	79.20
CS 200	48 m	41.01	1968.48	18.01	864.48	35.22	1690.56	0.87	41.76
2Tkm 4	48 m	50.28	2413.44	7.43	356.64	35.32	1695.36	2.04	97.92
Total	144 m		6098.88		1487.52		5963.52		218.88
AMC		42.35		10.33		41.41		1.52	

5th TRIANGLE									
SAMPLE	DEPTH (h)	KAOLINITE (%)	KAOLINITE h*(%)	ALUNITE (%)	ALUNITE h*(%)	SILICA (%)	SILICA h*(%)	ACCESSORIES (%)	ACCESSORIES h*(%)
3Tkm 5	48 m	35.77	1716.96	5.55	266.40	53.70	2577.60	1.65	79.20
CS 200	48 m	41.01	1968.48	18.01	864.48	35.22	1690.56	0.87	41.76
2Tkm 2	48 m	25.04	1201.92	23.66	1135.68	44.98	2159.04	0.85	40.80
Total	144 m		4887.36		2266.56		6427.20		161.76
AMC		33.94		15.74		44.63		1.12	

6th TRIANGLE									
SAMPLE	DEPTH (h)	KAOLINITE (%)	KAOLINITE h*(%)	ALUNITE (%)	ALUNITE h*(%)	SILICA (%)	SILICA h*(%)	ACCESSORIES (%)	ACCESSORIES h*(%)
Tkm 2	48 m	50.70	2433.60	11.13	534.24	34.24	1643.52	1.81	86.88
CS 200	48 m	41.01	1968.48	18.01	864.48	35.22	1690.56	0.87	41.76
2Tkm 2	48 m	25.04	1201.92	23.66	1135.68	44.98	2159.04	0.85	40.80
Total	144 m		5604.00		2534.40		5493.12		169.44
AMC		38.92		17.60		38.15		1.18	

7th TRIANGLE									
SAMPLE	DEPTH (h)	KAOLINITE (%)	KAOLINITE h*(%)	ALUNITE (%)	ALUNITE h*(%)	SILICA (%)	SILICA h*(%)	ACCESSORIES (%)	ACCESSORIES h*(%)
Tkm 2	48 m	50.70	2433.60	11.13	534.24	34.24	1643.52	1.81	86.88
CS 200	48 m	41.01	1968.48	18.01	864.48	35.22	1690.56	0.87	41.76
2Tkm 5	48 m	38.12	1829.76	30.84	1480.32	29.09	1396.32	0.59	28.32
Total	144 m		6231.84		2879.04		4730.40		156.96
AMC		43.28		19.99		32.85		1.09	

8th TRIANGLE									
SAMPLE	DEPTH (h)	KAOLINITE (%)	KAOLINITE h*(%)	ALUNITE (%)	ALUNITE h*(%)	SILICA (%)	SILICA h*(%)	ACCESSORIES (%)	ACCESSORIES h*(%)
3Tkm 3	48 m	47.37	2273.76	5.56	266.88	41.30	1982.40	1.05	50.40
CS 200	48 m	41.01	1968.48	18.01	864.48	35.22	1690.56	0.87	41.76
2Tkm 5	48 m	38.12	1829.76	30.84	1480.32	29.09	1396.32	0.59	28.32
Total	144 m		6072.00		2611.68		5069.28		120.48
AMC		42.17		18.14		35.20		0.84	

9th TRIANGLE									
SAMPLE	DEPTH (h)	KAOLINITE (%)	h*(%)	ALUNITE (%)	h*(%)	SILICA (%)	h*(%)	ACCESSORIES (%)	h*(%)
3Tkm 3	48 m	47.37	2273.76	5.56	266.88	41.30	1982.40	1.05	50.40
2Tkm 4	48 m	50.28	2413.44	7.43	356.64	35.32	1695.36	2.04	97.92
CS 200	48 m	41.01	1968.48	18.01	864.48	35.22	1690.56	0.87	41.76
Total	144 m		6655.68		1488.00		5368.32		190.08
AMC		46.22		10.33		37.28		1.32	

The calculated mineral compositions of the surface samples in Table 3 were adjusted by adding or subtracting the values shown in Table 28, to more truly reflect the average composition in the subsurface. Each of the surface samples so modified represents the apex of a triangle used in the reserve calculation. In the following step, the average percentages of the minerals were determined for each of the nine specified (blocks) triangles in Plate 4 (Table 29). Next, the volume and the tonnage of the ore were calculated from the areas of the triangular blocks (Table 30). For the tonnage calculation, the depth of the blocks is assumed to be 48 m and the density of kaolin was determined as an average of 1.22 g/cc.

On the basis of average grade, the available contained mineral weights of the kaolin deposit were determined as shown by Table 31. For the economic analysis, the tonnage was reduced by 50 % due to the possible mining loss caused by overburden, presence of NM 59 right of way, difficulty of deep mining, and also siliceous and alunitic zones. Theoretically, the gross value of the deposit after mining loss was based on the recent structural clay price and the tonnage calculated (Table 32).

Table 30: The volume and tonnage of triangles.

The triangles	The length of triangle side and its height a h_a (m)	$A = a \times h_a/2$ (m^2)	$V = d \times A$ d=45 m (m^3)	$T = V \times (1.22)$ (mtons)
1	262.5 207.0	27169	1304112	1591017
2	259.5 84	10899	523152	6382451
3	168 52.5	8820	423360	516499
4	93 57	2651	127248	155243
5	181.5 35.25	6398	307104	374667
6	162 87	7047	338256	412672
7	211.5 72	15228	730944	891752
8	255 148.5	18934	908832	1108775
9	255 84	10710	514080	627178
Total			5177088	6,316,048

Table 31: The available contained mineral weights (Tonnage taken from Table 30 and AMC taken from Table 29).

Proven ore is calculated by the following equation:
Tonnage × AMC × 0.01 = 1591017 × 44.00 × 0.01 = 700047 m tons for the kaolinite content of the 1st triangle.

TRIANGLE	KAOLINITE	ALUNITE	SILICA	ACCESSORIES
1	700047	160693	644362	20047
2	204111	166837	236534	7021
3	167656	114714	206600	7334
4	65745	16037	64286	2360
5	127162	58973	167214	4196
6	160612	72630	157434	4870
7	385950	178261	292941	9720
8	467570	201132	390289	9314
9	289882	64787	233812	8279
TOTAL	2568735	1034064	2393472	73141
AVERAGE[1] PERCENTAGES	40.67 %	16.37 %	37.89 %	1.16 %

[1] T = 6,316,048 m tons (from Table 30) ☞ (2,568,735m tons / 6,316,048 m tons) × 100 % = 40.67 % for the kaolinite average percentage.

Table 32: The value of available kaolin after mining loss.

ORE	PRICE ($)	TONNAGE (mton) (From Table 30 reduced to 1/2)	GROSS VALUE ($)
Kaolinitic clay (kaolinite, silica, alunite, and accessories)	5.18*(fob)	3,158,024	16,358,564
* personal communication, Robert L. Virta, U.S. Bureau of Mines, on June 21, 1993.			

7.2.2. Mine Life

The company's production is 1,250,000 bricks per month. Each brick weighs 4.6 lbs, which is called king size brick. Therefore, the company needs to recover 5,750,000 lbs of clay (2,875 short ton or 2,608 m tons, 1 metric ton (m ton) = 2205 lb) to manufacture the monthly brick production. For a year, the company needs to recover 31,296 m tons of clay. Due to the recovered clay loss as a result of loading, transporting, dumping, grinding, processing and extruding, the company requires 36,000 m tons of clay per year to meet its annual clay need, including the above stated mining losses, which comprises 15 % of 31,296 m tons of clay.

Due to the possible mining loss caused by overburden, right of way of the road NM 59, difficulty of deep mining, siliceous zone, and alunitic zones the reserve of the clay deposit is reduced 50 % to 3,158,024 m tons as shown in Table 32. Thus, mine life can be calculated as shown by the following equation:

From Table 32 ☞ 3,158,024 mtons/36,000 m tons.year^{-1} ≅ **88 years**

7.2.3. Cost of Goods

In order to calculate cost per thousand bricks sold, the following calculations are made to estimate the elements of the cost. The elements of the cost for the clay deposit are: mining (Table 33), royalty (Table 34), environmental (Table 35), loading (Table 36) and transportation (Table 37). Costs for mining were estimated from Stebbins (1987). The fol-

lowing are the costs associated with production of bricks at the plant: labor (Table 38), natural gas (Table 39), electricity (Table 40), additives (Table 41), cost of #3 and #1 local clay (Table 42), and packaging (Table 43). Fuel and lubrication were estimated from Stebbins (1987). Afterwards, the estimated cost of goods sold was based on mine and plant costs (Table 44) per thousand white brick made with Kline Mountain clay by the American Eagle Brick Company with a small amount of local clay from Cerro de Cristo Rey. All costs are converted to "per thousand" king size bricks, each of which is 4.6 pounds weight. Operating expenses (Table 45) were estimated as 25 percent of the gross revenue per year, as indicated by Dr. George. F. Cudahy, President of American Eagle Brick Company.

The calculation of annual net income and operating cash flow was based on the American Eagle Brick Company's calculations (Table 46), which is similar to that employed in standard references such as Peters (1987). The investments necessary for utilizing Kline Mountain clay production are as shown by Table 47. The net present values were calculated under the assumption that all estimated costs, revenues, and reserve are reasonably accurate. Of the two calculated net present values, one was determined by the Hoskold factors (Tables 48 and 49). The determination of the discounted cash flow return on investment (Table 49) was based on an equation taken from Peters (1987).

7.2.3.1. Mining Cost

The clay deposit is in an area of moderate relief with warm summers and mild, snowy winters. The cost of mining is estimated as $1.00 per metric ton for the brick company (Table 33). It is assumed that the daily clay recovery will be 1,000 mtons with the company's already owned equipment as seen below (Dr. George F. Cudahy, pers. comm., July 1993):

Dozer operator[1]($18.75 per hour × 8 hours per day)	$150 per day
Fuel (200 gallons per day)	$200 per day
Maintenance and labor	$200 per day
Amortize equipment haul ($1,000 per year)	$30 per day
Food, clothes, water, generator, camping, lost time and general services etc	$420 per day
Total	$1,000 per day

The planned production is 1,000 mtons per day; therefore, the cost of a metric ton of clay is estimated as $1.00 per ton. In order to calculate the costs of one brick (4.6 lbs) and one thousand bricks, a dollar per metric ton is divided by 2,205 lbs which yields $4.53514 × 10^{-4} lb^{-1}. Then, a pound value is multiplied by 4.6 lbs. Since 75 percent of a brick is assumed to contain Kline Mountain clay, the brick cost is multiplied by 0.75 and the result is multiplied by a thousand to get the mining cost of one thousand bricks. A mining loss of 15 percent is also taken into account for one thousand bricks, as shown below:

[1] Operator hourly burdened wage is $18.42. It is assumed as $18.75 per hour for 1993 (Western Mine Engineering, Inc., 1992).

Table 33: Mining cost per thousand bricks.

Mining* **(only consists of ripping, pushing and selecting with bulldozer)**
$\$1.00\ mton^{-1} = (\$4.53514 \times 10^{-4}\ lb^{-1})$[1]
$4.6\ lbs \times \$4.53514 \times 10^{-4}\ lb^{-1} = \$2.08616 \times 10^{-3}$ per king size brick[2] (hereafter brick)
$0.75 \times \$2.08616 \times 10^{-3} = \$0.00156462$ per brick (Kline Mountain clay portion)[3]
1,000 brick × $0.00156462 per brick= $1.5646 per thousand bricks (15 % mining loss)
$1.5646 per thousand bricks × 1.15 = $1.7993 per thousand bricks
*Estimated from Peters, 1987, pp. 267.

Table 34: Royalty cost per thousand bricks.

Royalty* **(See Appendix 3 for claim maps of the clay deposit)**
$\$1.00\ mton^{-1} = (\$4.53514 \times 10^{-4}\ lb^{-1})$[1]
$4.6\ lbs \times \$4.53514 \times 10^{-4}\ lb^{-1} = \$2.08616 \times 10^{-3}$ per brick[2]
$0.75 \times \$2.08616 \times 10^{-3} = \$0.00156462$ per brick (Kline Mountain clay portion)[3]
1,000 bricks × $0.00156462 per brick= $1.5646 per thousand bricks
* Estimated by Dr. G. F. Cudahy, President of the American Eagle Brick Company (pers. comm., June,1993).

[1] 1 metric ton = 2,205 pounds

[2] The company manufactures primarily the standard size brick (also known as king size brick), which is 2.625 by 3.00 by 9.625 inches in size and weighs 4.6 pounds, for residential construction. However, it also produces standard modular size brick, that is smaller than the king size brick, for commercial markets such as bank, school and office construction. All units in this economic analysis were calculated with respect to the king size brick.

[3] According to the firing experiments (Figure 93 and 94), good results were achieved with 25 % use of #3 local clay (Cerro de Cristo Rey). Therefore, it is assumed that white brick consists of 75 percent of Kline Mountain clay and 25 % of #3 and/or #1 of the local clay.

The mining operation takes approximately 2 months in the summer season of each year to recover annual clay production to meet the company's yearly need; therefore, camping is assumed to be sufficient. Thus, tent and camping equipment is needed, in addition to a storage shed with an estimated cost of $1,013 per year.

As stated previously, there are no electricity facilities in the mine area. Hence, it is assumed that camp electricity will be provided by a generator at a estimated cost of $2,700 per year. Finally, it is assumed that potable water can be provided either by a close creek or ground water at an estimated cost of $1,620 per year. These supplemental cost figures are estimated as intermediate values and taken from Stebbins (1987).

In order to calculate the supplemental costs of a thousand bricks, all these units are reduced to 1,000 bricks. The company makes 13,500,000 bricks per year. Thus, the supplemental costs in Table 44 are determined per thousand bricks.

7.2.3.2. Environmental Cost

Environmental costs elements are listed by the Bureau of Mines Information Circular (IC 9142, 1987), as surface water, ground water, air quality, geology, soil, vegetation, wild life, visual, archeological, and socioeconomic. It is also stated that environmental costs can vary drastically with respect to land type and mining impact.

As previously stated, Kline Mountain clay deposit is located in the Gila National Forest. For a project in a national forest, Paulsen (1982) reported that the environmental cost for an operational phase is between $20,000 and $50,000 per year. He also stated environmental cost from $10,000 to $30,000 per year for closure and reclamation phase. The environmental costs figures below are moderate range estimates from published case study figures by Paulsen (1982).

Table 35: Environmental cost per thousand bricks.

Environment*
Operating phase.....$36,000 year^{-1} Closure and reclamation phase.....$18,000 year^{-1}
Total.....$54,000 year^{-1}
$54,000 year / 36,000 mton.year^{-1} = $1.50 mton
$1.5 mton / 2205 lb = $6.80272 x 10^{-4} lb^{-1} $6.80272 x 10^{-4} lb^{-1} × 4.6 lb = $3.12925 x 10^{-3} per brick 0.75 × $3.12925 x 10^{-3} = $2.34693 x 10^{-3} per brick (Kline Mountain clay portion) 1,000 bricks × $2.34693 x 10^{-3} = $2.3469 per thousand bricks
* Estimated from Bureau of Mines Information Circular (IC 9142), 1987 and Paulsen, 1982.

7.2.3.3. Loading Cost

The company will employ its own loader, whose bucket capacity is 10 tons. Operation time of the bucket is 4 minutes every time. A full workday is assumed to be 8 hours. Thus, the loader is estimated to load 1,000 tons per day including breaks at predicted daily costs below (Dr. G. F. Cudahy):

Loader operator[1]($18.75 per hour × 8 hours per day)	$150 per day
Fuel (200 gallons per day)	$200 per day
Maintenance and labor	$200 per day
Amortize equipment haul ($1,000 per year)	$30 per day
Food, clothes, water, generator, camping, lost time and general services etc	$420 per day
Total	$1,000 per day

As previously stated, the planned clay production is 1,000 mtons per day. Therefore, loading costs is estimated as $1.00 per metric ton. In order to calculate the cost of one brick (4.6 lb) and one thousand bricks, a dollar per metric ton is divided by 2,205 lbs which yields 4.53514×10^{-4} lb^{-1}. Then, a pound value is multiplied by 4.6 lbs. Since 75 percent of a brick is assumed to contain Kline Mountain clay, a brick cost is multiplied by 0.75 and the result is multiplied by a thousand to get the one thousand bricks loading cost, as shown below:

[1] Operator hourly burdened wage is $18.42. It is assumed as $18.75 per hour for 1993 (Western Mine Engineering, Inc., 1992).

Table 36: Loading cost per thousand bricks.

Loading*
$1.00 mton^{-1} = ($4.53514 × 10^{-4} lb^{-1})[1]
4.6 lbs × $4.53514 × 10^{-4} lb^{-1} = $2.08616 x 10^{-3} per brick[2]
0.75 × $2.08616 x 10^{-3} = $0.00156462 per brick (Kline Mountain clay portion)[3]
1,000 bricks × $0.00156462 per brick= $1.5646 per thousand bricks
* Estimated by Dr. G. F. Cudahy, the President of the American Eagle Brick Company (pers. comm., June,1993).

[1] 1 metric ton = 2,205 pounds

[2] The company manufactures primarily the standard size brick (also known as king size brick), which is 2.625 by 3.00 by 9.625 inches in size and weighs 4.6 pounds, for residential construction. However, it also produces standard modular size brick, that is smaller than the king size brick, for commercial markets such as bank, school and office construction. All units in this economic analysis were calculated with respect to the king size brick.

[3] According to the firing experiments (Figure 93 and 94), good results were achieved with 25 % use of #3 local clay (Cerro de Cristo Rey). Therefore, it is assumed that white brick consists of 75 percent of Kline Mountain clay and 25 % of #3 and/or #1 of the local clay.

7.2.3.4. Transportation Cost

The Kline Mountain clay deposit is located about 170 miles away from El Paso, where the American Eagle Brick Company is located. Since trucking charges are usually computed in terms of round trip miles, the round trip miles (340 miles) are used to determine rates from a graph by Schumacher (1993). In order to determine the total cost to haul a short ton of clay 170 miles one way, the carrier revenue minimum potential rate per ton mile ($0.038) is found from the graph for a 340 mile distance, and this revenue is multiplied by 340 (Figure 100).

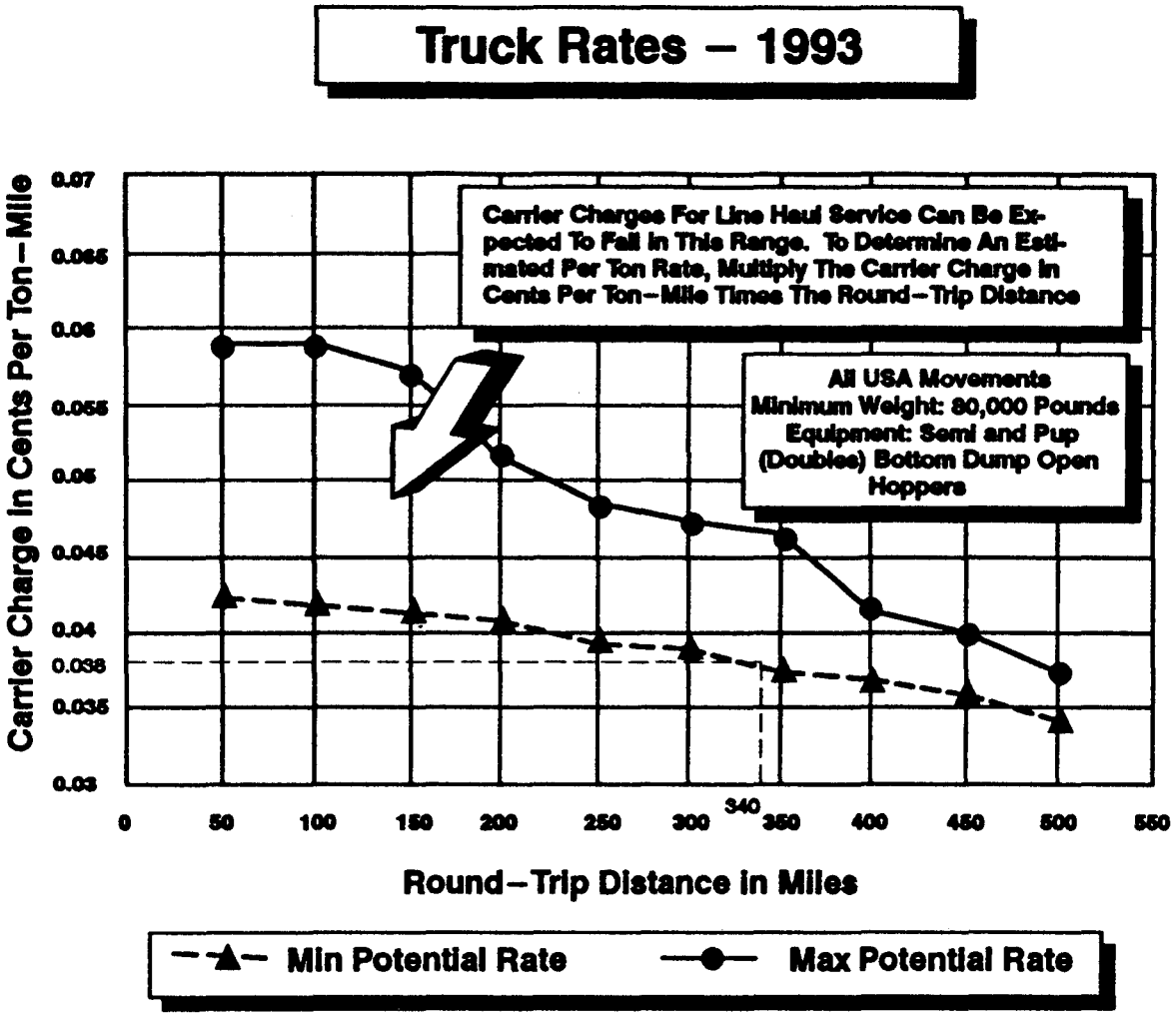

Figure 100: Transportation cost for trucks for 1993 showing carrier charge in cents per ton–mile versus round–trip distance in miles (Schumacher, 1993).

In order to estimate the transportation cost of one thousand bricks Kline Mountain clay portion, transportation costs is converted to a pound by dividing $12.92 per ton into 2,000 pounds. The transportation costs per pound is multiplied by 4.6 pounds. The result is multiplied by 0.75. For one thousand bricks transportation cost, a brick cost of Kline Mountain clay portion is multiplied by 1,000 as shown below:

Table 37: Transportation cost per thousand bricks.

Transportation*
340 miles (round trip) x \$0.038 $ston^{-1}$ = \$12.92 $ston^{-1}$ \$12.92 $ston^{-1}$ / 2,000 lbs^{1} = \$6.46 x 10^{-3} lb^{-1} \$6.46 x 10^{-3} lb^{-1} × 4.6 lbs = \$0.029716 per brick 0.75 × \$0.029716 per brick = \$0.022287 per brick (Kline Mountain clay portion)★ 1,000 bricks × \$0.022287 per brick = \$22.29 per thousand bricks
* Derived from Schumacher (ed), 1993. ★ It is assumed that white brick consists of 75 percent of Kline Mountain clay and 25 percent of #3 and/or #1 of local clay.

[1] 1 short ton = 2,000 pounds

Table 38: Labor cost per thousand bricks.

Labor*	
Grinding	2 people
Mining	2 people
Extruding	2 people
Loading kiln cars	6 people
Unloading cars for packaging	6 people
Kiln	4 people
Supervisors	2 people
Total	24 people
24 people x \$6.00♣ h^{-1} x 8 h.day^{-1} = \$1,152 day^{-1} \$1,152 day^{-1} x 250 days.$year^{-1}$ = \$288,000 $year^{-1}$ \$288,000 $year^{-1}$ x 15,000,000 bricks.$year^{-1}$= \$0.0192 $brick^{-1}$ 1000 brick x \$0.0192 $brick^{-1}$ = \$19.2 per thousand bricks	
* Dr. G. F. Cudahy, President of the American Eagle Brick Company (pers. comm., June,1993). ♣ Average including fringe benefits (A laborer works 40 hours a week).	

7.2.3.5. Natural Gas Cost

It is stated that 1,200 Btu (British thermal unit) is the generally accepted value for firing one pound of brick in a tunnel kiln (Dr. G. F. Cudahy, pers. comm., July, 1993). A brick weighs 4.6 pounds. Therefore, the required natural gas unit is 5,520 Btu to fire a brick. Since \$2.60 is the estimated cost for one million Btu (Dr. G. F. Cudahy, pers. comm., July, 1993), the natural gas estimated cost for one brick is calculated by multiplying \$2.60 by 5,520 Btu and dividing by a million. Then, the natural gas estimated cost for one brick is multiplied by one thousand to get the estimated natural gas cost for a thousand bricks.

Table 39: Natural gas cost per thousand bricks.

Natural Gas*
1,000,000 Btu estimated unit cost is $2.60. 1,200 Btu required for one pound brick firing 4.6 lb x 1,200 Btu = 5,520 Btu required per brick ($2.60 x 5,520Btu) / 1,000,000 = $0.014352 per brick 1,000 bricks × $0.014352 per brick = $14.35 per thousand bricks
* Estimated (Dr. G. F. Cudahy, pers. comm., President of the American Eagle Brick Company, June, 1993).

Table 40: Electricity cost per thousand bricks.

Electricity*
$5.49 per thousand bricks
*Estimated (Dr. G. F. Cudahy, pers. comm., President of the American Eagle Brick Company, June, 1993).

Table 41: Additives cost per thousand bricks[1].

Additives*
$5,000 per month additives cost × 1,250,000 bricks.month^{-1} = $4.0 x 10^{-3} per brick 1,000 bricks × $4.0 x 10^{-3} brick^{-1} = $4.00 per thousand bricks
* Calcium lignosulfonate (calcium salt plus inorganic salts, oxidized sugars, pentose sugars and carbohydrates), a byproduct of paper industry produced by Georgia-Pacif ic Cooperation, Bellingham, WA (Dr. G. F. Cudahy, President of the American Eagle Brick Company, pers. comm., June,1993).

[1]Calcium lignosulfonate is used by the company as an additive to improve extrudability and green strength in making brick. The company also uses iron oxide, ball clay, fire clay, manganese oxide as other additives to color brick's face.

7.2.3.6. Cost of #3 and #1 Local Clay Mining Operation

According to the firing experiments (Figure 93 and 94), good results were achieved with 25 % use of #3 local clay from Cerro de Cristo Rey where the company is currently mining for brick production. Therefore, it is assumed that white brick consists of 75 % Kline Mountain clay and 25 % of #3 and/or #1 local clay. The local clay contains smectite and organic material(s) (Ntsimanyana, 1990) both of which also improve plasticity and green strength which are desirable in white brick making. Thus, it is projected that 25 % of the local clay will be used in making white brick.

It is postulated that local mining cost is $2.00 per metric ton. In order to calculate a brick (4.6 lb) mining cost, one pound mining cost is determined by dividing the $2.00 into 2,205 lbs. The result is multiplied by 4.6 lb to get per brick cost, which is multiplied by 0.25 to determine the local mining cost per brick. Finally, this cost is multiplied by one thousand to determine a thousand brick local mining cost as shown in Table 42:

Table 42: Cost of #3 and #1 clay mining operation per thousand bricks.

Cost of #3 and #1 clay (mining operation)*
$\$2.00\ mton^{-1} / 2{,}205\ lb = \$9.07029 \times 10^{-4}\ lb^{-1}$ $4.6\ lb \times \$9.07029 \times 10^{-4}\ lb^{-1} = \$4.17233 \times 10^{-3}$ per brick $0.25 \times \$4.17233 \times 10^{-3} = \$1.04308 \times 10^{-3}$ per brick (Local clay portion) $1{,}000\ bricks \times \$1.04308 \times 10^{-3} = \$1.043$ per thousand bricks
* Dr. G. F. Cudahy, the President of the American Eagle Brick Company (pers. comm., June,1993).

Table 43: Packaging material cost per thousand bricks[1].

Packaging*
\$6,000 per month packaging cost / 1,250,000 brick.month^{-1} = \$4.8 x 10^{-3} per brick 1,000 bricks x \$4.8 x 10^{-3} brick^{-1} = \$4.80 per thousand bricks
* Dr. G. F. Cudahy, President of the American Eagle Brick Company (pers. comm., June,1993).

Packaging facilitates make brick ready for shipment by trucks. It gives important flexibilities such as handling, loading on trucks, unloading trucks on job site, and storing of bricks. The size of packages are adjusted to truck size. Packages are prepared by the company's fork lifting vehicle, since it is the cheapest method.

[1] The company spends \$6,000 per month to package monthly brick production of 1,250,000. In order to calculate a thousand brick estimated packaging cost, per brick packaging cost is determined by dividing \$6,000 into 1,250,000 bricks and the result is multiplied by 1,000. This cost does not include labor.

Table 44: Costs per thousand bricks sold.

Cost of Goods Sold* (per 1,000 brick)	
Mining (ripping and pushing with bulldozer)	$1.7993
Royalty	$1.5646
Supplemental★	
Camp	$0.0750
Generator	$0.2000
Pump	$0.1200
Environment	$2.3469
Loading	$1.5646
Transportation	$22.2900
Total (mine and transportation to plant)	$29.9604
Labor (average)	$19.2000
Natural gas	$14.3500
Electricity	$5.4900
Water[1]	$0.1800
Fuel and lubrication★ (machine, car, fork lift, loader, grinding equipment and extruder)	$1.4000
Additives	$4.0000
#3 and/or #1 clay	$1.0431
Packaging	$4.8000
Maintenance	
Parts (hammer mill, extruding machine, iron and steel, and replacement parts)	$1.9300
Labor (electrician and other outside labors)	$0.8500
Total (at the plant)	$53.2431
Subtotal ($29.9604 + $53.2431)	$83.2035
Contingency (10%)	$8.3203
TOTAL	$91.5238

* Assuming American Eagle Brick Company sells in that year only what the Company made that year and sells all that it made that year.
★Estimated from Stebbins, 1987.

[1] In order to extrude clay to make brick, clay has to be plastic. Plasticity can be achieved by the addition of water.

Table 45: Operating expenses of the American Eagle Brick Company per year.

Operating Expenses* (25% x Gross Revenue per year)	
Selling Expenses	
Fork lift lease	
Fuel	
Labor and its overhead	
Salesman	
Salesman's travel expenses	
Advertising	
Sales person at desk	
General and Administration (G&A)	
President	
Controller	
Assistant controller	
Secretary	
General insurance	
Office utilities	
Telephone	
Janitorial	
Office supplies	
Computers	
Interest payments on loans	
Short term	
Long term	
Depreciation	
Depletion	
Taxes	
Property (building and land)	
Excise (Texas state corporate excise tax)	
TOTAL (0.25 × $2,835,000, see Table 46	$708,750†

* Dr. G. F. Cudahy, President of the American Eagle Brick Company (pers. comm., June,1993).

† $59,063 per month
$52.50 per 1,000 brick

Table 46: Annual net income and operating cash flow.

Annual Net Income and Cash Flow (Per Year)	
Gross Revenue or Income (15,000,000 bricks.year^{-1} × 90% yield[1]) × ($210 per thousand bricks[2])	$ 2,835,000
Less Adjustments and Allowances[3] (0.5% × 2,835,000)	14,175
Net Revenue	2,820,825
Cost of Goods Sold ($91.5238 per thousand bricks × 15,000,000 bricks per year)	1,372,857
Gross Profit	1,447,968
Operating Expenses (25% × $2,835,000, see Table 45)	708,750
Operating Profit	739,218
Less depreciation for equipment[4] ($120,000 / 7 years)	17,143
Net Profit† (taxable income)	722,075
Income Tax[5] (20% × $722,075)	144,415
Net Income	577,660
Add: depreciation ($50,000 for plant equipment + $17,143 for mining equipment)	644,803
Add: depletion ($359.00 for 9,000 m tons of #3 and #1 local clay deposit)[6]	645,162
OPERATING CASH FLOW	**645,162**

* Estimated from Peters, 1987.

† The company is a SubS cooperation for tax purposes. Therefore, all the share holders pay their personal tax. All the operation profit is distributed to share holders (Dr. G. F. Cudahy, President of the American Eagle Brick Company, pers. comm., June 29,1993).

[1] According to Dr. G. F. Cudahy, the plant is on 90 % yield due to the 10 % substandard brick caused by drying and firing such as cracks, blistering and formation of black hearts.

[2] Estimated selling price per one thousand white bricks.

[3] Unpaid brick bills and returned brick due to faulty brick, brick color, and costumer dissatisfaction.

[4] The company equipment value for mining is estimated as $120,000. According to the tax law, value of mining equipment can be depreciated through 7 years (Arthur Valdez, II, CPA for American Eagle Brick Company, pers. comm., July,1993; U.S. Master Tax Guide, 1989).

[5] Federal income tax for share holders is estimated as approximately 20 %.

[6] Due to the royalty payment for the Kline Mountain clay deposit, no depletion amount is considered [9,000 m tons × 1.1 = 9,900 s ton (st.); 9,900 st. + 1.035 (3.5% mining loss) = 9,565 st.; 9,565 × $0.5 = $4,783; $4,783 × 7.5% depletion allowance (Mineral Commodity Summaries, 1990) = $359.00].

Table 47: Investments

Investments	
Environment[1]	
Planning phase	$40,000
Development and construction phase	$20,000
Supplemental	
Generator	$22,530
Camp equipment	$2,000
Water availability	$3,000
Overburden removal[2] ($0.6430 mton × 75m × 75m × 1m × 1.5 m^3 /mton)[3]	$5,425
Equipment and labor transfer[4]	$1,000
Subtotal	$93,955
Contingency (10%)	$9,395
TOTAL	$103,350

[1] Moderate range estimated from published case study figures by Paulsen (1982).

[2] Stebbins (1987) estimated overburden removal cost as $0.404 /LCY(loose cubic yard). Since 1 cubic yard is equal to 0.7646 cubic meter, the Stebbins figure is divided into 0.7646 cubic meters and the result is multiplied by 1.22 m^3/ton, the calculated density of clay, to get the estimated cost of overburden removal, $0.6430 per mton.

[3] It is assumed that an area of 75m by 75 m by 1 m will be removed for mining operation. The density of overburden is estimated as 1.5 m^3/ton.

[4] For mining operation at the mine site, the company has to transfer mining equipment and labor from its plant in El Paso, Texas.

Table 48: Present value of white brick made with the Kline Mountain clay in the American Eagle Brick Company Plant at a risk rate of return on invested capital of 15% and Hoskold sinking (redemption of capital) fund at a safe rate of 6%.

Profit per thousand brick ($210.00 × 0.995♠-$154.193*)	$54.7570
Profit per year ($54.7570 per thousand brick × 13,500,000 brick per year[1])	$739,220
Income Tax (20% × $739,220)	$147,844
Net Income	$591,376
Present value of operations ($591,376 × 6.148♣)	$3,635,780
Outlay for investment[2]	$103,350
NET PURCHASE VALUE (NPV)[3]	$3,532,430

♠1/2% adjustments and allowances, see Table 46.
* $91.5238/0.90[1] (Table 44) + $52.50 (Table 45) = $154.193 per thousand brick.
♣ Peters (1987), p. 275, Factor for present value during 30 year period.

[1] As stated earlier, the plant is on 90 % yield due to the 10 % substandard brick caused by drying and firing such as cracks, blistering and formation of black hearts. Thus, 1,500,000 bricks out of an annual 15,000,000 brick production are assumed to be discarded each year.

[2] It is assumed that the present American Eagle Brick Company in El Paso is free of liens. If not, these costs must subtracted from the net income.

[3] The NPV by Hoskold Method is conservative and tends to undervalue the property as a protection against risk (Peters, 1987, p. 274).

Table 49: Net Present Value (NPV) for the property.

Year	Cash Flow (CF)[1]	15% Discount Factor* (DF)	Present Value (PV)
1	645,162	0.870	561,291
2	645,162	0.756	487,742
3	645,162	0.658	424,517
4	645,162	0.572	369,033
5	645,162	0.497	320,646
6	645,162	0.432	278,710
7	645,162	0.376	242,581
8	645,162	0.327	210,968
9	645,162	0.284	183,226
10	645,162	0.247	159,355
11	645,162	0.215	138,710
12	645,162	0.187	120,645
13	645,162	0.163	105,161
14	645,162	0.141	90,968
15	645,162	0.123	79,355
16	645,162	0.107	69,032
17	645,162	0.093	60,000
18	645,162	0.081	52,258
19	645,162	0.070	45,161
20	645,162	0.061	39,355
21	645,162	0.053	34,194
22	645,162	0.046	29,677
23	645,162	0.040	25,806
24	645,162	0.035	22,581
25	645,162	0.030	19,355
26	645,162	0.026	16,774
27	645,162	0.023	14,839
28	645,162	0.020	12,903
29	645,162	0.017	10,968
30	645,162	0.015	9,677
TOTAL			$4,235,488
Investment (-)			$103,350
NET PRESENT VALUE (NPV) (acquisition value)			$4,132,138
* Single payment present value factors taken from Benjamin et al, 1989.			

[1] Assumes uniform cash flow over 30 year period.

The discount factor in Table 49 yields a present value over 30 year period without a separate safe rate of return on invested capital used in the Hoskold method above.

The actual value of the plant and equipment considering equipment replacement and set up is approximately $840,000 (Dr. G. F. Cudahy, pers. comm., June 29,1993). This value and capital investment in the new mine at Kline Mountain is $943,350. Then, by using the "rule of thumb" approach indicated by Peters (1987, p. 277-278), the DCFROI is calculated as 48 %.

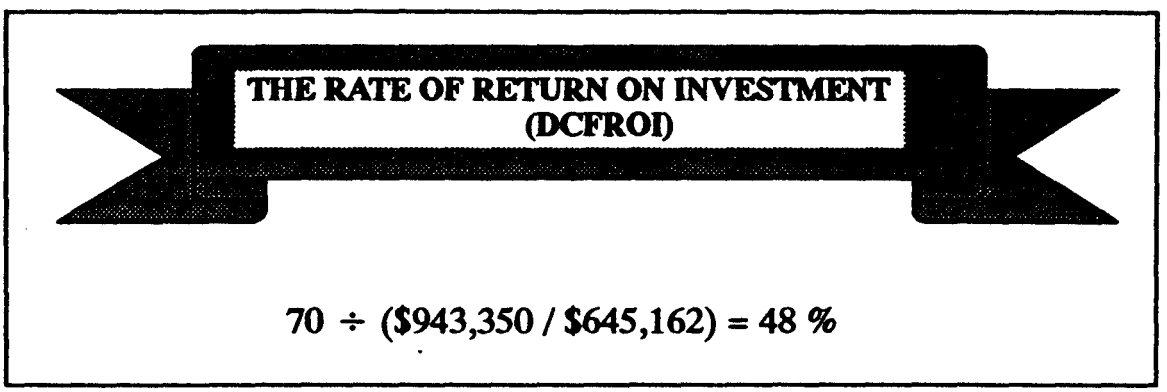

7.2.4. Results

On the basis of drill core calculated average mineral compositions, there are mineral percentage variations in the kaolinization zone (48 m) with respect to surface sample such that kaolinite, alunite, and accessories increase by 7.61, 4.60 and 0.10 % respectively, and silica decreases 12.73% (Table 27 and 28).

The probable reserve of clay is 6,316,048 m tons (Table 30)

On the average, the available clay is calculated to be composed of (Table 31):

Kaolinite: 40.67 %

Alunite: 16.37 %

Silica: 37.89 %

Accessories: 1.16 %.

Due to the possible mining loss caused by overburden, right of way of the road NM 59, difficulty of deep mining, siliceous and alunitic zones, the reduced tonnage of recoverable clay is 3,158,024 m tons (Table 32).

The nominal value of the clay is $16,358,564 fob at site of use (Table 32), using a nominal price of $5.18 per metric ton.

The life of the mine is about 88 years, at a mining rate of 36,000 mtons per year.

The cost of goods sold (per 1,000 brick) is $91.5238 (Table 44).

The operating expenses of the brick company are $708,750 per year (Table 45).

The annual operating cash flow, after 90% yield and 0.5% adjustments and allowances in brick making, are $645,162 per year (Table 46).

The total investment (Table 47) is $103,350.

The NPV by the Hoskold method (Table 48) is $3,532,430. This includes 15 % interest on investment and redemption of capital at 6 %.

The NPV of brick made with Kline Mountain clay at American Eagle Brick Company for the following 30 years (Table 49) using the single factor Discounted Cash Flow method is $4,132,138.

The DCFROI is 48 %.

7.2.5. Discussion of the Economic Analysis

Although the two NPVs are similar in order of magnitude, the difference between the two NPVs is due to the Hoskold method which tends to undervalue the property as a protection against risk, as described by Peters (1987). The rate of discounted cash flow return on investment (DCFROI)–48 %–is higher than a possible and acceptable hurdle rate of 15%. On the basis of the NPV and DCFROI, manufacturing white brick by recovering the Kline Mountain clay at the American Eagle Brick Company plant in El Paso is found to be economically viable under the projected conditions.

The company presently sells one thousand regular bricks for an average of $150.00. The cost of white brick appears to be about $30.00 per thousand brick above the company's present cost. It is expected that the company will recover two times the marginal cost by making white brick ($60.00), at a market price of $210.00 per thousand brick. Currently, the demand for white brick in the El Paso area is being supplied from the Athens Brick Company, Athens, Texas; Acme Brick Company (Perla Plant), Perla, Arkansas; and Summitt Brick Company, Pueblo, Colorado; which are about 800 miles, 1200 miles and 700 miles from El Paso, respectively. This adds significant incremental cost to the brick in the local market (Isik, 1992). About half of American Eagle's brick is sold in the El Paso area. The other half is sold to locations as far east as Dallas, Texas and as far north and west as northern New Mexico, Arizona, Nevada, and California. Also, the company sells a relatively small amount of brick to Mexico (per. commun., Dr. G. F. Cudahy, June 12, 1993). Since there are no white brick producers in the local area, one thousand white bricks are usually sold between $250.00

and $300.00 in the local market. Obviously, local market conditions are especially favorable for the company's white brick production, where the company markets between 50 and 60 % of sales.

As seen in Table 44, transportation of the clay to the company, energy (natural gas and electricity), and labor will be the largest parts of the brick manufacturing costs. Therefore, any reduction in these costs will increase the company's ability to impact the local white brick market. Also, increasing the current yield ratio (90%) will give another flexibility to the company for market penetration. To be ready for the possible free trade implementation consequences in the future, additional production cost reduction should be considered by the company to compete with Mexican brick products where the production costs are relatively lower. A supplier of white brick from the Chihuahua city area in Mexico, discontinued brick production in approximately 1988, in favor of tile manufacture (Dr. K. F. Clark, pers. commun., July 19, 1993).

The brick manufacturing business is somewhat seasonal and is also driven by the cyclical nature of the building industry. While the brick manufacturing facilities in the southwest part of the USA are presently near capacity, it is expected, as is usual, that the demand for brick products will wane in the future. What is more important to the brick manufacturer located in the El Paso area than an increase in profit margins is the expansion of the brick products and subsequent expansion of the brick market that white brick allows. This should help augment any future low demand period. This amelioration of the cyclical nature of the

business yields even greater benefit to the local brick manufacturers socially and economically such as retaining employees and marketing bricks throughout the year.

CHAPTER 8
CURRENT ACTIVITIES

In June 1993, Internacional de Ceramica S. A. (Interceramic) of Chihuahua, Mexico reported the company's interest in manufacturing white wall and floor tiles from the Kline Mountain kaolin (Dr. K. F. Clark, pers. comm., June 1993). The Interceramic Company was founded in 1981 and its plant is located 240 miles south of El Paso. It is currently employing 2200 people to manufacture floor and wall tiles by employing three shifts, 24 hours a day. The company manufactures 1.2 million square meters of tile per month. The company is primarily marketing in Mexico, but is also exporting tiles to the USA. In the future, it plans to locate a clay deposit in Texas or New Mexico and build a plant in the Dallas area (Diario de Juarez, August 3, 1993).

From Interceramic's preliminary studies, Javier Holguin L. (Interceramic geologist) recovered samples randomly from the Strip Mine site of the Kline Mountain kaolin deposit at the beginning of June 1993. On the basis of the company's preliminary firing studies, SO_3 within the Kline Mountain clay was reported a potential problem in making tiles due to its undesirable effect to the atmosphere, kiln, and tile. According to the chemical analysis done on the sample for Interceramic, SO_3 content was reported to be 5.54 weight percent (Max Medrano H., research and development manager of the Interceramic, pers. comm., July 31, 1993), while it was detected between 0.00 and 17.20% on the six samples recovered on July 31, 1993.

The Kline Mountain kaolin (100 %) was molded as tile and fired at 1080 °C. For the second experimental tile, the Kline Mountain clay (59 %) was mixed with ball clay (22 %), silica (12 %) and calcite (7 %) and molded as tile followed by firing at 1080 °C. As seen in Figure 101, the firing color of these tiles is reported to be attractive for the company's needs (Max Medrano H. and Javier Holguin L., Interceramic Company, pers. comm., July 31, 1993). According to the preliminary studies, the company decided to further explore on the Kline Mountain clay for the manufacturing of white tiles.

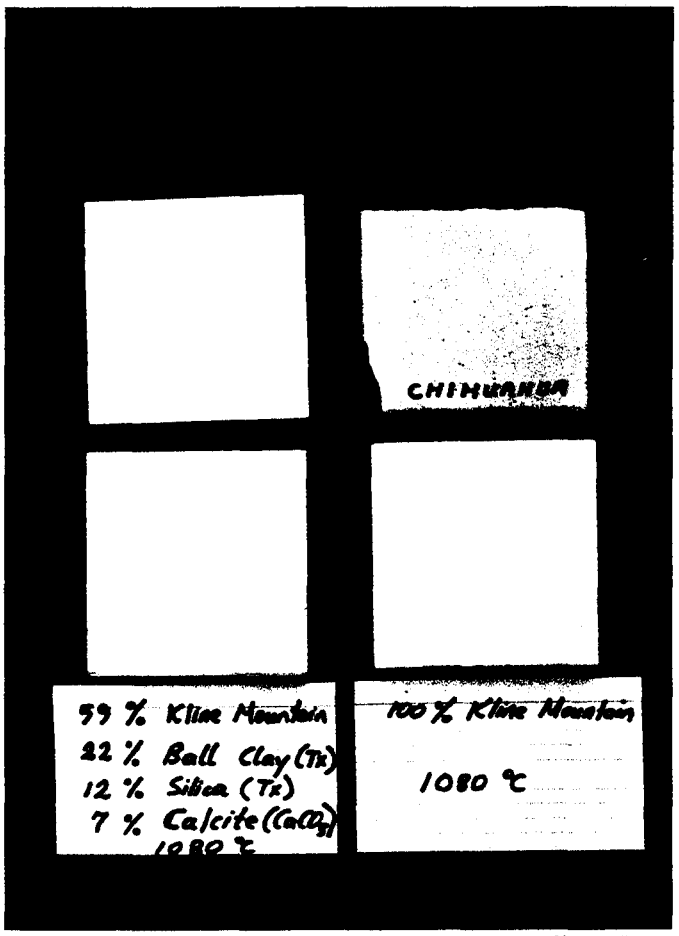

Figure 101: Tiles manufactured from a pure and a mixture of the Kline Mountain kaolin by the Interceramic Company, Mexico, showing the white fired tiles in comparison with the Chihuahua tile.

On July 31, 1993, Dr. K. F. Clark and I were asked by the interceramic company geologists to accompany them to show the deposit on site and to recover samples for their ongoing evaluation. During our latest trip to the deposit, a bulldozer equipped with drilling equipment (Figure 102) was seen. Moreover, several locations in and around the Strip Mine were already drilled, most likely by this drilling equipment indicating serious exploration of the deposit. Holes were approximately 10 cm in diameter and from 5 to 10 m depth. Part of the pulverized material was also sampled by Interceramic at two borehole localities. As of today, no information has been obtained as to who accomplished this drilling program. Thus, three different groups currently have interested in the Kline Mountain kaolin deposit: American Eagle Brick Company, El Paso, Texas; Internacional de Ceramica, Chihuahua, Mexico; and one unknown group that performed drilling between February and July, 1993.

Figure 102: Bulldozer equipped with drilling equipment in the Strip Mine location of the deposit (The picture was taken on July 31, 1993).

CHAPTER 9
CONCLUSIONS

The Kline Mountain kaolin deposit is located in the Black Range which lies on the eastern margin of the Mogollon Plateau volcano–tectonic province. The stratigraphy in the Kline Mountain clay deposit area consists of mid–Tertiary bimodal volcanic and volcanoclastic deposits that consist of basaltic andesite lavas, high–silica rhyolite lavas, and pyroclastic material.

Local faults in the study area could have originated by the intrusion of Kline Mountain rhyolitic domes, which may be a set of ring fracture intrusions possibly related to the Gila Cliff Dwellings cauldron to the west. These faults have probably been reactivated by the Basin and Range extension in the past 21 Ma and/or the Rio Grande rift. The study area lies on the Black Range, which is reported as a west–dipping homocline bounded on the east by the range–margin–fault of the Winston graben that has dropped relative to the Black Range uplift. Faults in the study area display two dominant trends: northwest and northeast. They are silicified, altered and mineralized in some localities.

Volcanic units in the field have undergone hydrothermal alteration. Alteration is most intense near the intrusive contact of the Kline Mountain Rhyolite Porphyry and gradually diminishes distally. The Kline Mountain rhyolite intrusion is also altered. Four distinct alteration assemblages are recognized in the study area. These assemblages are: (1) weak propylitic alteration, (2) argillic alteration, (3) advanced argillic alteration, and (4) silicification. Alteration of the volcanic units occur primarily by replacement. Of these, the advanced

argillic alteration zone contains commercial kaolin deposits which have been exploited intermittently. Advance argillic alteration, characterized by a kaolinite–alunite–silica (chalcedony, tridymite, and quartz) mineral assemblage, is widespread in the study area. This pervasive alteration in the area developed in situ and is related primarily to hydrothermal regimes developed concurrent with or subsequent to the intrusion of the rhyolite porphyry of Kline Mountain. Kaolinite and alunite are the most diagnostic indicators of advance argillic alteration. On the basis of calculated mineral composition, kaolinite is the dominant clay mineral in the northern part of this alteration zone where the abandoned mines are located, while alunite is the dominant mineral to the south near the contact of the intrusive. The resulting alteration mineral assemblages may best be described, from north to south, as a kaolinization zone with alunite to alunitization zone with kaolinite.

On the basis of representative drill core fragments, the depth of the kaolinization zone is 48 m. Between 0 and 48 m the tuff is completely altered to kaolinite–alunite–silica mineral assemblage with a characteristic white color and softness.

In the advanced argillic alteration assemblage adjacent to the Kline Mountain intrusive, alunite inevitably contaminates the kaolin deposit. Based on the calculated average mineral composition within the 48 m kaolinization zone of the drill core, kaolinite and alunite proportions increase with depth; on the other hand, the silica proportion decreases with depth.

Silicification is considerable in the study area, and is primarily restricted to three localities within the tuff of Kline Mountain and Kline Mountain Rhyolite Porphyry. They are :

(1) silicified tuffs at the top of the tuff of Kline Mountain, (2) chalcedonic quartz within the kaolin deposit, and (3) widespread silicification at the top of the Kline Mountain Rhyolite Porphyry.

Hydrothermal activity was responsible for silicification as well as kaolinization in the study area. Thus, it appears that silicification in the study area was formed as a result of precipitation from cooling waters supersaturated with dissolved SiO_2, as evidenced by colloform and botryoidal habits of chalcedonic silica in the SEM images, and also as a result of a strong acidic environment that altered volcanic units (pumice and rhyolite) mostly to kaolinite and alunite by dissolving SiO_2.

Some of the silicified unit (sinters) readily breaks down into fragments when the deposits become desiccated due to shifting hydrothermal activity and exposure to weathering. Depending on the weathering environment, the fragments may remain in place, or more commonly may be transported locally by wind or water, and occasionally become cemented by later hot-spring activity. A great amount of chalcedonic nodules and fragments distributed in the north of the open pit mine location are believed to be eroded silica fragments possibly from the top of the silica cap.

In the kaolinitic clay, SiO_2 shows an inverse relationship with Al_2O_3. In the alunitic samples (Tkm 18 and 20), SiO_2 has the lowest percentage, while Al_2O_3, K_2O and loss on ignition (LOI) are the highest percentages. Also, the ratio K_2O+LOI:SiO_2 is very low in the kaolin clays and is high in the alunite samples.

From chemical analyses of samples, the calculated mineral percentages correspond to minerals present from XRD data. Minerals are calculated under four categories: kaolinite, alunite, silica, and accessory minerals. Silica should be accounted for as quartz, tridymite, opal, and cristobalite. Semiquantitative calculated mineral composition of outcrop samples from chemical analysis shows an inverse relationship between kaolinite percentage and proximity to the intrusion. Conversely, it displays a proportional relationship between alunite content and the proximity of the intrusion. This evidence suggests that around the intrusion the advanced argillic alteration zone contains dominantly alunite, while in the more distantly located pits kaolinite predominates. Variations in the proportions of minerals were found with respect to depth of the drill core. Within the kaolinization zone, the kaolinite proportion is between 30.97 % and 58.20 %. However, this percentage drops drastically down to 5.27 %, with 72.63 % of silica in the basal breccia zone, which is the kaolin deposit.

On the basis of X-ray diffractogram patterns, most of the whole-rock minerals is composed of kaolinite, alunite, tridymite, quartz, cristobalite and accessory minerals. Kaolinite is present in both whole-rock and clay size fractions of each sample. However, alunite dominant samples (Tkm 18 and Tkm 20) in both sizes show weak, small peaks of kaolinite reflection that would indicate very minor kaolinite content. Cristobalite is detected in only one of the bulk samples as a chief constituent. Tridymite is present in both sample sizes in a different intensity with the exception of alunitic tuff (Tkm 20).

Kaolinite is the most common clay mineral detected in <2μm samples. However, smectite was identified in two samples as the second clay mineral present. No change in or-

dering of XRD patterns of the glycolated and heated samples were observed in the preliminary study of deposit, indicating no significant amount of expandable clay minerals. The kaolinite is well–crystallized as evidenced by the sharp 001 and 002 reflections.

XRD data indicates that the mineralogy of the clay–size fractions is different from that of the drill core. The mineralogical difference among the different size fractions within given samples show that quartz is concentrated in the coarse fractions (>2 μm). In the < 2 μm fraction, kaolinite predominates in 14 out of 24 samples and quartz is absent in 19 out of 24 samples. In the drill core samples, kaolinite is the chief mineral followed by alunite and tridymite. However, alunite is the chief mineral followed by kaolinite in the deepest core sample obtained.

SEM photomicrographs of three outcrop samples show different varieties of kaolinite textures: columnar covered by very fine silica silcretes, well–crystallized, relatively poorly crystallized, and stacks. Even though all the SEM photomicrographs demonstrate evidence for fine–size silica content (lepispheres) and one sample displays these fine–size silica textures with high porosity associated with alunite flakes. Energy–dispersive spectroscopy indicates aggregates of bladed crystals composed of individual lepispheres consisting dominantly of silica minerals (tridymite and/or cristobalite). SEM images of alunite demonstrate identical crystal forms (hexagonal and pseudorhombohedral) and flakes within the typical texture (tightly packed and associated with lepispheres). The SEM images show that alunite crystals are hexagonal and pseudorhombohedral associated with bladed silica crystals, which are intergrown with lepispheres.

Particle-size analyses show that the shallowest drill core sample, which includes silica (tridymite, quartz, and cristobalite), kaolinite, and alunite, has the highest percentage of clay-size particles. With the exception of alunitic clay, there is a proportional relation between kaolinitic content percentages and clay-size fraction percentages of kaolinitic surface samples. Larger clay-size fractions in some samples indicate larger amounts of kaolinite. The two open pit samples show more sand-size fraction than the other samples. For the drill core samples, the majority of the material is clay-sized, less so silt-sized, and sand^{+}-sized particles. On the other hand, two kaolinitic surface samples have clay-sized particles as a principal dominant fraction. The alunitic clay sample (Tkm 18) has the silt-sized fraction as the chief constituent. The open pit mine sample SM 200 contains the least percentage of clay-sized fraction, while the shallowest drill core sample contains the least percentage of sand+ sized fraction.

In the firing experiments, four different sets of samples were prepared. The first set was prepared without any additive fluxing agent, while the others were prepared with a certain amount of fluxing agents. Also, the laboratory extruder of American Eagle Brick Company was employed for the second set of the samples. In order to determine if there was vitrification without adding any flux to the clay, the patties (molds) were fired at different temperature by using the Standard Large Orton Pyrometric Equivalents (PCE) cones to observe the temperature.

From the average absorption of water point of view for each experimental brick specimen, the following conclusions can be drawn:

1) The fluxing agents influence the water absorption rates of experimental brick positively (reduce absorption) with the exception of hydrated lime.

2) Increase of firing temperature appears to play a greater role in lowering the water absorption.

3) In increasing order, talc, nepheline syenite+white silica and #3 clay+nepheline syenite+white silica decreases the water absorption in the lower temperatures.

4) Pure kaolin displays the second highest percentages of water absorption exceeded only by hydrated lime additive in the clay body.

5) There is an inverse linear relationship between water absorption and temperature.

6) Kaolin+#3 clay+nepheline syenite+white silica mixture shows a minimum amount of water absorption at lower temperatures.

There is a proportional linear relation between compressive strength and temperature. Kaolin+#3 clay+nepheline syenite+white silica shows the highest compressive strength at lower temperature (3617 psi at 1900 °F) which is higher than the required compressive strength (2500 psi for Grade SW, 2200 psi for grade MW, and 1250 psi for Grade NW). Kaolin+#3 clay and/or #1 clay with nepheline syenite and white silica should be the best mixture for high compressive strength at low temperature. Thus, this mixture appears to be not only favorable for lowering the water absorption but also for providing highest compressive strength at low temperature. In addition, #3 clay improves plasticity and green strength of brick made from Kline Mountain kaolin. To make a comparison between the Chihuahua white brick and the Kline Mountain kaolin brick, a compressive strength test was

conducted on the Chihuahua white brick. It was determined to be 1005 psi, which is weak under the required standards for all weathering grades, Negligible Weathering (NW), Moderate Weathering (MW), and Severe Weathering (SW).

The fired brick specimens also demonstrated excellent white color properties. The bright whiteness of the fired specimen can give more market flexibility to the local brick company to produce various shades of white colored brick from Kline Mountain kaolin by adding from 15 to 50 % of #3 and/or #1 clay with nepheline syenite to the kaolin so that a complete range of white to gray colored brick can be produced. This has the additional advantage of lowering the cost of producing white brick, because the #3 and/or #1 clay have negligible transportation cost to the firing plant, both of which are located on the eastern flank of Cerro de Cristo Rey in the El Paso area.

The water absorption was the only physical property determined to be high for the specimens. However, all the brick specimens were prepared without using a vacuum which can reduce the porosity in a brick body and thus reduce water absorption. Water absorption is determined in the lowest percentages at lower temperatures in the specimens containing kaolin+#3 clay+nepheline syenite and white silica. Thus, using #3 clay and/or #1 clay in various percentages from 15 to 50 % with nepheline syenite and by extruding under vacuum the brick would have not only color manipulation but also reduced water absorption. By using these clay mixtures followed by extrusion with vacuum, water absorption should be reduced in the fired brick to the required limit and possibly lower than the required limit which is 20 percent for Grade SW, 25 percent for Grade MW, and no limit for Grade NW.

The firing experiments have determined that the experimental brick specimens made with the Kline Mountain kaolin have the plasticity, green strength, workability and extrudability properties needed for utilization by the brick industry without any defects as a result of firing and chemical composition.

The degree of success of any new project will ultimately depend on the underlying economic strength of the project as well as how successfully the parties involved can coordinate their interests. In the case of the Kline Mountain kaolin deposit, which had been used only sparingly by industry, the most striking attractions are its convenient location (crossed by NM Highway 59), large reserves, high brightness, cheap extraction methods, and readiness to be sold. Furthermore, there are no water flooding problems, although snow cover will be a hindrance in winter time.

On the basis of drill core calculated average mineral compositions, there are mineral percentage variations in the kaolinization zone (48 m) with respect to surface sample such that kaolinite, alunite, and accessories are higher by 7.61, 4.60 and 0.10 % respectively, and silica is lower by 12.73%. The probable reserve of clay is 6,316,048 m tons, as calculated by the triangular area of influence method constructed between chemically analyzed surface samples and one core hole sample. On the average, the available clay is calculated to be composed of: Kaolinite (40.67 %), alunite (16.37 %), silica (37.89 %) and accessories (1.16 %). Due to the possible mining loss caused by overburden, right of way of the road NM 59, difficulty of deep mining, siliceous and alunitic zones, the reduced tonnage of recoverable clay is considered to be 3,158,024 m tons.

The economic parameters of the Kline Mountain deposit are as follows. The corresponding value of the clay is $16,358,564 Fob at site of use, using a nominal price of $5.18 per metric ton. The life of the mine is about 88 years, at a mining rate of 36,000 m tons per year. The cost of goods sold (per 1,000 brick) is $91.52. The operating expenses of the brick company are $708,750 per year. The annual net income and operating cash flow, for 90% yield and 0.5% adjustments and allowances for defective brick and unpaid bills, are $645,162 per year. The total investment is $103,350, and the value of the production plant is estimated to be $840,000. The Net Present Value (NPV) by the Hoskold method is $3,532,430. This includes 15 % interest on investment and redemption of capital at 6 %. The NPV of brick made with Kline Mountain clay at American Eagle Brick Company for the next 30 years using the single factor Discounted Cash Flow (DCF) method is $4,132,138. The Discounted Cash Flow Return On Investment (DCFROI) is approximately 48 %. Although the two NPVs are similar in order of magnitude, the difference between the two NPVs is due to the Hoskold method which tends to undervalue the property as a protection against risk. The DCFROI rate–48 %–is significantly higher than a possible and acceptable hurdle rate of 15% as an investment opportunity. On the basis of the NPV and DCFROI, manufacturing white brick by recovering the Kline Mountain clay at the American Eagle Brick Company plant in El Paso is found to be economically viable under the projected conditions.

REFERENCES

ASTM Standard Specifications for Brick and Applicable Testing Methods for Units and Masonry Assemblages, 1975: Brick Inst. America, 80 p.

Barnes, C. G., Ensenat S. E., and Hoover, J. D., 1991, Mineralogy and Geochemistry of Eocene Intrusive Rocks and their Enclaves, El Paso Area, Texas and New Mexico: Am. Mineral., v. 76, pp. 1306–1318.

Barnes, H. L., 1979, Geochemistry of hydrothermal ore deposits (2nd ed): New York, John Wiley and Sons, Inc., 798 p.

Benjamin, J. J., Francia, A. J., and Strawser, R. H., 1989, Principles of Accounting (5th ed.): Dame Pub., Inc., Houston, Texas, 1007 p.

BIA News, 1993, Brick Institute of America, v. 6, n. 6, June 1993, Reston, Va, 22 p.

Brickell, T. G.,1989, Reference Manual for the Clay Mineral Analysis Laboratory of the New Mexico Bureau of Mines and Mineral Resources: New Mexico Inst. Min. Tech., Socorro, New Mexico, (unpub. report) 22 p.

Brindley, G. W. and Brown, G., 1980, Crystal structures of clay minerals and their X-ray identifications: Mineralogical Society, London, 495 p.

Browne, P., 1992, Hydrothermal Processes and Their Mineralogical Signatures: Unpub. course notes, New Mexico Tech, Socorro, New Mexico.

Bureau of Mines Cost Estimating System Handbook (in two parts) 1. Surface and Underground Mining: (compiled by staff, Bureau of Mines), 1987: U.S. Bur. Mines Inf. Circ., IC 9142, 630 p.

Chowdhury, J., 1980, New Mexico Kaolin: Unpub. report, Dresser Industries, 11 p.

Coney, P. J., 1976, Progress report on the Mogollon Plateau volcanic field southwestern New Mexico, No. 3–surface expression of a pluton, Cenozoic Volcanism in Southwestern New Mexico, W. E. Elston and S. A. Northrop (eds): New Mexico Geol. Soc., Spec. Pub. 5, pp. 29–41.

DeVilliers, T. E., 1962 a, The evaluation of a new kaolin clay for use in coating and filling of paper: Unpub. report, Project 2343, Inst. Paper Chemistry, Appleton, Wisconsin, 33 p.

DeVilliers, T. E.,1962 b, The evaluation of a new kaolin clay for use in coating and filling of paper: Unpub. report, Project 2343, Inst. Paper Chemistry, Appleton, Wisconsin, 9 p.

DeVilliers, T. E.,1962 c, The evaluation of a new kaolin clay for use in coating and filling of paper: Unpub. report, Project 2343, Inst. Paper Chemistry, Appleton, Wisconsin, 10 p.

Dixon, J. B. and Weed, S. B., 1989, Minerals in Soil Environments: Soil Science Soc. America, Madison, Wisconsin, USA., 2 nd ed.

Eggleston, T. L., 1987, The Taylor Creek District, New Mexico: geology, petrology, and tin deposits: Unpub. Ph. D. dissert., New Mexico Inst. Min. Tech., Socorro, New Mexico, 473 p.

Eggleston, T. L., and Norman, D. I., 1983, Taylor Creek tin district–stratigraphy, structure, and timing of mineralization: New Mexico Geology, v. 5, pp. 1–4.

Elston, W. E., Rhodes, R. C., Coney, P. J., and Deal, E. G., 1976, Progress report on the Mogollon Plateau volcanic field southwestern New Mexico, No. 3–surface expression of a pluton, Cenozoic Volcanism in Southwestern New Mexico, W. E. Elston and S. A. Northrop (eds): New Mexico Geol. Soc., Spec. Pub. 5, pp. 3–28.

Elston, W. E., 1984, Mid–Tertiary ash flow tuff cauldrons, southwestern New Mexico: Jour. Geophys. Res., v. 89, pp. 8733–8750.

Ericsen, G. E., Wedow, H. Jr., and Eaton, G. P., 1970, Mineral resources of the Black Range Primitive area, Grant, Sierra, and Catron counties, New Mexico: U.S. Geol. Surv. Bull. 1319-E, 162 p.

Eslinger, E., and Pevear, D., 1988, Clay Minerals for Petroleum Geologists and Engineers: Soc. Econ. Paleontol. Mineral., short course notes, n. 22, 428 p.

Grim, R. E., 1968, Clay Mineralogy: New York, McGraw-Hill, 2nd ed., 596 p.

Grimshaw, R. W., 1971, The Chemistry and Physics of Clays and Allied Ceramic Materials: New York, Wiley-Interscience, 4 th ed., 1024 p.

Harrison, R. W., 1986, General geology of Chloride mining district, Sierra and Catron counties, New Mexico: New Mexico Geol. Soc. Guidebook, 37th Field Conf., pp. 265-272.

Isik, I., 1990, The characteristics of the Kline Mountain kaolin deposit, Black Range, New Mexico: Unpub. rept., New Mexico Inst. Min. Tech., Socorro, New Mexico, 26 p.

Isik, I., 1992, Proposal for Ph. D. Research : Department of Geological Sciences, Univ. Texas, El Paso, Texas, 29 p.

Isik, I., and Clark, K. F., 1992, A comparison between two hydrothermally formed extensional environment related kaolin deposits: Balikesir-Duvertepe, Turkey and Kline Mountain, Sierra County, New Mexico: Abstracts with Programs 1992, Annual Meeting, Cincinnati, Ohio, USA, Geol. Soc. America, p. A63.

Keller, W. D., 1978, Method of kaolin investigation in International Clay Conference 1978, M.M. Mortland and V. C. Farmer (eds), Developments in Sedimentology 27: New York, Elsevier, 1979, pp. 581-590.

King, D., 1953, Origin of alunite deposits at Pidinga, South Australia: Econ. Geol., v. 48, pp. 689-703.

Klinefelter, T. A. and Hamlin, H. P., 1957, Syllabus of Clay Testing: United States Dept. Interior, Bureau of Mines, Washington, 67 p.

Kyle, J. R. and Clark, K. F., 1990, Geology of the Allamoore Talc District, West Texas: Soc. Econ. Geol., Guidebook, v. 8, pp. 181–190.

Long, D. T., Fegan, N. E., McKee, J. D., Lyons, W. B., Hines, M. E., and Macumber, P. G., 1992, Formation of alunite, jarosite and hydrous iron oxides in a hypersaline system: Lake Tyrrell, Victoria, Australia: Chem. Geol., Amsterdam, v. 96, pp. 183–202.

Lovejoy, E. M. P., 1976, Geology of Cerro de Cristo Rey Uplift, Chihuahua and New Mexico: New Mexico Bur. Mines Memoir, 31:84.

Meyer, R. and Reis, R. B. P., 1985, Paleosols and alunite silcretes in continental Cenozoic of western Portugal: Jour. Sedimentary Petrol., v. 55, no. 1, pp. 76–85.

Mineral Commodity Summaries, 1990: U.S. Bureau Mines, Washington, 199 p.

Moore, D. M., and Reynolds, R. C., 1989, X-Ray Diffraction and the Identification and Analysis of Clay Minerals: Oxford Univ. Press, Oxford, U.K., 332 p.

Ntsimanyana, M., 1990 a, Mineralogy and Exploitation of the Anapra and Messilla Valley Formations for the Production of Brick and Tile, Anapra, Dona Ana County, New Mexico: M. S. thesis, Dept. Geol. Sciences, Univ. Texas, El Paso, Texas, 186 p.

Ntsimanyana, M., 1990 b, El Paso Brick Company, Geology, Mining, Processing and Marketing: To Accompany A Visit by American Institute of Mining, Metallurgical and Petroleum Engineers: Dept. Geol. Sciences, Univ. Texas, El Paso, Texas, 18 p.

Patterson, J. A., 1959, Estimating Ore Reserves Follows Logical Steps: Eng. Min. Jour., v. 160, No: 9, pp. 111–115.

Patterson, S. H. and Holmes, R. W., 1965, Clays in Mineral and Water Resources of New Mexico: New Mexico Bur. Min. Min. Res. Bull. 87, pp. 312–322.

Paulsen, K. R., 1982, Environmental and Regulatory Costs of Mining Projects in Mineral Industry Costs (compiled by J. R. Hoskins): Northwest Mining Assoc., pp. 27–32.

Peters, W. C., 1987, Exploration and Mining Geology: New York, John Wiley and Sons, Inc., 685 p.

Sallee, G. L., 1962, Evaluation of a New kaolin clay for use in coating and filling of paper: Unpub. report., Project 2343, Inst. Paper Chemistry, Appleton, Wisconsin, 9 p.

Scholle, P. A., 1979, A Color Illustrated Guide to Constituents, Textures, Cements, and Porosities of Sandstones and Associated Rocks: Tulsa, Amer. Assoc. Petrol. Geol., 201 p.

Schumacher, O. L. (ed), 1993, Mining Service Cost: Spokane, Western Mine Engineering, Washington, pp. TRiv.

Stebbins, S. A., 1987, Cost Estimation Handbook for Small Placer Mines: U. S. Bur. Mines Inf. Circ. I.C. 9170, 94 p.

Subasic, C., A., 1993, Brick Institute of America, E.I.T., Engineering and Research Division, pers., commun., June 1993.

Tichane, R., 1990, Clay Bodies: New York, The New York Glaze Institute, 339 p.

U.S. Master Tax Guide, 1989: Commerce Clearing House Inc., 72nd ed., 2801 p.

Valdez, A., II, 1993, CPA for American Eagle Brick Company: pers. comm., July,1993.

Velde, B., 1985, Clay Minerals in series developments in sedimentology, New York, Elsevier, v. 40, 427 p.

Waggoner, J., 1993, Realty specialist for the Bureau of Land Managment, Las Cruces, New Mexico, per., comm., July 9, 1993.

Welton, J. E., 1984, SEM Petrology Atlas: Tulsa, Amer. Assoc. Petrol. Geol., 237 p.

Woodal, R., 1991, Director of exploration, Western Mining Corpation Limited Exploration Division, Unley, South Australia: written communication.

Woodard, T. W., 1982, Geology of the Lookout Mountain area, northern Black Range, Sierra County, New Mexico: M. S. Thesis, Univ. New Mexico, Albuquerque, 95 p.

Appendix 1: Quantitative Determination of Mineral Content

The method used in this calculation, which is best described as semi-quantitative, is based on the major element chemical analyses of the each sample. For this calculations to be most informative, the calculated mineralogical balance of the each sample in this way is matched with its X-ray diffractogram, where the major mineral entities are obtained. The agreement is observed between the calculated mineralogical composition and obtained major minerals by X-ray diffractometer for each sample. Moreover, the SEM photomicrographs and EDS analyses are also consistent with the calculated mineral compositions.

For these calculations, the following assumptions are made in the result of major element chemical analysis in Table 1 and 2:

1) the K_2O content comes from alunite (no residual K-feldspar in tuff).

2) the Al_2O_3 content comes from both alunite and kaolinite, but knowing the content of former, the latter can be calculated

3) LOI (loss on ignition) content comes from alunite as (SO_3+H_2O) and from kaolinite as (H_2O)

4) the remaining silica after subtracting that present in the kaolinite, will be as quartz, tridymite, cristobalite or opal(?) forms of free silica.

On the basis of above stated assumptions, the mineral compositions of the samples are determined as shown below in the example of R5-I:

THE CALCULATIONS OF THE MINERAL COMPOSITIONS:

The chemical formula of kaolinite: $Al_2Si_2O_5.(OH)_4$ or $Al_2O_3.2SiO_2.2H_2O$

The formula weight of kaolinite: 102+2x60+2x18=258 g

The chemical formula of alunite: $KAl_3.(SO_4)_2.(OH)_6$ or $K_2O.3Al_2O_3.4SO_3.6H_2O$

The formula weight of alunite: (2x39+16)+3x102+4x80+6x18=828 g

Quartz, tridymite, and cristobalite: SiO_2

The formula weight of SiO_2: 60 g

In the example of R5-I:

ALUNITE			
Chemical compounds	Theoretical proportion (%)	R5-I from the Table 1	Calculated
K_2O	11.4	1.69	1.69
Al_2O_3	37.0	17.90	5.50
(SO_3+H_2O)=LOI	51.6	12.52	7.69
Total	100.0		14.88

94 g K_2O is being used for 828 g alunite. Proportionally, 1.69 g K_2O should be used for 14.88 g alunite, as seen in the Table above. By the same token, 828 g alunite requires 306 g Al_2O_3. Likewise, 14.88 g alunite requires 5.5 g Al_2O_3. Also, 828 g alunite requires 428 g (SO_3+H_2O) and thus 14.88 g alunite requires 7.69 g (SO_3+H_2O), which is assumed as LOI in the Table 1.

ALUNITE			
Chemical compounds	Theoretical ratio (%)	R5–I from the Table 1.	Calculated
Al_2O_3	39.5	17.90	12.40
SiO_2	46.5	68.51	14.59
H_2O=LOI	14.0	12.52	4.37
Total	100.0		31.36

After being used in alunite, the remaining Al_2O_3 is 12.40 g. On the basis of alumina content, 102 g alumina makes 258 g kaolinite and proportionally 12.40 g Al_2O_3 makes 31.36 g kaolinite. Similarly, 258 g kaolinite requires 120 g SiO_2 and thus 31.36 g kaolinite requires 14.59 g SiO_2. The remaining amount, 53.92 g, forms free silica. Also, 258 g kaolinite requires 36 g H_2O, while 31.36 g kaolinite requires 4.37 g H_2O. The amount of accessory minerals is 0.63 g (or weight percent).

In Table 1, total R5–I is 101.25 % by analysis and consequently, the calculated mineralogical proportions for this sample are shown below:

Kaolinite	(31.36/101.25)x100	30.97 %
Alunite	(14.88/101.25)x100	14.70 %
Silica (quartz, tridymite, cristobalite, and opal)	(53.92/101.25)x100	53.25 %
Accessory minerals	(0.63/101.25)x100	0.62 %
Total		99.54 %

Appendix 2: Particle Size Analysis Procedure

After disaggregating the dried samples down to approximately 0.5 inch in diameter by a hammer, a crusher and a mortar, about 20 grams of sample split is placed in an oven to be dried at 105 °C in a previously weighed 80 ml. beaker about one and half hours. Then, the beaker is removed from the oven and is placed in a desiccator for about 30 minutes. The beaker is removed from the desiccator and is weighed with the sample and the weight recorded as weight of the original sample as seen in the particle size analysis sheet below. In the next step, the sample is placed in a 1000 ml. beaker with about 200 ml. of distilled water and a 10 ml. of dispersant (prepared by mixing 50 gr. sodium hexametaphosphate with 100 ml. distilled water). Then, the sample is mixed thoroughly and allowed to settle overnight. On the following day, the mixture is stirred vigorously with a glass stirring rod and then placed in an ultrasonic agitator for about 45 minutes.

When the sample is unflocculated, it is wet sieved through a number 230 sieve to remove all sand–plus sized material and then dried in a preweighed beaker in an oven at 105 °C. The sand–plus size is weighed and the weight recorded as weight of drying dish with dried sample. The silt– and clay–sized particles are placed in a 1000 ml. beaker and distilled water added to make a 1000 ml. suspension. Then, the mixture is stirred vigorously to distribute the clay and silt particles uniformly and allowed to settle for 30 minutes. Then, from the upper 2 mm, 50 ml. of suspension is extracted with a pipette and is placed in a preweighed beaker for drying in an oven at 105 °C. The clay–size fraction contained in the beaker is weighed and

the weight recorded as weight of drying dish with dried sample. By multiplying the clay-sized fraction by 20, the weight of this fraction in the original sample is obtained.

The results are reported as a weight percentages of the original sample as seen on the sheet below.

PARTICLE SIZE SHEET SHOWING THE CALCULATION AND RESULTS OF SAMPLE R5-VI FRACTIONS

Sample: R5-VI
Date: March 9, 1993

SAND-PLUS FRACTION

Weight of drying dish with dried sample	54.8898 gr.	
Weight of drying with dish empty	52.3913 gr.	
Weight of sample (sand-plus fraction)	2.4985 gr.	11.47 %

CLAY FRACTION

Weight of drying dish with dried sample	52.8892 gr.			
Weight of drying with dish empty	52.4026 gr.			
Weight of sample (clay fraction)	0.4866 gr.	x20	9.7320 gr.	44.66 %
Total (sand and clay)	12.2305 gr.			

SILT FRACTION

Weight of the original sample	21.7901 gr.	
Weight of sand-plus and clay	12.2305 gr.	
Difference (Weight of silt fraction)	9.5596 gr.	43.87 %

TOTAL _____ 100 %

Appendix 3: Placer Claim Map of the Kline Mountain Clay Deposit

(Judith Waggoner, Realty Specialist for the Bureau of Land Managment, Las Cruces, New Mexico, per., comm., July 9, 1993).

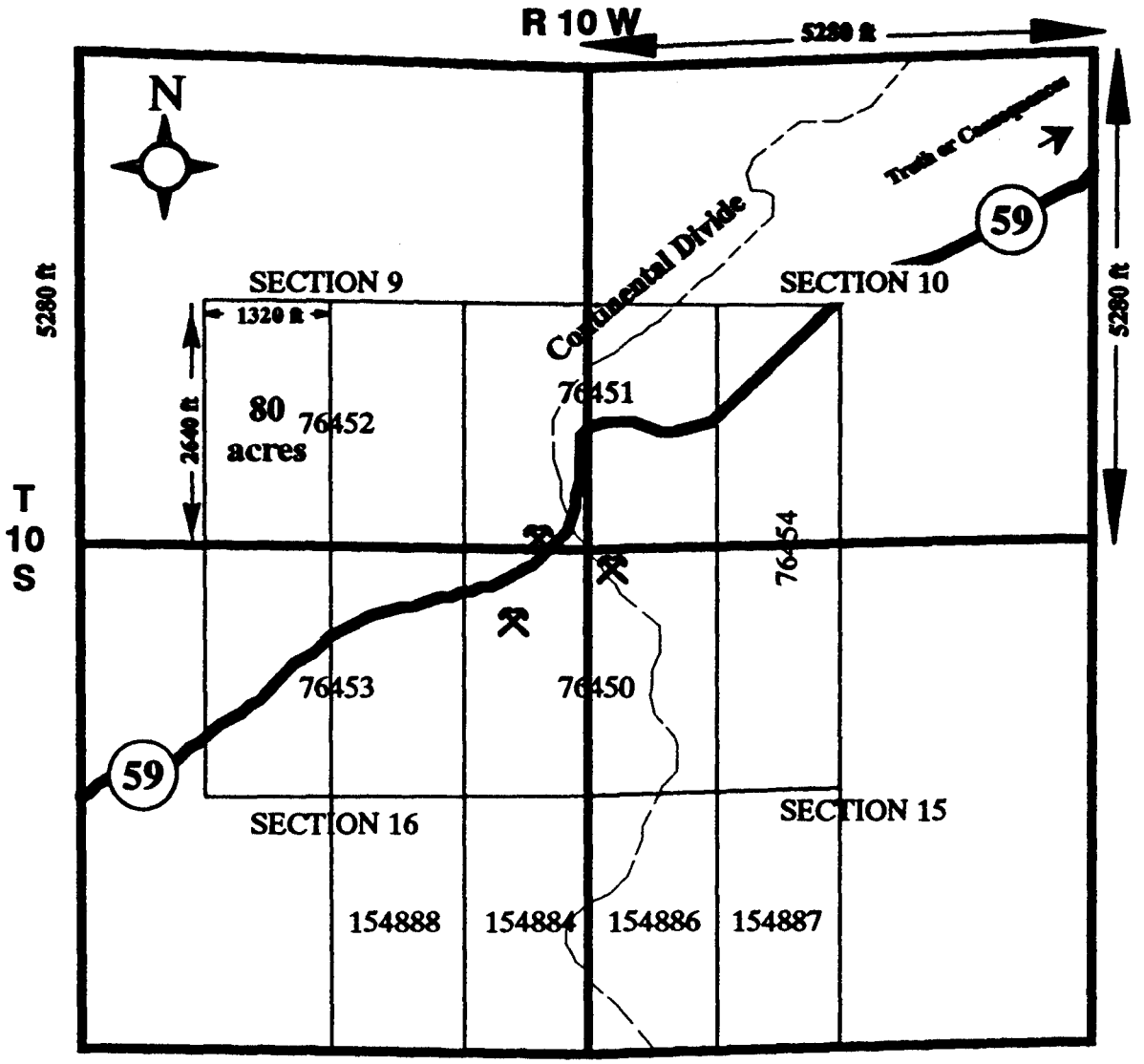

Owner Name	The Serial Number of New Mexico Placer Mining Claims
Ruth Wilson Hurley	NMMC 76450 through NMMC 76454
Richard and Carolyn Johnson Virgil and Carolyn Earles	NMMC 154884, 154886, 154887, and 154888

Curriculum Vitae

Iskender Isik was born in Gole, Turkey (Turkiye), on May 1, 1955, the son of Abdulkadir Isik and Gulnaz Isik. After graduating from Alpaslan High School in Kars, Turkey, he entered Black Sea Technical University by passing the University Entrance Examination held by the government and began his studies in geology in 1975. He graduated in June, 1979 with a geological engineering degree. Upon graduation, he was appointed for about 2.5 years as an geological engineer at the Electric Power Resources Survey and Development Administration (known as Electric Isleri Etud Idaresi, EIEI) for investigating dam sites, from where he won a scholarship when he was a senior.

By taking an examination, he became a teaching assistant at the Department of Mining Engineering of Anadolu University in the middle of 1982, where he received his master's degree in geology in the fall of 1985. He began his Ph.D. studies at Dokuz Eylul University in Izmir, Turkey, in 1986. Then, he transferred to the Anadolu University. After completing required Ph. D. course work and successfully passing the Ph.D. qualifying examination, he was granted a scholarship by Anadolu University to pursue his Ph. D. studies in the United States.

In July 1989, he enrolled at New Mexico Tech, Socorro, New Mexico. In January 1990, he transferred and entered the Graduate School of the University of Texas at El Paso. He has several publications on industrial minerals in Turkish and English languages. He is currently a faculty member of Anadolu University, Turkey.

Permanent address: Department of Mining Engineering

Anadolu University

Eskisehir, Turkey

This dissertation was typed by Iskender Isik.